CONTROLLED PARTICLE DEPOSITION IN A RETICULATED VITREOUS CARBON ELECTROCHEMICAL ADSORPTION CELL

A Thesis submitted to the

University of Manchester

Institute of Science and Technology

for the degree of Doctor of Philosophy

by

Majid Bahmani-Makvandzadeh

Department of Chemical Engineering

1996

DECLARATION

I hereby certify that no portion of the work referred to in the thesis has been submitted in support of any application for another degree or qualification of this or any other university of other institution of learning.

Majid Bahmani-Makvandzadeh

ACKNOWLEDGEMENTS

I wish to express my sincere gratitude to:

Prof. R.A.Williams for his enthusiastic support, patience and invaluable advice throughout the course of this work.

The technicians in the Department of Chemical Engineering, UMIST, for assisting the author with the construction of experimental apparatus.

The departmental computer staff for their assistance.

Postgraduate students in the Chemical Engineering Department, UMIST.

TABLE OF CONTENTS

NOMENCLATURE

α	displacement angle from the forward stagnation point
β	voidage
γ	collision efficiency factor
δ^+	minimum separation distance
ε_r	relative permittivity of medium$_o$
ε_o	permittivity of a vacuum
ε	dielectric constant of the medium
ζ	zeta potential
η_R	single collector efficiency
η	single collector efficiency based on physical forces
κ	Debye-Huckel reciprocal length
λ	filter coefficient
λ_{the}, λ_{exp}	theoretical and experimental filter coefficients
μ	fluid viscosity
ρ	volume density of charge
ρ_p, ρ_f	particle and fluid densities
σ_o	surface charge density
σ_C	collision diameter
υ	kinematic viscosity
Ψ	stream function
Ψ_{limit}	stream function for the limiting trajectory
ψ	surface potential
ψ_s	Stern's layer potential
Ω	angular velocity
ω	characteristic wavelength

a, a_f	particle and collector radii
A	Hamaker constant
A_F	flow parameter
A^+	dimensionless coefficient (a^2A_1/U) where A_1 a constant)
B	dimensionless coefficient (B_1a/U) where B_1 a constant
C, C_o	inlet and outlet particle number concentration
D	centre-to-centre separation distance (h/a)
d_p, d_c	particle and collector diameters
D^+	dimensionless coefficient (D1 a/U) where D1 a constant
e	electronic charge
E	electric field strength

F	force
F_1, F_2, F_3, F_4	hydrodynamic retardation factors
F_{Gr}, F_{LO}, F_{EDL} , F_I	gravitational, London, double layer and inertial forces
F_{st}, F_{ext}	hydrodynamic and external forces
F_{ret}	van der Waals retardation factor
f^t_r, f^m_r	drag correction factors
g	acceleration due to gravity
g^r_θ, g^t_θ, $g^m_{1\theta}$, $g^m_{2\theta}$	torque correction factors
h	surface-to-surface separation distance
H	dimensionless gap (h/a)
i_α, i_R	tangential and radial unit vectors
I	ionic strength
k^*, k^*_o	outlet and inlet conductivity
k	Boltzmann constant
l	axial distance in bed
l_c	axial distance of a unit collector
L	total filter bed depth
M	molar concentration
N_A	Avogadro's number
N_{LO}, N_G, N_R	London, gravity and interception dimensionless numbers
N_{D1}, N_{D2}, N_{D3}, N_{D4}	dimensionless double layer numbers
n_i,	number of ions per unit volume
$n_{i\infty}$	number of ions per unit volume in the bulk
NE1	electrokinetic group $(\upsilon\kappa(\zeta^2_1\zeta^2_1))/(12\ \pi\mu U)$
NE2	electrokinetic group $(2\zeta_1\zeta_2)/(\zeta^2_1+\zeta^2_1)$
NDL	double layer group (κa)
NLO	London group $A/(9\pi\mu a^2 U)$
P	pressure disturbance field
r	radial distance
R	proportionality ratio
RET	retardation correction factor
S_1	$(f^t_\theta\ g^r_\theta - f^r_\theta\ g^t_\theta)/\ g^r_\theta$
S_2	$(f^r_\theta\ g^m_{1\theta} + y\ f^m_{1\theta}\ g^r_\theta)/\ g^r_\theta$
S_3	$(f^r_\theta\ g^m_{2\theta} + y\ f^m_{2\theta}\ g^r_\theta)/\ g^r_\theta$
S_o	apparent rate constant
S_{planar}, $S_{spherical}$	planar and spherical surface areas
T	absolute temperature
t_{calc}	mean hydraulic residence time
Δt	time interval
U	fluid velocity
U_e	electrophoretic mobility
u_e	electrophoretic velocity
v_R, v_α	radial and tangential velocities
U_{st}, U_{sh}	stagnation point flow and shear flow velocities
V_A, V_R	van der Waals and electrical double layer energies
V_B, V_T	Born and total interaction energies

VF	volumetric flowrate
V_{total}, V_{void}, V_{beads}	total, void and beads volumes in the glass beads column
W	weight of particle deposited
WFT	total weight of particles in feed
WT	total weight of particle deposited
y	$r-a_f$
Z_i	valency of ion of type i

ABSTRACT

The ability to selectively separate specific colloidal particles from a mixed species is a long standing need of many industrial processes. The aim of this study was to investigate the use of surface forces for controlling the deposition process with a view to, ultimately, of addressing this goal. The effect of potentiostatic control of potential of filtration media on the deposition rate was investigated. The objective was to establish the experimental conditions wherein the surface forces (e.g. van der Waals and electrical double layer forces) were important. Deposition of 5.4 μm polystyrene latex and 7 μm *Hypercarb* (graphitised carbon) particles onto a carbon substrate was studied. The substrate used was Reticulated Viterious Carbon (RVC) which formed a rigid foam-like structure. An electrochemical adsorption cell was designed to perform the experiments. The cell consisted of RVC as the working electrode and stainless steel as the counter electrode. The effect of varying experimental conditions such as superficial fluid velocity, electrolyte concentration and electrode potential on the deposition process was examined. The results of deposition of polystyrene latex showed that, provided there were no Faradaic currents present, the effect of electrical double layer on the deposition process became evident at intermediate electrolyte concentration, typically 0.001 mol dm^{-3}, and low superficial fluid velocity, typically 2.26×10^{-5} m s^{-1}. The experimental results were compared with the DLVO theory. Theoretical collection efficiency and filter coefficients were obtained using trajectory analysis methods for the deposition of non-Brownian particles onto *cylindrical* collectors. The difference between theoretical and experimental values was typically of order 10. Reasons for these discrepancies are suggested and discussed. The important conclusion obtained from this study is that it is possible to extend the established deep bed filtration techniques utilising spherical glass bead collector to the use of rigid foam-

like electronically conducting materials such as RVC. The overall conclusion of the experiments was that the variation of RVC collector potential externally produced significant variation in the deposition rate under favourable deposition condition, whereas under unfavourable deposition condition the same effect was not obtained.

CHAPTER 1

INTRODUCTION

Separation of solids from liquid may be required to remove valuable products or to retain undesired contaminants. Deep bed filtration of waste waters is perhaps the most prominent example of the need to remove particulate contaminants from the liquid.

The conventional solid/liquid separation processes such as filtration usually involve removal of total solid content *mechanically* irrespective of type or shape. However, it is sometimes required to selectively separate one species of solids from a mixed species.

Studies reported in literature for selective separation usually involve *physical* attachment of solids onto larger substrates. Possibility of separating finely divided minerals from mixed slurries by selective aggregation using flocculants has been reported by Attia (1982). However, other studies have dealt with deposition of colloidal sized particles onto planar collectors as possible route for selective separation.

Deposition of colloidal particles is encountered in many chemical and biochemical engineering processes. Naturally occurring examples include the particulate fouling of the heat exchangers, thrombus formation in vascular prostheses and other artificial organs and aerosols carrying gaseous pollutants entering the lungs. The process of deposition as shown in Figure 1.1 involves two stages namely the *transport* stage where the particle is brought to the vicinity of the collector by the fluid flow and diffusion, followed by the *attachment* stage

where the particle is physically deposited. The attachment stage is governed by short range colloidal interaction forces namely the London-van der Waals attraction and the electrical double layer. The sum of these two forces represents the total interaction energy between the particle and collector and this forms the underlying assumption for the Derjaguin, Landau, Verwey and

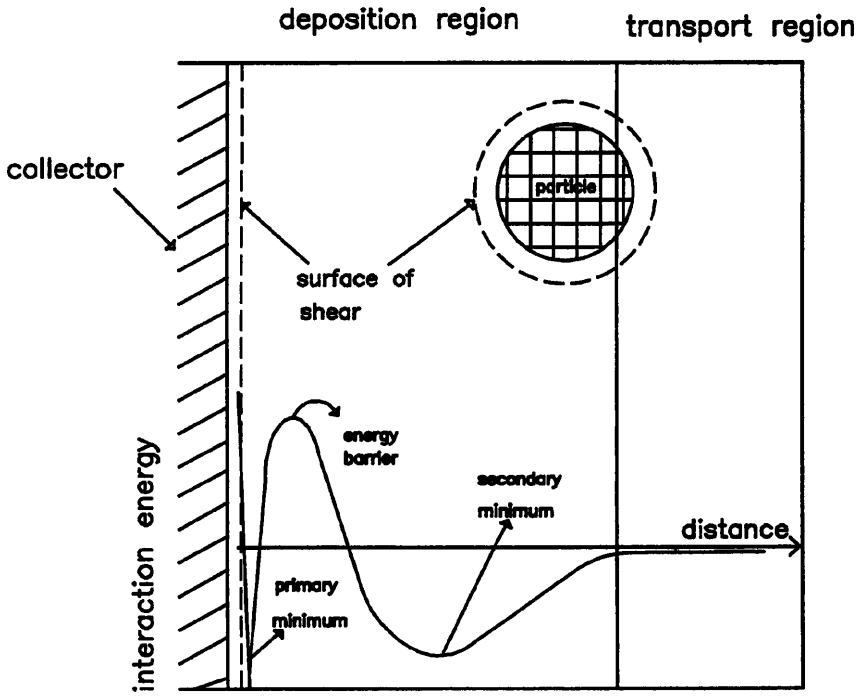

Figure 1.1 Schematic representation of particle deposition stages (upper diagram) and a typical (DLVO) interaction energy profile between the particle and collector (lower diagram).

Overbeek (DLVO) theory of colloid stability. Depending on electrolyte concentration, different interaction energy profiles may be obtained. At high electrolyte concentrations (e.g. 0.1 mol dm^{-3}) a primary minimum and no energy barrier may be obtained in which case deposition of particles is possible. At low electrolyte concentrations (e.g. below 10^{-4} mol dm^{-3}) no energy minimum and an energy barrier may be obtained resulting in repulsive forces and hence no particle deposition is possible. At intermediate concentrations two minima (primary

and secondary) and a maximum may occur. It can be seen from Figure 1.1 that deposition into the deep primary minimum usually involves surmounting the energy barrier and any particle deposited into the primary minimum is said to be irreversibly trapped. In contrast the secondary minimum is usually shallow compared to the primary minimum and additionally no energy barrier must be surmounted prior to deposition. Consequently, particle deposition into the secondary minimum is said to be reversible which means that it is easier to desorb the particles from the secondary minimum than those in the primary minimum. From the aforementioned statements the secondary minimum seems a suitable option for possible selective separation processes.

A possible scheme utilizing the secondary minimum for selective separation would involve depositing the desired species of particle from the mixed suspension by manipulating the experimental conditions so that other species do not deposit and thereafter the deposited particles are desorbed by reversing the experimental conditions.

A feasible selective separation technique should be applicable to a variety of experimental conditions. Particle size, concentration and density could play decisive roles even if a selective separation technique has been proven successful. For example, the occurrence of the blocking phenomena is attributed to the deposited particles reducing the sites available for deposition. Additionally problems associated with the scale-up of a laboratory scale selective separation technique renders it vulnerable unless it is modified to be applicable to process scale.

Jia and Williams (1990) argue that selectivity could be achieved by exploiting inherent

differences in the surface properties of colloidal species or by applying an external field which may be of gravitational, magnetic or electrical in nature.

This thesis addresses the problem of selective separation of colloidal particles from a mixed species aqueous suspension. The objective of this study is to investigate the aforementioned theory, particularly the use of secondary minimum, for devising a separation technique which utilises *externally controlled electrical potential of the collector*. Based on experimental results it will be argued whether this technique is practical for selective separation of a species of non-Brownian particle from a mixed species suspension.

Prior to any attempt to design a selective separation process based on these principles several important issues must be clarified. Correct selection of an appropriate experimental system and procedure for carrying out deposition experiments is of considerable importance. For example it could well be possible to achieve selective separation for one combination of particle/collector system and not for another. Designing the experimental system consists of detailed design of the adsorption column, nature of the relevant external field and determination of the duration of experiments. In the research presented here deposition of different colloidal particles onto different collectors have been investigated in order to provide guidelines for the design of a selective deposition system. It has been possible to examine the effects of different experimental parameters such as pH, electrolyte concentration and superficial fluid velocity on the adsorption rate.

Two types of collectors with different packing characteristics have been employed.

1. *Glass beads* which are representative of the conventional deep bed filtration collector. Such materials have been employed widely in colloid filtration. These can be formed into a packed bed by pouring them into the column.

2. *Reticulated Vitreous Carbon (RVC)* which is used to examine the possibility of selective separation. This forms a fixed rigid flow through electrode.

An electrochemical RVC adsorption cell has been designed thus allowing the effect of different experimental conditions, particularly the effect of applying of an external electric field, on adsorption rate to be investigated.

Spherical polystyrene latex and *Hypercarb* (graphitised carbon) have been used as particulate feed materials. Use of an external electric field as means of controlling deposition has been investigated for the two particle types. The total interaction energy between the collector and particle is estimated for a variety of parameters such as the collector potential, particle potential, ionic strength and pH. The best combination of these parameters predicting suitable experimental conditions for selective deposition is investigated.

1.1 ORGANISATION OF THESIS

The layout of the thesis is briefly described below:

Chapter 2 introduces the scientific concepts which are most relevant to this research. This Chapter comprises four parts. The first part discusses the solid/liquid interface and the characterisation of surface potential by use of the zeta potential. The second part reviews

existing quantitative relationships for estimation of colloidal particle-particle and particle-collector interaction forces. The last two parts provide a critical summary of techniques which can be used in the study of deposition processes.

Chapter 3 describes the experimental apparatus which was designed and constructed for deposition. Associated theoretical background relevant to the tests used (turbidimeter, zeta potential analyser and potentiostat etc.) is also included here.

Chapter 4 describes the characterisation of the particulate materials, the collectors and the experimental procedures that were developed for the deposition experiments.

Chapter 5 presents experimental data for the spherical glass bead collector. These are then compared with the deep bed filtration models available in literature.

Chapter 6 compares the effect of different experimental conditions on deposition rate of polystyrene latex and *Hypercarb* particles onto RVC collector and then investigates possible means of achieving selective separation based on this information .

Chapter 7 presents a theoretical approach to quantify adsorption in the RVC system based on trajectory analysis theory.

Finally Chapter 8 presents the conclusions and recommendations for future work which are likely to result in further improvements to the present system.

CHAPTER 2

PRINCIPLES OF COLLOID DEPOSITION

A CRITICAL REVIEW

This chapter seeks to provide a summary of the underlying principles relevant to understanding deposition processes. The subject area has been divided, for convenience, into four sections. In section 2.1 a summary of terms and relevant theories for describing the solid/liquid interface are introduced. Section 2.2 provides a glossary of expressions available for estimation of colloidal interactions relevant to this research project (emphasising the electrical double layer and London-van der Waals energies). Section 2.3 deals with packed bed techniques which have been reported in the published literature for investigation of deposition processes. Section 2.4 introduces basic electrochemical concepts which are relevant to the present study. Section 2.5 focuses specifically on work reported in the literature where attempts have been made to control colloid adsorption using an external electric field. The scope of this previous work, both theoretical and experimental, is assessed.

2.1 THE SOLID/LIQUID INTERFACE

Most substances exhibit a surface electric charge when immersed in a polar (e.g. aqueous) medium. Jia and Williams (1990) have discussed this in some detail and state that possible routes for the charge transfer could be ionisation, ion adsorption and ionic dissolution. This surface charge forces the distribution of nearby ions in the polar medium in such a way to establish electroneutrality. Ions of opposite charge (counter ions) are attracted towards the surface and ions of like charge are repelled away from the surface. This together with the mixing

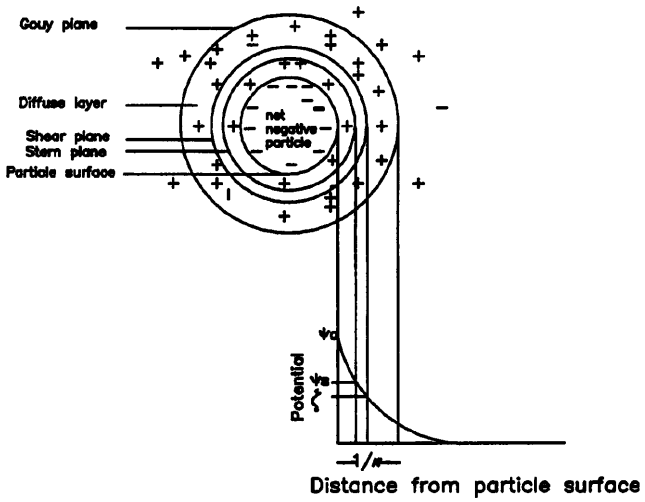

Figure 2.1 Electrical double layer for a spherical particle with different 'conceptual planes'

tendency of thermal motion leads to the formation of an electrical double layer made up of the charged surface and a neutralising excess of counter ions in the polar medium.

Quantitative treatment of electrical double layer presents a difficult problem which has been tackled by several workers. The classical approximate theory for electrical double layer was given by Gouy (1910), Chapman (1913), Debye and Huckel (1923) and modified by later work of Stern (1923) and particularly Graham (1948). Among these models the simplest is the capacitor model in which the interface is envisaged to be a parallel-plate capacitor. The variation of the electrical potential (ψ) with distance from a charged surface of arbitrary shape is known to be described by Poisson equation:

$$\nabla^2\psi = -\frac{\rho}{\epsilon} \qquad (2.1)$$

where ρ is the volume density of charge and ε is the dielectric constant of the medium given by $\varepsilon_0\varepsilon_r$ (as defined in the nomenclature). The volume density of charge found from the total

number of charge per unit volume of electrolyte, i.e. $\rho=e\ \Sigma n_i Z_i$ where e is the electronic charge, n_i is the number concentration of ions of species i and Z_i is the valency of the ions, noting that the sign of the charge is implicit in Z_i. In order to usefully describe the distribution of charge about the particle a Boltzmann distribution is adopted. Boltzmann's distribution law indicates that if each state of a system has a characteristic and distinct energy level, $Z_i e\psi$, then the number of ions having this energy is:

$$n_i = n_{i\infty} \exp\left[\frac{-Z_i\, e\, \psi}{k\, T}\right] \tag{2.2}$$

where n_i is the number of ions of type i per unit volume, $n_{i\infty}$, the bulk concentration, k the Boltzmann constant and T the absolute temperature. Combining equations (2.1) and (2.2) yields the Poisson-Boltzmann equation (2.3):

$$\nabla^2\psi = -\frac{e}{\epsilon}\sum Z_i n_{i\infty} \exp\left(-\frac{Z_i e\psi}{kT}\right) \tag{2.3}$$

This is an important equation since it forms the basis of our understanding of electrolyte solutions, electrode processes, colloid interactions and transistor behaviour and this forms the basis of the Debye and Huckel theory (1923). The Poisson equation implies that the potentials associated with charges combine in an additive manner. On the other hand, the Boltzmann equation involves an exponential relationship between the charges and the potentials. Consequently, a fundamental inconsistency is introduced when equations (2.1) and (2.2) are combined. Equation (2.3) does not have an explicit general solution and therefore must be solved for certain limiting cases.

For the case of a planar collector surface at a low positive potential (i.e. when electrical

energy is small compared to thermal energy: $Z_i e\psi \ll kT$), the exponential on the right-hand of equation (2.3) can be expanded as a power series. If only first-order terms are retained and electroneutrality is taken into account, equation (2.3) becomes:

$$\frac{d^2\psi}{dx^2} = \frac{e^2\psi}{\epsilon kT} \sum Z_i^2 n_{i\infty} \tag{2.4}$$

The parameter κ, called the Debye-Huckel reciprocal length, is defined as:

$$\kappa^2 = \frac{e^2}{\epsilon kT} \sum Z_i^2 n_{i\infty} \tag{2.5}$$

This parameter, is very important for quantitative description of electrical double layer and is often regarded (but imprecisely) as the 'thickness' of the double layer. If n_i is expressed as the number of ions per cubic meter and related to the molar concentration, M_i, of the ions by $n_i = 1000\ N_A\ M_i$, equation (2.5) becomes:

$$\kappa = \left[\frac{1000 e^2 N_A}{\epsilon kT} \sum Z_i^2 M_i \right]^{1/2} \tag{2.6}$$

where N_A is Avogadro's Number. For aqueous solutions of symmetric (Z:Z) electrolyte at 25 ^{0}C equation (2.6) becomes:

$$\kappa = 3.28\ (\ Z^2 M\ )^{1/2} = 3.28\ I^{1/2} \tag{2.7}$$

where κ is in nm^{-1} and I is the symmetrical electrolyte ionic strength in mol dm^{-3} in which $Z_1 = Z_2 = Z$ and $M_1 = M_2 = M$ so that:

$$I = Z^2 M \tag{2.8}$$

substitution of equation (2.5) into the one dimensional form of equation (2.4) allows one to

write:

$$\frac{d^2\psi}{dx^2} = \kappa^2\psi \tag{2.9}$$

with the appropriate solution for the potential decay from a flat plate is:

$$\psi(x) = \psi_0 \exp(-\kappa x) \tag{2.10}$$

It has to be born in mind that the above approximation is only applicable to low potentials (ψ_o <25 mV). However, it is a limiting case which applies to all equations that are derived for general applications, i.e. at low potentials all equations should reduce to (2.10).

2.1.1 Gouy-Chapman model

The Gouy (1910) and Chapman (1913) model is based on the nonlinear Poisson-Boltzmann relationship for a diffuse electrical double layer. The later linearisation is known as the Debye and Huckel (1923) approximation. This model is based on the assumptions that the surface is flat, of infinite size and uniformly charged. Additionally, the ions in the electrolyte are treated as point charges and distributed according to the Boltzmann law, whilst the dielectric constant is assumed to be uniform throughout the diffuse part of the double layer and no other solvent-specific effects are allowed for.

Hence for one dimensional problem and a single symmetrical electrolyte equation (2.3) can be written as:

$$\frac{d^2\psi}{dx^2} = \frac{2 Z e n_\infty}{\epsilon} \sinh\left(\frac{Z e \psi}{kT}\right) \tag{2.11}$$

whose solution with boundary conditions $\psi(x)\big|_{x=0} = \psi_0$ and $\psi(x)\big|_{x=\infty} = 0$ can be written

either in the following form:

$$\psi(x) = \frac{2\,k\,T}{Z\,e} \ln\left(\frac{1 + \Upsilon_0 \exp(-\kappa x)}{1 - \Upsilon_0 \exp(-\kappa x)}\right) \qquad (2.12)$$

or as

$$\Upsilon = \Upsilon_0 \exp(-\kappa x) \qquad (2.13)$$

where $\Upsilon = \tanh(Ze\psi/4kT)$ and $\Upsilon_0 = \tanh(Ze\psi_0/4kT)$.

When the exponential in Υ are expanded and only one term in the series is kept, both in the numerator and denominator, the expected Debye-Huckel expression, equation (2.10) is obtained. At large values of distance, x, the potential falls to a very small value regardless of its initial value and under this interesting conditions equation (2.13) becomes:

$$\psi(x) = \frac{4\,k\,T\,\Upsilon_0}{Z\,e} \exp(-\kappa x) \qquad (2.14)$$

2.1.2 Stern model

Stern (1924) recognised that two underlying assumptions for the derivation of the models discussed above were unsatisfactory i.e.:

1) The ions constituting the indifferent electrolytes are assumed to behave as point charges. This assumption is acceptable for the bulk region of dilute solutions. The finite size of the ions whether hydrated or not, limits their maximum concentration at the wall, and their distance of closest approach to it.

2) The assumption that the solvent could be treated as a structureless dielectric of constant permittivity.

Stern proposed a model in which the double layer is divided into two parts separated by a

hypothetical boundary, the Stern layer, being located at about a hydrated ion radius from the actual surface. He also considered the possibility of specific adsorption of ions at the interface. Specifically adsorbed ions are those which are attached (albeit temporarily) to the surface by electrostatic and/or specific chemical forces strong enough to overcome the thermal agitation. They may be dehydrated, at least in the direction of surface. The centres of any specifically adsorbed ions are located in the Stern layer, i.e. between the surface and the Stern plane. When specific adsorption takes place, counter-ion adsorption usually predominates over co-ion adsorption and it is possible, especially with polyvalent or surface active counter-ions, for the reversal of charge to take place within the Stern layer, i.e. for ψ_0 and ψ_s to have opposite signs (see Figure 2.1). Adsorption of surface-active co-ions could create a situation in which ψ_s has the same sign as ψ_0 but is greater in magnitude. Stern assumed that a Langmuir-type adsorption isotherm could be used to describe the equilibrium between ions adsorbed in the Stern layer and those in the diffuse part of the double layer. The Stern model of double layer predicts a more realistic picture of the double layer than the previous models since it allows for surface saturation (due to specific adsorption) and consequently it overcomes the objection to the Gouy-Chapman theory which predicts excessive surface concentration of adsorbed ions.

However, there are several shortcomings associated with the Stern model of double layer. First, Stern theory is difficult to apply quantitatively because several of the parameters (such as the dielectric constant of the Stern layer and the specific chemical energy term) cannot be evaluated experimentally. Secondly, in the Gouy-Chapman theory the functional dependence of ψ on x involves only parameters κ and ψ_0. The former is known and the latter may be evaluated for some surfaces. The Stern theory of the double layer introduces parameters which

are not only difficult to estimate but also demand knowledge of specific characteristics of different ions. Thirdly, the generality of the Gouy-Chapman model is lost when the specific adsorption effects are taken into accounts.

2.1.3 Zeta potential

It would be ideal if the potential ψ_s (see Figure 2.1) could be experimentally determined, however, in practice the best possible estimate is provided by the zeta potential (ζ) at the surface of shear which can be estimated by electrokinetic measurements. Surface of shear is an important concept encountered in electrokinetics and this is an imaginary surface which lies close to the surface and within which the fluid is stationary (see Figure 2.1) and with its exact location unknown.

Shaw (1992) discusses electrokinetic phenomena and states that electrophoresis occurs due to the movement of a charged surface relative to a stationary liquid under the influence of an applied field. The surface of shear envelopes the particles and all the materials inside the envelope form a kinetic unit so that the particle moves along with a certain quantity of the surrounding liquid and its contained charge. Measurement of electrophoretic mobility will provide an estimate of the charge on the particle.

To obtain a relationship between experimentally measured electrophoretic mobility, U_e, (defined as the ratio of the electrophoretic velocity, u_e, of a particle to the electric field strength, E) and its corresponding zeta potential, two extremes have been studied. For curved surfaces the double layer can be described in terms of the dimensionless quantity 'κa' which is the ratio of radius of curvature to the double layer thickness.

1) when 'κa' is small (less than one), a charged particle may be assumed to behave as a point charge in an undisturbed electric field. Huckel (1923) considered this assumption and from the Debye-Huckel approximation obtained the following equation:

$$U_e = \frac{u_e}{E} = \frac{2 \epsilon \zeta}{3 \mu} \qquad (2.15)$$

Where μ is the fluid viscosity. Normally this equation does not apply to particle electrophoresis in aqueous media since for example particles of radius 10^{-8} m suspended in a 1-1 aqueous electrolyte solution would require an electrolyte solution as low as 10^{-5} mol dm^{-3} to give κa=0.1. This equation, on the other hand, has possible attractions in particle electrophoresis in non-aqueous media of low conductivity.

2) Large values of 'κa' (greater than one) present the other extreme and electrophoretic mobility is related to the zeta potential by the Smoluchowski's (1917) equation, which is written:

$$u_e = \frac{\epsilon \zeta}{\mu} \qquad (2.16)$$

It can be concluded from this equation that the electrophoretic mobility of a uniformly charged non-conducting particle, for which 'κa' is large i.e. the thickness of the double layer is small compared to the radius of curvature of the particle, should be independent of its size and shape provided the zeta potential is constant.

When a particle is in an electric field the ions in the mobile part of the double layer move in the opposite direction to that of the particle and this creates a local movement which opposes the particle motion. This movement is called electrophoretic retardation. Another

effect arising from this movement which should be taken into account is that the ions in the mobile part of the double layer take a finite time, called the relaxation time, to restore the original symmetry by diffusion and conduction. The resulting asymmetric movement of the ions imposes another retarding force known as the relaxation effect. The relaxation effects can be ignored for small values of $\kappa a < 0.1$ and for large values of $\kappa a > 300$, but it must be taken into account for intermediate values.

The equipment used to determine the zeta potentials of the particles and collectors used in the adsorption experiments in this study is briefly described in Chapter 3. Smoluchowski's equation is used to calculate the zeta potentials of the particles and collectors and this will be discussed in section 3.4.

2.2 COLLOIDAL INTERACTIONS

As discussed in Chapter 1 deposition processes consists of two steps namely *transport* of particles towards the collector followed by the *attachment* of particles onto the collector. The attachment step is dominated by colloidal interaction energy in the vicinity of the collector. These colloidal interaction energies include the electrical double layer, the London-van der Waals, Born repulsion, hydration (structural), hydrophobic interactions for hydrophobic surfaces and the steric interactions when macromolecules adsorb onto the interface of the interacting particle and collector. In the theoretical section of this work it will be assumed that the mainenergies contributing to adsorption interaction between the surfaces will be due to the electrical double layer and the London-van der Waals. It is the the sum of the energies that provide the total interaction energy between the surfaces and this constitutes the underlying assumption for the classical Derjaguin, Landau, Verwey and Overbeek (DLVO)

theory of colloid stability. A typical interaction energy curve can be seen in Figure 2.2. The occurrence of the primary and secondary minima and the energy barrier has already been briefly discussed in Chapter 1.

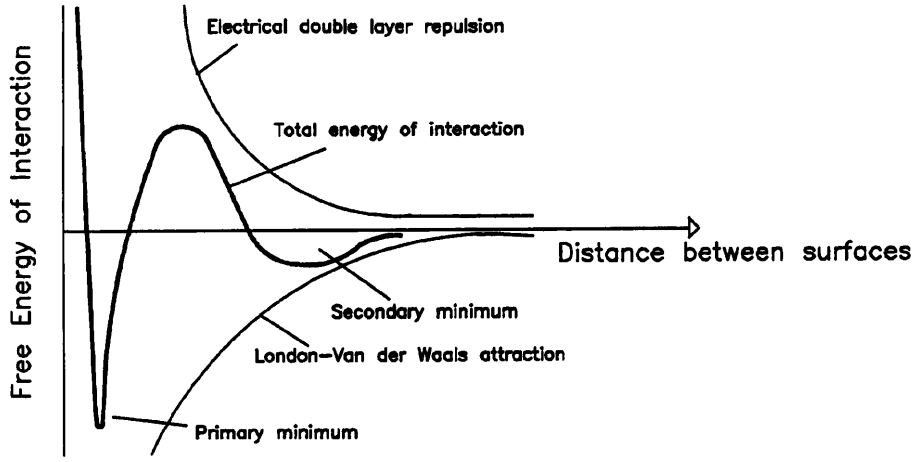

Figure 2.2 Schematic diagram of a typical energy of interaction curve for two spherical particles

Depending on the electrolyte concentration an energy minimum and no energy barrier or two energy minima and an energy barrier may be obtained.

There are some fundamental shortcomings associated with the DLVO's theory for instance flocculation experiments show that adding electrolyte to colloidal suspension induces floc formation and removal of electrolyte by dialysis reverses this process. The classical DLVO theory explains the flocculation process but it does not allow reversibility. Consideration of London-van der Waals and electrical double layer as the only energies between particles results in the flocs being held together in an infinitely deep energy well.

Another shortcoming observed by Overbeek (1977) was that the DLVO theory did not allow for dependency of initial rate of flocculation on the particle size.
Nir et al. (1978) investigated this dependency and carried out aggregation experiments and confirmed the above statement and argued that the reason for failure of DLVO theory was that there were two modes of aggregation i.e. a primary and a secondary minimum.

Elimelech (1991) investigated the applicability of DLVO theory for adsorption experiments. He argued that theoretical predictions within the framework of DLVO resulted in particle size having a pronounced effect on the collision efficiency. This was the result of the London-van der Waals and electrical double layer energies and subsequently the height of energy barrier depending on particle size. In contrast, experimental results showed that the experimental collision efficiency was virtually independent of the particle size. He stated that the classical DLVO theory, although elegant, cannot be used to predict the collision efficiency in the initial stages of the colloid deposition. An alternative approach is needed for predicting the collision efficiency in natural and technological colloidal processes.

Jia and Williams (1990) and Jia (1992) in reviews gathered the most common expressions for the plate-plate and sphere-sphere double layer interactions and London-van der Waals energies and discussed their shortcomings and limitations. Some of these expressions are collated in an edited form in Tables 2.1-2.3.

2.2.1 Electrical double layer

When two colloidal particles are brought together so that their double layers overlap there

will be an interaction between the double layers resulting in distortion and a change in the free energy but eventually an state of equilibrium will be reached. Study of electrical double layer interaction is usually undertaken with two approaches. These are the *constant potential* and *constant charge* approximations originating from the behaviour of double layers from the time of interaction to the final equilibrium.

If double layers relax so rapidly that equilibrium is restored almost immediately then double layers are assumed to be at equilibrium and a constant potential will be assumed. In contrast if double layers restore equilibrium very slowly then the surface charge will be assumed to be constant. In reality due to uncertainty about the choice of plane to represent the surface potential which in turn plays the major role in the interaction of double layers Bell et al. (1970) recommended that an alternate method based on the Linear Superposition Approximation (LSA) provides a useful intermediate approach.

Figure 2.3 shows typical values for the expressions quoted in Table 2.1. Evidently all the expressions predict similar double layer energies at separations greater than 30 nm. The largest descrepancies are found at closer separations. The expression due to Hogg et al.(1966) for constant surface potential interactions is always the lowest, while that of Bell et al.(1970) always is close to the average of all the expressions. In the present study the double layer energy expressions due to Bell et al.(1970) and Hogg et al.(1966) have been used. The former is found to be appropriate since it is not clear what sort of interaction is occuring and this approximation gives the average of both CCA and CPA. The expression due to Hogg et al.(1966) is popular in the literature and allows direct comparison with other published results.

Table 2.1 Summary of sphere-sphere double layer interactions

Interaction expression	Method	Validity	Source
$V_R=\frac{128a_1a_2\pi n_\infty kT}{(a_1+a_2)\kappa^2}\psi_1\psi_2\exp(-\kappa h)$	LSA DIM	$h < a_1$ symmetric $\kappa a_1 > 5$	Verwey & Overbeek (1948)
$V_R=\frac{2a_1a_2\pi n_\infty kT}{(a_1+a_2)\kappa^2}(\psi_1^2+\psi_2^2)\left[\frac{2\psi_1\psi_2}{\psi_1^2+\psi_2^2}\ln\left(\frac{1+\exp(-\kappa h}{1-\exp(-\kappa h}\right.\right.$ $\left.\left.+\ln(1-\exp(-2\kappa h))\right]\right.$	CPA LPB DIM	small Φ_1 $h < a_1$ $\kappa a_1 > 1$	Hogg et al. (1966)
$V_R=\frac{2a_1a_2\pi n_\infty kT}{(a_1+a_2)\kappa^2}(\psi_1^2+\psi_2^2)$ $\times\left[\frac{2\psi_1\psi_2}{\psi_1^2+\psi_2^2}\ln\left(\frac{1+\exp(-\kappa h)}{1-\exp(-\kappa h)}\right)\right.$ $\left.-\ln(1+\exp(-2\kappa h))\right]$	CCA LPB DIM	small ψ_1 $h < a_1$ $\kappa a_1 > 1$	Wiese & Healy (1970)
$V_R=4\pi\epsilon\psi^2\frac{a(h+a)}{(h+2a)}\ln\left[1+\left(\frac{a}{h+a}\right)\exp(-\kappa a)\right]$	LSA	$\kappa a < 1$	Bell et al. (1970)
$V_R=\frac{\pi a_1a_2}{a_1+a_2}\left[(2\sigma_2\psi_1/\kappa)\times\left(\frac{\pi}{2}-\tanh^{-1}\sinh(\kappa h)\right)\right.$ $\left.-\left(\frac{4\pi\sigma_{02}^2}{\epsilon\kappa^2}-\frac{\epsilon\psi_1^2}{4\pi}\right)\ln(1+\exp(-2\kappa h))\right]$	mixed CP & CC LPB DIM	weak interaction symmetric $h < a_1$ $\kappa a_1 > 1$	Kar et al. (1973)

Note:
LPB=Linear Poisson-Boltzmann equation solution
CCA=constant-charge approximation
CPA=constant-potential approximation

LSA=linear superposition approximation
DIM=Derjaguin Integration Method

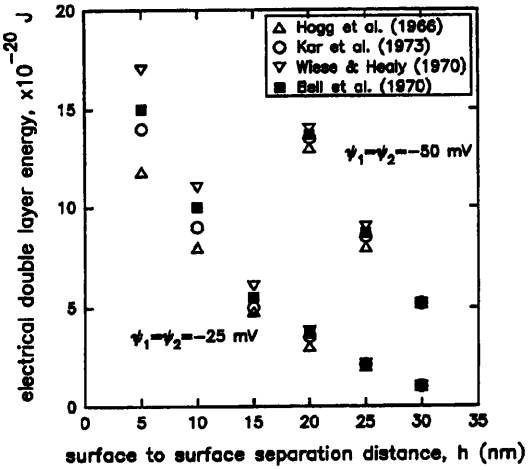

Figure 2.3 Variation of electrical double layer energy with separation between two spherical particles of the same radii of 0.1×10^{-6}m in an electrolyte of concentration 1×10^{-3} mol dm^{-3}

2.2.2 London-van der Waals energy

This is an attractive energy exerted by all atoms or molecules, whether polar or not. They arise from fluctuation in the electron charge distribution around the atoms or molecules. These fluctuations produce an instantaneous dipole so that one molecule in the neighbourhood of another experiences attraction.

There are basically two approaches for estimation of the London-van der Waals energy. One is due to Hamaker (1937) in which the attractive energy between two particles is calculated as the pairwise summation of all intermolecular interactions. This method of pairwise addition has three main inadequacies:

- If atom 1 in A interacts with atom 1 in B the presence of neighbouring atoms to A and B will undoubtedly influence the interaction between A and B.
- The Hamaker approach does not provide information regarding to whether the finite dielectric property of the medium between bodies 1 and 2 should be taken into account.
- As a result of point 2 above it is not clear how the dielectric property of the medium should

enter the equation for pairwise addition.

The second approach is based on the Lifshitz (1956) theory which attempted to overcome the above inadequacies by calculating the attractive energy in terms of the bulk properties of the particles and of the intervening material.

In both approaches a value for the Hamaker constant, A, having units of energy is required. In the Hamaker approach, A is taken as a constant and an average value for the particles immersed in a medium can be estimated as shown by equation (2.17).

$$A_{312}=\left(A_{33}^{1/2}-A_{11}^{1/2}\right)\left(A_{22}^{1/2}-A_{11}^{1/2}\right) \qquad (2.17)$$

where A_{33} and A_{22} are the Hamaker constant for the material 3 and 2 and A_{11} is the Hamaker constant for the medium. In contrast the Lifshitz theory considers A as being dependent upon the distance between the materials.

As discussed before, the London-van der Waals attractive energy arises from the instantaneous dipoles produced when two bodies are near each other. If the distance between atoms is larger than 50 nm, by the time electric field from one atom has reached and polarised the other, the electron configuration of the first atom will have changed. There will be poor interaction between the two dipoles and atoms experience what is called the 'retarded' London-van der Waals attraction energy. Therefore, calculation of London-van der Waals attractive energy falls into two categories:

1) particles at separations greater than 50 nm where retarded London-van der Waals energy

is in operation.

2) particles at separations less than 10 nm where particles experience non-retarded London-van der Waals attractive energy. The most common expressions for the unretarded and retarded London-van der Waals energy can be seen in Tables 2.2 and 2.3 respectively.

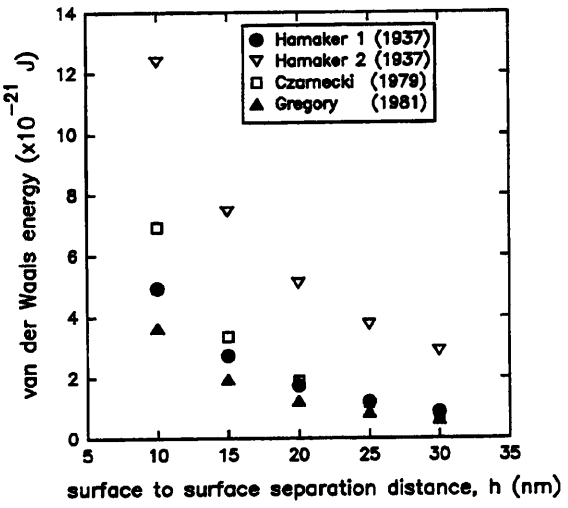

Figure 2.4 Variation of van der Waals energy with separation distance for spherical particles of equal radii of $0.1x10^{-6}$ m and hamaker constant of $1x10^{-20}$J

Figure 2.4 shows the variation od London-van der Waals energy with separation distance between spherical particles of equal radii of 100 nm. The more recent results of Gregory (1981) and Czarnecki (1979) are used in the present study. This is because they include the retardation effects which are not included in the Hamaker (1937) results. It is clear that the expression for the unretarded van der Waals energy are higher than that for the retarded. The largest differences between the various expressions are found at close separations. Both expressions are used herein because each is considered to be more appropriate for specific separations.

Comparison of Figures 2.3 and 2.4 shows that the energy values found in V_A and V_R suggest that both are comparable and neither can be neglected at the expense of the other.

Table 2.2 Summary of common expressions for the unretarded van der Waals interaction

Interaction expression	Validity	Source
$-\frac{A}{6}\left[\frac{2a_1a_2}{h^2+2a_1h+2a_2h}+\frac{2a_1a_2}{h^2+2a_1h+2a_2h+4a_1a_2}+\ln\left(\frac{h^2+2a_1h+2a_2h}{h^2+2a_1h+2a_2h+4a_1a_2}\right)\right]$	sphere-sphere	Hamaker 1 (1937)
$-\frac{A}{6}\left[\frac{a}{h}+\frac{a}{h+2a}+\ln\left(\frac{a}{h+2a}\right)\right]$	sphere-plate	Hamaker 2 (1937)

Table 2.3 Summary of principal expressions for retarded van der Waals interaction

Interaction expression	Validity	Source
$A\left[\frac{2.45\omega}{60\pi}\left(\frac{h-a}{h^2}-\frac{h+3a}{(h+2a)^2}\right)-\frac{2.17\omega^2}{720\pi^2}\left(\frac{h-2a}{h^3}-\frac{h+4a}{(h+2a)^3}\right)+\frac{0.59\omega^3}{5040\pi^3}\left(\frac{h-3a}{h^4}-\frac{h+5a}{(h+2a)^4}\right)\right]$	sphere-sphere $h > \omega/4\pi$	Czarnecki (1979)
$\frac{-Aa_1a_2}{6h(a_1+a_2)}[1-(bh/\omega)\ln(1+\omega/bh)]$	sphere-sphere $h < a_1$ $b = 5.32$	Gregory (1981)

2.2.3 Other static energies

Apart from the London-van der Waals and electrical double layer energies there are other

interaction energies which operate between surfaces at short distances of operation. Examples of these energies include the Born repulsion and structural energies. These energies are usually small in magnitude compared to the London-van der Waals and electrical double layer energies. Effects of these energies are usually considered important when anomalies occur in the expected property of colloidal suspensions. Failure of the DLVO theory to explain the reversibility of flocculation discussed before is one such example. These energies are briefly discussed in the following paragraphs.

Born repulsive energy arises from the overlapping of electron shells as atoms come close to each other. The realistic way of determination of Born energy involves the Hamaker type summation of individual effects from all molecules. Ruckenstein and Prieve (1976) were the first to take Born repulsion into account in order to determine the rate of adsorption/desorption.

Structural energy is the collective name given to describe the energy arising from the adsorption of solvent, surfactant and macromolecules. There are basically three energies.

- Repulsive hydration energy which is discussed in some detail by Hunter (1989). He argued that at close distances the van der Waals attraction should pull surfaces together, however, at KCl concentrations higher than about 10^{-4} mol dm^{-3} there arises short-range repulsive energy that is stronger than the attractive energy. This repulsion has been shown to be due to the hydration of adsorbed K^+. Because of the short-range nature of this energy it does not affect the double layer interaction, except when the surfaces are in close proximity (< 5 nm). At high KCl concentrations, e.g. 1 mol dm^{-3}, where the double layer becomes compact the

hydration energy should dominate the interaction energy.

- Attractive hydrophobic energy which was studied in detail by Israelachvili and Pashley (1982). They measured the interaction energies between two hydrophobic surfaces in aqueous solutions. They found that the attractive component of this energy exceeded the amount predicted by the DLVO theory. By subtracting the excess attractive energy from that predicted by the DLVO theory they arrived at a value which they attributed to the hydrophobic attraction. The hydrophobic attraction arises from interaction between organic nonpolar molecules, such as hydrocarbons, in water.
- Repulsive steric energy arises from the interaction of nonionic polymers adsorbed or attached onto the surface of colloidal particles.

The theoretical section of the present thesis assumes that the major energies contributing to the total interaction energy between the collector and particle are the electrical double layer and the van der Waals energies. In Chapter 6 the results of deposition experiments onto RVC collector are presented followed by Chapter 7 wherein a theoretical modelling of these experiments is undertaken using trajectory analysis. Any observed discrepancies between the experimental and theoretical results are discussed in Chapter 7 and it is believed that the Born and hydration repulsive energies may contribute to anomalies in the expected deposition behaviour.

2.3 EXPERIMENTAL TECHNIQUES FOR DEPOSITION STUDIES

The importance of the fundamental principles of adsorption and their potential applications in industry has been introduced in Chapter 1. It would be of great value if a theoretical

framework could be constructed that was capable of predicting the behaviour of adsorption processes encountered in real life. However, the great number of factors involved give rise to discrepancies between 'theoretical' and 'real' deposition studies. Hence there is a need to improve the theoretical principles and to achieve this ideal systems have to be utilised. Conventional adsorption theories that are available apply to ideal colloids which are generally defined as monodispersed uniform spherical particles of narrow size distribution.

Similarly collectors used in the present study are those which offer characteristics such as particle-collector energy of interaction and hydrodynamics that can be described within existing theoretical frameworks. Therefore collectors with either flat or curved geometries are favoured. In this section packed bed techniques utilising spherical collector and fibre filters with their unique hydrodynamic properties are discussed.

2.3.1 Packed bed

The planar-geometry collector used in techniques such as rotating disc (Marshall & Kitchener (1966)), stagnation point flow (van de Ven & Dabros (1983)) and parallel plate channel (Bowen & Epstein (1979)) have allowed important developments of theoretical and practical deposition studies. However, for many technological applications (e.g. the deep bed filtration of waste waters) the packed bed technique is used and therefore, a number of relevant studies have been reported in this area. Ives (1960) carried out a macroscopic examination of the problem involving solution of the conservation equation. Deep bed filtration studies using spherical collectors can be divided into two classes:

1) Deposition studies of non-Brownian particles, usually having diameters greater than 1 μm,

with different modes of double layer interaction between particle and collector.

2) Deposition studies of sub-micrometer (Brownian) particles with different modes of double layer interaction between particle and collector.

Theoretical investigation of deposition of non-Brownian particles on spherical collectors was facilitated by the introduction of the trajectory concept by Yao (1968) which had been adopted primarily in aerosol deposition. The trajectory analysis in essence involves carrying out force and torque balances on the particle approaching the collector.

Rajagopalan and Tien (1976) argue that, trajectory analysis of deposition of non-Brownian particles involves two steps:

1) Selection of an appropriate porous media model to describe the hydrodynamics of the packed bed.

2) Selection of a suitable technique capable of describing the retention of particles within the bed and the resulting change of structure of the filter media.

The requirement of the second step is fulfilled by the trajectory concept and for the first step there are several models put forward such as spherical, capillaric and constricted tube models depending on the geometry of the pores between solid particles. They considered the deposition to occur by the four main mechanisms of diffusion, interception, gravitional and collection due to surface forces. They used Happel's (1958) sphere in cell model as shown in Figure 2.5 to describe the flow fields. The limiting trajectory separating the trajectory for collection from that of non-collection was obtained by integrating the trajectory equation. The

trajectory equation in turn was obtained by writing a force balance on the suspended particle.

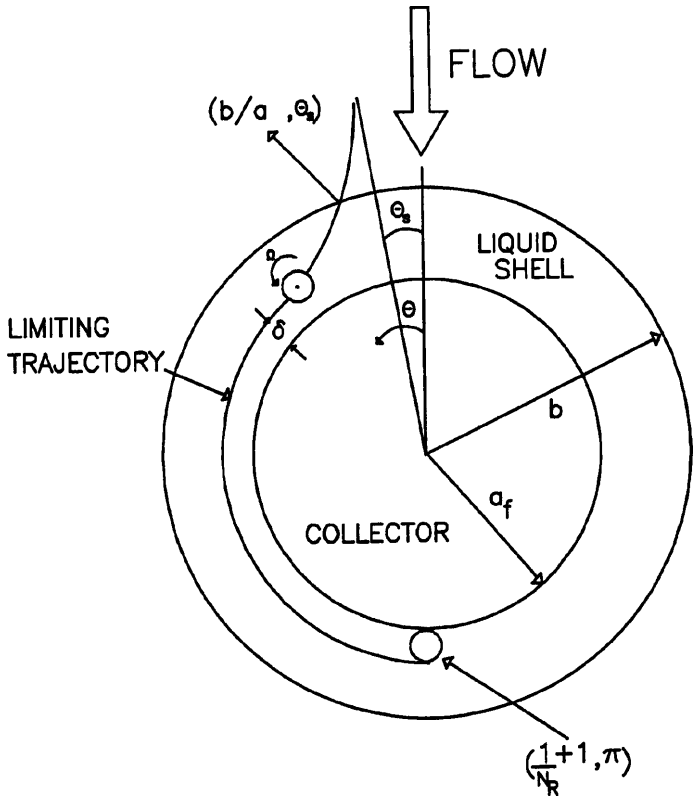

Figure 2.5 Happel's sphere-in-cell porous media model (a_f) collector radius (b) liquid envelop radius (θ) angular coordinate (Ω) angular velocity (δ) distance between surfaces (N_R) a/a_f

At equilibrium the appropriate force and torque balances are written:

$$F_{Gr} + F_{LO} + F_{EDL} + F_D + F_I = 0$$
$$t_{Gr} + t_{LO} + t_{EDL} + t_D + t_I = 0 \qquad (2.18)$$

where F and t are forces and torques acting on the particle and the subscripts Gr, LO, EDL, I and D represent gravity, London, electric double layer, inertia and drag respectively.

The resulting expressions for the radial, r, and azimuthal, θ, velocities are written:

$$u_r^* = \frac{1}{U}\frac{dr}{dt} = \frac{1}{f_r^t}\Big([\, -A^+ (1 + \delta^+)^2 f_r^m N_G \cos\theta \,] + N_{E1} [\, N_{E2} - e^{-N_{DL}\delta^+} \,] [\, e^{-N_{DL}\delta^+} / (1 - e^{-2N_{DL}\delta^+}) \,] - [\, N_{LO}\, RET (\delta^+; N_{Rid}) / (\delta^{+2}) (2+\delta^+)^2 \,] \Big) \qquad (2.19)$$

$$u_\theta^* = \frac{r}{U}\frac{d\theta}{dt} = \frac{1}{s_1}\left[B^+ s_2 + D^+(1+\delta^+) s_3 + N_G \sin\theta \right] \qquad (2.20)$$

The symbols are defined in the nomenclature. The trajectory equation is obtained by eliminating the time derivative between equations (2.19) and (2.20).

Rajagopalan and Tien (1976) solved the resulting differential equation by using a Runge-Kutta method with the initial condition r_0^* defined as:

$$r_0^* = \left[\frac{1}{N_R} + 1 \, , \, \pi \right] \qquad (2.21)$$

which describes the position at the rear of the collector.

The filter coefficient, λ, which is commonly used to present the filtration data was defined by Ives (1960) as:

$$\lambda = - (1/C) \frac{\delta C}{\delta l} \qquad (2.22)$$

Where C is the particle concentration of suspension and l the axial distance in filter. If deposition is assumed to be uniform anywhere in the bed then each elemental slice of the bed is supposed to behave similarly and the filter coefficient is a constant.

From the above relationship Rajagopalan and Tien (1976) arrived at the following expressions

for the initial filter coefficient (λ_o):

$$\lambda_o = - \frac{3\,(1-\beta)}{2\,d_c} \ln\,(1-\eta_o) \qquad (2.23)$$

Where β is the bed porosity and η_o is defined as the initial collection efficiency.

From their simulations these authors were able to derive an approximate closed form expression for the initial collection efficiency:

$$\eta \approx 0.72\,A_s\,N_{LO}^{1/8}\,N_R^{15/8} + 2.4x10^{-3}\,A_s\,N_G^{1.2}\,N_R^{-0.4} + 4\,A_s^{1/3}\,N_{Pe}^{-2/3}\;;\; N_R<0.18 \qquad (2.24)$$

This relationship essentially estimates the amount of deposition occurring on a unit collector arising solely from physical forces. The contributions arising from surface chemistry are discussed below. The terms in equation (2.24) are defined in Table 2.4. Where N_R accounts for deposition of particles by interception. N_G is a dimensionless parameter giving the ratio of particle deposition due to gravity to that due to transport by fluid flow. N_{LO} is a dimensionless parameter giving a ratio for deposition due to London-van der Waals forces to that due to Stoke's flow. N_{Pe} is a dimensionless providing a ratio for deposition due

Table 2.4 Definition of terms used in equation (2.24)

PARAMETER	DEFINITION
N_R	a / a_f
N_G	$[\,2\,(\rho_p - \rho_f)\,g\,a^2\,] / [\,9\,\mu\,U\,]$
N_{LO}	$A / [\,9\,\pi\,\mu\,a^2\,U\,]$
N_{Pe}	$[\,12\,\pi\,\mu\,d_c\,d_p\,U\,] / k\,T$
A_s	$[\,2\,(1 - p^5)\,] / [\,2 - 3p + 3p^5 - 2p^6]$
p	$(1 - \beta)^{1/3}$

to transport by convection to that due to diffusion. A_s is porosity dependent parameter used in equation (2.24). Rajagopalan and Tien (1976) compared results obtained using equation (2.24) with the experimental data obtained by Fitzpatrick (1972), as shown in Figure 2.6, and concluded that equation (2.24) is a sufficiently accurate approximate solution to the trajectory analysis.

Tobiason and O'Melia (1988) utilised the approach used by Rajagopalan and Tien (1976) to include the effects of surface chemistry on the rate of deposition. They argued that surface chemistry as determined by such parameters as pH and ionic strength of the electrolyte solution plays an important role in occurrence of favourable,

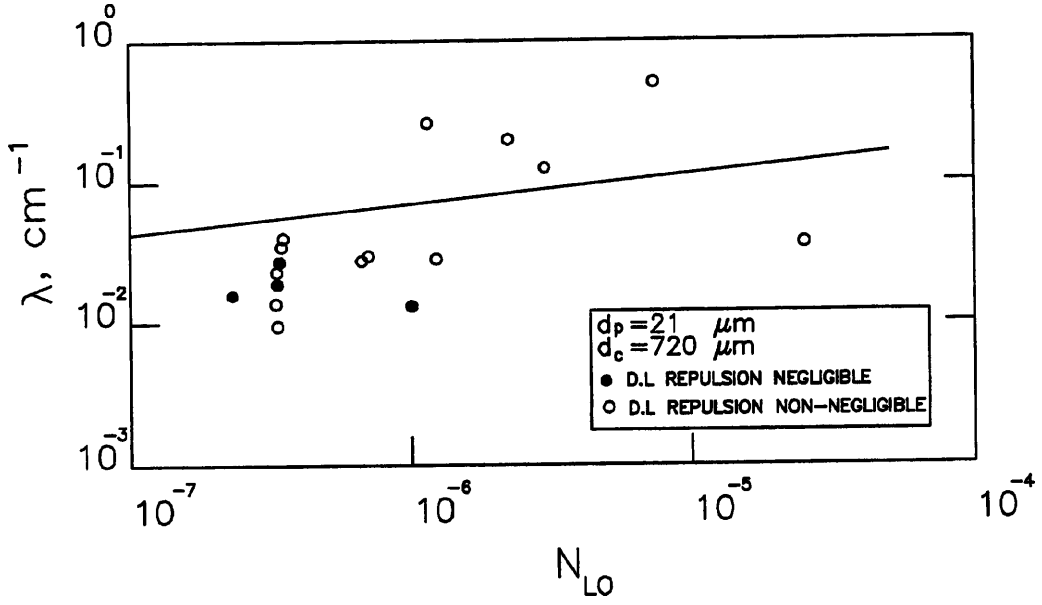

Figure 2.6 Comparison of simulation results with experimental data obtained by Fitzpatrick (1972) for deposition of latex particles on to glass beads

referring to the situation when electrostatic barrier does not exit, as against the unfavourable situation when there is an electrostatic barrier present. To include chemical effects on the

deposition rates, use was made of γ, the collision efficiency factor as defined by Gregory (1980):

$$\gamma = \frac{\eta_R}{\eta} \tag{2.25}$$

Where η_R is defined as single collector efficiency and η is the collector efficiency calculated from theories that only include physical effects on deposition.

Therefore γ will have a value of 1 under favourable conditions. Applying a mass balance over an incremental depth of the bed, and then integrating over the entire bed, an expression for the fraction of the particles remaining in the filtrate was obtained by Yao(1968)):

$$\frac{C}{C_O} = \exp\left[- \frac{3\,(1-\beta)}{2\,d_c}\,\gamma\,\eta\,L \right] \tag{2.26}$$

Where C and C_0 are the effluent and influent concentrations, β is the bed porosity, d_c is collector diameter and L is total bed length.

Tobiason and O'Melia (1988) concluded :

1) For favourable chemical conditions (i.e. no electrical double layer repulsive energy) the models based on the fundamental physical theories can quantitatively describe the deposition process.

2) Theories available for deposition can describe the onset of an unfavourable condition (i.e. repulsive electrical double layer energy present), however, these models greatly underestimate particle deposition for unfavourable conditions.

2.3.2 Fibre bed

Studies using fibres as collectors have received some attention due to potential application to such industries as papermaking where optimum retention of a variety of wet-end additives on

pulp fibres is desirable. In addition in gas-solid systems, aerosol and clean-room technology have utilised sophisticated fibre filters. Despite the growing practical interest in fibrous filters the majority of studies in the literature are concerned with deep bed filtration in granular beds. The literature for fibrous filters lacks information in both theoretical and experimental aspects. Lack of information in theories for filtration through fibrous bed arises from complex fibre mat geometries with complex hydrodynamical behaviour resulting in adsorption study in such media complicated. Two experimental studies into use of fibres as collector will be briefly discussed.

Alince et al. (1978) utilised two cationic latexes, polystyrene (PS) and polystyrene butadiene (PSPB) and carried out deposition experiments on to anionic pulp fibres and observed that the behaviour of PS and PSPB latexes differ due to a combined effect of latex stability, separation distance of deposited latexes and fluid shear. They stated that the PS particles deposited as individual particles and PSPB particles appeared to deposit as doublets.

In one of several studies carried out by Tamai et al. (1982), deposition of PMMA latex particles on fabrics such as polyamide Nylon 6, polyester Tetoron, polyacrylonitrile Vonnel and cotton were investigated. The amount of latex on fibre was measured using a weighing method. Two grammes of fabric was weighed and immersed in 50 cm^3 of latex solution (4 x 10^{-2} g dm^{-3} solid content). The amount of latex deposition was determined from the dry weight of 25 cm^3 of latex dispersion before and after immersion. The effect of pH on the rate of deposition was investigated and correlated against zeta potential measurements of the fibres and particles. The point of zero charge (PZC) of each material determined and upon application of heterocoagulation theory the interaction energies were determined. It was

observed that the rate of deposition increased with increasing pH and the maximum occurred in the vicinity of the isoelectric points of the particles as shown in Figure 2.7. The rate constants in the plot have been obtained by assuming that the deposition follows first order kinematic with respect to the particle concentration.

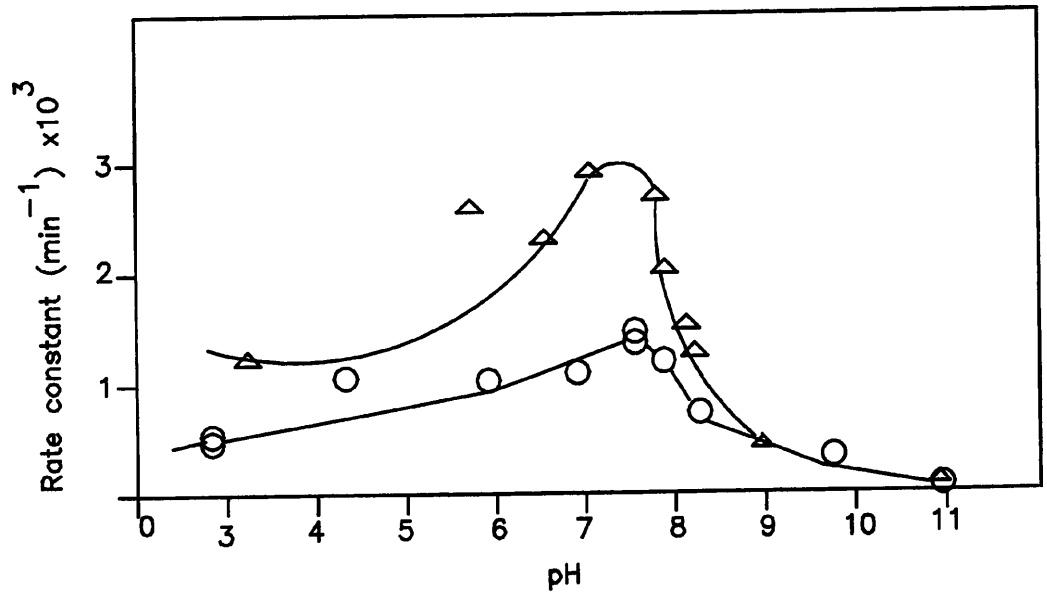

Figure 2.7 Variation of deposition rate constant of latex with pH at 0.001 M electrolyte concentration (○) Nylon (△) Tetoron fabrics (after Tamai et al. (1982))

As described in Chapter 1, in the present research thesis deposition experiments have been carried out onto different collectors. An attempt is made to theoretically investigate these experiments. For adsorption experiments onto spherical glass bead collector, use is made of equation (2.24) to analyse the results (see Chapter 5).

Over the last decade there has been continued development in employing more elaborate modelling techniques to colloidal dispersions. Elimelech et al. (1995) discuss the most recent developments in utilising Eulerian and Lagrangian techniques for deposition studies. Such

techniques as the Monte Carlo, Molecular Dynamic and Brownian Dynamics are discussed by Elimelech et al. (1995) and guidelines are provided for implementation of these techniques.

Table 2.5 Principal theoretical studies of deposition on to cylindrical collectors

AUTHOR	FLOW MODEL	FORCES CONSIDERED	REMARK
Natanson (1957)	Lamb's distribution (1932)	convective diffusion equation	collection efficiency correlated
Stechkina et al. (1968)	Kuwabara model (1959)	interception and Brownian diffusion	parallel cylinders considered
Spielman et al. (1968)	Brinkman model (1947) and Lamb's distribution (1932)	interception and Brownian diffusion	different fibre mat geometries considered
Spielman et al. (1970)	Lamb's distribution (1932), Happel (1959) and Kuwabara (1959)	electrostatic, drag and gravity	trajectory analysis employed
Adamczyk et al. (1981)	Lamb distribution (1932)	convective diffusion equation	dimensionless mass transfer number predicted for a single cylinder and a fibre mat
Choo et al. (1991)	Happel (1959), Kuwabara (1959), swarm theory	drag, electrostatic, gravity	trajectory analysis employed

The discrepancies observed between the reported experimental results and theory particularly under the unfavourable deposition conditions are discussed in detail. Of direct relevance to the present study is the discussion of trajectory analysis by Elimelech et al. (1995). This analysis is used to simulate the experimental results in Chapter 7.

For the case of adsorption onto RVC collector a theoretical study based on the trajectory analysis for non-Brownian particles onto cylindrical collectors developed by Spielman (1968), (see Table 2.5) will be utilised. Certainly, several important underlying assumptions are necessary prior to adopting this model to the RVC electrochemical adsorption cell. These assumptions as well as the equations will be elaborated in detail in Chapter 7. Table 2.5 shows theoretical studies located in the literature for deposition onto fibre (cylindrical) collectors.

2.4 ELECTROCHEMICAL CONCEPTS

The RVC flow-through electrode system in the present study bears a resemblance to an electrochemical reactor, with the exception that there is no reaction taking place. Therefore, to have a better understanding of the behaviour of the present RVC electrochemical adsorption cell some electrochemical concepts relevant to the present cell are introduced in this section.

A simple electrochemical cell as shown in Figure 2.8 consists of a working electrode where the electrochemical reaction is taking place. In order to measure the changes taking place at the working electrode a reference electrode is used through which no current flows. This zero current condition ensures that the potential difference across the reference electrode-solution interface remains constant. The third electrode, the counter electrode, completes the circuit in the cell and the current that passes through the working electrode passes through the counter electrode.

Within the cell these electrodes must be arranged symmetrically to minimise the potential gradients at the working electrode arising from ohmic drops through variation in the electrolytic path between the working and counter electrode. Furthermore the working

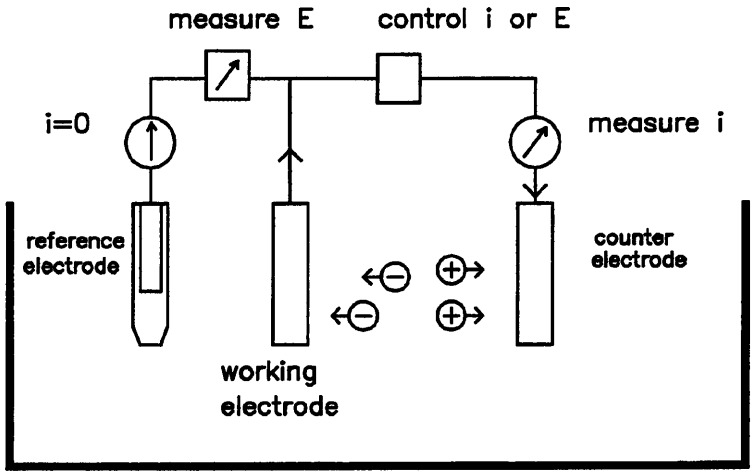

Figure 2.8 A simple electrochemical cell

electrode potential is known to depend on the placement of both the reference and counter electrodes.

The potential of an electrode can only be measured with respect to another electrode, since voltmeters only measure potential differences between two positions. The absence of a reliable zero potential electrode makes it impossible to determine the absolute electrode potential. It is, however, possible to choose an electrode and to consider it as the zero level of the potential, even if that electrode has an absolute unknown potential. The conventional zero electrode is the standard hydrogen electrode (SHE).

$$SHE = 0\ V \text{ (by convention)}$$

Reference electrodes are electrodes that provide a stable and reproducible potential against the SHE and they are convenient to use. Reference electrodes can thus be used to measure the potential of the working electrodes. One of the most common reference electrodes in the laboratory and in industry is the Saturated Calomel Electrode (SCE). The potential of the SCE

depends on the anion chloride concentration. A platinum wire is immersed in the liquid mercury covered by mixture of Hg and Hg_2Cl_2 , called calomel, on top of the calomel is a KCl solution. The Saturated Calomel Electrode uses a saturated KCl solution because it provides a more stable potential and the presence of KCl crystals makes it easy to verify the saturation of the solution.

A problem encountered with using reference electrodes such as the SCE is the liquid junction potential developed at the interface between the reference electrode electrolyte and the electrolyte in which the working electrode is immersed and this potential introduces an error into the working electrode potential measurement. One way of avoiding this problem is to use the same electrolyte such as KCl for the reference and the cell electrolytes.

Another problem is the ohmic drop due to the resistance offered by the electrolyte to the passage of electricity. The value of the ohmic drop depends on the position of the reference electrode in the cell and to overcome this problem condition has to be sought that renders ohmic drop towards zero.

One way of overcoming the contribution of ohmic drop is to use a luggin probe. This technique consists of putting a glass tube between the reference electrode and the working electrode as shown in Figure 2.9. The upper part of the tube is large allowing the reference electrode to be immersed and the lower part is elongated to form a capillary near the working electrode. The capillary minimises the screen effect on the working electrode. The luggin probe is filled with electrolyte and the current that passes through the electrolyte can not enter the luggin probe since there is no exit for the current.

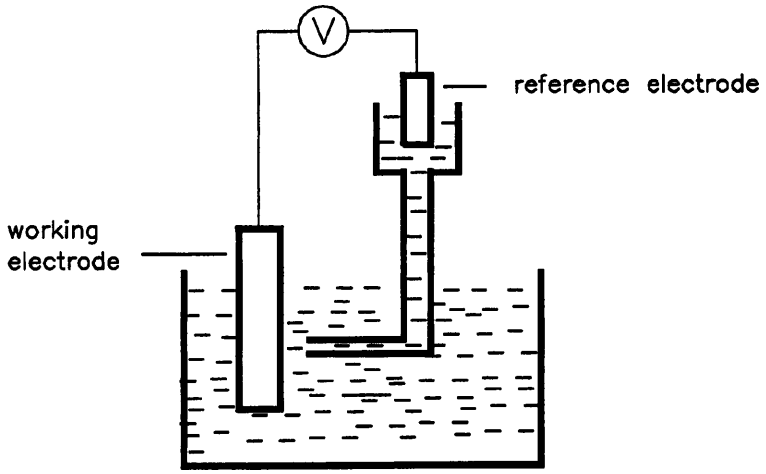

Figure 2.9 The luggin capillary technique

The ohmic drop can be approximately measured in the laboratory with a high impedance digital voltmeter using the current interruption technique. This technique depends on the fact that the ohmic drop disappears immediately when the current is cut off. A known potential difference (vs SCE) is applied between the working and the counter electrodes and when a steady current flow is established the current is interrupted. The value of the working electrode at the instant of the current interruption can be measured using a high impedance voltmeter. Figure 2.10 shows the plot of working electrode potential against time before and after current interruption. Line A to B represents a steady current flow through the working electrode whence the current is interrupted at point C. The potential difference between points B and C represents the ohmic drop. The potential at point D achieved after long time is commonly referred to as the rest potential which is defined as the potential of the electrode under the no current condition.

When current flows through a dilute aqueous electrolyte in an electrochemical cell electrolysis of the electrolyte occurs. Electrolysis of the electrolyte is accompanied in the cathodic direction by the reduction of H^+ and in the anodic direction by the oxidation of water

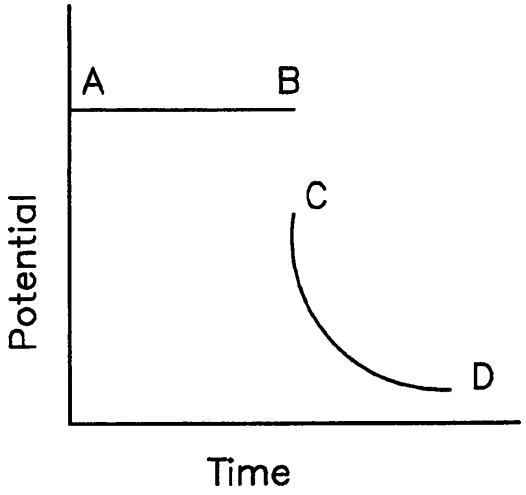

Figure 2.10 Graph of potential vs time

according to the following schemes:

$$4H^+ + 4e \rightarrow 2H_2\uparrow \qquad (2.27)$$

$$2H_2O \rightarrow 4H^+ + 4e + O_2\uparrow \qquad (2.28)$$

It is therefore important to determine the minimum potential that need to be applied to set the above reactions going.

2.5 ELECTROCHEMICAL ADSORPTION CELL

Electrochemical cells utilising RVC type packings may provide some information for the design of the present RVC adsorption column. Therefore, this section reviews some particle adsorption studies using *electronically conducting material* as the filter media and the use of *externally-controlled electrode potential.*

When the direction of current and solution flow are parallel to each other (flow-by arrangement), the thickness of the porous electrode is limited by the ohmic drop

considerations and as a result it is difficult to obtain a uniform potential distribution as well as a high reactant conversion. Consequently the flow-through arrangements where the current flow is perpendicular to the solution flow is mostly favoured. Potential variations can be minimised by having the electrode thin in the direction of current flow and for high reactant conversion a long electrode in the direction of solution flow should be used. From the above argument a flow-through arrangement has been chosen for the electrochemical adsorption cell to be used in this study.

There has been a great deal of attention paid to electrically conducting materials (usually carbon or graphite based) for use as adsorption media. These studies may be divided into two categories according to the method of application of external electrical potential:

method 1) Those in which the fibre bed is allowed to be polarised between two electrodes.

method 2) Those where the fibre bed is used as the working electrode.

Tables 2.6 and 2.7 show some of most important studies found in the literature with the use of fibres as in method 1 and 2 respectively.

Table 2.6 Previous adsorption studies using an external electric field (method 1)

Author	Particle type	Collector	Remark	Electrolyte	Particle conc.
Zebel(1965)	aerosol particles from air stream	cylindrical fibre	theoretical investigation	air	-
Judd et al. (1989)	polystyrene latex 0.432,1.13 and 2.09 μm diameter	ion exchange fibre (Actilex) 25.8 μm diameter	429-4290 V m^{-1} electric field strength	2 x 10^{-4} mol dm^{-3} trishydro xymethyl methyl amine and 10^{-4} M HCl	0.018-3.0 x 10^{14} particles per cm^3
Judd et al. (1994)	polystyrene latex 1 μm diameter	Rayon, Cotton, Nylon and Actilex 25-30 μm diameter	experimental and theoretical	same as above	40 g m^{-3}

Of particular relevance to the present thesis is Table 2.7 which provides the most up to date summary of achievements in this area of research. In this section several important studies mentioned in Table 2.7 will be elaborated.

Table 2.7 Major previous investigation of adsorption using flow-through electrodes (method 2)

Author	Particle type & diameter	Collector	Remark	Electrolyte	Particle conc.
Tobias et al. (1983)	*E.coli* Bacteria	porous carbon bed	180-1100 mV	0.01 mol dm^{-3} NaCl at 0.03 cm^3 s^{-1} flow rate	2 x 10^7 particles per cm^3
Soffer et al. (1987)	alumina particles 0.1 μm	graphite felt 8-10 μm diameter	-200 to 550 mV vs SCE	0.05 mol dm^{-3} buffered $NaNO_3$ at 0.5 cm^3 s^{-1}	10 mg per dm^3
Oren et al. (1983)	Mercury ions	graphite felt 9 μm diameter	flow-by or flow-through	0.5 mol dm^{-3} NaCl at velocity of 0.03-0.45 cm s^{-1}	30 ppm Hg^{2+}
Tobias et al. (1987)	alumina 0.5-0.6μm	carbon felt 8-10 μm diameter	18-50 volts and 15 mA current	water at 0.17-0.5 cm^3 s^{-1}	6 ppm
Oren et al. (1987)	latex 0.15 μm	graphite felt 10 μm diameter	-500 and +500 mV	0.1-0.001 mol dm^{-3} NaCl at 0.27-1.27 cm^3 s^{-1}	
Albery et al. (1990)	carbon black 0.23 μm	microscope slide in impinging cell	deposition into secondary minimum -1.0-1.0 V applied	$NaClO_4$ at rate of 0.062 cm^3 s^{-1}	6 x 10^8 particles per cm^3
Jia et al. (1990)	alumina and titania mixture	pt/platinum oxide	theoretical study into feasibility of selective separation	KCl	
Joscelyne (1993)	polystyrene latex 0.243 μm diameter	graphite fibre 9 μm diameter	pH=4.8, potential of -200 to +1100 mV	$NaClO_4$ at flow rate 0.0.004-0.0.005 cm^3 s^{-1}	2.8 x 10^8 to 2.8 x 10^9 particles per cm^3

Oren et al. (1987) studied the electrically induced adsorption of colloidal particles from aqueous suspension onto a carbon electrode. They varied the electrode potential in a wide

range to allow study of colloidal adsorption under the condition of double layer charging and the condition when water electrolysis occurring. They proposed a scheme for the redox reactions occurring when the carbon electrodes were charged to the proper potential range. They argued that due to the high surface area of electrodes these reactions can change the pH of the bulk suspension and this in turn changes the surface charge of colloidal particles and consequently the adsorption rates change. They observed that at the potential range where the charging of the double layer was the main process taking place, no effect of potential variations on the extent of adsorption was observed and this contradicts the results obtained by other workers (Hull & Kitchener (1969), Tamai (1982)) where electrostatic repulsive or attractive energies (between similar or oppositely charged surfaces respectively) were clearly

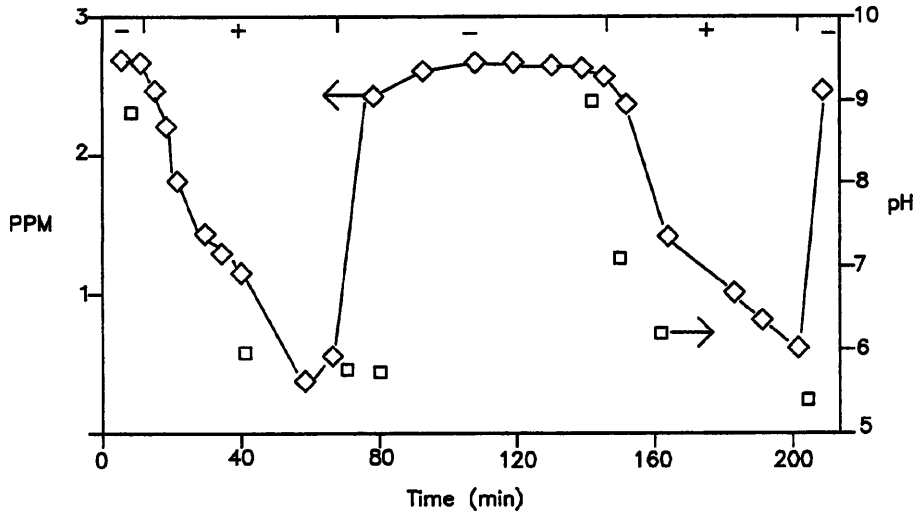

Figure 2.11 Variation of colloid pH (□) and concentration (◇) with time for deposition of latex particles onto graphite felt

found to govern colloidal adsorption. Consequently they studied the adsorption of colloidal particles as a result of electrochemically induced pH variations (see Figure 2.11) and observed that when potential was 500 mV, pH decreased followed by a decrease of colloidal concentrations whereby the potential was changed to -500 mV and consequently the pH and

the particle concentration increased. They concluded that in cases where the colloid was not so highly charged with respect to the electrode, adsorption and desorption could be induced by mutual interaction of the two double layers rather than by pH variation.

Albery et al. (1990) carried out deposition experiments using an impinging jet type apparatus as shown in Figure 2.12. The substrate was a microscope slide coated with tin-doped indium

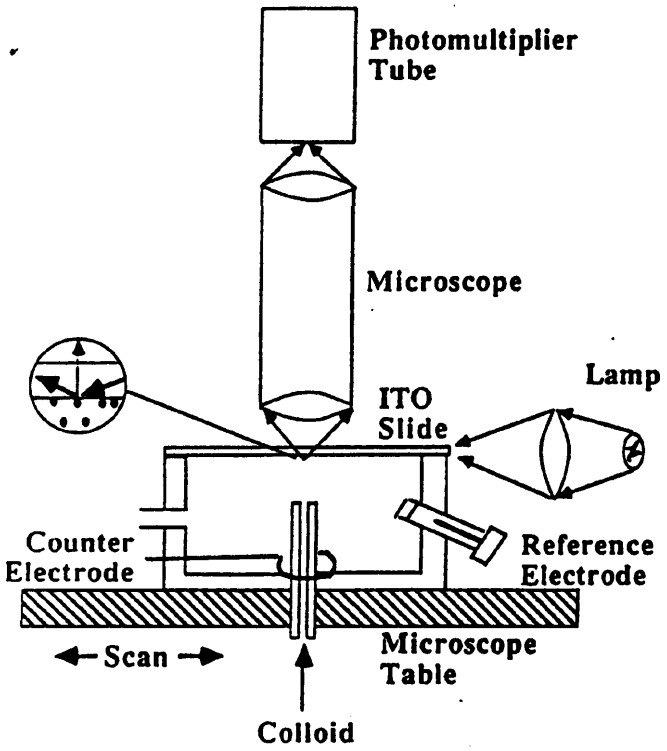

Figure 2.12 schematic diagram of the impinging jet cell used by Albery et al. (1990)

oxide. Connection between potentiostat and the slide was made via a copper wire attached to the electrode surface with silver loaded epoxy resin. Colloidal suspensions of carbon black particles, having a mean radius of 0.23 μm and concentrations in the range of 6×10^8 particles cm^{-3}, were used. The counter electrode was a ring of platinum wire circling the jet at the bottom of the cell.

The rate of deposition was obtained from the intensity of the light from the evanescent wave

scattered by deposited particles. They concluded that for potentials more positive than -400

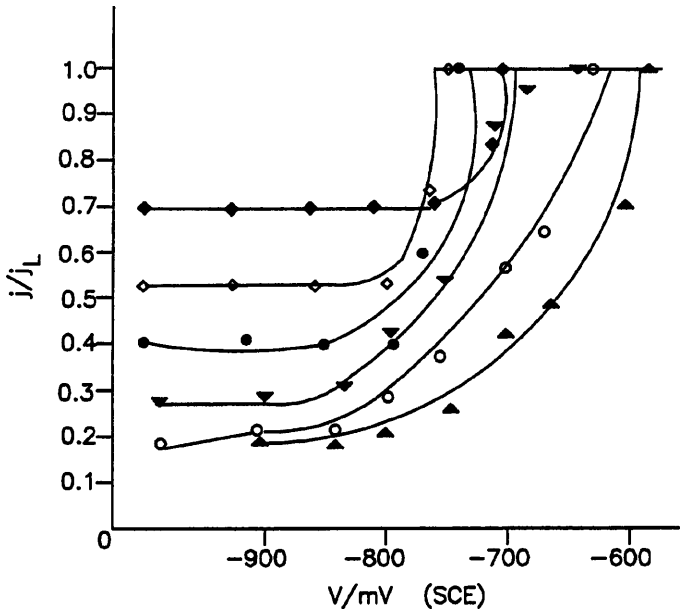

Figure 2.13 Variation of the apparent flux ratio with the electrode potential, for deposition of carbon black particles onto an indium tin oxide electrode, for various ionic strengths (mmol dm^{-3}) as follows:(▲) 0, 0.5; (O), (▼)1.0; (●), (◊)2.0; (♦) 5.0

mV vs SCE there were no barrier against deposition into primary minimum and at these potentials deposition was always mass transfer controlled.

Figure 2.13 shows a typical experimental result obtained, expressed as the ratio of apparent flux j to the limiting flux j_l found at positive potentials.

For more negative potentials different results were obtained ranging from no deposition for some surfaces to mass transfer controlled deposition for others and they explained these results by proposing that particles were held in secondary minimum. The lower the electrolyte concentration, the further was the secondary minimum from the electrode surface and the lower was the intensity of evanescent wave.

Jia and Williams (1990) carried out a theoretical investigation into the feasibility of separating a mixed species suspension of titania and alumina. They considered such parameters as the Hamaker constant, particle diameter, particle surface potential, collector surface potential and electrolyte concentration. They simulated the effect of above parameters on the interaction energy profile, depth of secondary minimum and the height of energy barrier. This demonstrated that:

- The secondary minimum does not seem suitable for separating the above mixture.
- For the range of parameters considered, use of primary minimum along with the energy barrier seems a more suitable route for the separation.
- In a mixed suspension the actual surface charge of each particle is affected by the adsorption of soluble species originating from the other solid.

These findings, notably the first, contradict the work by Albery et al. (1990) where it was proposed that particles were held in the secondary minimum for a set of experimental conditions.

The theoretical study of Jia and Williams (1990) demonstrated that for the set of parameters considered the prerequisite of the presence of high energy barrier along with a deep secondary minimum for appreciable deposition could not be obtained. However, Albery et al. (1990) stated that the experimental data of deposition into the secondary minimum were not reproducible owing to surface heterogeneity (roughness).

Recently Joscelyne (1993) carried out deposition of 0.243 μm and 1.03 μm diameter polystyrene latex particles on to 9 μm diameter graphite fibre in a flow through electrochemical cell as shown in Figure 2.14.

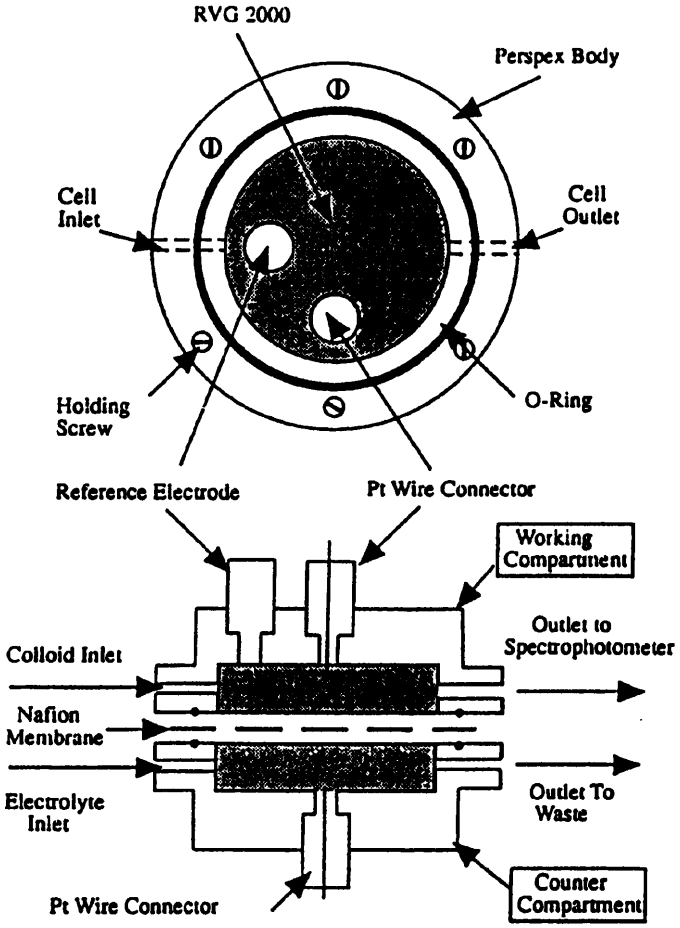

Fig 2.14 Sketch of deposition cell 1 used by Joscelyne (1993)

Two other configurations of the cell were also designed mainly differing in the positioningof the cell outlet and the counter electrode. The counter electrode used was the same graphite fibres for two of the cell configurations. An Ag/AgCl electrode was used as the reference electrode. The electrolyte solution used was sodium perchlorate having its pH adjusted to 4.8 using acetate buffer. The particle number concentration used for the 0.24 μm particles was 2.82×10^9 particles/cm^3 and 7.3×10^7 particles/cm^3 for the 1.03 μm particles. The inlet and outlet suspensions were monitored by UV spectrophotometry. Figure 2.15 shows a typical experimental result.

The principal findings were that at positive potentials (>+900 mV) and/or high electrolyte solution (e.g. 0.1 mol dm^{-3}) high adsorption rates were obtained and the deposited particles were deposited irreversibly into the primary minimum. However, at low and intermediate concentrations, deposition into the secondary minimum occurred for the case when the collector and particle were similarly charged. Deposition into the secondary minimum was justified by arguing that these particles were removed by flowing distilled water through the column. This destroyed the secondary minimum and released the particle back into the solution.

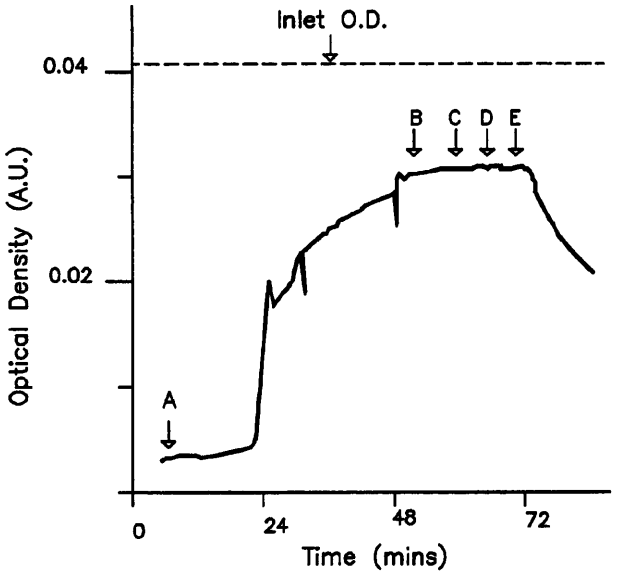

Figure 2.15 Effect of potential on the optical density of outlet for the following experimental conditions: Particle concentration: 2.8 x 10^8 particles cm^{-3}, Flow rate: 0.25 cm^3 min^{-1}, $NaClO_4$ concentration: 0.5 x 10^{-3} mol dm^{-3}, A: colloid in, no potential applied, B: +500 mV, C: +600 mV, D: +700 mV, E:+800 mV
(after Joscelyne (1993))

Additionally Joscelyne carried out experiments to study effect of other important parameters on the release of deposited particles from the secondary minimum namely:

- reversing the electrode potential
- wash-out using doubly-deionised water
- effect of temperature
- effect of aging
- evolution of hydrogen
- saturation of irreversible site

The conclusions drawn from these experiments were:

- reversal of electrode potential did not affect the rate of release of deposited particles.
- flushing the cell with electrolyte followed by doubly-deionised water causes the release of majority of deposited particles.
- as the temperature increased the extent of release decreased.
- as the aging time of deposited particles increased, the extent of release decreased.
- use of evolution of hydrogen gas to knock off deposited particles was not successful.
- after deposition time of 66 hours, release of particles using doubly-deionised water did not improve upon the rate of release for the short deposition times.

Similar to conclusions obtained by Albery et al. (1990) Joscelyne centres his argument around the point that particles can be trapped in the secondary minimum and this contradicts the theoretical results obtained by Jia and Williams (1990). Indeed, there has not been any direct evidence to support loading into the secondary minimum and this still remains the central issue in these deposition studies.

CHAPTER 3

EXPERIMENTAL APPARATUS

This chapter describes the experimental apparatus constructed to allow measurements of the deposition of colloidal particles as a function of an externally applied electrical potential. The packed bed employed is an electrically-conducting packing.

Initially experiments were performed using a conventional spherical bead packed bed to demonstrate the reproducibility of experimental procedures and also to provide guidelines for choosing the scale and geometry of the system for the electronically-conducting bed. As a result there are two main experimental arrangements, namely one for the *spherical collector* system and the other for *Reticulated Vitreous Carbon (RVC) collector* system.

This chapter is divided into four parts. The first describes the spherical collector system. The second part illustrates how the RVC collector system was designed and fabricated including the column dimensions, material of construction etc. A brief introduction to the background of potentiostatic control will be given since this is relevant to the operation of the bed at controlled potential. The third section introduces the theory of light scattering properties of colloidal suspension and its use in the determination of particle number concentration using a commercial turbiditimeter. Finally, the last part describes the measurement of zeta potential. Other data on the physical and surface chemical characteristics of the particulates are given in Chapter 4.

3.1 ADSORPTION COLUMN FOR THE SPHERICAL COLLECTOR SYSTEM

As discussed in section 2.3, theoretical analysis of deposition onto spherical collectors has received great deal of attention due to its application to deep bed filtration of waste waters. Therefore, the experimental set-up for these type of experiments is well documented (see 2.3.1). In this study the adsorption column was made of plexiglass tubing, purchased from AMARI Plastics (Oldham), 200 mm high and having an inside diameter of 22 mm and wall thickness of 3 mm. The inlet and outlet pipes, Perspex tubes of 4 mm inside diameter, were glued onto Perspex flanges 30 mm diameter, of the same thickness as the column, and attached to the column by means of eight plastic screws. A rubber o-ring was placed between the flange and column to prevent any leakages. At a distance of 30 mm from the bottom the column was cut into two pieces and a stainless steel mesh was placed between them. These pieces were then glued together using Perspex adhesive (Tensol). This stainless steel mesh acts as the support for the glass beads. A schematic diagram of the experimental flow circuit and adsorption column is given in Figures 3.1 and 3.2 respectively.

The polystyrene latex feed suspension was delivered using a peristaltic pump built inhouse with a system 101 pump head (R.S components Ltd) having a maximum speed of 8 rpm. The KCl solution was delivered using a Watson-Marlow peristaltic pump model 502 with the maximum speed of 100 rpm. The procedure for carrying out deposition experiments will be discussed in Chapter 4.

Determination of the particle number concentration was achieved by means of a turbiditimeter, discussed in section 3.3. A 250 cm^3 beaker was used as the feed vessel for the polystyrene latex and a 7 dm^3 glass vessel was used as the KCl feed tank. The suspension was

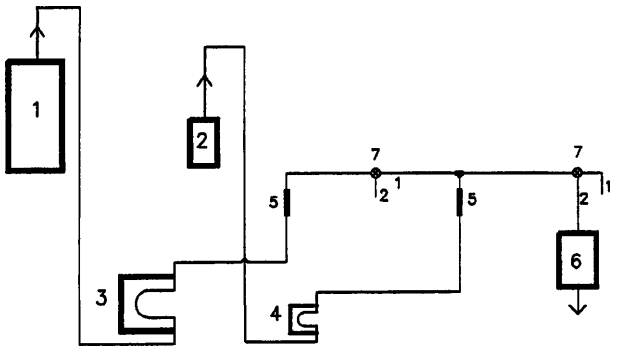

Figure 3.1 Flow diagram for the spherical collector arrangement 1: KCL feed, tank, 2: polystyrene latex feed tank, 3: high output peristaltic pump, 4: low output peristaltic pump, 5: rotameter, 6: adsorption column, 7: two-way valve

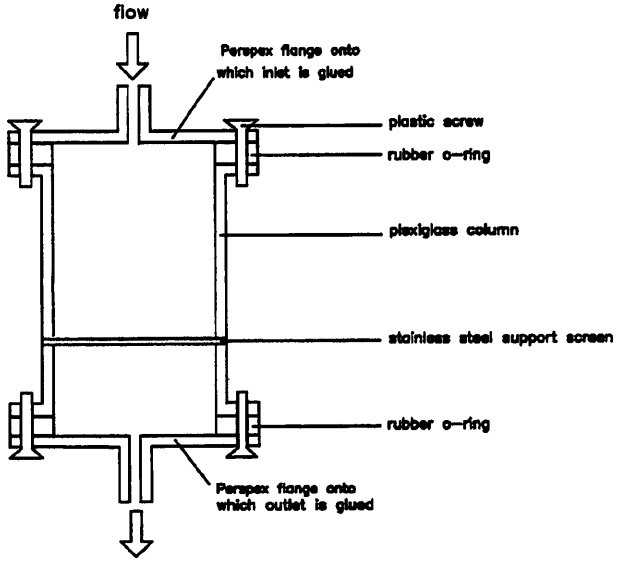

Figure 3.2 Schematic representation of the spherical collector adsorption column

delivered to the column by means of silicon rubber tubing having inside diameter of 4 mm and 2 mm wall thickness. The latex suspension flow rate was monitored using a BOC gas type rotameter which showed a reading fluctuating between 120 $\pm$ 5 for a 1 cm^3 min^{-1} flowrate. KCl solution flow rate was monitored using rotameter tube (Rotameter MFG Co.Ltd, 292303/1004/G1) and its reading fluctuated between 1.5 $\pm$ 0.1 for an output flow rate of 34 cm^3 min^{-1}.

3.2 RVC COLLECTOR SYSTEM

The main objective of this thesis was to investigate deposition under the influence of an externally applied electrical potential. To achieve this, an electronically- conducting bed has to be utilised and, as discussed in section 2.4, there have been several studies carried out using carbon/graphite based fibres as packing. The material used in the research reported here is Reticulated Vitreous Carbon (RVC).

Cowlard and Lewis (1967) state that carbonization of certain cross-linked polymers under carefully controlled conditions yields a non-graphitising carbon which because of its high lustre and conchoidal fracture is called 'vitreous carbon'. They compared some properties of several forms of carbon with vitreous carbon as shown in Table 3.1. It is evident from the table that vitreous carbon is much stronger than any of the other carbon or graphite cited. Its thermal and electrical conductivities are similar to those of baked carbon but they are considerably smaller than graphite. Most forms of carbon are inert to a wide range of chemical reagents but vitreous carbon because of its low permeability, negligible porosity and a low specific surface tends to be even more inert.

Table 3.1 Comparison of some properties of different types of carbon (data from Cowlard and Lewis (1967))

PROPERTY	BAKED CARBON	ELECTRODE GRAPHITE	VITREOUS CARBON
apparent density (kg/m^3)	1570	1550	1470
transverse strength (10^6 kg/m^2)	0.77	0.70	7.0 - 21.1

The RVC used was purchased from Electrosysnthesis (N.Y, U.S.A) and the product specification provided by them is that reproduced in Table 3.2. Figure 3.3 shows the

Table 3.2 Summary of properties of RVC used in this study (data from Electrosynthesis)

BULK VOID VOLUME (%)	BULK DENSITY(kg/m^3)	STRUCTURAL DENSITY (kg/m^3)	STRUCTURAL RESISTIVITY (Ohm m)
97	49.6	1490.0	0.5

scanning electron micrograph of the RVC. It can be seen from this figure that RVC is an open pore material with a honeycomb (foam) structure consisting of hexagonal units providing it with symmetry and rigidity. Each hexagonal unit is made up of rectangular plates approximately 300 μm long and 37 μm wide and with the thickness being negligible in comparison with the length. The RVC structure provides rectangular elements parallel, perpendicular and inclined to the flow path. Thus, when adsorption experiments are carried out the colloidal particles may deposit on these rectangular plates positioned parallel, perpendicular and inclined to the flow path. The manufacturer reported that there are 100 pores per inch of RVC yielding a structure with 97% porosity.

The first part of this section briefly describes the construction of the adsorption column, its dimensions and the RVC slab insert. In the second part a brief summary of theory and

principle of operation of the potentiostat will be presented.

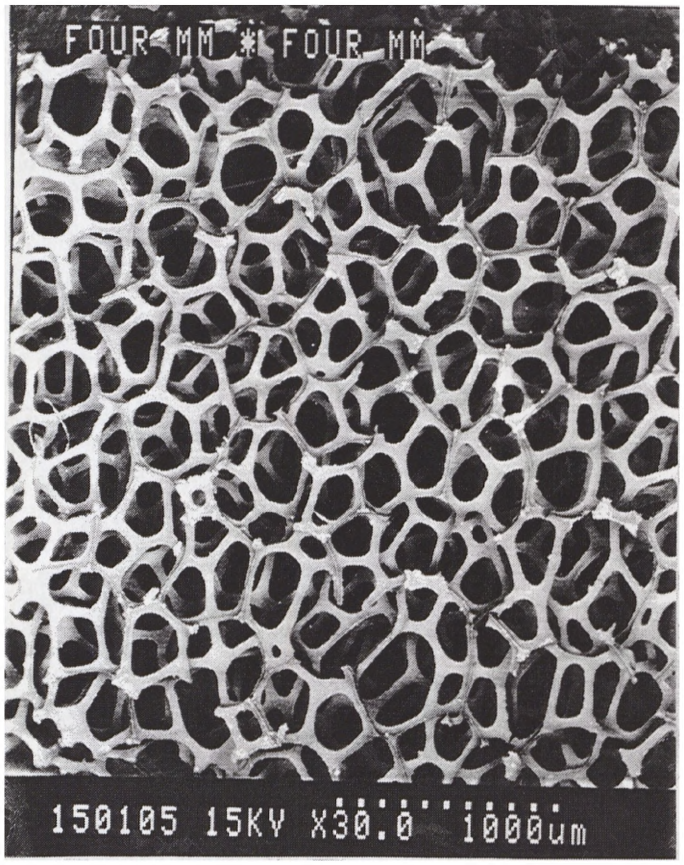

Figure 3.3 Scanning Electron Micrograph of RVC

3.2.1 Adsorption column

The main problems that were encountered in designing the RVC-flow-through- electrode were as follows:

1) Selection of the appropriate dimensions of the RVC slab.

2) Finding a suitable method of attachment of wire to the RVC electrode.

3) Selection and installation of counter electrode.

The above points have been considered individually and are briefly discussed below;

1) Dimensions of RVC slab

In designing the cell it was believed that achieving uniformity of current distribution in the cell was of importance. The only practicable shape which provided symmetry for the flow of current from the RVC electrode to the counter electrode was a rectangle. Hence this formed the basis of the collector geometry as shown in Figures 3.4 and 3.5 in which the current flow was normal to the direction of the fluid flow in the cell.

To decide upon the dimensions of such a system poses a more difficult task since there is no defined design procedure available in the literature to obtain the dimensions. However, use can be made of criteria available for the adsorption of particles onto *model* packings such as glass beads. Hence to *estimate* the length of the RVC slab a semi-empirical relationship developed by Rajagopalan and Tien (1976) was utilised, although it should be noted that this is applicable to the deposition of non-Brownian particles onto *spherical collectors*. Due to its three dimensional porous structure, RVC offers different pathways for the flow of electrolyte. Previous examination of the SEM of RVC (Figure 3.3) showed that each rectangular element in the hexagonal unit is approximately 37 μm wide. For the purpose of providing an estimate of the length of packed bed of RVC it will be assumed that the bed consists of hypothetical spherical collectors of the same diameter as the width of the hexagonal elements within the RVC matrix but having the *same* void volume as that of conventional spherical collector bed. Once this has been used to obtain an approximate value for the length of this hypothetical bed, constraints imposed by the different collector geometry and void volume will be applied to this estimate to deduce a more reasonable approximation.

Using equation 2.24 involving the terms defined in Table 2.4 provides the following values for the relevant parameters:

A_s=37.96 using a value of 0.4 for the porosity

N_{Pe}=3.1x10^{14} using the following values:

d_p=5.4x10^{-6}m, d_c=37x10^{-6}m, U=1.7x10^{-3}m/s, T=298 K,

k=1.3805x10^{-23}J/K, μ= 1 mPa s

N_{Lo}=4.943x10^{-13} using the following values:

A=1.73x10^{-20}J (see Chapter 6 for this estimation)

N_G=4x10^{-9}

substituting these values into equation (2.24) yields:

$$\eta = 0.029 \tag{3.1}$$

For favourable chemical conditions i.e. when there is no repulsive double layer present, the collision efficiency factor (γ) equals to 1 and for complete adsorption of particles C will approach zero. Hence assuming a very small value for (C/C_0) e.g. 1x10^{-9}, equation (2.26) will yield a value of 20.4 mm for the length of the bed. This value is an estimate of the length of a bed containing hypothetical RVC spheres of the same diameters as the width of each rectangular element within the matrix of RVC slab and consequently this value has to be adjusted for different geometry of the RVC pore structure and void volume. By looking at equation (2.26) it can be seen that the length is directly proportional to the collector diameter and indirectly proportional to the voidage. Therefore the following ratio has been applied to the estimated bed length:

$$R=\frac{S_{planar}\ (1-\beta)^{1/3}{}_{spherical}}{S_{spherical}\ (1-\beta)^{1/3}{}_{planar}} \tag{3.2}$$

where S_{planar} is the surface area of each planar element in the matrix of the RVC and, from Figure 3.3, the width of each element equals 37x10^{-6} m and the average length of each

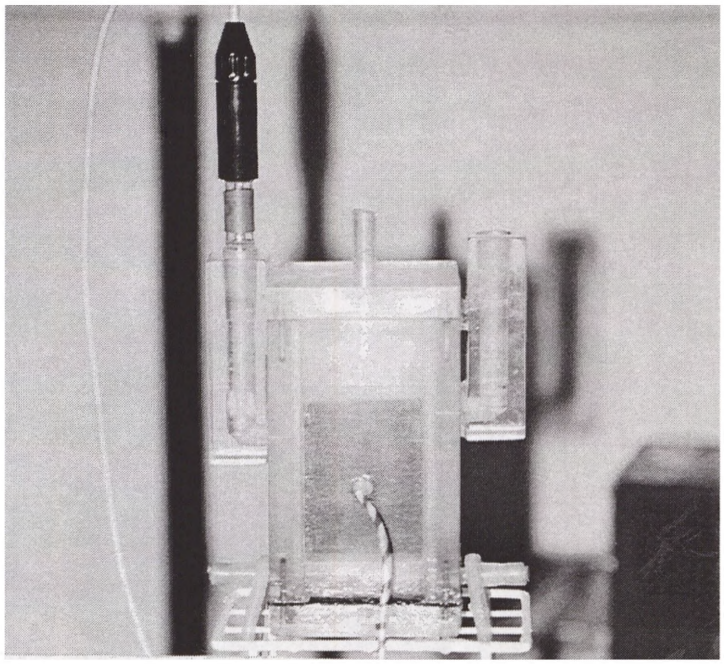

Figure 3.4 Photograph of the RVC electrochemical adsorption cell

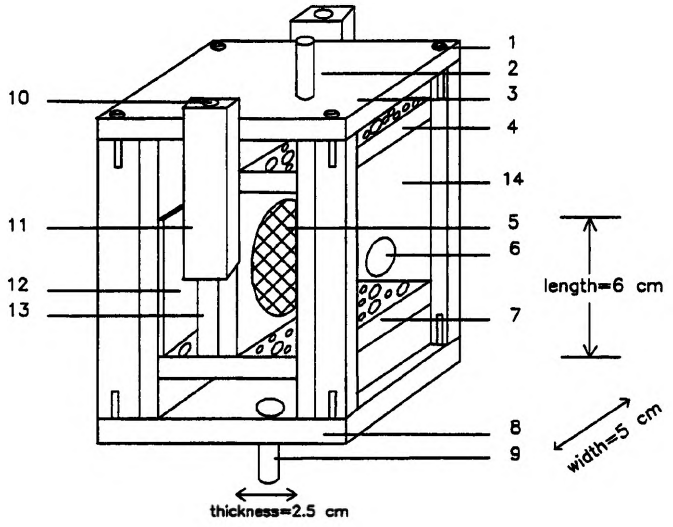

Figure 3.5 Schematic representation of the electrochemical adsorption cell 1: plastic screw, 2: inlet pipe, 3: top Perspex cover, 4: perforated upper plate, 5: membrane, 6: hole for wire connecting RVC to potentiostat, 7: bottom perforated plate, 8: bottom Perspex cover, 9: outlet pipe, 10: hole to allow insertion of reference electrode, 11: 'side arm' for reference electrode, 12: stainless steel counter electrode, 13: Perspex membrane carrier, 14: area for RVC slab

element equals to 300×10^{-6} m, Hence:

$$R = \frac{11100 \times (1-0.4)^{\frac{1}{3}}}{4301 \times (1-0.97)^{\frac{1}{3}}} = 7.0 \qquad (3.3)$$

Consequently a value of 143 mm for the length of RVC slab would seem reasonable.Although the above assumptions are simplistic, in the absence of the alternative correlations the simplistic equations provide us with some logical basis on which to base the design.

Consider next the thickness and the width of the slab. Since the direction of current and fluid flow are perpendicular to each other, electrode size normal to these paths can be adjusted independently. Axial potential variations can be minimised by making the electrode thin in the direction of current flow. Since the stock of RVC available was limited to a thickness of 25 mm, the slab was cut to a thickness of 25 mm and to preserve symmetry it would be ideal to use the same value for the width. From the above argument, one is able to conclude that the appropriate theoretical dimensions for the RVC-flow-through-electrode are 25 x 25 x 143 mm. However, in reality it proved impractical to fabricate such a geometry due to the mechanical frailty of the RVC and the block size. Hence the optimum size adopted, after several fabrication attempts, was adjusted to as shown in Figure 3.5:

length=60.0 mm, thickness=25 mm, width= 50.0 mm

Where the length is taken to be the distance from the top to the bottom of the RVC piece, the width is the size of the side of the RVC piece at which the electrical connection is made (resting against the side 2 wall in Figure 3.6). The collector was housed in a shell made from Perspex acrylic sheet (ICI, ISO 9002-BS5750 part2) of thickness 7 mm for the inside walls (sides 1 & 2 in Figure 3.6) and 10 mm for the outside walls.

The column had to be designed in such a way that removal of the used RVC and mounting of new piece could be carried out with ease. Subsequently, the column was constructed as shown in Figure 3.6 where the four sides were glued together using Perspex cement (Tensol). The stainless steel slab acting as the counter electrode was screwed onto the side facing the RVC electrode. At the end of each experiment the column was dismantled by removing the top and bottom Perspex covers with their associated rubber gaskets and then the top and bottom perforated plates and eventually the membrane carrier which left the RVC slab

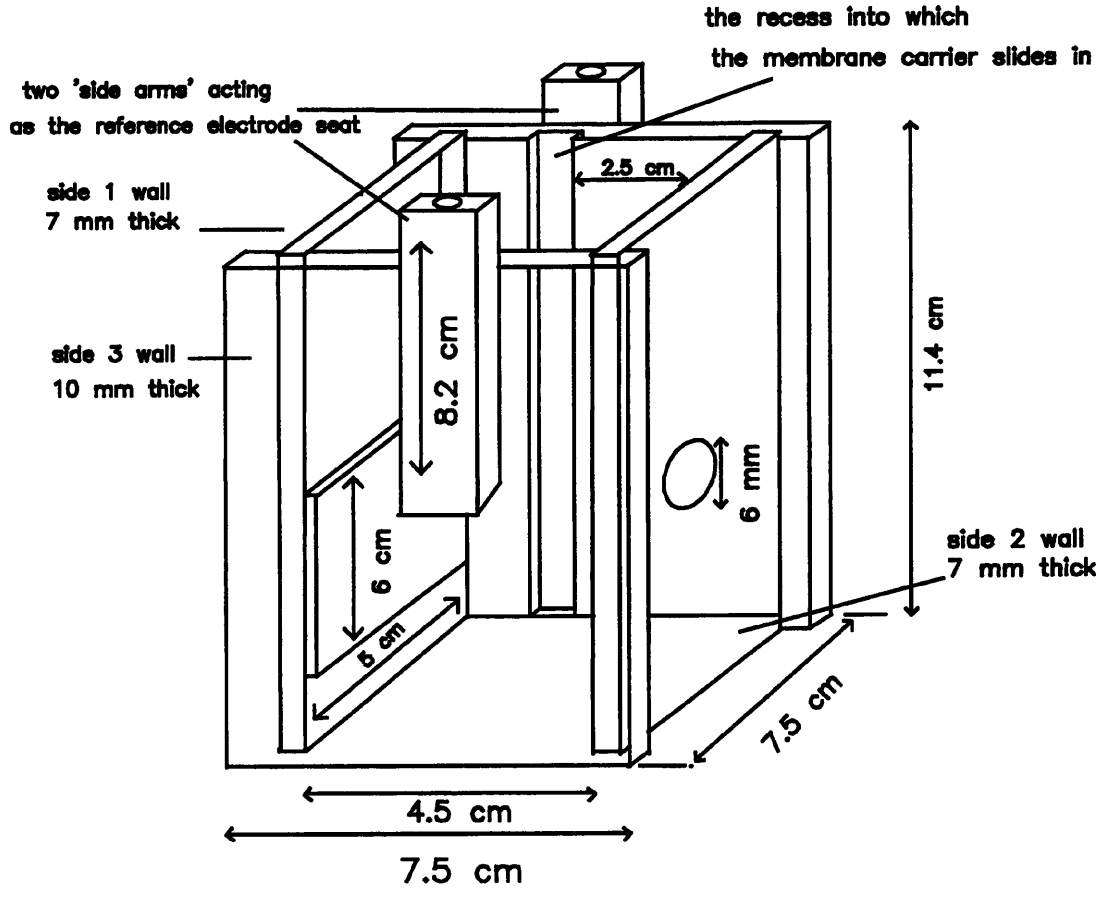

Figure 3.6 This figure shows different parts of the column that were glued together and were non-removable, namely: the 'side arms', counter electrode, four faces of the column made up of four Perspex slabs of 7 and 10 mm thickness

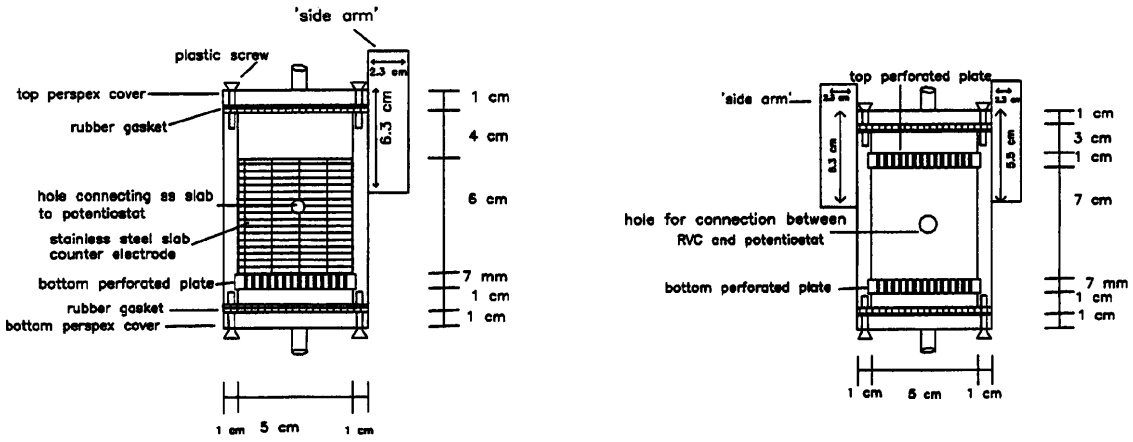

Figure 3.7 Schematic diagram of (a,b) side views and (c) plan view of RVC column

accessible for removal. Mounting a newpiece of RVC involved the above steps but in reverse order. The '*side arms*' which acted as the reference electrode seat and the Luggin probe were also glued onto the column. In order to allow the effect of variation of the reference electrode location onthe potential applied to be studied, two reference electrode seats were used. These were constructed by drilling a 15 mm diameter hole in a Perspex rectangular block 23 mm wide and 80 mm long and then these were mounted onto the opposite sides of the column, Figures 3.7 and 3.8. Figure 3.7 shows side and top views of the column. Contact was made between the reference electrode and the electrolyte solution at the vicinity of the RVC using a small diameter hole in the membrane carrier facing the RVC. This hole was drilled into the membrane carrier to a depth of 3 mm where it met (at right angle to it) with a capillary inside the membrane carrier which led into the 'side arm'. The mechanism of operation of the Luggin probe and the reason for its use is discussed in section 2.4.

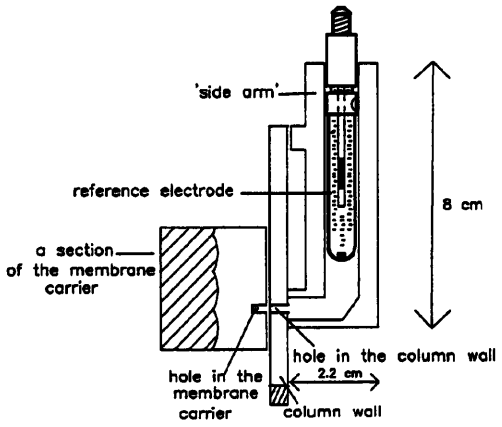

Figure 3.8 The 'side arm' and its location in the column

When electrolyte solution was being pumped through the column it slowly penetrated up through the capillary causing the bottom half of the 'side arm' to slowly fill up and a pool

of electrolyte was formed. Upon insertion of the reference electrode into the pool, contact was established between the cell electrolyte solution and the reference electrode's electrolyte. The reference electrode used was a saturated calomel (mercury/mercurous chloride/saturated KCl). The mechanism of operation of the reference electrode has been discussed in section 2.4.

The *membrane carrier* was made up of two Perspex slabs each 5 mm thick with the centre drilled to the same diameter as the circular membrane (see Figure 3.9) one acting as male and other as the female counterpart. A cellulose acetate membrane having pore size of 0.1 μm was sandwiched between Perspex slabs in the carrier and held in place by means of four plastic screws.

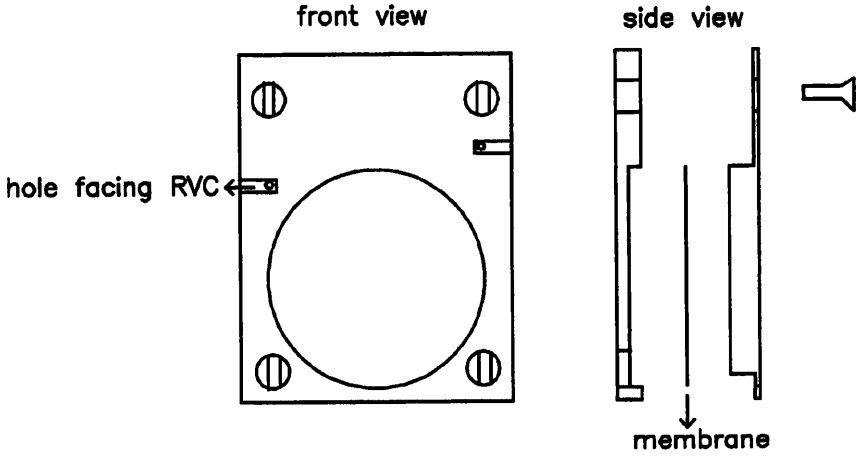

Figure 3.9 Sketch of the membrane carrier showing front and side elevation

2) Wire attachment to RVC

Contact was made between the RVC electrode and the potentiostat using a copper wire. At the point of attachment care had to be taken to ensure that leakage was avoided and at the same time the wire had to be isolated from contact with electrolyte. The simplest way was

found to be direct attachment of wire using silver-loaded epoxy resin (R.S Components Ltd). To reduce the area for contact between electrolyte and wire the attachment point was enclosed within a small length of a small diameter glass tubing (see Figure 3.10). The point of attachment was further protected from electrolyte by applying a layer of silicon rubber outside the glass tubing. The RVC with the wire attached were left in a 50 ^{0}C oven for half a day to speed up the curing period of the silver loaded epoxy resin. The length of wire used to connect the RVC to the potentiostat was 550 mm.

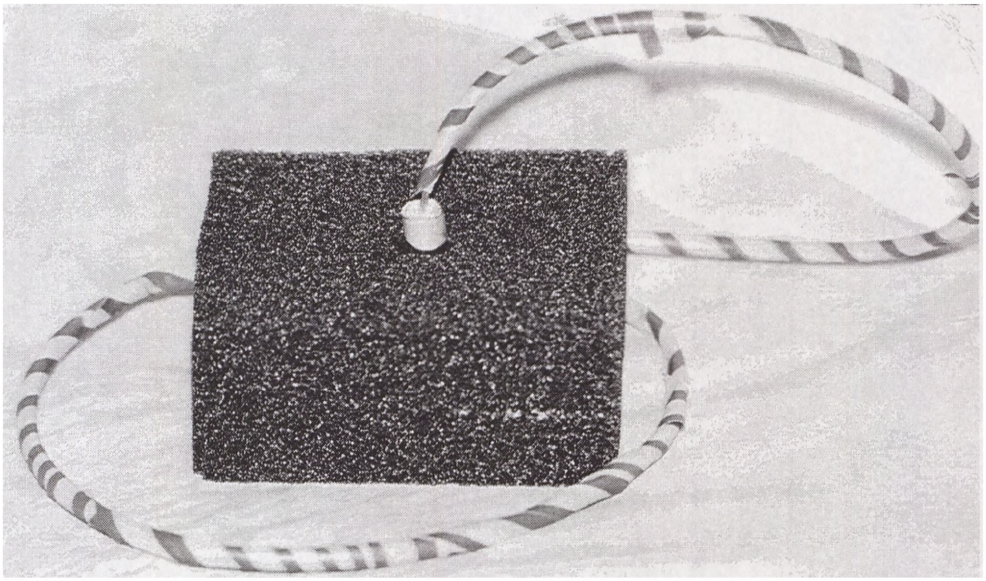

Figure 3.10 Photograph of a piece of RVC cut for an adsorption experiment

3) Selection of counter electrode

As explained in section 2.4 an electrochemical cell consists of working, reference and counter electrodes. The current flows from the working electrode through the electrolyte to the counter electrode into the potentiostat and back to the working electrode. The counter electrode used in this study was a stainless steel slab having the same dimensions as the RVC slab, i.e. 60 mm (length) and 50 mm width. The counter electrode was screwed on to the side exactly

opposite (see Figure 3.6) to the RVC slab to minimise current non uniformity. A copper wire 440 mm long was used to connect the counter electrode to the potentiostat.

3.2.2 Potentiostat

An Autostat model Auto401 (Thompson Electrochem Ltd) was used for controlling the potential between the working electrode and the reference electrode at a fixed and

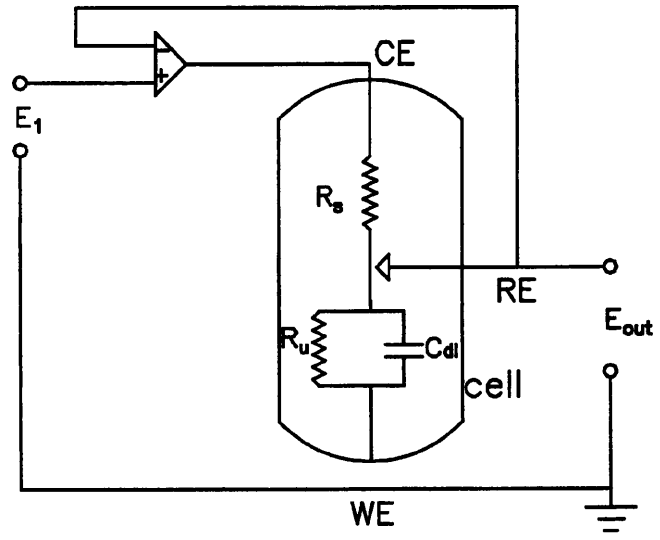

Figure 3.11 Basic arrangement for the potentiostatic control of the RVC's potential

selected potential (sometimes this potential was also varied with time). The underlying principle of operation can be seen in Figure 3.11. Von Fraunhofer (1972) discusses the basic principles of a potentiostat and state that potentiostat is simply a voltage follower with the task of controlling the potential, between reference electrode (RE) and the RVC working electrode (WE), at E_1. The working potential which is at ground potential, has a potential of -E_1 relative to the reference electrode, hence the input voltage is inverted in the cell.

The cell resistance is made up of individual contributions from the solution resistance, R_s,

between the reference electrode probe and the counter electrode, CE, the resistance between the luggin tip and the working electrode, R_u, and the double layer capacitance of the working electrode, C_{dl}.

The potentiostat was software-controlled connected to an Archimedes 310 BBC computer via an RS232/423 serial communication link. The interface supported the following functions:

- setting control potential.
- monitoring potential in both 'run' and 'isolate' modes.
- current range changing.
- selecting an isolate/run mode.

The computer software was selected by means of a menu offering two programs. A general purpose program for cyclic voltammetry, and a slightly different program for linear polarisation experiments.

When the cyclic voltammetry is selected the program requires values for the desired initial and final working electrode's potentials and also the rate (mV/min) at which the initial working electrode's potential must be increased to the final value. If the same value is entered for the initial and final working electrode's potential then the software automatically takes the value entered for the rate to be the duration of time during which the electrode must be maintained at the entered potential. In deposition experiments carried out the cyclic voltammetry was selected and a predetermined potential was entered into the program for the initial and final potentials and a long time was entered for the duration of the scan (e.g. 4 hours) to allow the equilibration of RVC and then with ample time left for carrying out the deposition experiment. During an experiment the resulting current and

potentials were remotely measured and stored to a floppy disc. The potentiostat required approximately 30 minutes to 'warm up' before use. During deposition experiments to ensure correct and accurate control of potential a high impedance digital voltmeter (DVM) was placed between the potentiostat's electrode input terminals. It was found that the potential entered into the interface program was slightly different (see Chapter 6) from the direct reading obtained by the DVM, however, the later was utilised in the experimental results reported here.

3.3 TURBIDITIMETER

In the literature for adsorption studies, several techniques are used to measure particle number concentrations in the inlet and outlet streams. One method is the Coulter Counter technique which is based on counting the number of particles going through a small aperture immersed in the suspension based on an electrical measurement (see 3.5). The most common technique utilises the light scattering properties of the colloidal suspension. This property was first recognised by Faraday when he transmitted a beam of light through a gold suspension. Further study by Tyndall led to this property being called the Tyndall effect. The experimental technique for measurement of the light scattering is very simple and can be seen in Figure 3.12. The intensity of light scattered at an angle δ is measured at a distance r from the scattering object by a suitable detector.

The British Standard BS 6068 defines turbidity as the reduction of transparency of a liquid caused by the presence of undissolved matter. The particle number concentrations in the present experiments were measured by a portable turbiditimeter (model 6035, Jenway Equipment Ltd). The light source was a 5V, 230 mA Tungsten lamp and the detector was a silicon diode with enhanced blue response. The scattering measurements were obtained at 90^0

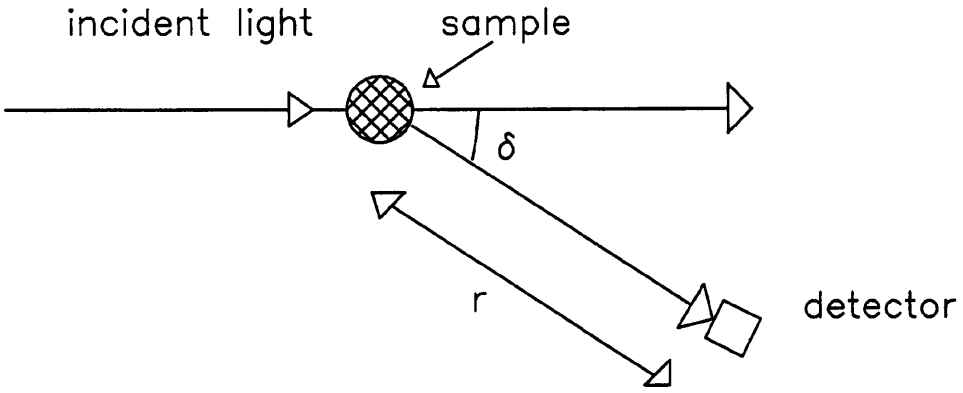

Figure 3.12 Basic arrangement for the light scattering experiments

to the incident light beam. The sample vials provided by Jenway had a volume of approximately 21 cm^3 and these vials had an etched mark for alignment against the marking on the hole in the meter where the vial was inserted.

A 5.0 Nephelometric Turbidity Unit (NTU) standard was also purchased which was used to calibrate the meter for correct turbidity readings. The procedure for calibration of the turbiditimeter to convert turbidity readings into particle number concentration is described in section 4.1.

3.4 ZETA POTENTIAL ANALYSIS

The concept of zeta potential and assumptions required to derive expressions for its estimation have been discussed in section 2.1.3. Zeta potential signs and values are measures of the surface charge carried by particles. Therefore a negative value means the surface is negatively charged and vice versa. The equipment used in this study, a ZetaPlus (Brookhaven Instruments Corporations, USA), was based on measuring the electrophoretic mobility. In this

device charged particles in a dilute suspension move between two oppositely charged electrodes. Due to motion of the charged particles a frequency shift, or Doppler shift, ω_s, occurs in the light scattered by particles. This light is a focused laser beam of wavelength λ_0=670 nm, Figure 3.13. The particles move perpendicularly to the incident beam. As a result the angle between the field and the incident beam is half the scattering angle δ. The scattering angle is 15^0 in the ZetaPlus.

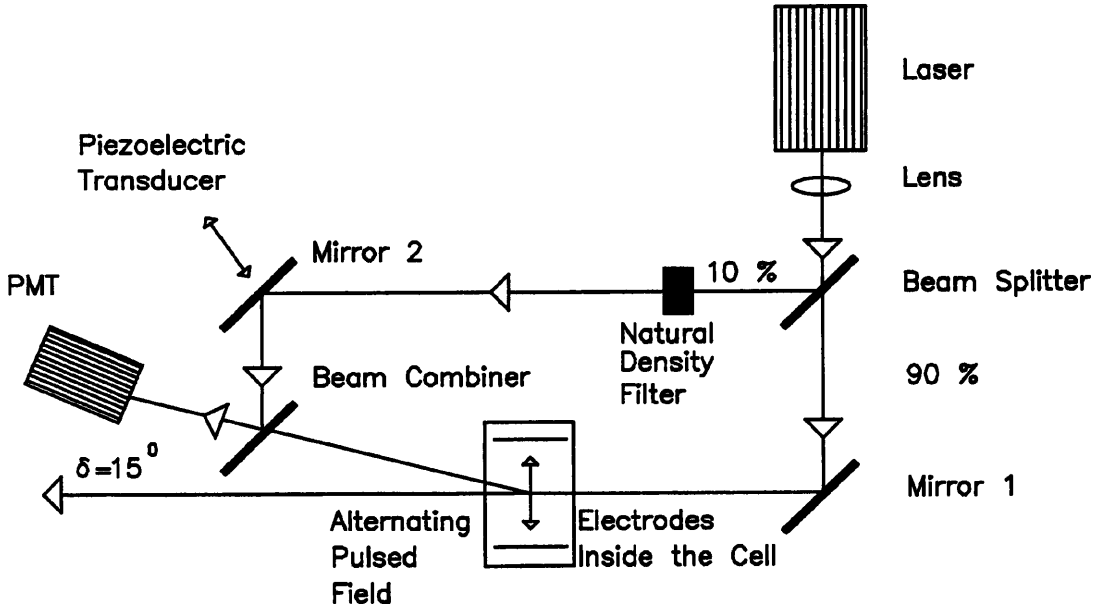

Figure 3.13 Principle of operation of the ZetaPlus instrument

The ZetaPlus is supported by a menu-driven software and when zeta potential measurement is selected the menu for run options appears on the monitor. Some of the data in this menu had been pre-selected by the manufacturing company namely:

- wavelength of 670 nm
- modulation frequency of 250 Hz
- temperature set point of 25 ^{0}C

- refractive index of 1.332

Usually two runs consisting of two cycles, with a sampling time of 256 μsec, were carried out on the same suspension sample.

The ZetaPlus measures the electrophoretic mobility of the particles and the zeta potential is calculated by the software using the Smoluchowski relationship (equation 2.16).

3.5 COULTER COUNTER

A Coulter Counter (Model TAII, Coulter Counter Electronics Ltd) was used to calibrate the turbiditimeter so that its NTU readings can be converted into particle number concentrations. The procedure for the calibration will be elaborated in Chapter 4.

The principle of counting and sizing particles was developed by Wallace H. Coulter in the late 1940's originally designed for rapid counting of blood cells. A schematic diagram of the Coulter Counter can be seen in Figure 3.14. The particles suspended in the electrolyte solution (usually a brine solution called ISOTON) flow through a small aperture (or orifice) in the wall of an electrical insulator. A current path is established between the two electrodes setting a base impedance to the electrical circuitry. As every particle goes through the aperture, it displaces electrolyte of equal volume to its own immersed volume. The base impedance is therefore modulated by an amount equal to the displaced volume of the particle resulting in an electrical pulse of short duration the height of which is proportional to the volume of particle. This pulse may be measured from the change in the resistance, current or voltage across the electrodes. When there are a number of particles going through the aperture a train of pulses result which can be monitored on an oscilloscope and subsequently analysed by the counter and the pulse height analyser circuits to produce particle volume, or equivalent

spherical diameter, distribution.

The coulter Counter can be set to analyse the sample in three modes: the manometer, total and time. These correspond to sampling until a preset value is reached for volume, counts and time respectively. In the present research the sampling switch was set to manometer and consequently the Coulter Counter was set to analyse 0.5 cm^3 of the suspension. The standard polystyrene latex suspension was made up as described in Chapter 4. Counts were performed, using a 140 μm orifice, by opening and closing the sample control stopcock. The reset, accumulate and stop switches illuminated during their respective portion of the cycle. The procedure for dilution of samples prior to the Coulter Counter analysis is further discussed in Chapter 4.

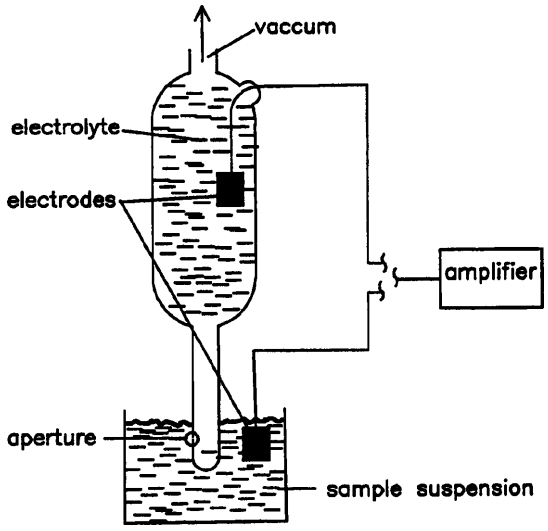

Figure 3.14 The basic principles of the Coulter Counter

CHAPTER 4

EXPERIMENTAL PROCEDURES

Having discussed the experimental apparatus and reasoning behind the choice of experimental apparatus, the procedure for carrying out deposition experiments will now be considered. The underlying principle of the deposition experiments utilising different experimental arrangements are similar and only differ in the nature of collector and the method utilised to prepare the collector for a deposition experiment.

Colloidal interaction energies of interest operating at the distance of separation concerned are discussed in Chapter 2.2. The total energy of interaction, can predict whether a *favourable* condition for deposition is prevalent. This condition is met when there are attractive energies operating between collector and particles. This is in contrast to an *unfavourable* condition which occurs when there are net repulsive energies operating between the collector and particles. To determine the total interaction energy information on both the zeta potential of the collector and particles are required.

Other information which is needed to facilitate full understanding of the deposition experiments such as the surface charge of the particles and the range of operating potentials of the RVC collector must be sought.

This chapter seeks to explain the methodology adopted during the deposition experiments and also discusses the relevant theories of deposition. This chapter has been divided into seven

parts as follows:

- construction of the calibration chart for the turbiditimeter.

- characterisation of the polystyrene latex particles by determining their zeta potentials and also their surface charge density. A separate part within this section has been designated to an introduction to dialysis as a technique for 'cleansing' polystyrene latex particles.

- characterisation of the spherical *Hypercarb* particles.

- characterisation of the spherical glass beads.

- characterisation of RVC.

- experimental procedure for deposition experiments onto glass beads.

- experimental procedure for deposition onto RVC collector.

4.1 CALIBRATION OF TURBIDITIMETER

Turbidity measurement has been widely used in colloid science (section 3.3). However, readings obtained from a turbiditimeter only indicate how much scattering of an incident light beam is caused when it is directed through the sample under study. Construction of a particle break-through curve encountered in adsorption experiments requires information on the particle number concentration. Consequently, data from the turbiditimeter has to be quantified

to allow generation of a calibration chart to convert the turbidity readings into particle number concentration. For this purpose, standard samples of polystyrene latex particles were made up and then the number of particles present were determined by means of Coulter Counter (model TAII, Coulter Counter Electronics Limited). Having obtained the turbidity values the calibration chart was constructed by plotting the Coulter Counter readings against the turbidity values.

A 0.5 g aliquot of polystyrene latex powder (see section 4.2) having mean diameter of 5.4 μm were weighed and made up to 20 cm^3 with distilled water filtered through a 1 μm membrane filter.

Different volumes of this stock particle suspension were taken and made up to 16 cm^3 with distilled water which had been filtered through a 1 μm membrane filter. To 1 cm^3 of these standard suspensions, 100 cm^3 of ISOTON (brine solution) was added. Before the Coulter Counter reading could be obtained, background measurements were carried out on a blank sample of ISOTON.

When the background reading obtained, the Coulter Counter aperture (140 μm) was allowed to immerse in the suspension diluted with 100 cm^3 of ISOTON and then the total counts obtained. The Coulter Counter was set to analyse 0.5 cm^3 of sample. The counts obtained were then subtracted from the reading for the blank sample and this corresponded to the actual number of particles in 0.5 cm^3 of the original stock suspension.

Table A1 in Appendix A shows the background and total counts and the final particle number concentrations for different turbidity values.

The results in Table A1 have been plotted as shown in Figure 4.1 and the equation that best

fits these data was found to be:

$$Y = (-1.1\times10^{-4}) X^2 + (2.27\times10^{-2}) X \quad (4.1)$$

Where Y is the particle number concentration ($x10^6$ particles cm^{-3}) and X is turbidity (NTU).

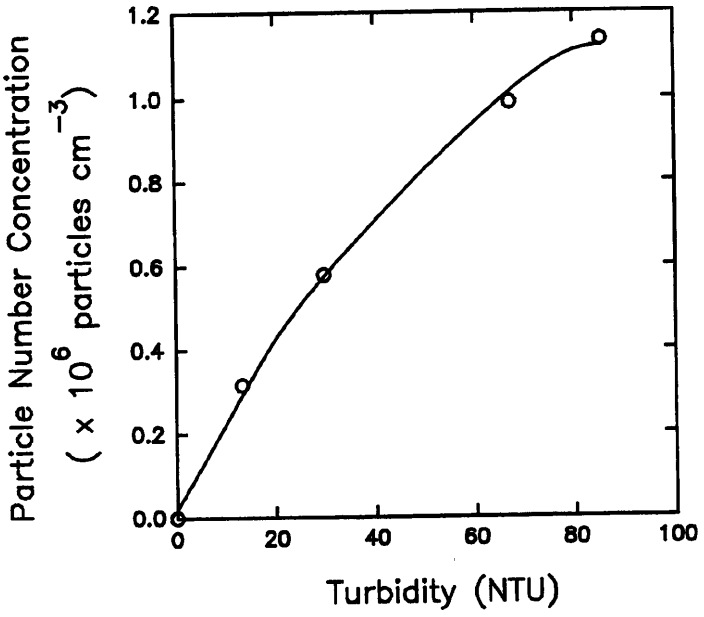

Figure 4.1 Particle number concentration (particles/cm^3) against turbidity (NTU)

4.2 CHARACTERISATION OF POLYSTYRENE LATEX PARTICLES

Two types of colloidal particles have been used and this section deals with characterisation of polystyrene latex particles. These particles were produced at Bradford University following the dispersion polymerisation method developed by Almog (1982). Following Coulter Counter analysis the size distribution of these particles exhibited a median size of 5.4 μm. Figure 4.2 shows the Scanning Electron Micrograph of the particles in dry state. Amongst the by-products of the dispersion polymerisation are alcohols, surfactant and polymeric monomers

and despite washing it is quite possible that these remain in solution and may interfere with attempts to characterise the particles and therefore they should be removed.

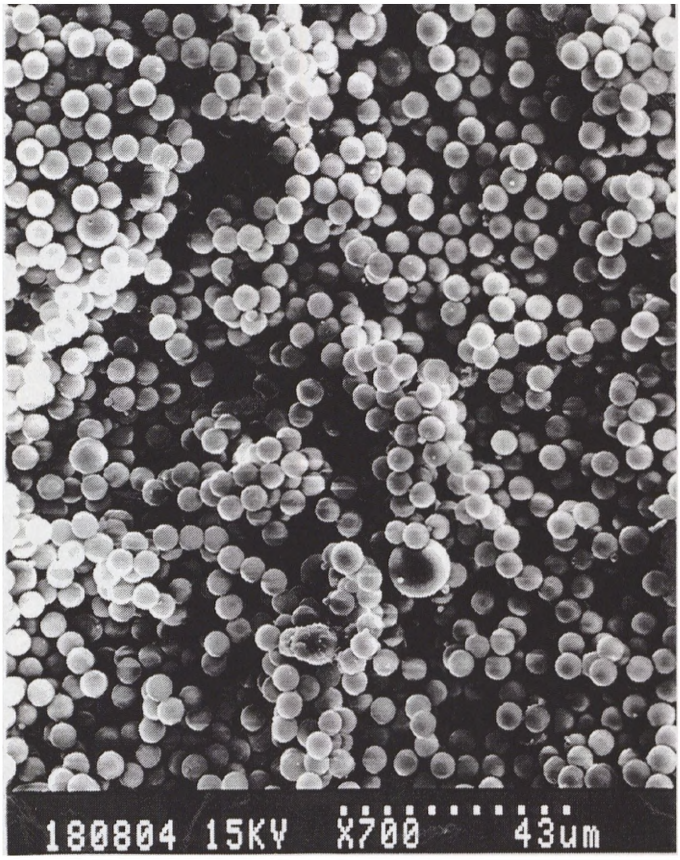

Figure 4.2 Scanning electron micrograph (SEM) of polystyrene latex particles used in this study

In an excellent article, van den Hull et al. (1972), describe an ion-exchange-and-conductometric technique to give 'clean' (i.e. emulsifier and electrolyte free) latexes. The surface charge of latexes were determined by conductometric titration. They found that the surface charge remained constant after three ion-exchanges, however, it reduced by a great deal after the first ion-exchange. They also investigated dialysis as another (well known) method for 'cleansing' latexes and concluded that in their experience this method did not give

complete removal of impurities. A major advantage of ion-exchange over dialysis is that in ion-exchange a complete exchange of anions such as Na^+ and K^+ ions for H^+ ion occurs and this is very useful when attempts are made to measure the surface charge by conductometric titration since this method only measures the number of H^+ and any anion which has Na^+ or K^+ counter-ions will go undetected.

In this study due to non-availability of ion exchange equipment, the particles used in adsorption experiments were placed in dialysis membrane (see section 4.2.3) immersed in distilled water for at least one month prior to experimentation. The conductivity of the surrounding distilled water was regularly checked and when it exceeded 20 μS the water was renewed. The rise in the conductivity of water was due to the transport of ions from inside the tubes to the surrounding water.

In the following three sections measurements of the zeta potential of the latexes are considered. Then an attempt will be made to determine their surface charge and finally an introduction is made to dialysis as a technique for cleaning particles.

4.2.1 Zeta potential measurement

Using the equipment, described in section 3.4, measurements were performed as reported in Tables A2-A5 in Appendix A for different KCl concentrations. The suspensions were made up so that the particles had a volume fraction of approximately 0.0008.

The ZetaPlus analyser was supported by a software which allowed the measurements to be made in two cycles on a single sample. Hence the data reported in the tables have been

presented as two in one box meaning that these measurements were carried out on the same sample. Normally two runs, each consisting of two cycles, were performed on the same sample before small amount of bubbles was observed in the sample. These bubbles were thought to have been created by the electrolysis of the solution due to passage of current between the electrodes.

Another source which was speculated to contribute to error in the measurements was the surface markings of the sample cell walls, produced when the electrodes were pushed into the cell against the walls. These markings were in the path of the laser beam and they may have interfered with measurements. Generally after 10 measurements a new cell was used.

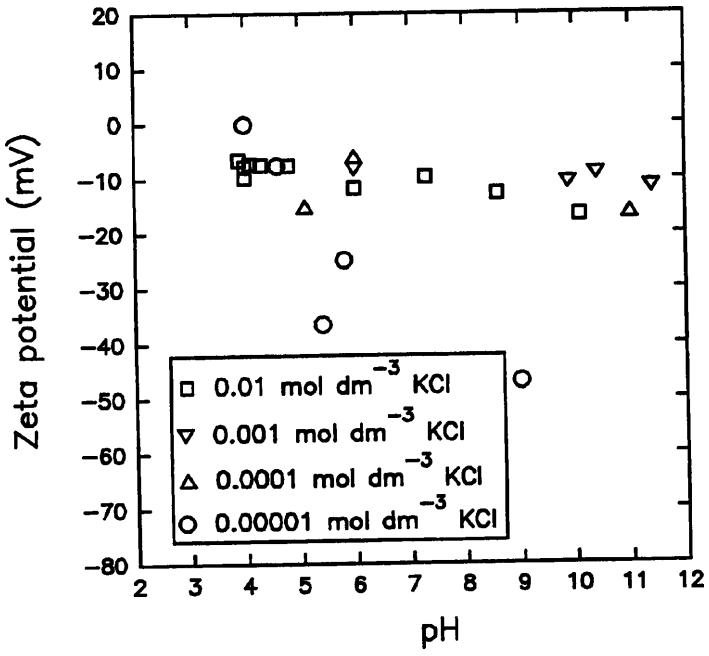

Figure 4.3 Zeta potential of polystyrene latex particles measured for different values of pH and KCl concentration

These results have been plotted as shown in Figure 4.3. It can be observed that at high to

moderate KCl concentrations pH does not appear to affect the zeta potential values drastically but at a lower concentration, typically 10^{-5} mol dm^{-3}, a pronounced effect can be observed. It is evident from this figure that the isoelectric point of these particles occurs at pH of 3-4 since at this range of pH highly unstable mobility readings were obtained.

The standard deviation is widely taken as the measure of spread of a batch of data about their arithmetic mean and therefore a large value represents a large spread of data.

The standard deviations calculated for the zeta potential values are quoted in the tables and the values lie in the range 2.8-7.4 but the majority are around a value of 4.0. The higher values for standard deviations were obtained for high and low pH measurements, typically pH of 4.0 and 11.0. This is to be expected since the point of zero charge of the particles lies at a low pH. To obtain a stable high pH involved using larger volumes of alkali. This meant that there were more ions present in the suspension and these consequently may have interfered with the measurements.

Elimelech et al. (1990a) discuss some anomalities observed with electrokinetic properties of latex particles that they had utilised. For example a maximum was obtained in the plot of zeta potential against pH. One explanation that was put forward for this was that of 'hairy layer'. According to this theory, the surface of polymer latexes comprised of polyelectrolyte chains carrying the surface charge. This layer expanded upon decreasing the ionic strength, due to repulsion of functional groups, and contracted with increasing ionic strength. The expansion and contraction of the 'hairy layer' affected the location of the plane of shear which consequently affected the zeta potential. They measured the electrophoretic mobility of surfactant free polystyrene latex for different concentrations of KCl and $CaCl_2$ as shown in Figure 4.4. They concluded that in the absence of KCl, as calcium chloride concentration

increases some of the Ca^{2+} counterions specifically interact with the surface sulphate functional groups and hence reduce the negative charge, while other calcium counterions neutralise the negative charge of the particles in a non-specific manner. simultaneously, co-ions enter the interfacial region adjacent to the particle surface and increase the negative charge of the particles.

To investigate the occurrence of this maximum for the present polystyrene latexes, the zeta potential values were determined for mixtures of equal volumes of KCl/$CaCl_2$, keeping the background KCl ionic strength constant and varying the $CaCl_2$ concentration, as shown in Tables A6-A8 and graphically in Figure 4.5. Surprisingly the effect of divalent Ca^{2+} ions are *opposite* to that observed by Elimelech (1990) despite careful retesting of the samples. Particles studied by Elimelech carried strong acidic functional groups and this is in contrast to the present particles which carry weak acid as their surface functional groups. Therefore, the mechanism proposed by Elimelech (1990) does not necessarily apply to latexes used in the present work.

The important effect of Ca^{2+} ions on the present particles is that for the same ionic strength of background KCl electrolyte, varying the $CaCl_2$ concentration can change the sign of zeta potential of the particles. This could have grave consequences when carrying out deposition experiments since any trace of Ca^{2+} impurity in appreciable concentration may affect the sign of zeta potential of particles which in turn may undermine the theoretically predicted occurrence of favourable/unfavourable deposition condition.

Another interesting point is the limiting Ca^{2+} ion concentration, above which for the same KCl

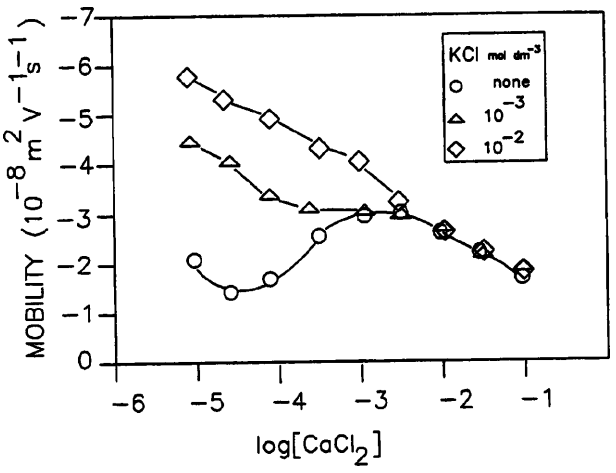

Figure 4.4 Electrophoretic mobility of latex particles as a function of $CaCl_2$ with KCl as a background electrolyte at pH 6.8 (after Elimelech et al. (1990a))

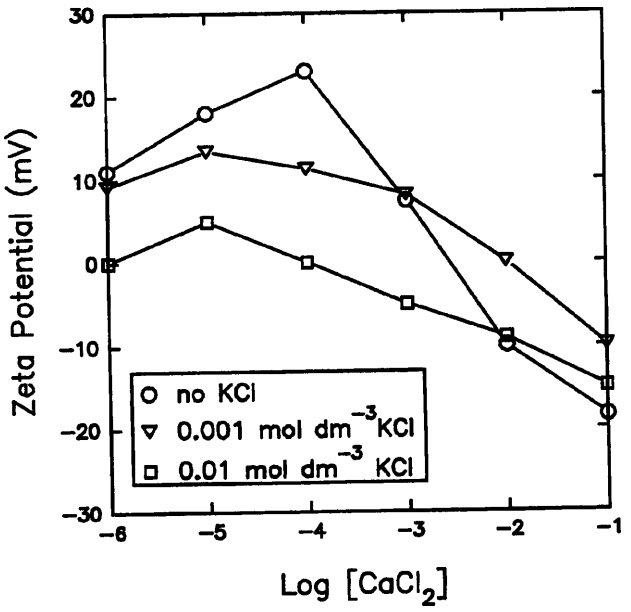

Figure 4.5 Variation of zeta potential of polystyrene latex particles with $CaCl_2$ concentration with equal volume of KCl solution as the background electrolyte (neutral pH)

electrolyte concentration the zeta potential bears positive charge and below which it is negative. The $(Ca^{2+})_{limiting}$ concentrations for the 0.0, 0.001 and 0.01 mol dm^{-3} of background KCl concentrations were 0.001, 0.01 and 0.0001 mol dm^{-3}.

4.2.2 Surface charge estimation

Estimation of surface charge density is based on expressions derived from the solution to the Poisson-Boltzmann equation. Jia and Williams (1990) reviewed the most prominent expressions relating surface charge and surface potentials. The following expression has been obtained by Ohshima et al. (1982) for a 1:1 electrolyte and for all κa values:

$$\sigma_0=\frac{2\,\epsilon\,k\,T\,\kappa}{e}\sinh\left(\frac{e\psi}{2kT}\right)\left[1+\frac{2}{\kappa\,a\cosh^2\left(\frac{e\psi}{4kT}\right)}+\frac{8\ln\left[\cosh\left(\frac{e\psi}{4kT}\right)\right]}{(\kappa a)^2\sinh^2\left(\frac{e\psi}{2kT}\right)}\right] \quad (4.2)$$

Another expression by Delahay (1965) is used to compare the surface charge density values:

$$\sigma_0 = 11.74\,(\,I\,)^{1/2}\sinh(\,19.46\,Z\,\psi\,) \quad (4.3)$$

The parameters used in these equations are defined in the nomenclature.

The argument of which plane (see Figure 2.1) to choose to represent the surface potential is discussed in section 2.2. It is argued that zeta potential at the surface of shear can be assumed to provide approximate value for the surface potential and this holds for low electrolyte concentration. The discrepancy between these potentials becomes pronounced at high electrolyte concentration when the diffuse layer contracts resulting in more potential drop from ψ_s to the Gouy plane to occur within the shear plane and consequently this affects the zeta potential value. The values used for estimation of surface charge density using the above

expressions are shown in Table 4.2.

Substituting the values in Table 4.1 into equation (4.2) yields a value of 0.019 μC cm^{-2} and the corresponding value from equation (4.3) is 0.018 μC cm^{-2}. Table 4.2 shows the surface

Table 4.1 Values for terms in equations (4.2) and (4.3) used for surface charge estimation

Parameter	Value
$\varepsilon=\varepsilon_0\varepsilon_r$	8.8542 x 10^{-12}(C^2/J m) x 78.5
k	1.3805 x 10^{-23} (J/K)
T	298 K
e	1.6 x 10^{-19} C
pH	6.0
ψ	-25 x 10^{-3} V
a	27 x 10^{-7} m
κ	3.28 $(I)^{(1/2)}$ (nm^{-1})
I	0.00001 mol dm^{-3}

Table 4.2 Surface charge density values estimated using equations (4.2) and (4.3)

Surface Charge Density (μC cm^{-2})		Zeta Potential (mV)	KCl Concentration (mol dm^{-3})
Equation 4.2	Equation 4.3		
0.137	0.137	-6.0	0.01
0.061	0.061	-8.5	0.001
0.020	0.020	-10.0	0.0001
0.019	0.018	-25.0	0.00001

charge density estimates utilising both expressions for zeta potential values at pH of 6.0 and for different KCl concentrations. From previous argument, values estimated at low electrolyte

concentration should be looked upon as better approximations. It can be seen from these values that the present polystyrene latex particles can at most be charged to 0.137 μC cm^{-2} for KCl concentration of 0.01 mol dm^{-3}. This raises the question that, in deposition experiments which will be carried out, whether the electrical double layer plays a significant role in the deposition processes.

The functional groups present at the surface of particles have to be identified if these low surface charge values need to be explained. Polystyrene latex particles have been produced following the procedure by Almog (1982) and the compound thought to be responsible for the surface charge is 2,2 Azobisisobutryronitrile (AIBN):

$$NC-C(CH_3)_2-N=N-C(CH_3)_2-CN \qquad (4.4)$$

It is envisaged that when in electrolyte solution the above compound dissociates and two molecules with CN^- endgroups will be produced. To validate the above statement, conductometric titrations were carried out to establish the nature of the surface functional groups.

To KCl solution containing 0.2 g of polystyrene latex particles, aliquots of 0.0001 mol dm^{-3} HCl were added but even after adding 70 cm^3 still no end-point was obtained. The same procedure was repeated but adding 0.0001 mol dm^{-3} NaOH and this time a slight end-point was obtained. It was therefore decided that the surface functional groups were only weak acids and it would be very difficult to titrate them unless a special air-free titration vessel was used.

As a last resort to identify these groups, an attempt was made to increase the strength of these weak acidic surface functional groups by addition of Mannitol as suggested by Vogel (1978). Mannitol produces complexes with these surface functional groups which then act as strong acids. Figures 4.6 and 4.7 show results of such titration with 2.0 g Mannitol added for non-dialysed and dialysed samples respectively.

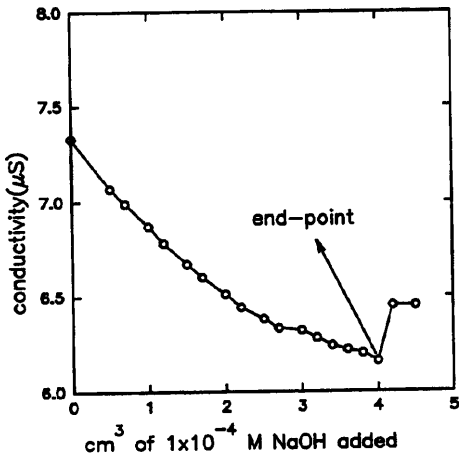

Figure 4.6 Conductometric titration of non-dialysed polystyrene latex particles

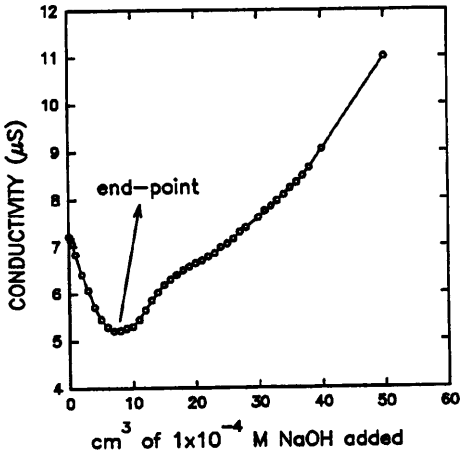

Figure 4.7 Titration of dialysed latex sample

It can be seen from Figure 4.6 that after addition of approximately 4 cm^3 of alkali an end-point was obtained and this subsequently confirms the supposition that these particles carry weak acid as their surface functional groups. The titration data for dialysed and non-dialysed latexes are shown in Table A9.

Since there was no access to an ion-exchange column, the only way the particles could be 'cleansed' was by leaving them in visking tubes (see section 4.2.3) for a long period of time, typically 3 months, prior to use in experiments. The titration curve for the dialysed sample shows an end-point of approximately 7 cm^3 which is 3 cm^3 more than that needed for the non-dialysed sample. This could be interpreted that, in spite of observation made by van den

Hall regarding dialysis technique, dialysis has indeed changed the surface charge of the latex particles by a small but significant amount.

4.2.3 Dialysis

Depending on the efficiency required for the separation of impurities such as small molecules and ions, from colloidal particles, a variety of separation techniques such as centrifuge, chromatographic techniques, ion-exchange and dialysis may be used.

The simplest of these to use is the dialysis in which the particles to be cleaned are placed in a membrane, usually cellulose based, tubing and this is then immersed in a wash solution. The impurities within the membrane tubing are made to flow, under the influence of the concentration gradient driving force, through the pores of the membrane outwards into the wash solution. For the case of removal of ions application of an electric field can enhance the removal rate.

The polystyrene latex particles employed in this study were cleaned using dialysis membrane (Medicell International LTD) having a molecular weight cut-off size of 12000-14000 Daltons.

4.3 CHARACTERISATION OF *HYPERCARB* PARTICLES

Polymer latexes, such as polystyrene latex used in the present study, are the most frequently used colloidal particles in adsorption studies. These particles offer attractive characteristics such as approximately uniform spherical shape, particle size and surface charge. One problem associated with these particles has been briefly discussed in the previous part as being the required 'cleansing' prior to use. The 'cleansing' stage is needed to remove undesired

polymerisation by-products and hence the true surface charge of particles arising from the surface functional groups will be revealed. It can be seen from Table 4.2 that the particles utilised in the present study had a low surface charge. It is believed that surface charge will play a major role in investigation of practicality of using an externally applied potential to manipulate the rate of deposition. Consequently, it was decided that alternative colloidal particle should be utilised with a view to investigate the universality of deposition experiments and to further analyse the applicability of externally applied control potential for manipulation of deposition.

Several attempts were made to produce various uniform monodispersed colloidal particles, with a narrow size distribution, following the procedures available in the literature notably by Matijevic (1985). Unfortunately it was observed that to produce colloidal particles, of the said characteristics, required exact experimental conditions such as pressure, temperature, inert atmosphere and most importantly the time for the reaction to be stopped. Hence it was more appropriate to purchase an alternative well characterised particle rather than attempt synthesis.

The material chosen was a carbon material which carried the tradename *Hypercarb*. It is a porous graphitic carbon manufactured, for use as a HPLC column packing by Shandon HPLC. The individual particles of *Hypercarb* were spherical but porous, reported by the manufacture to be at around 75% porosity, and to have a median pore diameter of 25 nm. The *Hypercarb* particle composed entirely of sheets of hexagonally arranged carbon atoms. The particles had a mean diameter of 7×10^{-6} m (and were in fact mechanically robust up to pressures exceeding 400 bars). Figure 4.8 shows a scanning electron micrograph of the *Hypercarb* particles used

in the present study. Due to high porosity, each particle carried within its pores trapped air bubbles and it was proved very difficult to disperse these particles into suspension even under a large vacuum pressure. Eventually, with the aid of the non-ionic surfactant TRITON X-405 (7 drops for a particle concentration of $5x10^{-4}$ g cm^{-3}) a reasonably stable suspension was obtained.

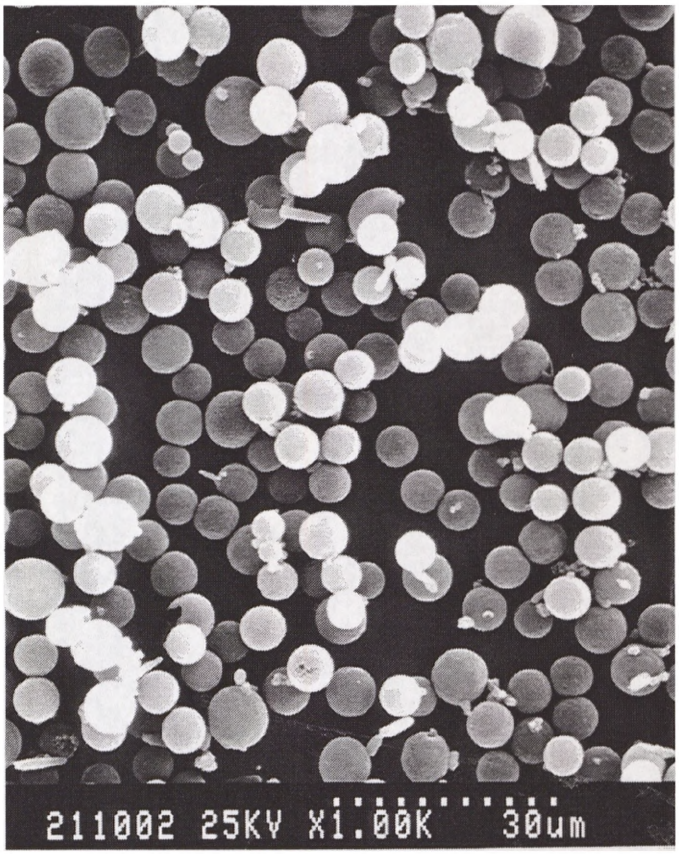

Figure 4.8 Scanning electron micrograph (SEM) of Hypercarb particles

Table A10 shows the zeta potential measurements performed on a sample of suspension having a neutral pH and for various KCl concentrations. Figure 4.9 shows a plot of these results from which it can be observed that at high concentrations these particles have low zeta

potential values whereas at 0.00001 mol dm^{-3} KCl high values are obtained. Table 4.13 shows the surface charge density values estimated using equations (4.2) and (4.3) and data in Table 4.1 (using the appropriate zeta potential value). It can be observed from these values that the *Hypercarb* particles have similar surface charge density and zeta potential values to polystyrene latex particles. It is expected that the *Hypercarb* particles may behave differently in deposition experiments mainly arising from factors such as different structure, different surface functional groups and relative Hamaker constant.

It can be observed from these values that the *Hypercarb* particles have similar surface charge density and zeta potential values to polystyrene latex particles. It is expected that the *Hypercarb* particles may behave differently in deposition experiments mainly arising from factors such as different structure, different surface functional groups and relative Hamaker constant.

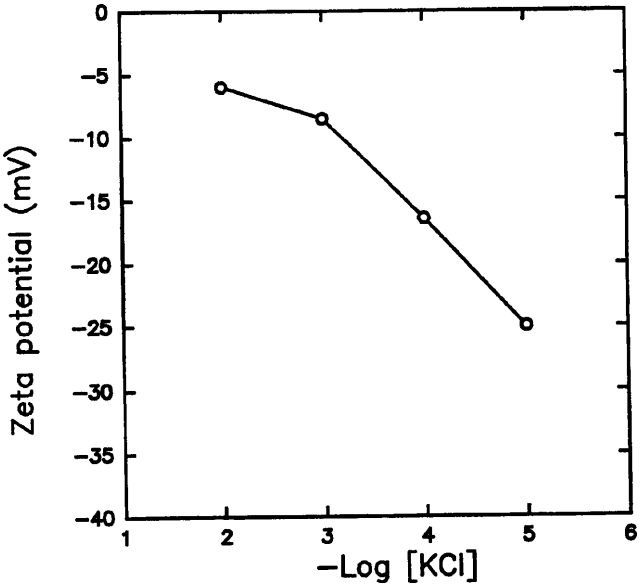

Figure 4.9 Variation of zeta potential of Hypercarb particles with potassium chloride concentration (pH 6.0)

Table 4.3 Surface charge density values of *Hypercarb* particles for different KCl electrolyte concentration at neutral pH

Calculated Surface Charge Density ($\mu C\ cm^{-2}$)		Zeta Potential (mV)	KCl Concentration ($mol\ dm^{-3}$)
Equation 4.2	Equation 4.3		
0.137	0.137	-6.0	0.01
0.061	0.061	-8.5	0.001
0.038	0.038	-16.4	0.0001
0.019	0.018	-24.9	0.00001

4.4 CHARACTERISATION OF GLASS BEADS

Lead glass beads (Jencons Ltd) were used in column tests having a specific gravity of 2.95, refractive index of 1.6 and diameter of 400-455 μm. Figure 4.10 shows a scanning electron

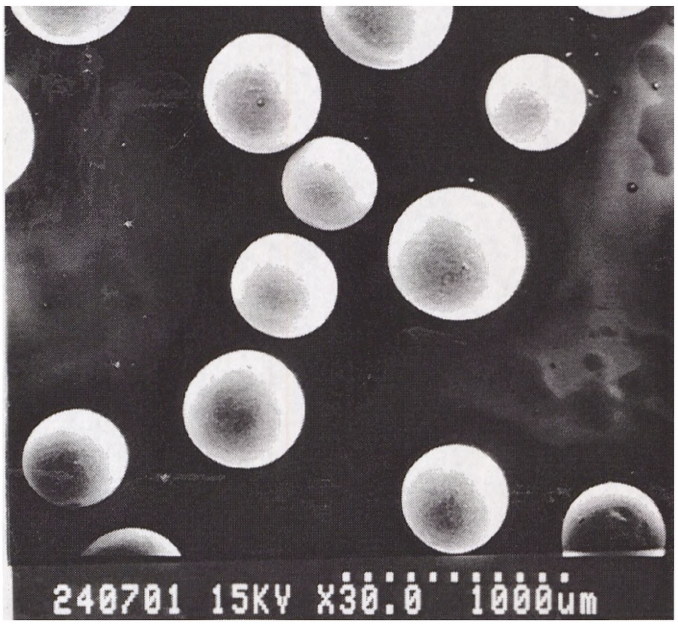

Figure 4.10 Scanning electron micrograph (SEM) of lead glass beads

micrograph of some typical beads. The beads generally had smooth surfaces, although it can be seen from Figure 4.10 that occasionally some beads had surface non-uniformities.

Amarasinghe (1990) measured zeta potential of similar soda lime glass beads for different pH and electrolyte concentrations as shown in Figure 4.11. It is believed that these values closely resemble the zeta potential of lead glass beads used in the present deposition experiments.

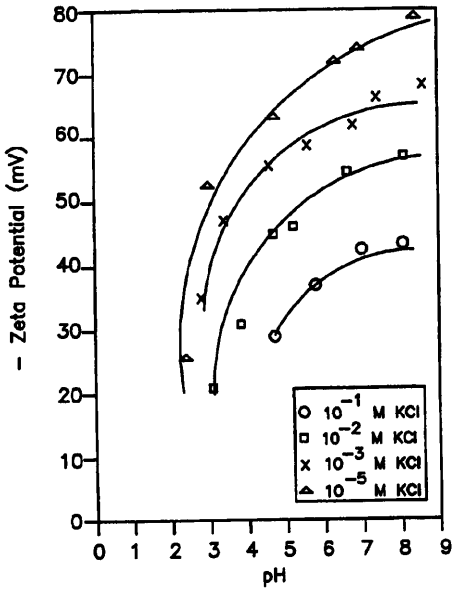

Figure 4.11 Variation of zeta potential of soda lime glass bead with pH and KCl concentration (after Amarasinghe (1987))

4.5 CHARACTERISATION OF RVC

Applying the DLVO theory to the present system would require knowledge of zeta potential values for the particle and collector. The zeta potential of polystyrene latex and the *Hypercarb* particles were described previously for various pH and electrolyte concentrations and in this part the zeta potential values for the RVC collector will be presented. Additionally the optimum range of operating potential of the RVC electrode will be discussed in section 4.5.2.

4.5.1 Zeta potential

In order to measure the zeta potential of RVC a small piece was taken and crushed to a fine

powder using mortar and pestle. 1.242 g of this powder was weighed and to this 25 cm^3 of distilled water, which had been filtered through a 1 μm membrane filter, was added. To 2 cm^3 of this, 12 cm^3 of KCl solution of the required concentration and pH was added. RVC has a density of 148.89 g/cm^3 and consequently the volume fraction of solids in the final suspension was $6x10^{-5}$ v/v. Tables A11-A14 show the measured values for various pH and electrolyte concentrations and these have been plotted as shown in Figure 4.12. Similar to polystyrene latex, these data are presented as two values in one box meaning that these values represent measurements on the same sample.

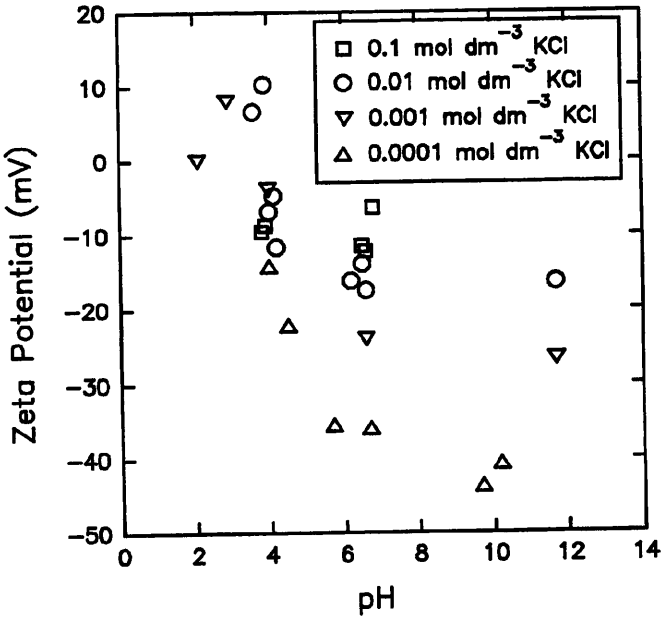

Figure 4.12 Zeta potential of RVC measured for different pH and KCl concentrations

The standard deviation calculated varied between 2.13-7.79 but similar pattern to that of polystyrene latex particles can not be observed. From Figure 4.12 the point of zero charge is estimated to occur around pH of 4.0.

Comparing Figures 4.3 and 4.12 it can be seen that RVC shows relatively higher zeta

potential values compared to the polystyrene latex particles, for the same pH and KCl concentration.

Similar to the procedures used for the polystyrene latex particles, it was decided to investigate the effect that the divalent ion Ca^{2+} has on the zeta potential values of RVC. These can be seen in Tables A15-A17 and graphically in Figure 4.13.

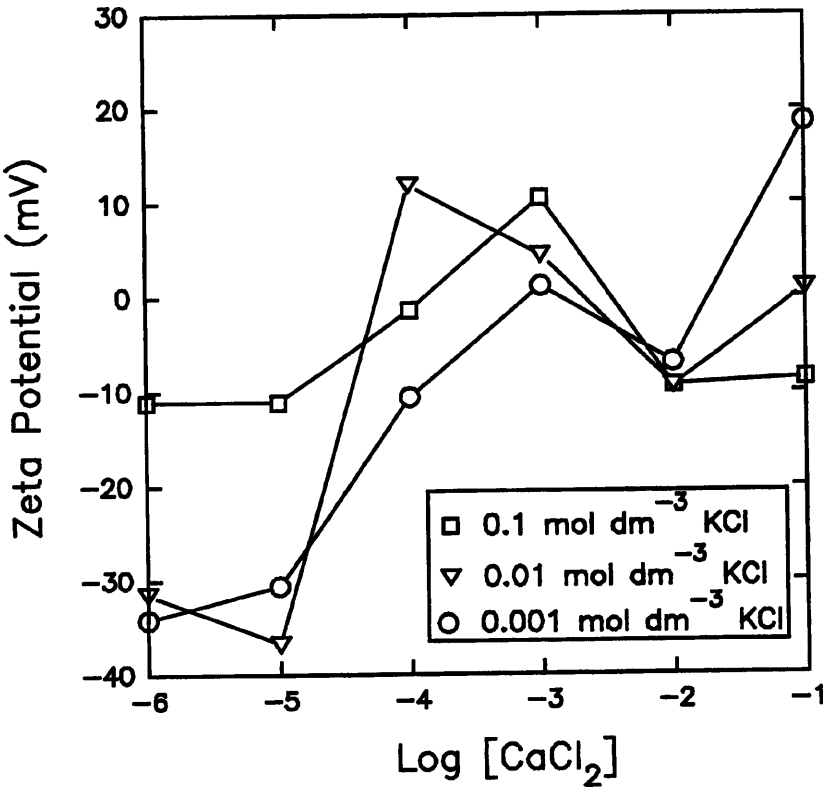

Figure 4.13 Effect of Ca^{2+} ions on zeta potential of RVC (pH 6.0)

As with the polystyrene latex particles for the same background KCl concentration varying the $CaCl_2$ concentration may change the sign of zeta potential. The difference is that for KCl concentrations higher than 0.001 mol dm^{-3} KCl the $(Ca^{2+})_{limiting}$ takes two values. As with the polystyrene latex particles these value may become important if Ca^{2+} ions are present in the

solution at appreciable concentration.

4.5.2 Operating region of the applied potential

The shape of the total interaction energy curve and existence of energy minima provide information about the possibility of deposition occurring and if so whether this deposition is permanent i.e. if particles are trapped in the primary minimum energy level. The equations that will be used to simulate the total interaction energy between the particles and the RVC collector will be elaborated in Chapter 6. From these simulations it will be decided for a set of experimental conditions e.g. electrolyte concentration, pH and RVC collector potential whether favourable or unfavourable deposition condition is prevalent. From these simulations the collector potentials which give the required deposition will be estimated.

To implement the collector potential determined care must be taken to ensure that this potential can be applied to the RVC electrode since the RVC collector potential is limited by gas evolution potentials in electrochemical cells which have been briefly discussed in section 2.4. A possible scheme for the mechanism of evolution of hydrogen and oxygen has also been provided. In section 2.5 the experiments carried out by Oren et al. (1987) were discussed. One of their conclusions was that due to high surface area of their electrodes and evolution of gases the pH in the suspension changed and thereby the deposition rate changed.

To investigate the range of operating potential for the present RVC adsorption cell, potentiometric scanning of the RVC cell was carried out. Electrolyte KCl solution of various concentrations and pH were made up and then pumped through the column.

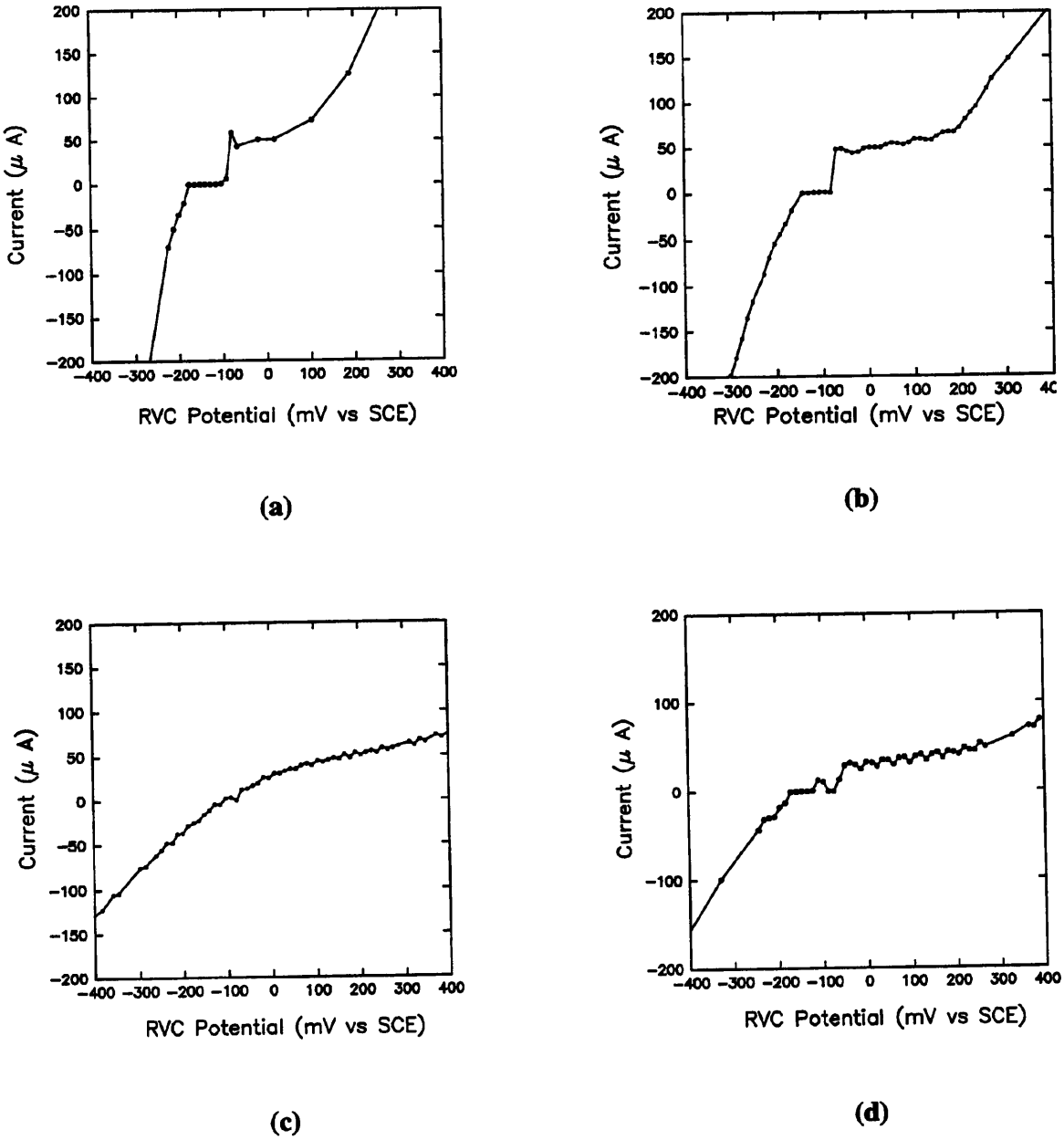

Figure 4.14 Decomposition curves:
a: 0.01 mol dm^{-3} KCl, rest potential 67.6 mV, pH 10.4, conductivity 1270 μS
b: 0.01 mol dm^{-3} KCl, rest potential 76.2 mV, pH 6.3, conductivity 1260 μS
c: 0.001 mol dm^{-3} KCl, rest potential 80.5 mV, pH 5.8, conductivity 128 μS
d: 0.001 M KCl, rest potential 60.6 mV, pH 9.4, conductivity 172 μS

When the cell's rest potential and the effluent pH and conductivity were stable and similar to the inlet then a potential scan of -1000 mV to 1000 mV was applied to the RVC electrode. Figure 4.14 shows some typical potential-vs-current (or decomposition curves). It can be deduced from these graphs that approximately within a potential range of -300 to +300 mV there will not be significant gas evolution but in fact the value for the hydrogen overpotential of the RVC is calculated in Chapter 6 (section 6.1.3) and it is approximately -130 mV.

4.6 PROCEDURE FOR ADSORPTION ONTO SPHERICAL COLLECTORS

There has been numerous reports of deposition experiments onto spherical glass beads in the literature, as discussed in section 2.3.1 and it has been mentioned that the procedure for this type of experiments is now well established. Following this established technique the flow set-up was arranged as seen in Figure 3.1. A typical adsorption run carried out consisted of the following steps:

1. Preparation of 6 dm^3 of KCl electrolyte solution of required concentration and pH.

2. Preparation of particle suspension. In this case 0.2 g of 5.4 μm diameter latex particle powders was weighed and dissolved in 15 cm^3 of distilled water which had been filtered through a 1 μm membrane filter. This was allowed to stand in an ultrasonic bath for 1.5 hours to help with formation of a stable monodispersed suspension. The particle number concentration ranged from $0.41x10^6$ particles cm^{-3} to $0.44x10^6$ particles cm^{-3}.

3. The amount of dry glass beads required to fill the column to a height of 160 mm was estimated:

specific gravity of glass beads=2.95

cross sectional area of the column= πr^2 =4.5 cm^2

a bed depth of 16 cm had a volume of 72.32 cm^3 and assuming a bed

porosity of 0.4:

$$V_{total} = V_{void} + V_{beads} \quad (4.5)$$

Therefore, the volume of glass beads required to fill the column to a height of 16 cm was 51.66 cm^3 and consequently 152.4 g of glass beads were required to fill the column to a height of 16 cm.

4. Glass beads provided by the manufacturer contained impurities and dust like glass particles and these had to be removed prior to an experiment. The equilibration of glass beads consisted of the following steps:

a) rinsing the glass beads with distilled water several times.

b) soaking in 0.1 mol dm^{-3} NaOH solution and then leaving in an ultrasonic bath for 30 minutes.

c) rinsing with distilled water

d) soaking in 0.1 mol dm^{-3} HNO_3 solution and then leaving in ultrasonic bath for 30 minutes.

e) rinsing with distilled water several times and if following several rinses the beads still left a turbid residue the steps (b) onwards were carried out until there was no trace of residues which could have affected the turbidity measurement readings.

f) the glass beads were left overnight in an oven set at 65^0 C until dry.

5. Column was filled with electrolyte solution and the glass beads were poured into the column.

6. Electrolyte was pumped, using a Watson Marlow peristaltic pump, in an upward flow mode followed by downward flow mode. This was done to remove air bubbles trapped between glass beads.

7. Step 6 was continued until the outlet had a stable pH, which in all experiments were higher than the inlet pH, and then the pump delivering the polystyrene latex particles was switched on. These particles were mixed with KCl electrolyte solution at plastic T-piece junctions and also bends in silicon tubing carrying the suspension into the column.

8. Analysis of the inlet and outlet for particle number concentration was carried out by means of the turbiditimeter (section 3.3).

The turbidity readings so obtained were converted into particle number concentration using the turbiditimeter's calibration chart (see 4.1) and these were then plotted as particle break-through curve. This involved plotting the ratio of the outlet particle number concentration to the inlet particle number concentration (C_o/C_i) against time (see Chapter 5).

4.7 PROCEDURE FOR ADSORPTION ONTO RVC COLLECTOR

Experiments in the RVC system was somewhat similar to the glass bead system as far as the method for construction of the break-through curve was concerned. However, the principle difference was the different column design and the shorter periods of RVC equilibration periods required for the RVC and in the application of electrical potential. The main objective of these experiments were to observe the effect of electrode potential on deposition and to seek ways to manipulate the electrode potential externally so that an effective tool for selective deposition may be obtained.

Prior to an experiment, two characteristics of the RVC adsorption cell were investigated, namely the mean residence time and ohmic drop, as discussed below.

4.7.1 Mean residence time

Due to the highly porous nature of the bed (97% porosity) low resistance to flow was offered and it would be informative if mixing characteristic and the residence time of fluid through the column could be estimated. This provides information regarding the complete break-through time when deposition experiments were to be carried out.

Levenspiel (1972) discusses in detail the varying degrees of mixing that occurs in open and closed vessels. To estimate the amount of dispersion in vessels, he proposes a stimulus-response technique which involves disturbing the system by means of a stimulus and then observing how the system responds to this stimulus. Analysis of the response gives the desired information about the system.

The procedure for carrying out tracer experiments is similar to that of adsorption with the difference that concentrated KCl solution was used instead of polystyrene latex particles.

The stimulus-response technique involved passing distilled water through the column until the pH and conductivity of outlet were stable and similar to the inlet whence KCl was introduced to a T-piece junction (see Figure 4.18) where it was mixed with water and subsequently this was fed into the column.

The effluent conductivity k^* at time t and the initial value k^*_0 at t=0 were measured using Jenway 4010 conductivity meter. The tracer break-through curve was constructed by plotting k^*/k^*_0 against t. Tobiason (1987) carried out similar type of investigation for his glass bead packed bed. He determined the mean hydraulic residence time of the filter from the break-

through curves by:

$$t_{calc}=\sum_{i}^{n}\Delta t_i\left[1-\left(\frac{k^*}{k^*_0}\right)_i^{avg}\right] \qquad (4.6)$$

Where Δt_i is the interval between samples taken at times t_i and t_{i-1} and $(k^*/k^*_0)_i^{avg}$ is the average value of k^*/k^*_0 for the time interval. The mean residence time can also be determined by finding the area between the experimental curve and a k^*/k^*_0 of 1.

The tracer experiments can also be used to find out about the extent of mixing occurring in the column. If there was no mixing in the column, *plug flow* should prevail and an step response from 0 to 1 for k^*/k^*_0 at t/t_{calc} of 1 should occur. Conversely, if there was complete mixing in the column then an exponential rise to a k^*/k^*_0 of 1 should occur.

Figure 4.15 shows a typical tracer break-through curve obtained for the RVC column from which it can be seen that plug flow was not achieved in the system. The corresponding mean residence time calculated for the data shown in Figure 4.15 is 8.3 minutes. Assuming equivalent transport for ions and fluid, the residence time calculated represents the average time for a fluid element to travel from the valve ahead of the filter to the discharge point from the filter effluent tubing.

Although the particle-break through curve obtained from a deposition experiment is different principally due to the presence of solid particles and consequently the corresponding mean residence time for the suspension containing polystyrene latex particles is different from the tracer, but guidelines may be obtained about their approximate mean residence time and

therefore duration of an adsorption experiment may be decided.

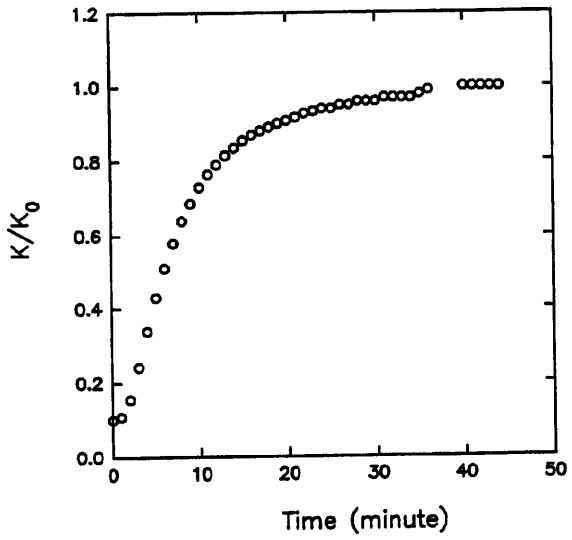

Figure 4.15 Tracer experiment for 34 cm^3min^{-1} volumetric flowrate

4.7.2 Ohmic drop measurement

Occurrence of ohmic drop in an electrochemical cell has been discussed in section 2.4. It is caused by the resistance to the flow of current offered by the electrolyte solution between the tip of reference electrode and the working electrode. One way of avoiding this problem was discussed in the same section to be the use of a luggin probe. The implementation of luggin probe into the present adsorption column has been explained in section 3.2.1 (see Figure 3.8). An approximate technique for measurement of ohmic drop is based on the *current interruption* principle which has been described in section 2.4 (see Figure 2.8). The ohmic drop measurement for the present system had a twofold purpose. First, the ohmic drop for the system under study was estimated and secondly it was utilised as a test for establishing whether all electrical connections in the system were satisfactory. Any loose connection or

short circuit would have produced an unstable cell current and rest potential values. A typical ohmic drop measurement as shown in Figure 4.16 involved applying 1.0 V between the working and counter electrodes using a power supply. The RVC potential was monitored remotely using the Archimedes computer connected via an interface to a Potentiostat as explained in Chapter 3. The current flow between the electrodes was monitored using a DVM connected in series onto the wire connecting one of the electrodes to the potentiostat. When the RVC potential and the cell current were stable (point A in Figure 4.16) then leads connecting the power source to the cell were removed. The RVC potential immediately after removal of power source (point B in Figure 4.16) was noted as accurately as possible and the consequent decay to the rest potential (point C in Figure 4.16) was also monitored. The difference between potentials A and B was taken to be the value for ohmic drop for the cell. In few cases the effect of positioning of the reference electrode upon the RVC potential and ohmic drop was examined and these are elaborated in Chapter 6.

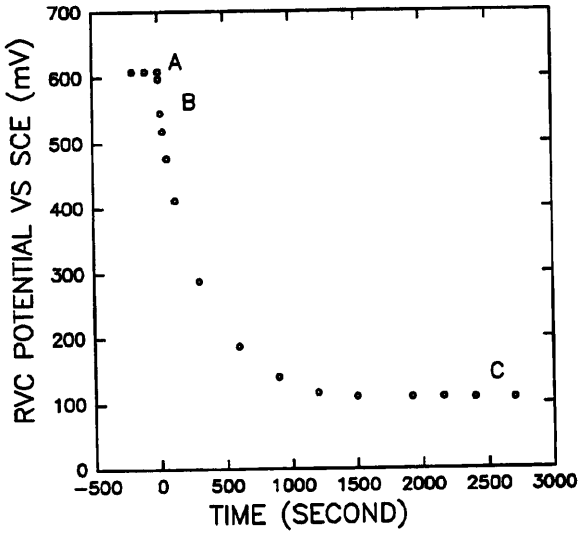

Figure 4.16 Typical current interruption cycle for measurement of ohmic drop

4.7.3 Adsorption experiments in the RVC system

A detailed description of the column has been given in section 3.2.1. It was mentioned that the column was designed so as to allow for easy access for insertion/removal of the RVC piece. The dismantled column (see Figure 3.6) was thoroughly cleaned and then the RVC piece was inserted with the small glass tube in the centre of the piece (see Figure 3.10) placed inside the arranged hole in the column (see point 6 in Figure 3.5). With the RVC piece inserted then the membrane carrier with a clean membrane was pushed into the column against the RVC so that when in the right position there was no gap left between the RVC and the Perspex membrane carrier.

Once the RVC was securely placed with its small glass tubing through the hole allocated then the hole was sealed using silicon rubber sealant.

Next the bottom and top perforated plates were placed in position. For the low velocity experiments (1.6, 4.5 and 5.6 $cm^3\ min^{-1}$ volumetric flowrates) it was found that the top perforated plate did not prove effective and consequently it was not used. The reason for this was that at these rates the flow was in the form of a few drops at a time and subsequently the drops hit the holes in the centre of the perforated plate. This was in contrast to the higher volumetric flowrates (12 and 34 $cm^3\ min^{-1}$) wherein the flow formed itself into a stream and when it hit the plate a thin layer of liquid was formed above it resulting in a better distribution of flow through all the holes.

It is interesting to note, as shown in Appendix E, that due to the high porosity of RVC structure (97%) the superficial velocity and the interstitial velocities do not differ by a significant amount, however, there is a significant difference between these velocities for the glass bead column (typical porosity 40%).

Finally the top and bottom covers were located in their positions by means of plastic screws. To prevent electrolyte leaking, neoprene rubber gaskets were placed between the covers and the column.

The set-up for these experiments can be seen in Figures 4.17 and 4.18. These experiment were fundamentally similar to those carried out onto glass beads. Prior to each experiment the RVC electrode was analysed for its mean residence time and the ohmic drop as described in previous parts.

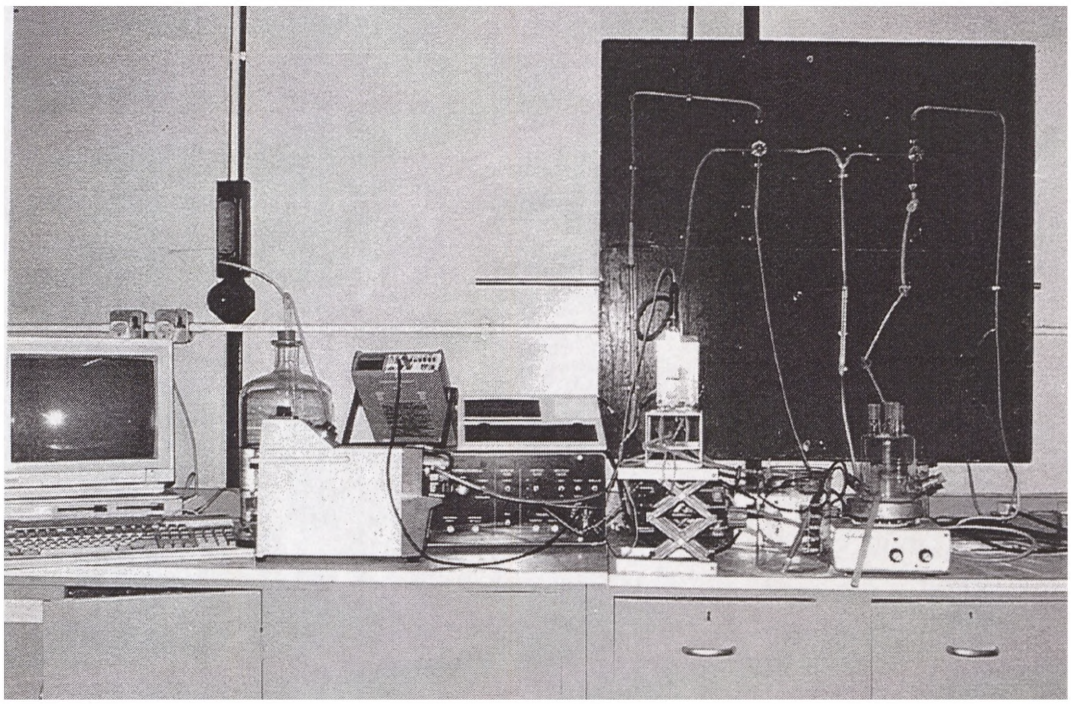

Figure 4.17 Photograph of the experimental assembly

Having established the integrity of the column, by means of tests for loose electrical connections and leakages, the equilibration of the RVC electrode commenced.

The two way valves (11a) and (11b) allowed flow in two directions namely directions (1) and (2) as shown in Figure 4.18. When valve (11a) was positioned at (1) it allowed the flow to

be directed towards the plastic T-piece (12) and consequently mixing with polystyrene latex occurred. Similarly when the two way valve (11b) was positioned at (1) it allowed the mixed electrolyte/latex suspension to be diverted to drain and when at position (2) the mixture was directed into the column. With the two way valve (11a) at position (2) and its outlet connected to the inlet of column, the equilibration of RVC began which consisted of passing potassium chloride solution, of the same concentration and pH as in deposition experiment, through the column from a 10 dm^3 glass vessel until the outlet achieved the same conductivity and pH as that of inlet. During the equilibration stage the Archimedes computer and the potentiostat had been switched on with the predetermined potential cycle entered into the computer's interface menu. Prior to starting the programe, the interface software allowed for the rest potential of the working electrode to be measured. The total cell potential was also measured using the DVM via a connection to the potentiostat's input terminal for the working and counter electrode. When it was decided that all readings were stable the potentiometric potential controlling of the RVC electrode began.

Prior to the introduction of polystyrene latex particles the following were monitored for their stability:

-Inlet stream pH, conductivity and turbidity

-outlet stream pH, conductivity and turbidity

-cell current

-RVC potential by means of crocodile clips attached to the input terminals of the potentiostat for the working and reference electrode

-cell potential with the same technique as for the RVC but using the input terminals for the working and counter electrode.

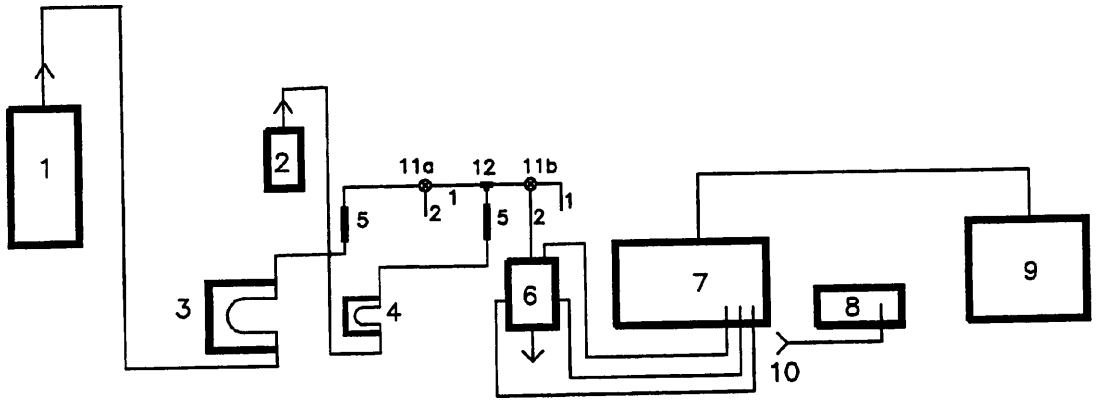

Figure 4.18 Schematic diagram of the flow arrangement for adsorption experiments, 1: KCl feed tank, 2: polystyrene latex particle feed tank, 3: high output peristaltic pump, 4: low output peristaltic pump, 5: rotameter, 6: adsorption column, 7: potentiostat, 8: DVM, 9: Archimedes computer, 10: crocodile clips, 11a,11b: two-way valves, 12: plastic T-piece

When all these readings, notably the cell current and RVC's potential, were steady and with the two way valve (11b) at position (1) then the low output peristaltic pump (4) was switched on. The peristaltic pump (4) operated at a low speed and it took approximately 1 hr to establish a steady output. With the peristaltic pump (4) having a steady output the valves (11a) and (11b) were positioned at (1) and (2) respectively and the resultant stream constituted the feed which was analysed for its turbidity, conductivity and pH. A stop clock was turned on the moment that the feed was introduced into the column.

Throughout the experiment the effluent was analysed for its turbidity, conductivity and pH and the cell was monitored for its current and potential. In few experiments after termination

of the potentiometric program the feed was allowed to flow through the column so that the effect of removal of external potential on deposition was investigated. Remotely measured cell current and RVC potential were stored in a floppy disc and this were then kept for further analysis.

At the end of an experiment the cell was dismantled by removing the top and bottom Perspex covers with their associated rubber gaskets and then the top and bottom perforated plates were removed. Next the membrane carrier was pushed out of the column and finally the RVC piece was taken out. Several attempts were made to observe the RVC under optical microscope but unfortunately it was found that light did not penetrate deep enough into the piece and at the same time the thought of taking SEM photographs was abandoned since it meant that the RVC piece had to be cut and this would probably have resulted in loss of particles.

The feed suspension was prepared using the same technique described in section 4.6. The feed particle number concentration varied slightly from one experiment to another but generally it was within the range 0.51-0.97 x 10^6 particles cm^{-3}.1

CHAPTER 5

ADSORPTION EXPERIMENTS ON GLASS BEADS

In the preceding chapters the experimental apparatus for adsorption experiments onto spherical glass bead and RVC collector have been described. It has also been noted that the objective of experiments using glass beads have been to provide guidelines for the adsorption studies onto the RVC collector.

This chapter discusses the results of deposition experiments of polystyrene latex particles onto spherical glass bead collectors and it is divided into three parts:

- Estimation of the interaction energies between particle and collector and between particle and particle.
- Discussion of the experimental data and comparison with prediction of the DLVO theory from the previous part.
- Comparison of the experimental results with the previously published data.

5.1 ESTIMATION OF INTERACTION ENERGIES

A particle in suspension approaching a collector interacts with both the the neighbouring particles and the collector. Therefore, a better representation of the adsorption process should involve discussion on both of these interactions. In the following paragraphs the equations utilised to estimate these interaction energies will be discussed.

Interaction energies between particles

The interaction energies between polystyrene latex particles in suspension is assumed to

consist of the attractive van der Waals and the repulsive electrical double layer and Born energies.

To estimate the van der Waals energy the expression due to Gregory (1981) quoted in Table 2.3 is used:

$$V_A = -\frac{A}{12h}\left[1 - \left(\frac{hb}{\omega}\right)\ln\left(1 + \frac{\omega}{bh}\right)\right] \qquad (5.1)$$

Where ω the characteristic wavelength is 100 nm.

The electrical double layer has been estimated using the expression due to Bell et al. (1970):

$$V_R = 4\pi\epsilon\psi_o^2 \frac{a(h+a)}{(h+2a)} \ln\left[1 + \left(\frac{a}{h+a}\right)\exp(-\kappa a)\right] \qquad (5.2)$$

The Born repulsive energy is estimated using the expression due to Feke et al. (1984).

$$V_B = \frac{A\,\sigma_c^6}{37800\,D\,a^6}\left[\frac{-2D^2+6}{D^7} + \frac{D^2+14D+54}{(D+2)^7} + \frac{D^2-14D+54}{(D-2)^7}\right] \qquad (5.3)$$

Where the collision diameter σ_c is 0.5 nm and D is the centre to centre separation distance between particles, (h+2a). The Hamaker constant for polystyrene latex in water has been taken from Jia (1992) to be 1×10^{-20}J. The total energy of interaction is given by:

$$V_T = V_A + V_R + V_B \qquad (5.4)$$

The Fortran programme PPENERGY (see Appendix C) written to calculate V_T from the above expression on Hewlett-Packard workstation which run HP-UX version 7.0, Hewlett Packard's implementation of AT&T's system V.2 Unix with Berkeley 4.3 extensions. The total interaction energies were evaluated for separation distances (h) up to 500 nm and these were

then plotted within the same programme by using the graphic software Uniras version 6v3a.

Interaction energies between particle and collector

The interaction energies operating between particle and collector are assumed to be the same as those between particles. The same expression for the London-van der Waals attractive energy is utilised. Since the diameter of the particle, 5.4×10^{-6} m, is small compared to that of the spherical glass bead, 400×10^{-6} m, then it can be assumed that the electrical double layer may be estimated from the expression for sphere-plane derived by Ruckenstein and Prieve (1976):

$$V_R = 16\epsilon \left(\frac{kT}{e}\right) a \tanh\left(\frac{e\psi_1}{4kT}\right) \tanh\left(\frac{e\psi_2}{4kT}\right) \exp(-\kappa h) \qquad (5.5)$$

The Born repulsive energy is estimated from the expression for a sphere and a plate derived by Ruckenstein and Prieve (1976):

$$V_B = \frac{A\sigma^6}{7560}\left[\frac{8a+h}{(2a+h)^7} + \frac{6a-h}{h^7}\right] \qquad (5.6)$$

The Fortran programme PCENERGY (Appendix C) was written to calculate the total interaction energies and to provide the plots of these data.

5.2 EXPERIMENTAL DATA

There were altogether 5 experiments carried out to investigate the reproducibility of the experimental procedures. The experimental data can be seen in tabular form in Appendix B. These experiments were all carried out at the same volumetric flowrate of 22 $cm^3\ min^{-1}$.

The particle break-through curves have been plotted as shown in Figure 5.1. The two runs at

0.01 mol dm^{-3} KCl were initially meant to have been carried out under exactly the same experimental conditions but the same outlet pH was not achieved thereby resulting in different profiles. The particle-particle and particle-collector interaction profiles can be seen in Figures 5.2 and 5.3 respectively. The data used for generating these graphs can be seen in Table 5.1.

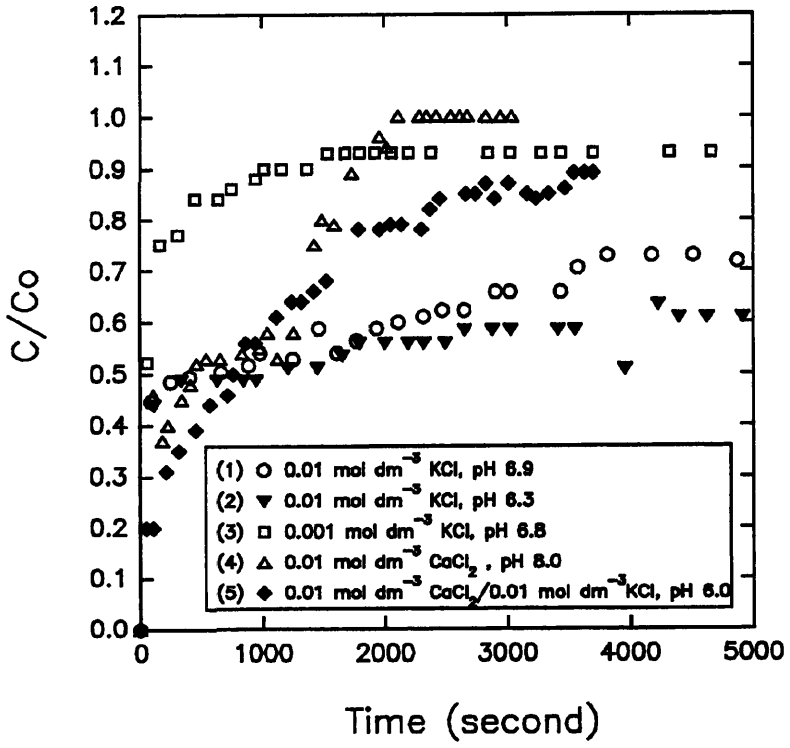

Figure 5.1 Particle break-through curves for deposition of polystyrene latex particles onto spherical glass beads

Figure 5.2 shows that at the range of parameters considered for the runs 1, 2 and 3 the electrical double layer of particles were compact leading to no interaction. This obviously means that the particles should aggregate but other static interaction energies such as the steric and hydration repulsive energies may contribute to the particles retaining a monodispersed state. The particle-collector interaction energy profiles for the runs 1 and 3 is also shown in Figure 5.2. The total interaction energy curve for run 1 shows that there is

mainly van der Waals attractive energy in operation between the particle and collector resulting in a favourable condition thereby high deposition rate is expected which is confirmed by the particle break-through curve for run1 in Figure 5.1. The total interaction energy curve for run3 shows a high energy barrier (>15 KT) and therefore the primary minimum is beyond reach for the particles and consequently the run3 in Figure 5.1.

Unfortunately the deposition experiments carried out using mixtures of $KCl/CaCl_2$, as shown in Figure 5.1, can not be analysed in the same fashion since the equations used to estimate low deposition rate is expected which is confirmed by the particle break-through curve for the total interaction energy are only valid for 1:1 electrolyte. However, it can be seen that addition of $CaCl_2$ to the KCl solution causes less deposition to take place and further reduction in deposition is caused by utilising only $CaCl_2$ solution. This can be interpreted that addition of $CaCl_2$ causes stronger repulsive energy between the particle and collector.

Table 5.1 Values for parameters used to estimate the interaction energy profile for the particle-particle and particle-collector

particle-particle		particle-collector	
Hamaker constant=$1x10^{-20}$ J		Hamaker constant=$1x10^{-20}$ J	
Run number	Particle zeta potential (mV)	Run number	Collector zeta potential (mV)
1	-8.5	1	-50.0
2	-7.0	2	-46.0
3	-10.0	3	-60.0

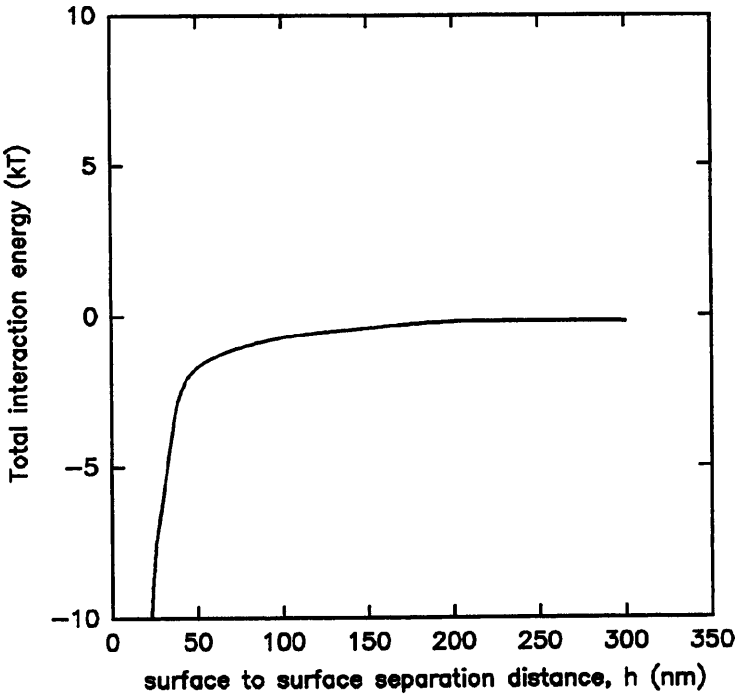

Figure 5.2 Energy of interaction between polystyrene latex particles for runs 1 and 3

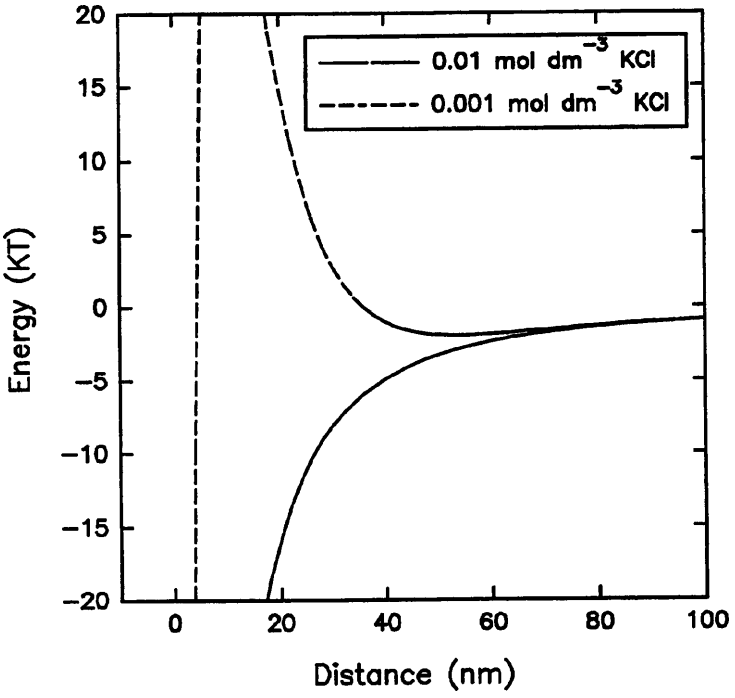

Figure 5.3 Energy of interaction between particle and collector for run1 and run3

5.3 COMPARISON OF RESULTS WITH OTHER PUBLISHED DATA

The same trend was observed by Elimelech and O'Melia (1990) when they carried out deposition of 0.753×10^{-6} m diameter latex particles onto 200×10^{-6} m diameter glassbeads. As the KCl electrolyte concentration increased the deposition rate also increased which they argued was due to the reduced repulsive energies caused by compression of the diffuse double layer.

The experimental results are compared quantitatively with the results obtained by Tobiason (1989) and Yoshimura et al. (1980). The results are analysed by calculating the single collector efficiency (η), the collision efficiency factor (γ) and the filter coefficient (λ). The single collector efficiency is calculated using equation (2.24), the collision efficiency factor using equation (2.26) and the filter coefficient using equation (2.23) which have all been discussed in section 2.3.1. Table 5.2 shows the values used for estimation of the single collector efficiency. Table 5.3 shows the values for the collision efficiency factor and filter coefficient.

Table 5.2 Estimation of single collector efficiency for run1

A_S	N_{Pe}	N_{Lo}	N_G	η
37.96	1.979×10^{16}	5.0×10^{-13}	8.0×10^{-9}	34.36×10^{-5}

Table 5.3 Values for the collision efficiency factor and the filter coefficient for runs 1, 2 and 3

Run number	Collision efficiency factor (γ)	Filter coefficient (λ)
1	1.96×10^{-2}	1.50×10^{-4}
2	3.46×10^{-2}	2.67×10^{-4}
3	5.60×10^{-3}	4.23×10^{-5}

Yoshimura et al. (1980) carried out deposition of 5.7×10^{-6} m latex particles onto 540×10^{-6} m glass beads at a superficial velocity of 1.1×10^{-3} m/s. They changed the NaCl electrolyte concentration and found that as concentration decreased the filter coefficient decreased. They argue that this was probably due to the increase in the repulsive energy of the electrical double layer as the ionic strength decreased. Similar pattern can be seen in the values for the filter coefficient for the present study although the exact values are different due to such factors as the different bed depth, superficial velocity and zeta potentials of the particle and collector.

Tobiason (1989) carried out deposition of 4 μm latex particles on 400×10^{-6} m glass beads (250 mm bed depth, 1.4×10^{-3} m/s loading rate, NaCl electrolyte). He quoted values of 5.2×10^{-3} and 3.2×10^{-2} for the collision efficiency factors for the 0.001 and 0.01 mol dm^{-3} NaCl solutions. The present study comprised deposition of 5.4 μm latex particles on 400 μm glass beads (16 cm bed depth, 0.097 cm/s loading rate, KCl electrolyte) which come very close to the experimental condition of Tobiason. The values for the collision efficiency factors quoted in Table 5.3 are similar to those obtained by Tobiason.

CHAPTER 6

ADSORPTION EXPERIMENTS ON RVC COLLECTOR

This chapter discusses the main objective of the present study as discussed in Chapter 1. The experiments investigated the possibility of utilising the application of a modest electrical potential to the RVC collector to manipulate the rate of deposition of colloidal particles.

The effect of varying a number of experimental conditions (listed below), on the deposition rate of *polystyrene latex* and *Hypercarb* particles, will be considered:

- variation of superficial fluid velocity.
- variation of RVC collector potential in combination with different electrolyte concentrations.

This chapter is divided into two parts. The first part (6.1) discusses the effect of changing the above variables on the deposition rate of polystyrene latex particles. The experimental results are compared with theoretical predictions based on the magnitude of primary/secondary minima in the DLVO plot of the total energy of interaction. The second part (6.2) discusses similar issues, but for the deposition of *Hypercarb* particles. The validity of applying the DLVO theory to interpret these experiments will be critically assessed in terms of occurrence of primary/secondary minima and an attempt will be made to justify any discrepancies. A more detailed analysis of relevant factors contributing to the discrepancies will be provided in Chapter 8.

6.1 DEPOSITION OF POLYSTYRENE LATEX PARTICLES ON RVC COLLECTOR

Adsorption of colloidal particles onto larger surfaces (composed of different materials to the dispersed particles), often termed heterocoagulation, involves the *transport* of particles to the vicinity of the collector and the *adhesion* to the collector surface by means of surface forces.

The transport step may occur in several ways:

-the particle may be transported towards the collector by means of the bulk fluid flow.

-the particles may be collected due to their size. This is often termed interception.

-the particles may collide with the surface of collector under the action of their own weight. This is termed sedimentation.

-the particle may collide with the surface of the collector due to their momentum. This is termed inertial impaction.

-the colloidal particles become bombarded by the movement of the molecules in the suspending medium. The resulting transport is termed diffusion.

For non-Brownian particles (diameter > 1 μm) the diffusion process becomes negligible compared to the bulk fluid flow. Since the polystyrene latex particles utilised in this study were 5.4 μm in diameter it then becomes possible to ignore the contribution due to diffusion. For reasonably low flowrates, Re < 1, the inertial impaction is usually assumed to be negligible compared to the hydrodynamic and surface forces. The highest particle Reynolds number employed in this study is 2.8×10^{-3} and provides sufficient justification for ignoring the contribution of the inertial impaction.

It may therefore be concluded that for the present system the dominant forces in the

deposition process are the hydrodynamic and surface forces. There has been several important studies carried out in the literature regarding the mechanism of operation of the surface forces. For example Adamczyk (1989) argues that for favourable deposition conditions the existing theoretical models agree favourably with the experimental results. However, when unfavourable deposition condition prevails and a high energy barrier of typically > 15 kT exists then great deal of disagreement occurs between the experimental results and theoretical models.

The simplest and yet most practical model for representing the colloidal interaction energies is the DLVO model. In this model the total energy of interaction between the particles and RVC are assumed to be the sum of London-van der Waals and electrical double layer. The expressions used for the estimation of individual contributions were given for the spherical collector system in section 5.1.

The experimental procedures have been explained in detail in Chapter 4. A series of twenty one experiments were performed as detailed in Appendix B.

To estimate the London-van der Waals energy a value for the Hamaker constant must be used for polystyrene-water-RVC and *Hypercarb*-water-RVC systems. Hamaker (1937) states that for most substances the Hamaker constant should lie in the range $1.0\text{x}10^{-19}$-$1.0\text{x}10^{-21}$ J. Values for the Hamaker constant can be estimated from the following relationship:

$$A_{12/3} = \left(A_{11/3} \times A_{22/3} \right)^{1/2} \qquad \textbf{(6.1)}$$

Where $A_{11/3}$ is the Hamaker constant for material 1 in medium 3, $A_{22/3}$ is the Hamaker

constant for material 2 in medium 3 and $A_{12/3}$ is the Hamaker constant between materials 1 and 2 in medium 3. The Hamaker constants for polystyrene-water and carbon-water were taken to be $1.0x10^{-20}$ J and $3x10^{-20}$ J, respectively, from Fowkes (1964). Utilising these values along with equation (6.1) yields values of $1.7x10^{-20}$ J and $3x10^{-20}$ J for polystyrene-water-RVC and *Hypercarb*-water-RVC respectively. Oren (1986) and Joscelyne (1993) used values of $3x10^{-20}$ J for polystyrene-water-carbon in their theoretical analysis.

6.1.1 Preliminary tests

As explained in Chapter 4, prior to a deposition experiment an inert tracer analysis and an ohmic drop measurement test were performed. These were carried out to provide useful information regarding the RVC slab to be used for an adsorption experiment. These will be elaborated further in the following paragraphs.

Inert tracer analysis

This analysis was carried out so that the mixing characteristics of the column and an estimate of the residence time of colloidal particles in the column could be obtained. The procedure for carrying out this analysis was discussed at length in section 4.7.1.

A wide range of volumetric flowrates was employed but, as discussed below, the majority of experiments were carried out at the lowest flowrate of 1.7 cm^3 min^{-1} and therefore more attention was given to the tracer analysis at this lower flowrate to confirm the reproducibility of the tracer break-through curves.

Figure 6.1 shows the tracer break-through curves for the volumetric flowrates of 34 and 1.7 cm^3 min^{-1}. Diagram (b) shows that the reproducibility of the tracer break-through curve was

examined by carrying out several tests and these are shown as different symbols. Note the different time scale for the Figures 6.1a and 6.1b. The complete break-through times for these flowrates are 46 minutes and 3.6 hours respectively. The hydraulic mean residence time was calculated for these curves using equation 4.6 (Chapter 4). The values for 34 and 1.7 cm^3 min^{-1} flowrates were 8.3 and 40 minutes respectively.

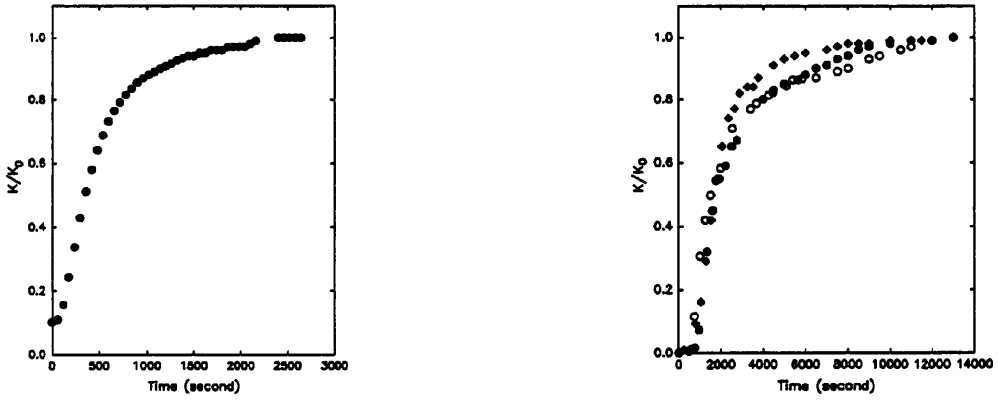

(a) (b)

Figure 6.1 Tracer break-through curves for volumetric flowrates of a:34 cm^3 min^{-1} and b:1.7 cm^3 min^{-1} repeated three times

It was explained in Chapter 4 that it may be assumed that ions, fluid and colloidal particles travel at the same rate and also that the residence time calculated represents the average time for travel from the valve upstream of the filter (part 2 in Figure 3.5) to the discharge point from the filter effluent tubing (part 9 in Figure 3.5). For example considering the tracer break-through curve at 1.7 cm^3 min^{-1}, it takes a single polystyrene latex particle approximately 40 minutes to travel from the inlet tubing through the column, and if not deposited, then out of the column through the outlet tubing.

Therefore prior to performing an experiment at the volumetric flowrate of 1.7 cm^3 min^{-1} it must be realised that for at least 40 minutes the outlet will have very low turbidity and consequently the duration of the experiment must be determined in such a way that at least 40 minutes is allowed before an observable effect of variation of RVC potential or the electrolyte concentration on the deposition rate may be noticed.

Ohmic drop measurement

It has been speculated that there would be two main problems associated with the application of potential to the RVC packing potentiostatically. First, the problem of establishing a good contact to the RVC packing - this has been discussed in Chapter 3. Secondly, the problem of the lack of knowledge about the *true* potential of the RVC electrode under potentiostatic control. This means that is there is no way of knowing with absolute certainty if the RVC potential in an experiment is the same as that which the potentiostat has been programmed to apply. It would be ideal if a technique could be devised to investigate whether the RVC potential is the same as that which potentiostat is applying.

There have been numerous studies dealing with the double layer characteristics of electronically conducting materials, such as carbon. The double layer characteristics of thin film electrodes, by means of surface conductance measurements, was studied by Hansen et al. (1978). The double layer characteristics of high surface area electrodes was studied by Oren et al. (1985, 1986a, 1987a) and by Soffer et al. (1972) by means of measuring the change in their interfacial tension which manifested in minute but detectable dimensional changes.

Within the scope of this project the only practical method for further analysis of the problem was to map the RVC surface for irregularities in the RVC potential and at best to establish that the potential is constant anywhere at the surface of the RVC. This was done by carrying out ohmic drop measurements with the reference electrode positioned at different locations along the length of the RVC packing. The ohmic drop was determined and the decay towards the steady state value was also observed.

Figure 6.2 shows one such measurement carried out prior to the deposition experiment (no Ex19). The ohmic drop was measured with the reference electrode positioned at four distinct locations. The first two measurements were done with the top Perspex plate and membrane carrier (parts 3 and 13 respectively in Figure 3.5) removed and then the reference electrode was inserted into the gap between the RVC piece and the stainless steel slab. The other two measurements were done with the reference electrode inserted into the 'side arms' 1 and 2 (see Figure 3.5).

The values for the ohmic drop measured were 3, 1, 4 and 4 mV for the reference electrode placed inside and middle of the column, inside and at the top of the column and 'side arms' 1 and 2 respectively. These figures show that the ohmic drop and the pattern for the decay towards the rest potential is approximately the same for all different locations. This result may be interpreted that positioning of reference electrode at different location does not produce irregularities in the measured RVC potential and everywhere the potential is constant but further analysis, such as those previously mentioned, is required to measure the magnitude of the potential. If the decay curve of the ohmic drop was seen to be unstable the experimental run was abandoned and a new RVC piece was chosen.

Additionally it must be borne in mind that the use of a SCE as the reference electrode means that the RVC potential readings obtained are with respect to the SCE. The potential of SCE is 0.242 V with respect to the SHE. This means that the RVC potential measured for example in run Ex12, -300 mV vs SCE as shown in Figure 6.17b, will in fact be measured at -85 mV vs SHE.

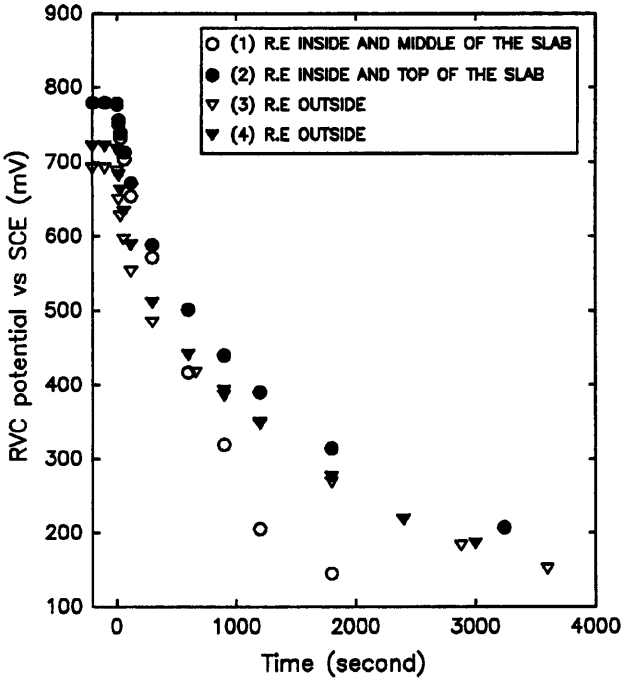

Figure 6.2 Ohmic drop measurement for run Ex19 with the estimated ohmic drop value for locations 1: 3 mV, 2: 1 mV, 3: outside and the left 'side arm' 4 mV 4: outside and the right 'side arm' 4 mV

6.1.2 Variation of superficial fluid velocity

The zeta potential of polystyrene latex particles was discussed in Chapter 4 and it can be seen from Figure 4.3 that the particles carry negative charge over a wide range of pH and KCl

concentrations. When a negatively charged particle approaches a positively charged RVC collector a net attractive energy develops between the surfaces and this condition, where no repulsive electrical double layer exists between the surfaces, is known as the favourable deposition condition. Figure 6.3 shows the DLVO prediction of the existing particle-collector interaction energies at KCl concentration of 0.0001 mol dm^{-3}. The profile corresponding to

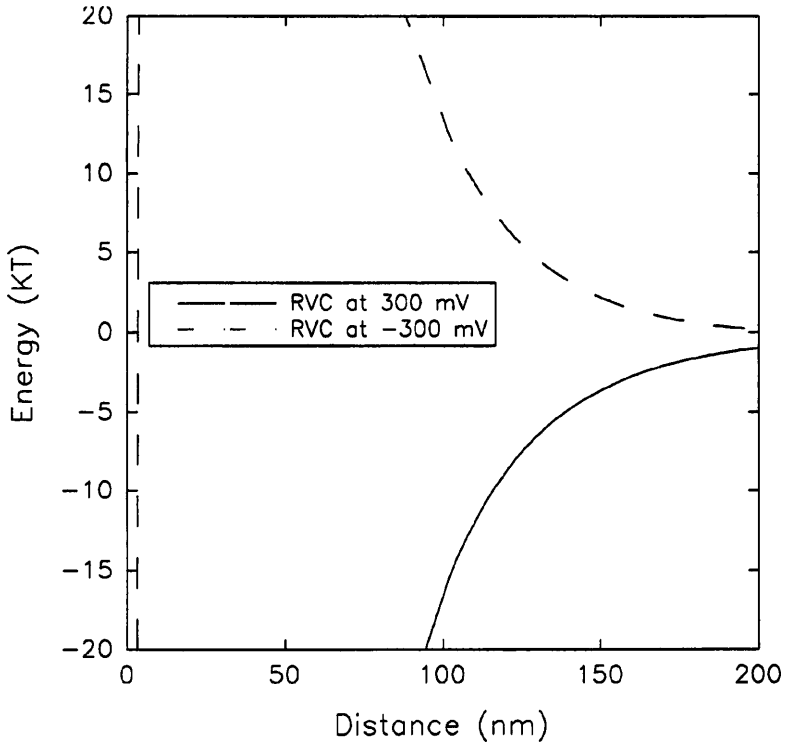

Figure 6.3 Interaction energy between polystyrene latex particles and RVC collector for KCl concentration of 0.0001 mol dm^{-3} and RVC potentials of +300.0 and -300 mV vs SCE

the RVC potential of +300 mV shows that there are only attractive forces operating between particle and collector and favourable deposition condition exists and it then follows from this profile that once the particles are in the vicinity of the collector they will be firmly held in the primary minimum by the collector.

At negative RVC potentials the negatively charged particles, when in the vicinity of the collector, experience a net repulsion due to the interaction of similarly charged double layers. This condition is commonly termed unfavourable deposition condition. The interaction energy profile at RVC potential of -300 mV vs SCE in Figure 6.3 shows that an energy barrier (>15 kT) exists and therefore for particles to reach the primary minimum they have to surmount this high energy barrier.

Considering the previous argument it can be seen that theoretically at negative RVC potentials the presence of the energy barrier provides an obstacle to the deposition of the polystyrene latex particles therefore it is expected that lower deposition rate should be obtained in comparison to case where the RVC is held at positive potentials leading to a barrierless deposition condition. However, real deposition processes are determined by many other factors (the particle size, particle density, hydrodynamic, feed concentration and so forth). Therefore the picture presented in the above may not account for many of these important factors.

The particles are shown, in Chapter 4 (section 4.2), to carry weak acid as their surface functional groups. Additionally the surface charge of the particles is estimated to be in the region of 0.01 $\mu C\ cm^{-2}$. It is argued that due to the low surface charge of the particles it is anticipated that the electrical double layer may not play an important role in the deposition process. However, the attractive particle-collector London-van der Waals are strong short-range colloidal forces and therefore theoretically their existence should be sufficient for producing significant deposition.

Several important forces affecting the deposition process were discussed previously and in this study the effect of hydrodynamics on the deposition process will be considered in more detail. It is believed that fluid has a dual role in the deposition process. The fluid provides a medium through which the particles are carried towards the collector and consequently the rate of particle transport towards the collector is largely determined by the fluid velocity. In situations where a high energy barrier develops between particle and collector, particles carried by fluid at high velocity may have enough kinetic energy to overcome the energy barrier and reach the primary minimum. Additionally under some circumstances it is envisaged that drag force on the particles may be strong enough to prevent particles from depositing or even to knock off the deposited particles.

To observe the effect of hydrodynamics on the deposition process the volumetric flowrates was varied in the range 1.7-34 $cm^3\ min^{-1}$ corresponding to the superficial velocity of 0.136-2.72 cm min^{-1}. Figures 6.4 and 6.5 allow comparison of the particle break-through curves for different flowrates (at the same electrolyte concentrations and RVC electrode potential corresponding to the particle-collector interaction energies shown in Figure 6.3).

The complete break-through times as shown in Figure 6.4 for 34 and 12 $cm^3\ min^{-1}$ flowrates are approximately 350 and 390 seconds respectively and at volumetric flowrate of 5.6 $cm^3\ min^{-1}$ steady state in not achieved in the time scale shown. Figure 6.6 shows the variation of the gradient, S_o, of the particle break-through curves determined at 300 seconds with flowrates for runs shown in Figure 6.4. S_o may represent an apparent rate constant and it can be seen from Figure 6.6 that S_o is directly proportional to the volumetric flowrate.

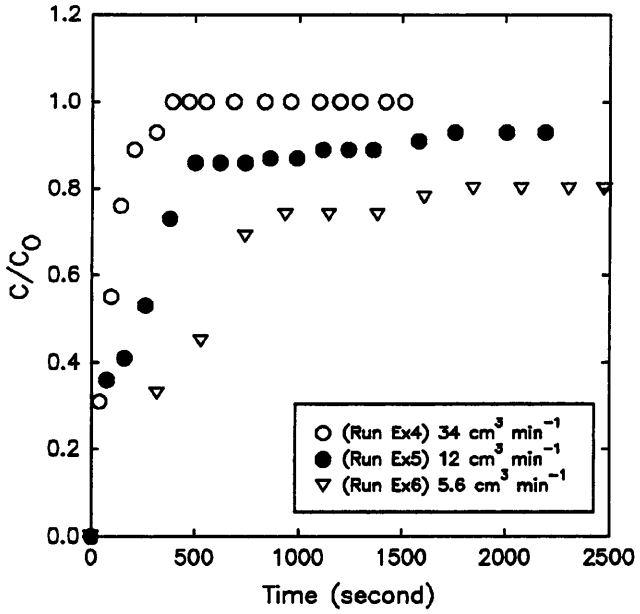

Figure 6.4 Particle break-through curves (runs Ex4, Ex5 and Ex6) with RVC at +300 mV vs SCE and KCl at 0.0001 mol dm^{-3}, for three different volumetric flowrates

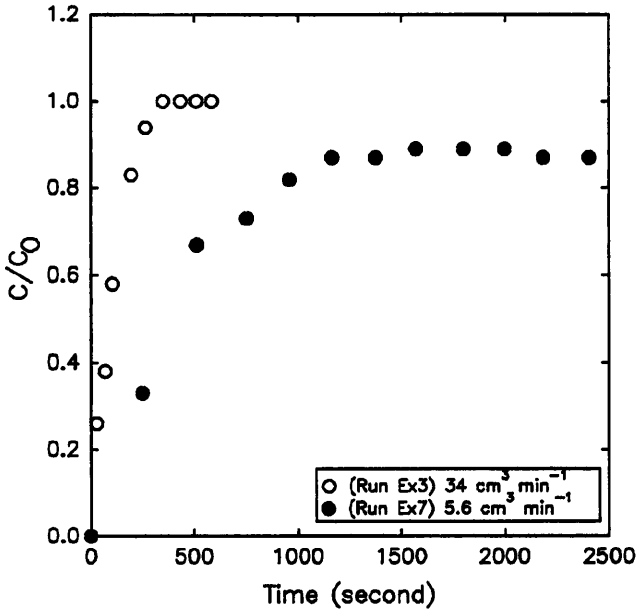

Figure 6.5 Particle break-through curves for runs Ex3 and Ex7 with RVC at -300.0 mV vs SCE and KCl at 0.0001 mol dm^{-3}

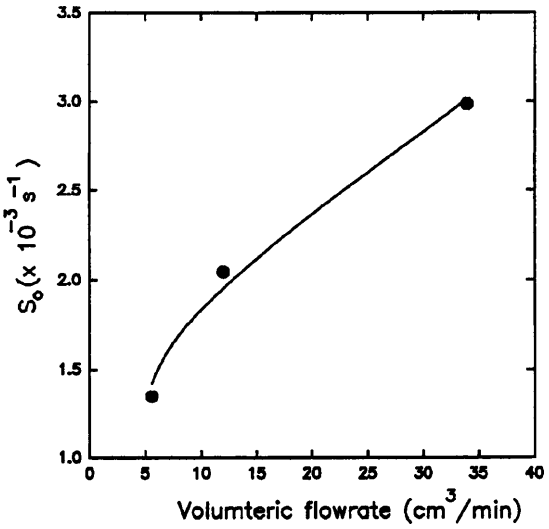

Figure 6.6 Variation of slope of the particle break-through curves with the volumetric flowrate for runs Ex4, Ex5 and Ex6.

The equation fitted to the line is:

$$S_o = 0.69\ VF^{0.42} \tag{6.2}$$

Where VF is the volumetric flowrate. One obvious reason for this may be said to be that at a given time the higher the flowrates the more feed suspension is available for deposition. Alternatively, at higher flowrates the particles have higher kinetic energy and consequently transport of particles to the vicinity of the collector takes place more effectively resulting in higher rate of capture of particles. The separation distance at which the magnitude of the total interaction energy is slightly larger than the kinetic energy of the particles and the total interaction energies can be seen in Table 6.1. The negative sign indicates that the total interaction energy consists of attractive forces as shown in Figure 6.3. Also included in this table are values of the drag force exerted on the particle by the fluid for the flowrates shown. The drag force was calculated from the Stoke's law (see equation (7.19)) and the total interaction force was also calculated for three typical cases where there were attractive

colloidal forces between particle and collector. The colloidal forces were calculated at a particle-collector separation distance where the magnitude of the force just exceeded the fluid drag force.

Table 6.1 Comparison of kinetic energy of particles with the particle-collector total interaction energy and comparison of fluid drag force with interaction force

Volumetric flowrate ($cm^3\ min^{-1}$)	Kinetic energy of particles ($/10^{-21}$ J)	Separation distance (nm)	Total interaction energy ($/10^{-21}$ J)	Run	Total interaction force ($/10^{-11}$ N)	Separation distance (nm)	Drag force ($/10^{-11}$N)
34	8.89	500	-9.29	Ex4	-2.43	140.0	2.05
12	1.10	710	-1.12	Ex5	-0.82	170.0	0.72
5.6	0.24	870	-0.25	Ex6	-0.41	190.0	0.34

Data in Table 6.1 should be interpreted as follows:

Consider run Ex5, the drag force is 0.72 x 10^{-11} N. At separation distances of less than 170 nm the total interaction force will be greater than the drag force since the value at this separation is -.82 x 10^{-11} N. The relationship between kinetic energy of particles and the total interaction energy is similar (e.g. consider the run at 34 $cm^3\ min^{-1}$ and at separation distances less than 500 nm the total interaction energy will be greater than the kinetic energy of particles.

The apparent rate constant S_o, calculated from the gradient of the particle break-through curves were determined at several points. These were then plotted against the value of C/Co at which point the tangent to the curve was drawn. The gradient is proportional to the deposition rate and these values have been plotted as shown in Figure 6.7 and it can be seen that at constant flowrate there exists an approximately linear relationship between C/C_o the change with time of the rate of deposition (gradient).

The equations fitted to these lines were:

$$S_o = 0.01 - 0.0096\frac{C}{C_o} \quad \textit{-flowrate of } 34\ cm^3\ min^{-1}$$

$$S_o = 0.0056 - 0.0059\frac{C}{C_o} \quad \textit{-flowrate of } 12\ cm^3\ min^{-1} \qquad (6.3)$$

$$S_o = 0.003 - 0.0039\frac{C}{C_o} \quad \textit{-flowrate of } 5.6\ cm^3\ min^{-1}$$

The amount of particles depositing can be deduced and consequently it may be speculated from this graph, provided the blocking of collector surface by deposited particles does not occur, at constant flowrate higher feed particle concentration may result in higher deposition rate.

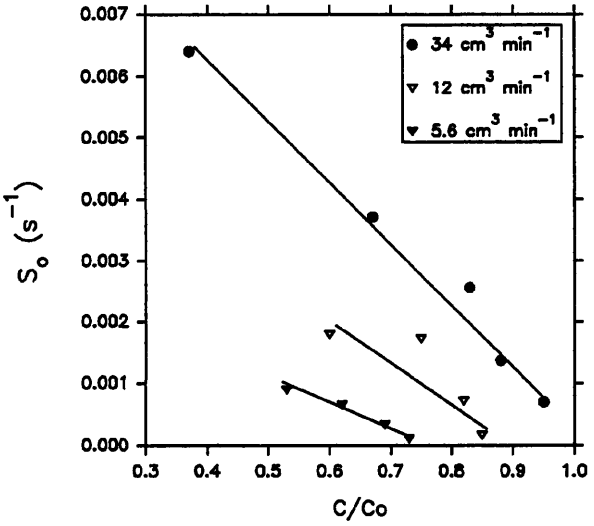

Figure 6.7 Variation of the gradient of the particle break-through curves with C/Co for the volumetric flowrates shown

To quantify the effect of filtration velocity on the deposition rate a better description would be obtained if the total weight of particles deposited after a time period can be estimated. Since the feed particle concentration varied slightly one experiment to another, then the total weight of particles thus calculated would need to be normalised by dividing them by the total

weight of feed particles that had entered the column during this time interval. The weight of particles depositing at a given time can be found by multiplying the outlet particle number concentration by the weight of one particle (86.57×10^{-12} g) and then subtracting it from the weight of particles entering in the feed.

The total amount of feed particles that had entered the column after a given period of time is found by:

$$\textit{WFT} = \textit{flow} \times \textit{weight of one particle} \times \textit{feed particle number concentration} \times \textit{time period} \quad (6.4)$$

Figure 6.8 shows a typical graph of the variation of the deposited particle weight on the left y-axis and the normalised deposited weight on the right y-axis against time for run Ex3.

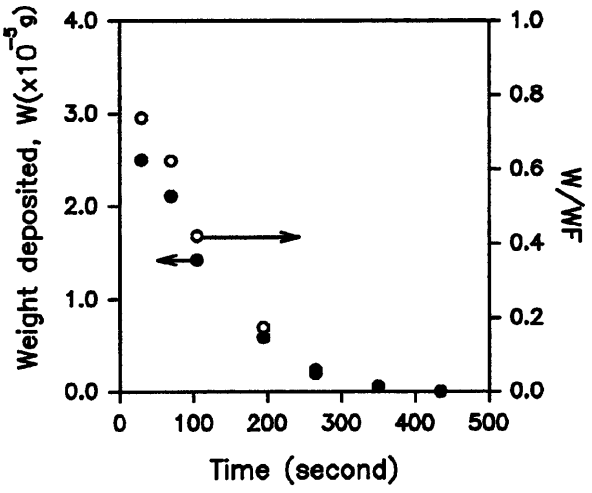

Figure 6.8 Weight of particles deposited (W) and the ratio of weight of particles to the weight of feed plotted against time for run Ex3

The deposition rate can be estimated from the slope of the curve corresponding to the variation of the deposit weight with time (the left y-axis). It can then be seen from Figure 6.8 that the slope decreases with time i.e the deposition rate decreases with time until a dynamic

equilibrium in reached which means that the rate of deposition attains a constant value until the saturation of the bed occurs.

Since the deposition rate varies with time the only way possible to compare the rates at different flowrates would be to fix the time on the x-axis and then find the slope of the curve corresponding to this x value. Unfortunately, the runs carried out at the high flowrate of 34 cm^3 min^{-1} reached equilibrium quickly compared to runs carried out at 5.6 cm^3 min^{-1} and therefore a common value on the x-axis could not be chosen for comparison of the deposition rates. For example comparing the particle break-through curves for runs Ex4 and Ex6, in Figure 6.4, it can be seen that run Ex2 reaches equilibrium at approximately 300 seconds while in run Ex6 the particles just start coming out of the column at 300 seconds.

The values for the weight of deposit at different times can now be read from Figure 6.8. Simpson's rule was used to find the total area under the curve, corresponding to the total weight deposited, up to a specific time. Table 6.2 shows the values of total weight of particles

Table 6.2 Values for the total weight deposited and the normalised weight after 390 seconds

	Ex1	Ex2	Ex3	Ex4	Ex5	Ex6	Ex7
Total particle weight entering, WFT($x10^{-3}$ g)	11.67	14.54	13.20	11.10	3.78	1.73	1.73
Total weight of particles deposited, WT($x10^{-3}$ g)	1.82	1.85	1.78	1.37	0.67	0.31	0.27
Normalised weight of deposit WT/WFT	0.15	0.13	0.13	0.12	0.17	0.18	0.16

deposited (equal to the total area under the curve) and the normalised weight, defined as the total weight deposited after 390 seconds divided by the total weight of feed particles that had

entered the column after 390 seconds, up to the time of 390 seconds. Figure 6.9 shows the plot of the values for experiments quoted in Figure 6.4, and this figure shows that the total

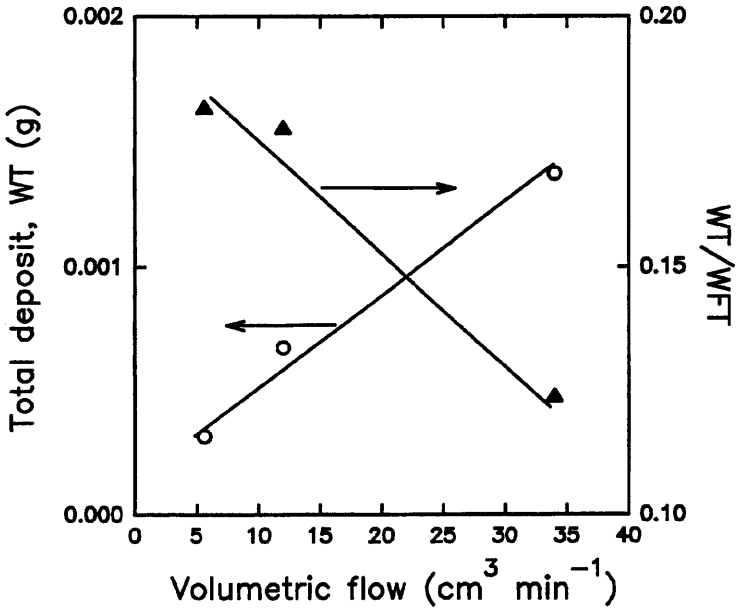

Figure 6.9 Variation of total weight of deposit with volumetric flowrate for RVC at +300 mV and KCl at 0.0001 mol dm^{-3}

weight deposited increased with increasing flowrate and the line corresponding to the right y-axis it appears that the particle removal efficiency *decreases* with increasing flowrate, i.e WT/WFT decreases.

The data in Figure 6.4 is replotted in Figure 6.10 where a filter time is used. The filter time is used to take into account the amount of time taken for the feed suspension to displace the electrolyte solution from the column. The filter time is defines as:

$$\tau = t - \frac{L\,\beta}{U_o} \qquad (6.5)$$

Where τ is the filter time, β is the bed porosity, L is the bed length and U_0 is the superficial velocity. Therefore, seriously speaking, τ=0 should be viewed as the start of a deposition

experiment. Use of the filter time has resulted in the data from Figure 6.4 to be shifted horizontally in the negative direction .

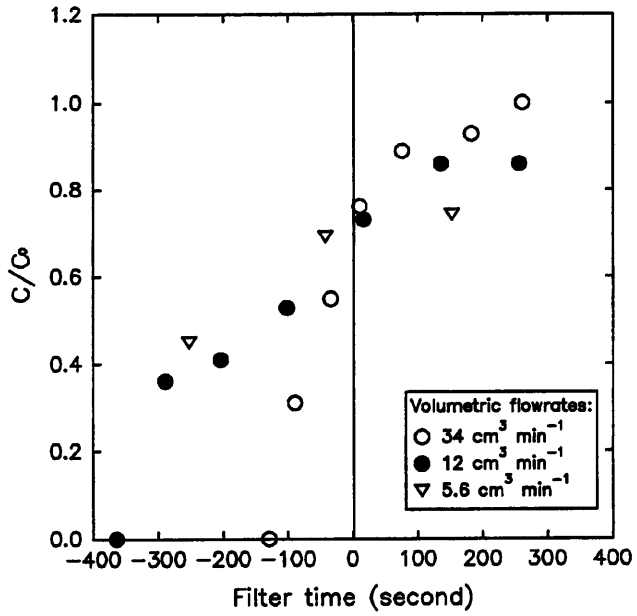

Figure 6.10 Particle break-through curves plotted against the filter time

To further investigate the effect of above forces on the deposition rate of particles the experiments carried out with RVC kept at potentials of +300.0 and -300.0 mV vs SCE were compared at 34.0 cm^3 min^{-1} (Ex4 and Ex3) and 5.6 cm^3 min^{-1} (Ex6 and Ex7) flowrates. Any effect of the external forces mentioned should manifest itself in the difference in the deposition rates.

The DLVO plot shown in Figure 6.3 suggests that when RVC is kept at -300 mV a high energy barrier exists but when RVC is kept at +300 mV only attractive forces exist between particle and collector. Therefore, favourable and unfavourable deposition conditions are predicted for the cases when RVC is kept at +300 and -300 mV respectively.

Comparing the particle break-through curves of runs corresponding to the RVC potentials of +300 and -300 mV in Figures 6.4 and 6.5 respectively, at volumetric flowrate of 34 cm^3 min^{-1}, it can be seen that similar steady state values are obtained. Similar comparison for the runs at lower flowrate of 5.6 cm^3 min^{-1} reveals that higher steady state value is obtained for the run where RVC is at +300 mV compared to the case where RVC is at -300 mV. The total deposit and the normalised weight ratio as shown in Table 6.2 reveal that at a flowrate of 34 cm^3 min^{-1} a higher total deposit weight and normalised weight ratio are obtained for the run where RVC is at -300 mV compared to the case where RVC is at +300 mV. On the contrary at 5.6 cm^3 min^{-1}, higher total deposit weight and normalised weight ratio are obtained for the run where RVC is at +300 mV compared to the case where RVC is at -300 mV.

If the double layer charging process is considered to play an important role in the total deposition process, then Ex4 should have higher deposition rate than Ex3. Similarly Ex6 should have higher deposition rate than Ex7. The higher deposited particle weight of Ex6 compared to Ex7 follows the predictions of the DLVO theory.

The discrepancy observed between the deposition rates seen in Ex3 and Ex4 and that predicted if the double layer charging process was the main contributor to the total deposition process can be explained as follows:

- Table 6.2 shows that considerably more feed had entered the column in Ex3 compared to Ex4 (13.2 and 11.1 $x10^{-3}$ g respectively). It was speculated from the trend observed in Figure 6.7 that the deposition rate was directly proportional to the concentration i.e. the higher the feed particle concentration the higher the deposition rate and this may have influenced the total weight deposited.

-the uncertainty regarding the exact magnitude of the RVC's potential under the potentiostatic control which will be elaborated in detail in section 6.1.3. It would have been ideal to carry out the same investigation under the non-electrophoretic condition which would eliminate the contribution of external variation of RVC potential as a source of error to the investigation of effect of fluid velocity on the deposition rate.

-the discrepancy becomes evident at higher flowrate of 34 cm^3 min^{-1} which means that at this flowrate external forces such as drag force and the particle inertia may exert stronger repulsive influence on the deposition process than the attractive colloidal interaction energies.

-at lower flowrate the particles have higher residence time resulting in a longer time for them to make successful attempt at deposition.

To conclude from the above argument the majority of deposition experiments were carried out at low volumetric flowrate of 1.7 cm^3 min^{-1} to minimise the probable interference of hydrodynamics with the deposition process.

6.1.3 Variation of RVC potential at KCl concentration of 0.001 mol dm^{-3}

The electrolyte concentration governs the form of the total energy of interaction obtained. It was discussed in Chapter 1 that at intermediate electrolyte concentration such as 0.001 mol dm^{-3} various shapes of total interaction energy profile exhibiting a combination of primary/secondary minima may be obtained. It was originally anticipated that it should be possible to asses how to utilise the secondary minimum in the total particle-collector interaction energy profile for depositing the polystyrene latex particles. However, the experimental results discussed in section 6.1.2 showed that for the present deposition system other important factors determined the total deposition process, consequently the rest of the

experiments were aimed at establishing the boundaries within which the double layer charging process is the controlling deposition route.

To this end, to avoid large ohmic drop values and yet offer low resistance to the passage of electricity, the main bulk of the runs in this study were carried out at KCl concentration of 0.001 mol dm^{-3}. As a result the sole effect of variation of electrolyte concentration on the deposition rate was not studied in depth. However, the combined effect of variation of ionic strength/collector potential was utilised as a tool for controlling the deposition rate.

Figure 6.11 shows the interaction energy profiles for runs Ex18, Ex19 and Ex20. Run Ex20 was carried out non-electrophoretically (i.e. there was no external application of potential to the RVC and the RVC collector potential was assumed to be the zeta potential at the experimental pH). The DLVO theory suggests that there is high energy barrier (>15 kT) for the experimental conditions of run Ex18 and consequently low electrostatically driven deposition rate is predicted. Under the experimental conditions prevailing in runs Ex19 and Ex20 the London-van der Waals forces are dominant and favourable deposition condition exists between particle and collector.

Figure 6.12 shows the particle break-through curves for runs Ex18, Ex19 and Ex20. The particle break-through curves resemble each other and the steady state values are also similar. The total area under the curve up to 1500 seconds corresponding to the total weight of particles deposited was estimated from the deposit weight vs time graphs using the Simpson's rule and the values can be seen in Table 6.3. Additionally the deposition rate, estimated from the slope of the deposit weight curve, are also presented in this table. The values quoted

in Table 6.3 show that runs Ex19 and Ex20 have similar total deposit and normalised weight values but Ex18 has unexpectedly high total and normalised weight values.

Table 6.3 Comparison of the total deposit weight for various RVC potentials at 9.6 cm^3 min^{-1} and KCl solution of 0.001 mol dm^{-3}

	Ex18	Ex19	Ex20
Total weight of particles deposited, WT(g)	$1.10x10^{-4}$	$6.50x10^{-5}$	$6.50x10^{-5}$
Total weight of particles entered in the feed, WFT(g)	$14.10x10^{-3}$	$15.10x10^{-3}$	$14.90x10^{-3}$
WT/WFT	$7.90x10^{-3}$	$4.30x10^{-3}$	$4.30x10^{-3}$
Deposition rate at 600 seconds (g/s)	$26.50x10^{-19}$	$17.70x10^{-19}$	$20.00x10^{-19}$

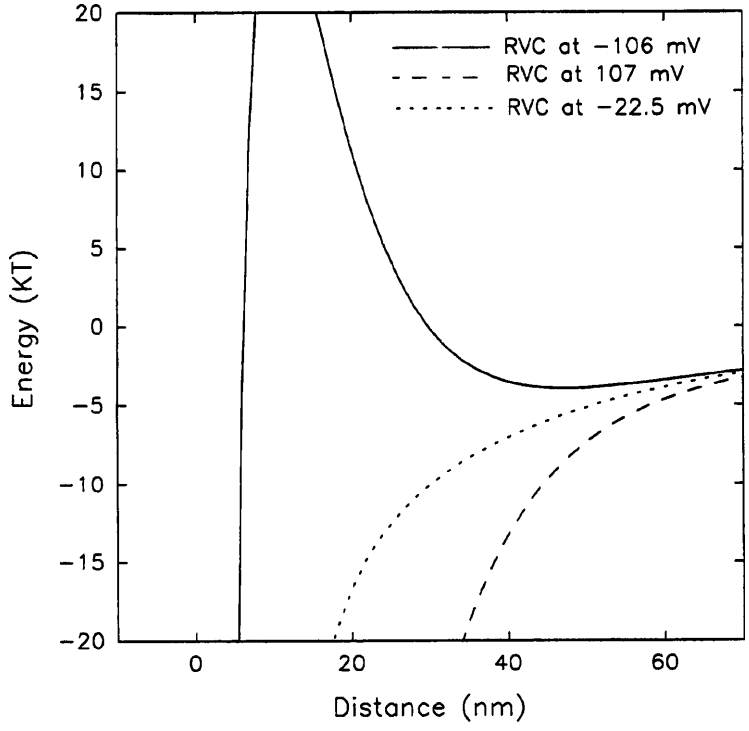

Figure 6.11 Interaction energy profile for KCl concentration of 0.001 mol dm^{-3} and volumetric flowrate of 9.6 cm^3 min^{-1} and RVC potentials vs SCE of -106 mV (Ex18), 107 mV (Ex19) and -22.5 mV (Ex20)

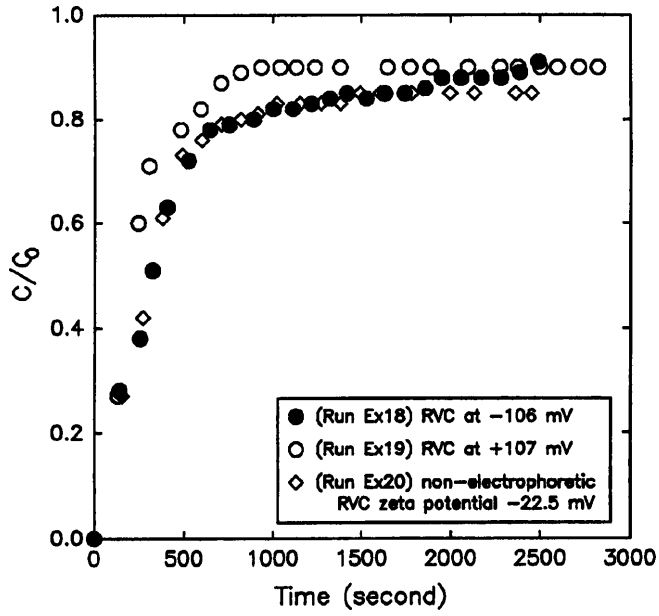

Figure 6.12 Variation of particle break-through curves with RVC potential for KCl concentration of 0.001 mol dm^{-3} and volumetric flowrate of 9.6 cm^3 min^{-1}

Thus it can be seen that these results contradict the DLVO prediction and similar reasonings to that previously adopted for explaining the observed discrepancy at high flowrate may be used to explain the discrepancy between the DLVO prediction and the experimental results. In addition to these reasonings the role of surface roughness must also be considered. The polystyrene latex particle can be assumed to have an ideal smooth surface but the RVC surface have surface heterogeneity. This will be discussed more in Chapter 7.

Figures 6.13 shows the experimental data for runs Ex18. The method for measurement of individual variables was explained in section 4.7.3. When interpreting these data care must be taken to differentiate the difference between the time axis on the break-through curves and that on the experimental parameter curves. The difference arises due to the fact that the equilibration period for the RVC collector was long. For example in Figure 6.13c it is shown that the feed suspension was introduced at approximately 3000 seconds and this point

corresponds to time=0 on the particle break-through curve of Figure 6.12. This means that it

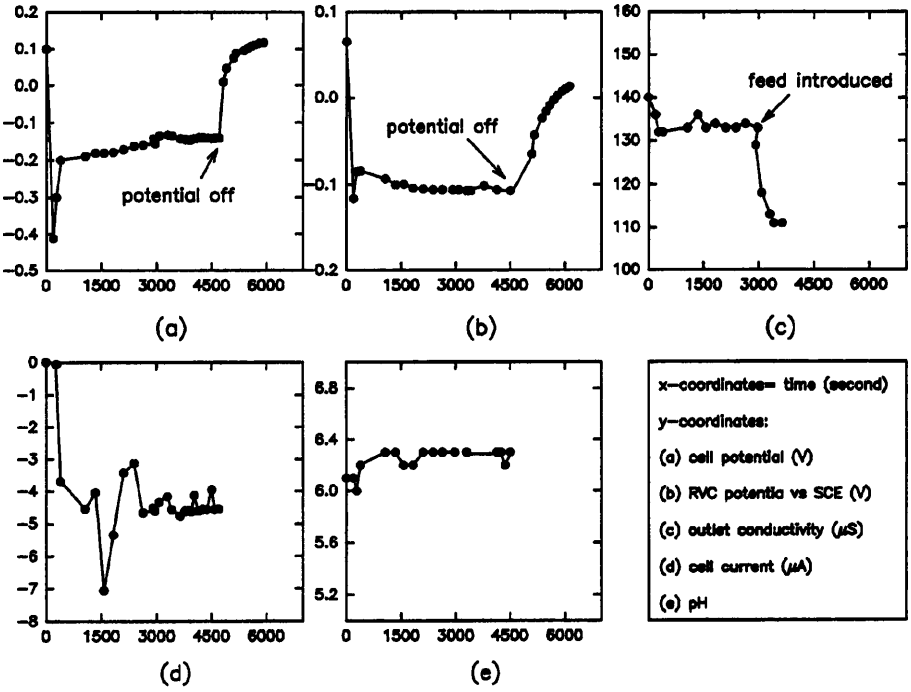

Figure 6.13 Experimental data for run Ex18 at volumetric flowrate of 9.6 cm^3 min^{-1} and KCl concentration of 0.001 mol dm^{-3}

took 3000 seconds for the system to achieve a steady state. The outlet pH and conductivity usually attained the inlet pH and conductivity fairly rapidly, but the RVC potential and the cell current were more susceptible to fluctuations and hence these took longer time to become steady. As explained in section 4.7.3 when all the readings shown in Figure 6.13 were perceived to be steady the feed was introduced.

An interesting point about experiment Ex18 is that at approximately 4000 seconds (1700 seconds on the particle break-through curve plot in Figure 6.12) the connection between the potentiostat and RVC was removed and consequently the RVC was allowed to decay towards its rest potential. This was done to observe the effect of removal of external voltage on the

deposition rate and it can be observed that in fact this did not alter the deposition process greatly. In the light of discussion previously presented for the analysis of deposit weight values (Table 6.3) it may be argued that at this flowrate, 9.6 cm^3 min^{-1}, the surface forces do not contribute greatly to the total deposition process and other external factors such as gravity and fluid flow may be argued to have a more pronounced effect on the deposition process.

Several times the RVC piece used after a deposition experiment was taken to be analysed under both a light microscope and a scanning electron micrograph, however, it was found that with the light microscope the light did not penetrate deep into the RVC structure and similarly to use a piece of RVC for analysis with the SEM meant that the slab had to be cut and this would have resulted in the loss of particles and concluding from these comments an exact amount of mechanical hold-up of particles in the column can not be accurately judged.

It was explained previously that the choice of KCl concentration of 0.001 mol dm^{-3} for carrying out the bulk of experiments was to allow passage of electricity with low resistance offered by the electrolyte. However, it is possible that as the KCl concentration increases the possibility of locally polarising the RVC electrode increases. This means that diffuse layer of the RVC electrode under the equilibrium condition (rest state) behaves as is envisaged i.e. the counter-ions accumulate around the surface. As an external potential is applied the bulk of the current flow takes place inside the conductive RVC but at high KCl concentrations a small amount of the current enters the electrolyte. This small current flow then travels the length of the pore within the matrix of RVC and again enters the RVC structure to join the bulk current flow. This process of leaving the RVC at some point and entering it at another point creates a temporary local anode and cathode and this may be said to counteract the

potentiostatically applied total potential. This in fact may explain the probable drop in the potential of RVC along the thickness of the RVC slab had it been possible to measure.

There were a further 9 runs carried out at the KCl concentration of 0.001 mol dm^{-3} but at a lower volumetric flowrate of 1.7 cm^3 min^{-1}, with the aim of reducing the probable effect of fluid drag and additionally to increase the residence time of the particles. Figure 6.14 shows the particle break-through curves. The inset shows the RVC potentials at which these

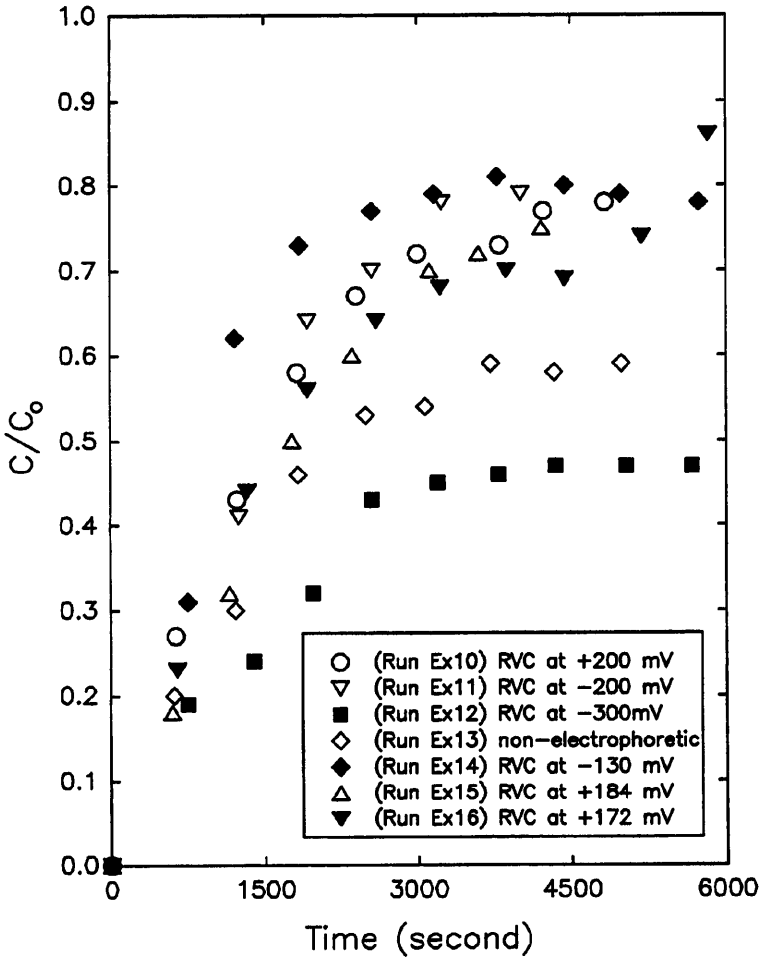

Figure 6.14 Particle break-through curves for experiments carried out at volumetric flowrate of 1.7 cm^3 min^{-1} and KCl concentration of 0.001 mol dm^{-3} and RVC potentials as shown in the inset

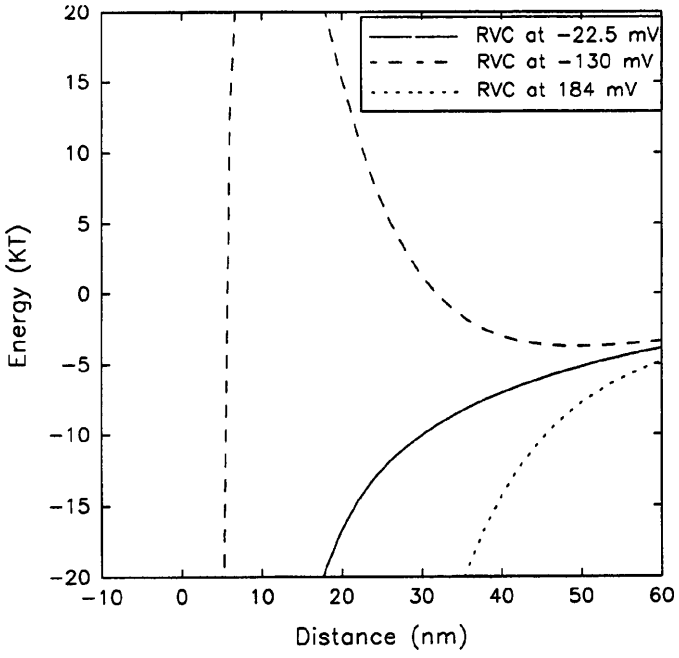

(a)

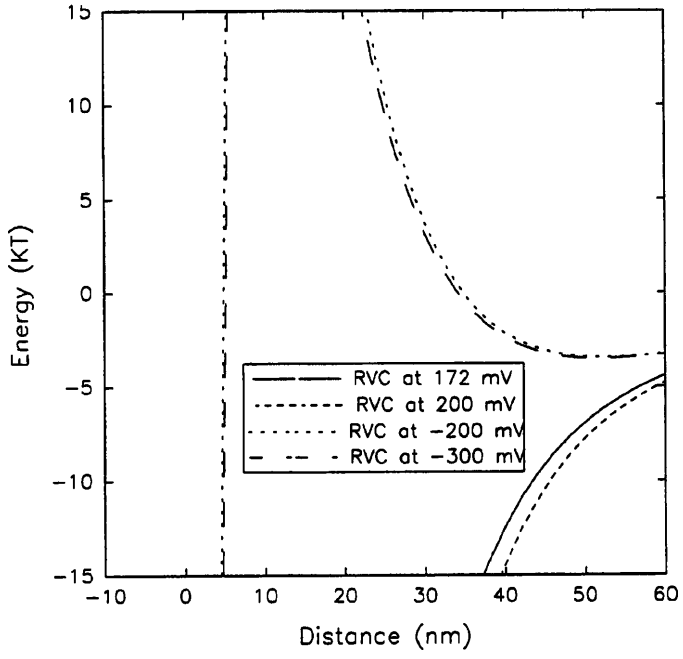

(b)

Figure 6.15 Interaction energy curves for deposition experiments carried out at volumetric flowrate of 1.7 cm^3 min^{-1} and KCl concentration of 0.001 mol dm^{-3} and RVC potentials vs SCE shown in the inset

experiments were carried out. Most strikingly in Figure 6.14, contrary to the results of previously discussed experiments, there seems to be differentiation of the curves according to the RVC potential and this must be examined closely to find out whether there is an underlying trend present.

Figures 6.15a and 6.15b show the interaction energy curves for these runs - presented as two figures to preserve clarity.

It can be seen from Figure 6.15a that the DLVO prediction is that the surface force controlled deposition is expected to occur in the order Ex15>Ex13>Ex14. However, the particle break-through curves in Figure 6.14 show that in fact deposition occurs in the order Ex13>Ex15>Ex14 and indeed this is additionally confirmed by the total deposit weight and normalised weight values shown in Table 6.4. It is apparent that the prediction of high energy barrier for run Ex14 is well justified by the lowest deposition rate obtained, but the discrepancy lies in the expectation that deposition rate should be more for Ex15 than Ex13. This will be discussed further in the light of comparison for other experiments at this experimental conditions.

Table 6.4 Total weight and the normalised weight of particles deposited

	EX10	EX11	EX12	EX13	EX14	EX15	EX16
Weight of feed entered WFT, $x10^{-3}$ g	4.78	6.25	6.99	6.54	5.44	7.13	6.32
Weight of particles deposited WT, $x10^{-5}$ g	0.08	0.56	3.48	2.62	0.90	2.25	1.95
WT/WFT ($x10^{-3}$)	0.17	0.89	4.90	4.00	1.67	3.16	3.08

Assuming that deposition into secondary minimum does not account for an appreciable amount of the total deposition taking place and additionally that the surface coverage of the

RVC collector is not 100%, i.e. there are still large areas of 'clean' RVC surface available for deposition and blocking by deposited particle does not occur. It may then be argued that the existence of any relationship between the external application of potential and the deposition rate may be manifested in the change in the deposition rate once the interface program has been terminated. It can be seen from Figure 6.16b that the RVC potential is negative at -130 mV vs SCE throughout the run and a high energy barrier is reported by the DLVO theory, as explained previously resulting in an unfavourable deposition condition. On the termination of the potential application program the RVC slowly returns towards its rest potential which in this case was +140 mV. Therefore as the RVC potential becomes more positive the deposition condition becomes less unfavourable which, theoretically, should

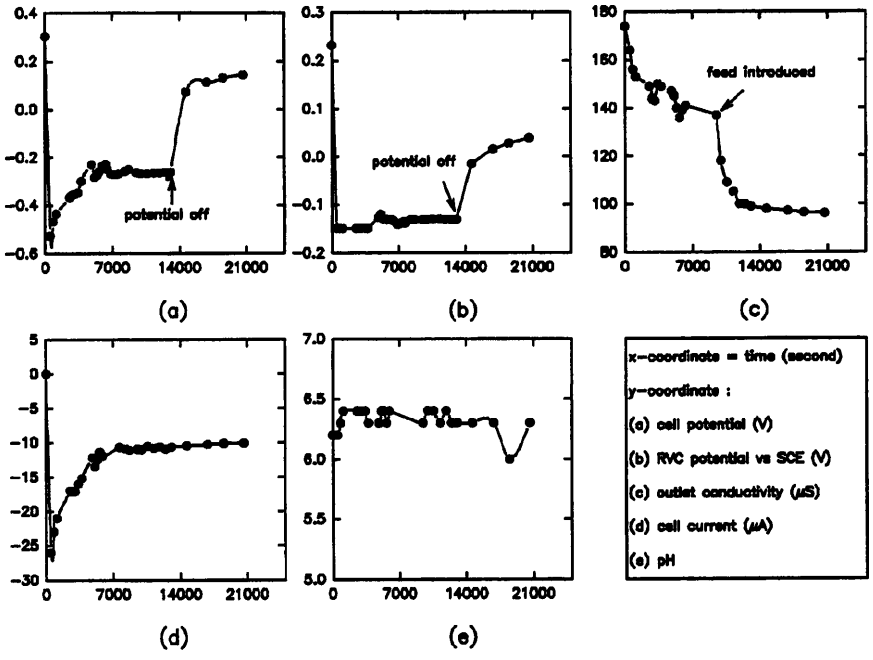

Figure 6.16 Experimental data for run Ex14 at volumetric flowrate of 1.7 cm^3 min^{-1} and KCl concentration of 0.001 mol dm^{-3}

result in more deposition occurring. Figure 6.17a shows the raw turbidity data for this run and

it can seen from this figure that immediately after termination of the applied potential there is indeed a slight increase in the deposition rate but it then retains the original turbidity value prior to the termination.

In run Ex15 at approximately 13000 seconds the potential- interface programe was terminated. The rest potential for this run was 140 mV and therefore on switching to open circuit the deposition rate should not be affected - this indeed was confirmed by the raw turbidity data shown in Figure 6.17b.

Figure 6.15b shows that the DLVO prediction for runs Ex10, Ex11, Ex12 and Ex16 is that surface force controlled deposition should occur in the order Ex10>Ex16>Ex11>Ex12. However, the experimental results in Figure 6.14 show that deposition occurs in the order

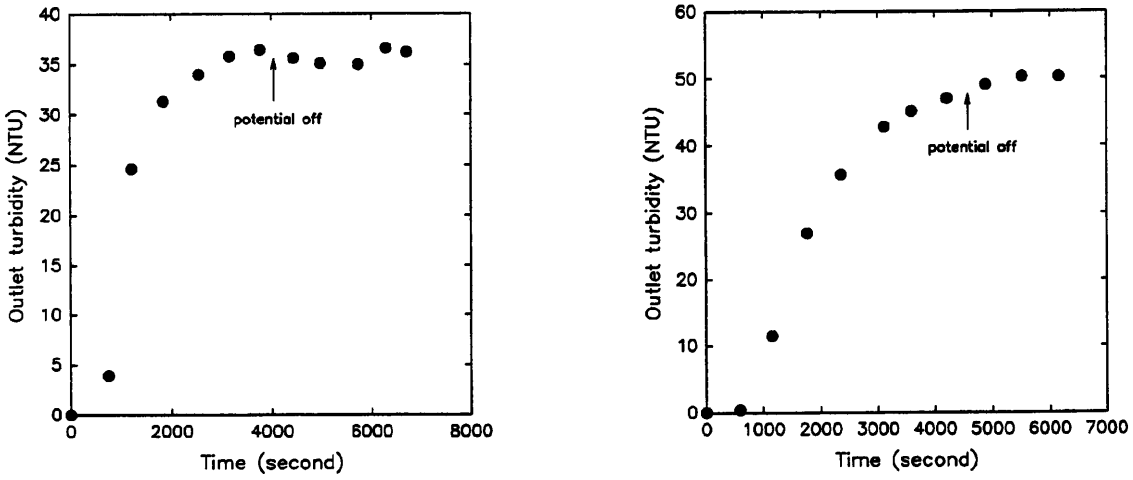

(a) (b)

Figure 6.17 Variation of outlet stream turbidity (NTU) against time for (a) Ex14 and (b) Ex15

Ex12>Ex16>Ex11>Ex10 and this is further confirmed by the total deposit weight and normalised weight shown in Table 6.4.

It is apparent that the discrepancy lies with the deposition rates obtained for runs Ex10 and Ex12 which can be seen to be opposite to the DLVO prediction.

The experimental findings of Oren et al. (1987) were discussed in detail in section 2.5. Figure 2.11 (Chapter 2) shows that as the graphite felt potential cycled between -500 and +500 mV the solution pH varied between 9 and 6 respectively, and this affected the zeta potentials of

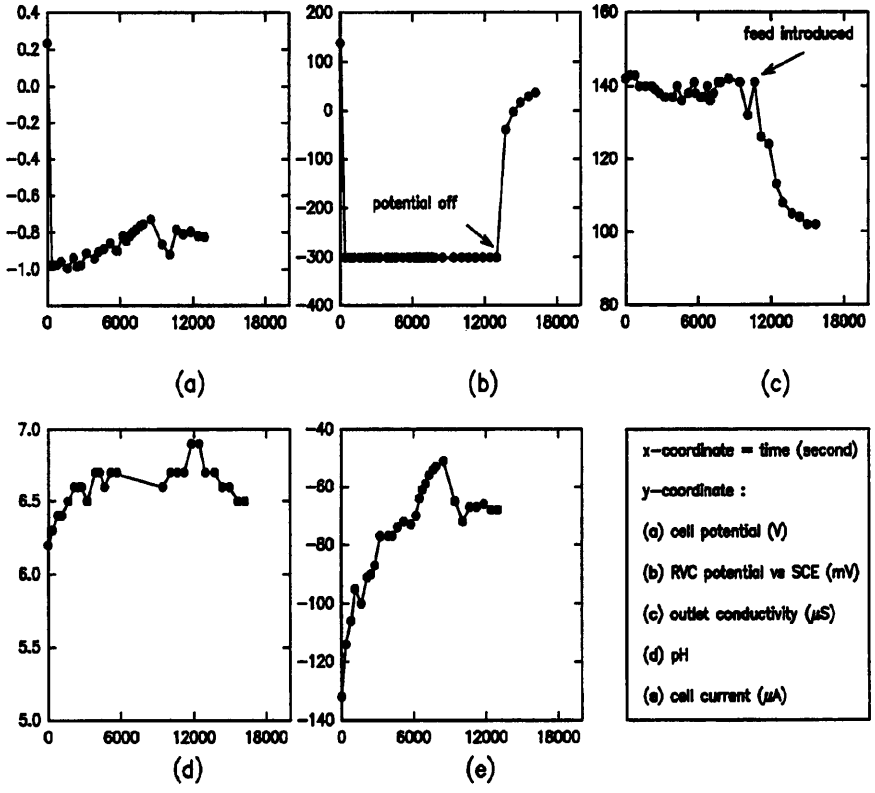

Figure 6.18 Experimental data for run Ex12 with KCl concentration of 0.001 mol dm^{-3} and volumetric flowrate of 1.7 cm^3 min^{-1}

the particles. It is believed that the unexpectedly high deposition rate obtained for run Ex12 could arise from the evolution of hydrogen which resulted in the increase in the deposition pH. This is illustrated by Figure 6.18d wherein the pH is shown to increase to 7 during the run.

Estimation of the hydrogen and oxygen overpotentials for an electrode is usually reported in the literature in terms of the Tafel law and Pickett (1979) provides the constants for various substances to be used in the Tafel law. The reported values for hydrogen overpotential for graphite were taken and under the experimental conditions of run Ex12 the estimated hydrogen overpotential was found to be approximately -130 mV.

The fact remains that in run Ex12 the there was unexpected rise in pH as shown in Figure 6.18d and the only explanation feasible seems to be the evolution of hydrogen. The increase in the deposition pH to 7.0 does not significantly affect the zeta potential of polystyrene latex but it is thought that evolution of hydrogen may undermine the deposition process in several ways and these will be discussed below.

To observe the effect of termination of the potentiostatic control of the RVC potential on the deposition rate the feed particle suspension was allowed to flow through the column while the potentiostat was switched off. Figures 6.19a, b, c show the raw turbidity data for runs Ex10, Ex12 and Ex16 respectively. The effect seems to be more pronounced for runs Ex12 and Ex16 where an appreciable decrease for Ex12 and an increase for Ex16 in the turbidity values are observed. These figures may be better interpreted alongside the RVC potential plots.

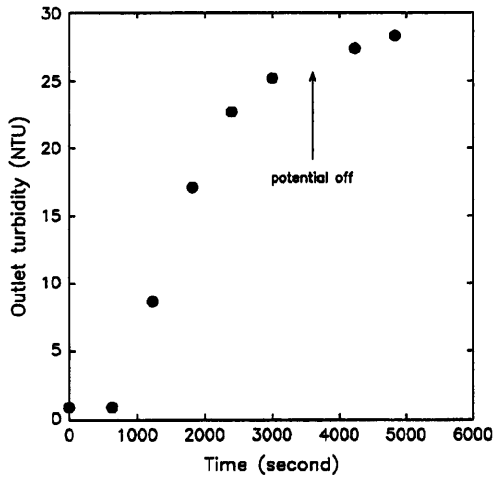

(a)

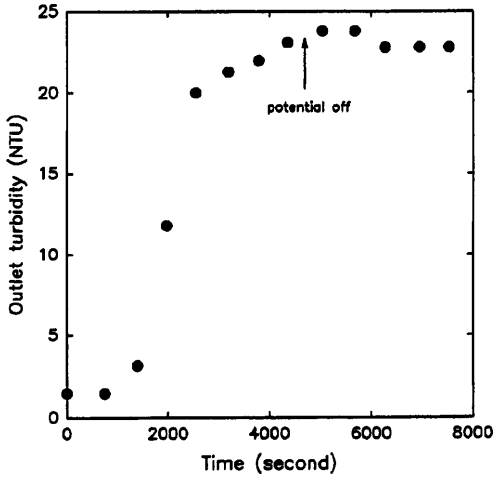

(b)

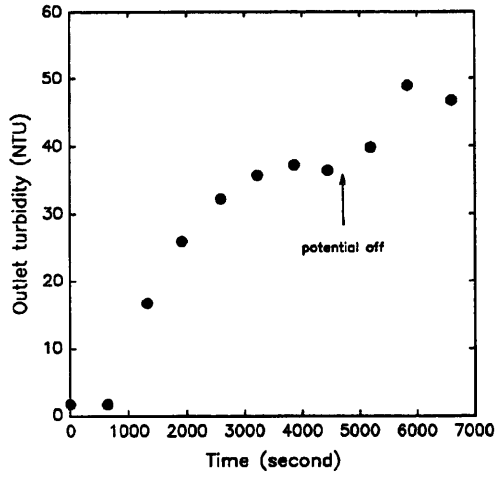

(C)

Figure 6.19 Variation of turbidity with time for runs a:Ex10, b:Ex12, c:Ex16

To investigate the findings by Oren et al. (1987) and analyse their relevance to this study since it was mentioned previously that gas evolution may have interfered with the deposition mechanism it was decided to carry out an experiment wherein the RVC potential was held at high negative values and the experimental data were recorded. Figure 6.20 shows the particle break-through curve for run PH1 where the RVC potential was kept at -417 mV vs SCE as shown in Figure 6.21b. Figure 6.21e shows that the observation made by Oren et al. (1987) is well justified i.e, at high negative potentials due to evolution of hydrogen the pH

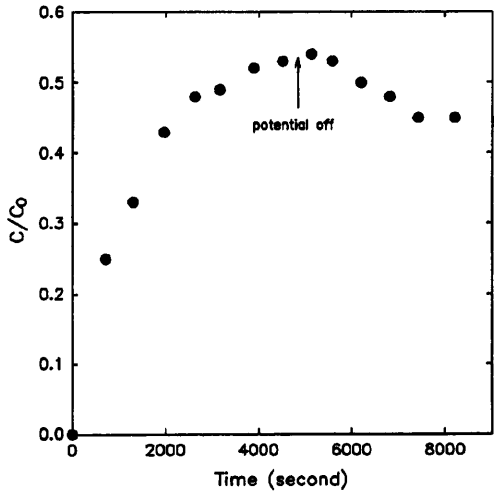

Figure 6.20 Particle break-through curve for run pH1

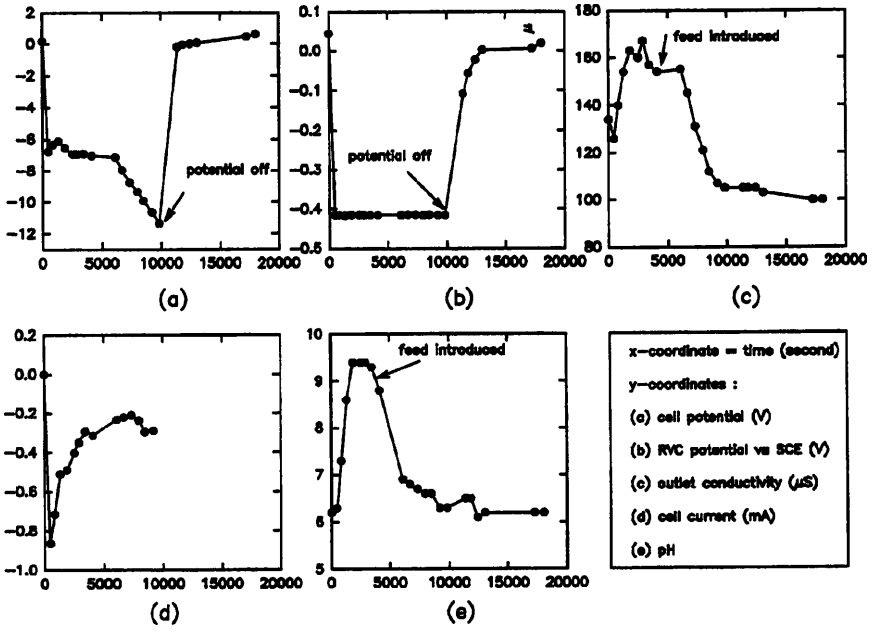

Figure 6.21 Experimental data for run pH1 at KCl concentration of 0.001 mol dm^{-3} and volumetric flowrate of 1.7 cm^3 min^{-1}.

rises from 6.2 to 9.4. After equilibration period of approximately 4200 seconds the feed suspension was introduced into the column. As seen from plot (e) introduction of the feed

suspension causes the outlet stream pH to be reduced to around 7.0. It may be concluded from these findings that the evolution of gases may affect the deposition process in several ways:

- as shown by Oren et al. (1987) the solution pH rises at high negative electrode potentials and also decreases at high positive potentials and consequently in either way the pH differs from the presumed value and this in turn changes the zeta potential values of the particles.
- gases emanating from the RVC surface may exert strong enough force on the deposited particles to overcome the colloidal adhesive forces and to dislodge them.
- due to the hydrophobic nature of the RVC there will be more affinity between the evolving hydrogen bubbles and the RVC surface. It is possible that latex particles may be attached to the evolving hydrogen bubbles which in turn carry them towards the RVC surface.

The interesting point in Figure 6.21 is that upon the termination of the interface program the RVC potential slowly returns towards its rest potential which in this case was +45 mV. DLVO theory suggests that the more positive the RVC potential becomes the more attractive the forces between the particle and collector become, leading to theoretically high deposition rates. It can be seen from Figure 6.20 that this is confirmed experimentally since upon termination of potentiostatic programm there seems to be more deposition occurring. In summary, whatever effect the evolution of hydrogen at high negative potentials may have on the deposition rate this effect is removed upon the termination of the applied potential.

To conclude for runs using KCl concentration of 0.001 mol dm^{-3}, there were 7 runs, with no unexpected complications, with varying RVC potentials. The DLVO theory predicted that deposition should occur in the order Ex10>Ex15>Ex16>Ex13>Ex14>Ex11>Ex12 according

to their shape of the interaction energy profile. Table 6.4 shows that deposition occurs in the following order:

Ex12>Ex13>Ex16>Ex15>Ex14>Ex11>Ex10

With the exception of runs Ex12 and Ex10, with the justification for the discrepancy already mentioned it may be said that, generally speaking, variation of RVC potential potentiostatically to obtain favourable and unfavourable deposition condition has been successful i.e. results can be distinguished according to the occurrence of favourable and unfavourable deposition conditions.

However it must also be said that, provided there were no Faradaic currents present, the difference between high and low loading rates corresponding to favourable/unfavourable deposition conditions respectively did not differ by large amounts.

To provide a better picture of the above conclusion the deposition rates were estimated, at 1400 seconds on the time-axis, from the slope of the deposit weight vs time plots. Figure 6.22 shows the variation of the deposition rate with the RVC potential. The negative values indicate the decreasing rate with time. It can be seen that under the unfavourable deposition condition the variation of RVC potential does not seem to affect the deposition rate as much as the equivalent for the favourable deposition condition.

It may then be concluded from this graph that the variation of RVC potential potentiostatically has the maximum effect under the favourable deposition condition and the shortcoming associated with the unfavourable deposition condition has to be speculated on further (see Chapter 7).

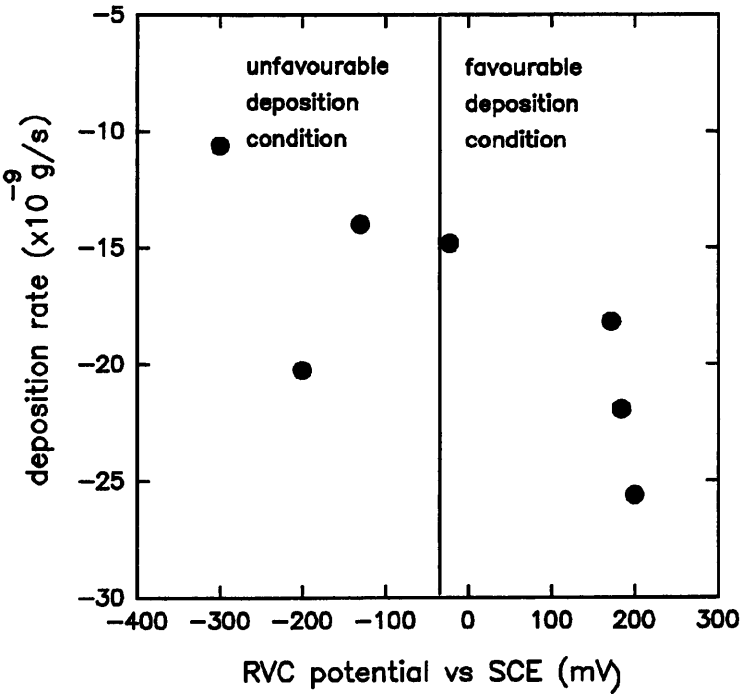

Figure 6.22 Variation of deposition rate at 1400 seconds with the RVC potential at KCl concentration of 0.001 mol dm^{-3}

6.1.4 Variation of RVC potential at 0.0001 mol dm^{-3} KCl solution

It was explained earlier that most of the experiments were carried out at the KCl concentration of 0.001 mol dm^{-3} to minimise ohmic drop effects. However, as the electrolyte concentration increases the thickness of the double layer decreases resulting in shorter range of double layer effects.

Further experiments at the KCl concentrations of 0.0001 and 0.01 mol dm^{-3} were carried out to find out if at all the double layer interaction can be confidently said to be taking part in the deposition process. The experimental results carried out at KCl concentration of 0.0001 mol dm^{-3} are discussed below.

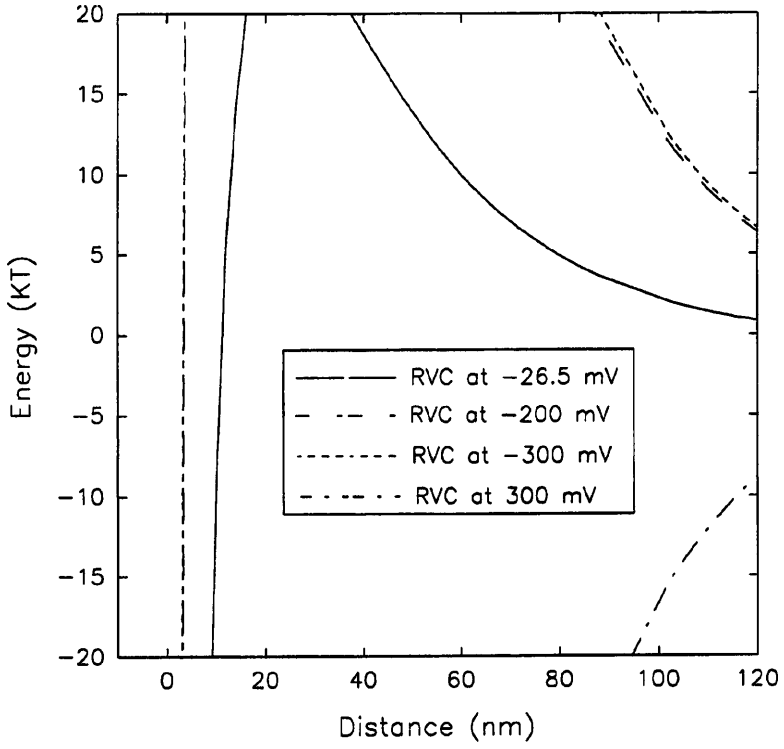

Figure 6.23 Interaction energy profile at KCl concentration of 0.0001 mol dm^{-3} and RVC potentials shown in the inset

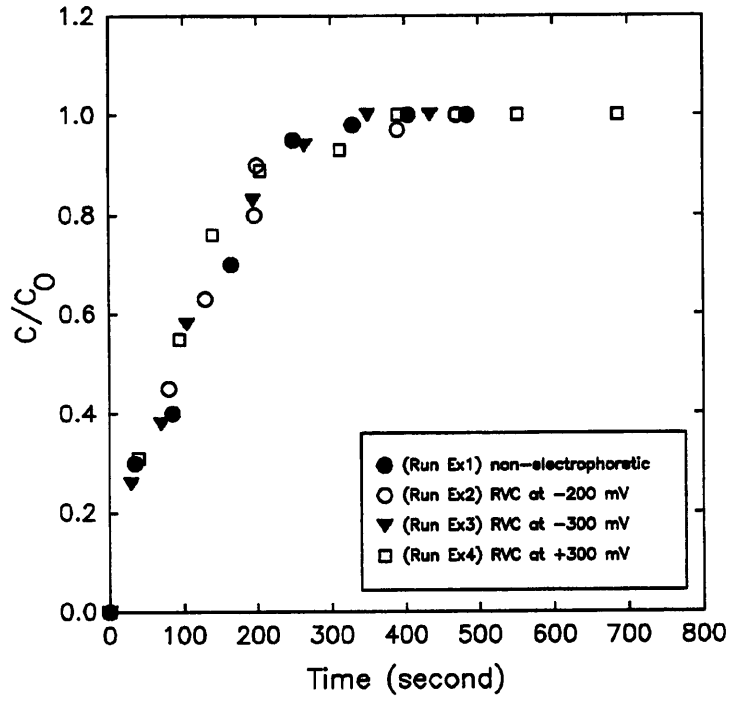

Figure 6.24 Particle break-through curves at KCl concentration of 0.0001 mol dm^{-3} and volumetric flowrate of 34 cm^3 min^{-1} and RVC potentials shown in the inset

Figures 6.23 and 6.24 show the interaction energy profile and the corresponding experimental particle break-through curves. The total energy of interaction predicts that at this KCl concentration (i.e. 0.0001 mol dm^{-3}) the more negative the RVC potential the more unfavourable deposition condition becomes (i.e. higher energy barrier, making the primary minimum less accessible to particles and consequently less deposition is expected). For experimental conditions of run Ex4, where RVC is kept potentiostatically at +300 mV vs SCE, the total energy of interaction shows only attractive London-van der Waals energy between particle and collector and therefore the total deposition process is aided by the surface forces.

At first glance at experimental results it seems that variation of RVC potential does not alter the deposition rates significantly since the same steady state value is reached in all cases after approximately 400 seconds.

Quantitative analysis of results, by means of graphs of weight plotted as a function of time may reveal further information. The total weight deposited after 390 seconds can be seen in Table 6.2. The total weight deposited also provide further evidence that at this KCl concentration and volumetric flowrate the variation of RVC potential does not affect the deposition rate and it is tempting to adopt the previously mentioned reasoning that the hydrodynamics has stronger impact on the deposition process.

Experiments carried out at lower volumetric flowrate may provide vital information for judging this argument. Figure 6.25 shows the particle break-through curves for runs Ex6 and Ex7 for KCl concentration of 0.0001 mol dm^{-3} and volumetric flowrate of 5.6 cm^3 min^{-1} and

RVC potentials of +300 and -300 mV vs SCE respectively.

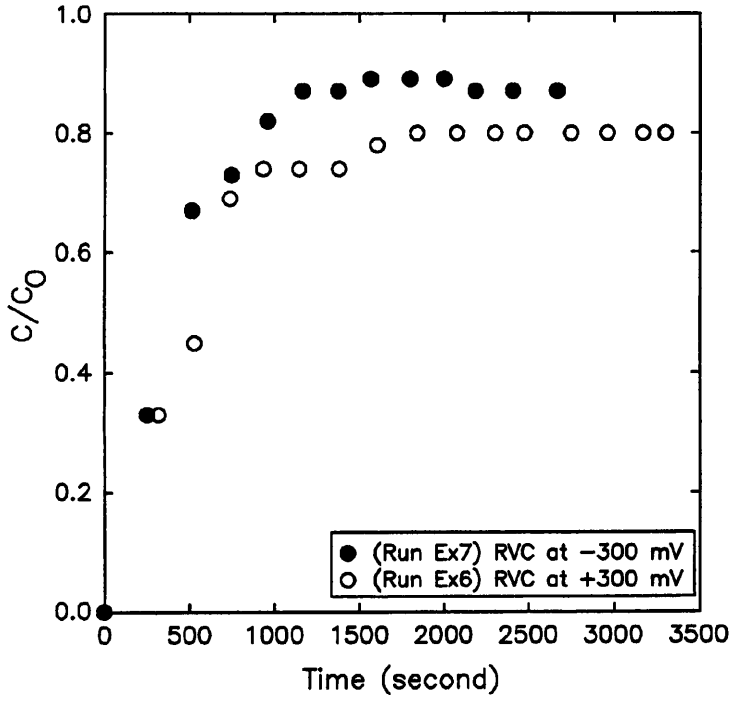

Figure 6.25 Particle break-through curves at KCl concentration of 0.0001 mol dm^{-3}, volumetric flowrate of 5.6 cm^3 min^{-1} and RVC potentials shown in the inset

At positive potentials at this electrolyte concentration DLVO theory suggests as shown in Figure 6.23 that favourable deposition condition exists between particle and collector and therefore the surface forces aid the total deposition process. On the contrary at negative RVC potentials a high energy barrier is reported to develop between particle and collector and the deposition rate should be lower. It can be seen from the particle break-through curves in Figure 6.25 that the curve corresponding to the RVC potential of +300 mV shows that indeed more deposition was obtained. In fact the steady state values of 0.88 and 0.8 for the runs where RVC was held potentiostatically at -300 and +300 mV, respectively, also provide evidence for agreement between the DLVO prediction and experimental results. The total deposit/feed weight ratio for runs Ex6 with RVC at +300 mV and Ex7 with RVC at -300 mV

as shown in Table 6.2 are 0.18 and 0.16 respectively. Additionally the deposition rate was determined from the slope of deposit weight vs time plots at the value of 700 seconds on the time-axis and these were 18.2×10^{-9} and 22.6×10^{-9} g/s respectively for Ex6 and Ex7.

The fluid drag force on the particle at flowrates of 34 and 5.6 $cm^3\ min^{-1}$ are shown in Table 6.1 to be 2.05×10^{-11} and 3.4×10^{-12} N respectively. It may be concluded from these values that as the flowrate decreased the fluid drag force on the particle also decreased resulting in an increase of the range of attractive energies from a separation distance of 100 nm to 190 nm and therefore a better correspondence between DLVO prediction and experiments obtained.

6.1.5 Variation of RVC potential at 0.01 mol dm^{-3} KCl solution

It was envisaged that the potentiostatic control of the RVC potential may produce the desired correspondence with the DLVO theory at intermediate KCl concentration, i.e. 0.001 mol dm^{-3}. Thus as explained previously the majority of runs were carried out at this concentration. However, two runs were carried out at 0.01 mol dm^{-3} with RVC potentials at -300 and +300 mV with their interaction energy profiles and particle break-through curves as shown in Figures 6.26 and 6.27 respectively. The main reason for this decision as seen in Figure 6.26 is that the DLVO prediction is that the electrical double layers for both cases are compact leading to the identical development of only attractive forces between particles and collector, i.e. the curves can not be distinguished from each other.

At first glance the particle break-through curves show that there are different steady state values obtained. The total weight of particles deposited after 1900 seconds as shown in Table 6.5 and the deposition rates, calculated from the slope of deposit weight vs time plot, reveal

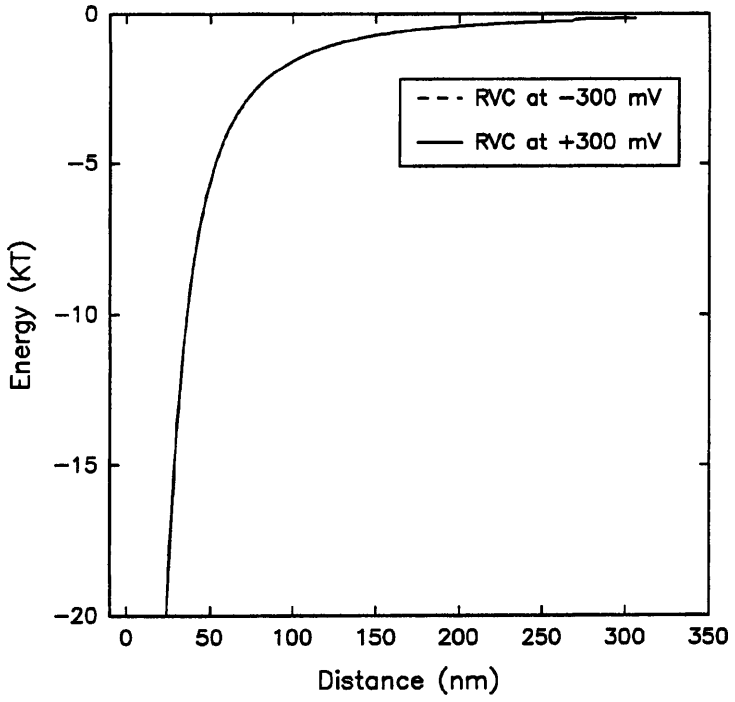

Figure 6.26 Interaction energy curves for runs with KCl concentration of 0.01 mol dm^{-3} and RVC potentials vs SCE at +300 mV and at -300 mV.

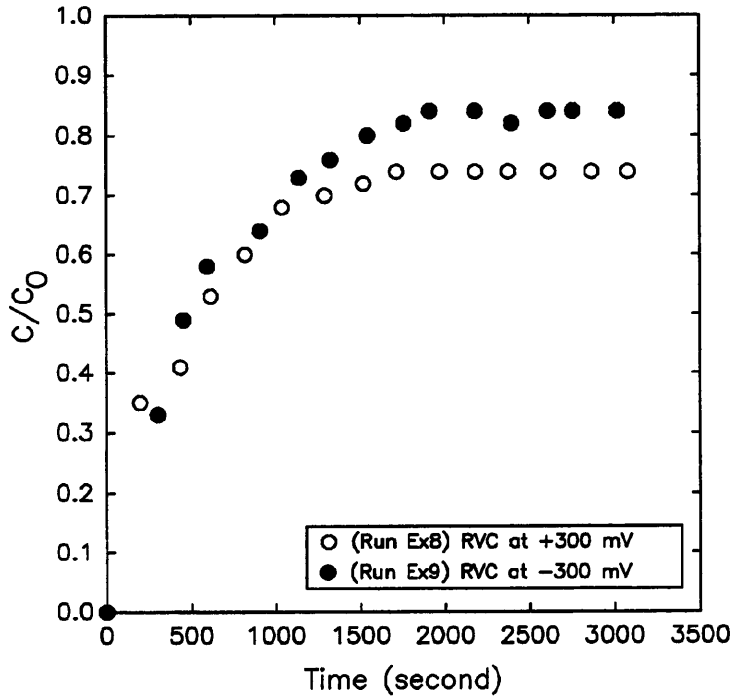

Figure 6.27 Particle break-through curves for runs with KCl concentration of 0.01 mol dm^{-3} and volumetric flowrate of 5.4 cm^3 min^{-1} and RVC potentials vs SCE +300 mV and -300 mV.

that in fact there are is more deposition occurring when RVC is +300 mV. This contradicts the DLVO prediction since the lower deposition obtained when RVC was held at -300 mV may in fact mean that there were an energy barrier against deposition. This discrepancy observed at unfavourable deposition will be more discussed in Chapter 8.

Table 6.5 Total and normalised weight of deposited particles for runs Ex8 and Ex9

	Ex8	Ex9
Total weight of feed entered, WF(g)	6.30×10^{-3}	6.70×10^{-3}
Total weight of particles deposited, WT(g)	2.70×10^{-5}	2.20×10^{-5}
WT/WF	4.30×10^{-3}	3.30×10^{-3}
Deposition rate at 1400 seconds (g/s)	4.60×10^{-9}	6.60×10^{-9}

Given the limited number of data sets, it was not possible to establish the reproducibility of experiments at 0.01 mol dm^{-3}, hence the reason for the discrepancy observed between the experimental measurement and DLVO can not be elucidated.

6.2 ADSORPTION OF *HYPERCARB* PARTICLES ON RVC

Another uniform monodispersed particulate system was investigated. The reason for this was to investigate further the universality of the deposition experiments so as to establish the possibility of manipulation of deposition process by externally controlled variation of RVC potential. The alternative particle employed was a graphitised carbon particle with the commercial name of *Hypercarb*. The zeta potentials and surface charge density values of *Hypercarb* particles were discussed in section 4.3.

The deposition experiments of polystyrene latex particles on RVC provided the experience that at high filtration flowrate (e.g >5.6 cm^3 min^{-1}) the effect of surface forces on the deposition process becomes negligible compared to the effect of hydrodynamics. Therefore the deposition experiments of *Hypercarb* on RVC were carried out at the low flowrate of 2.5 cm^3 min^{-1}.

Due to the cost of the feed stock purchased a total of 6 experimental runs were performed. The resulting data alongside with the experimental conditions can be seen in Appendix B. Three runs were carried out for KCl concentrations of 0.0001 mol dm^{-3} and three runs at KCl concentration of 0.001 mol dm^{-3}.

6.2.1 Variation of RVC potential at KCl concentration of 0.0001 mol dm^{-3}

Figure 6.28 shows the particle break-through curves and Figure 6.29 shows the corresponding interaction energy curves for these runs. As seen in Figure 6.29 the DLVO theory suggests that the more negative the RVC potential the higher the energy barrier leading to the prediction of lower surface force controlled deposition rate. Inversely at positive RVC potentials only attractive forces are predicted between the particle and collector leading to the prediction of high deposition rate. Therefore the deposition is predicted to occur in the order Hyp3>Hyp2>Hyp1.

However, the results in Figure 6.28 suggest that deposition occurs in the order Hyp3>Hyp1>Hyp2. Furthermore by comparing the total and normalised weights of deposited particles for these runs as shown in Table 6.6 it may also be concluded that the DLVO prediction was not obtained. The experimental data for runs Hyp1, Hyp2 and Hyp3 can be

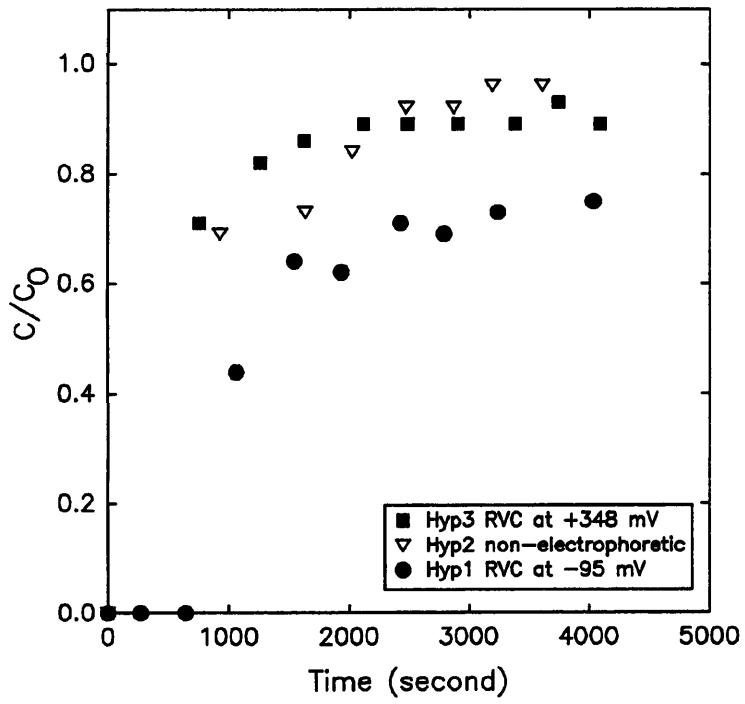

Figure 6.28 Particle break-through curves for deposition of *Hypercarb* on RVC at KCl concentration of 0.0001 mol dm^{-3} and volumetric flowrate of 2.5 cm^3 min^{-1} and RVC potentials as shown in the inset

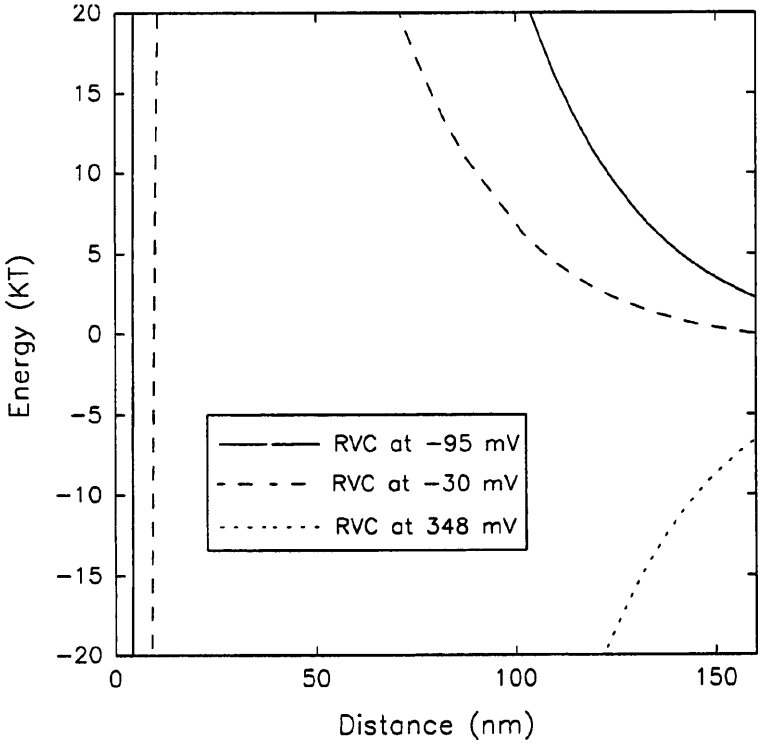

Figure 6.29 Interaction energy curves for deposition of *Hypercarb* on RVC at KCl concentration of 0.0001 mol dm^{-3} and RVC potentials vs SCE at -95 mV (Hyp1), -30 mV (Hyp2) and +348 mV (Hyp3)

seen in Appendix D. These figures show that there are no unexpected complication arising during the experiments and all the readings are fairly steady and therefore the experimental condition must be excluded from any fault finding investigations. Additionally the ohmic drop measurement carried out for these runs showed that the electrical connections were satisfactory.

The only other possible effect remaining which may have interfered with the deposition process is thought to be the presence of the non-ionic surfactant TRITON X-405 which was added to aid formation of a stable monodispersed suspension of *Hypercarb* particles. Hunter

Table 6.6 Total and normalised weight of deposited particles for runs Hyp1, Hyp2, Hyp3, Hyp4, Hyp5 and Hyp6

Time period of 3600 seconds	Hyp1	Hyp2	Hyp3	Hyp4	Hyp5	Hyp6
Total weight of feed, WF($x10^{-3}$ g)	5.80	3.30	3.60	4.40	4.20	4.20
Total weight of particles, WT($x10^{-5}$ g)	1.60	0.20	1.30	0.20	1.10	0.70
WT/WF($x10^{-3}$)	2.70	0.70	3.70	0.50	2.60	1.70

(1981) discusses the adsorption of non-ionic surfactant onto colloidal particles and argues that the experimental results in the literature show that adsorption of non-ionic surfactant near the c.m.c (critical micellar concentration) can sharply reduce the mobility values. Whereas adsorption of non-ionic surfactant well below the c.m.c value the adsorption of surfactant does not seem to affect the mobility values.

As explained in Chapter 4 the concentration of TRITON x-405 added to make up the *Hypercarb* suspension was 7 drops for a particle concentration of $5x10^{-4}$ g/cm^3 but the value for c.m.c for the present system could not be located in the literature.

Concluding from the above arguments the presence of the non-ionic surfactant may be partly responsible for the discrepancy observed with regard to the DLVO predictions.

Calculation of the London-van der Waals energy involves utilising an estimate for the Hamaker constant. As discussed at the beginning of this chapter, Hamaker (1937) states that for most substances the value for the Hamaker constant should lie in the range $1x10^{-21}$ to $1x10^{-19}$ J. Figure 6.30 shows the effect of variation of the Hamaker constant on the interaction energy profile for run Hyp1. The Hamaker constants employed were $1.0x10^{-21}$, $3.0x10^{-20}$ and $1.0x10^{-19}$ J, thus covering the range of values recommended by Hamaker (1937). It can be

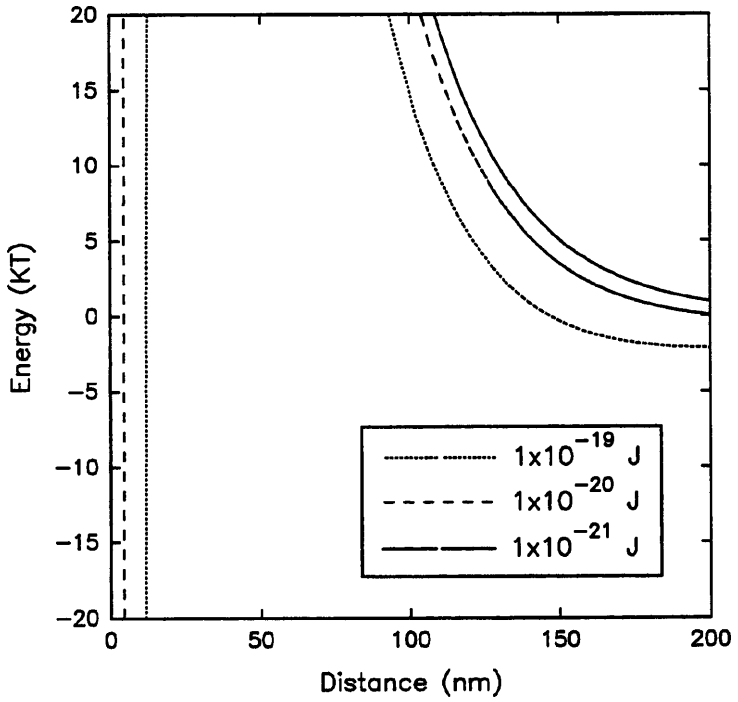

Figure 6.30 Effect of variation of Hamaker constant on the interaction energy profile for run Hyp1

seen from this figure that increasing the Hamaker constant from the adopted value of $3.0x10^{-20}$ J to $1.0x10^{-19}$ J increases the London-van der Waals interaction energy thus shifting the total

interaction energy profile downwards and reducing the height of the energy barrier. However, the total interaction energy profile still remains largely repulsive irrespective of this increase in the attractive energy therefore the adoption of larger value for the Hamaker constant does not seem to justify the observed discrepancy between DLVO prediction and experimental results.

6.2.2 Variation of RVC potential at KCl concentration of 0.001 mol dm^{-3}

In view of the discrepancies observed between the DLVO prediction and experimental results discussed in the previous section it was decided to perform three additional experiments at KCl concentration of 0.001 mol dm^{-3}. Figure 6.31 shows the particle break-through curves obtained for runs carried out at this concentration. Figure 6.32 shows the corresponding interaction energy profiles. The DLVO theory predicts the occurrence of secondary minimum for these runs but with a developing energy barrier from run Hyp4 to Hyp6. Therefore the DLVO theory predicts that surface force controlled deposition should occur in the order Hyp4>Hyp5>Hyp6. As seen in Figure 6.31 the experimental results show that deposition actually occurred in the order Hyp5>Hyp6>Hyp4. This result is also confirmed by the total deposited weight shown in Table 6.6. Close examination of the experimental data, as shown in Appendix D for runs Hyp4, Hyp5 and Hyp6 reveal that there were problems associated with gas evolution for run Hyp6 and to some degree for run Hyp5 manifested by the rise in the outlet pH during the experiments.

It is believed that it has been shown that the discrepancy may not have risen from the experimental procedures and neither could it have risen from the choice of *wrong* value of the Hamaker constant as it was shown for the run Hyp1 (see Figure 6.30) that changing the

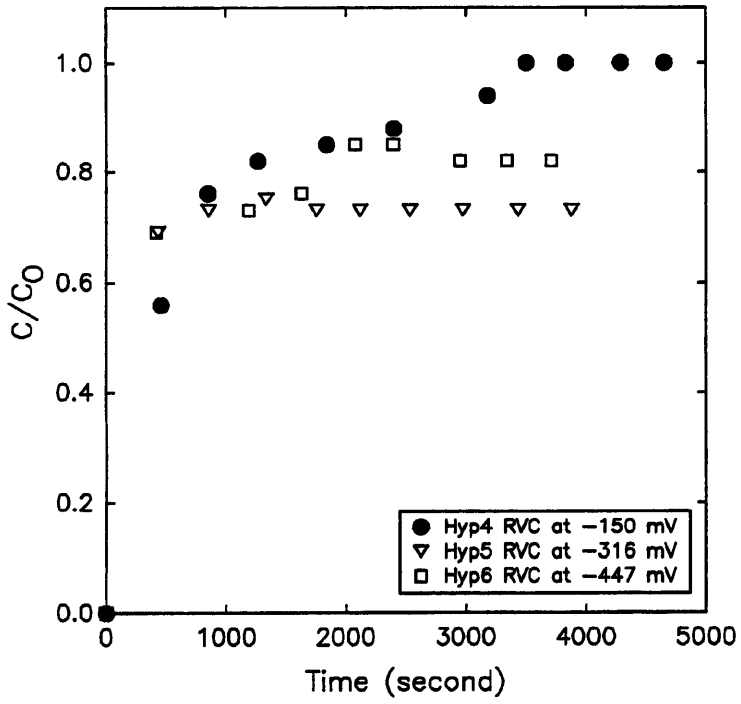

Figure 6.31 Particle break-through curves for deposition of *Hypercarb* particles on RVC at KCl concentration of 0.001 mol dm^{-3}, volumetric flowrate of 2.5 cm^3 min^{-1} and RVC potentials as shown in the inset

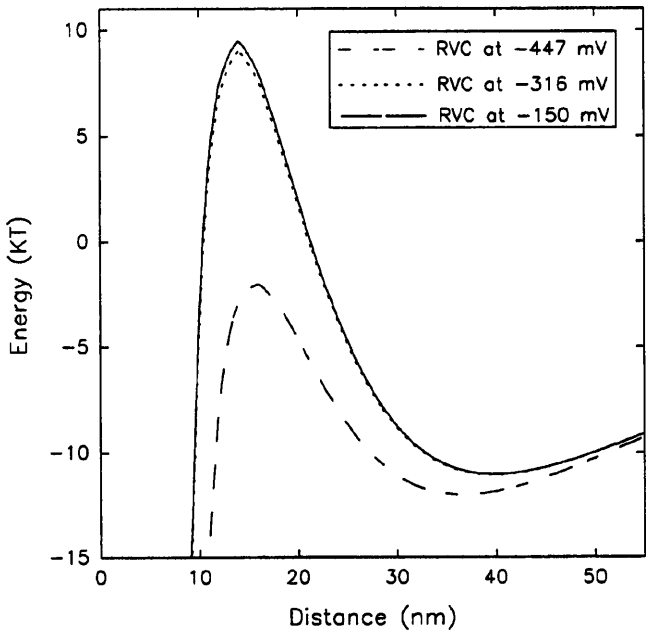

Figure 6.32 Interaction energy profiles for deposition of *Hypercarb* particles on RVC at KCl concentration of 0.001 mol dm^{-3}, volumetric flowrate of 2.5 cm^3 min^{-1} and RVC potentials vs SCE at -150 mV (Hyp4), -316 mV (Hyp5) and -447 mV (Hyp6)

Hamaker constant to extreme values did not produce significant change in the total interaction energy profiles.

There were several arguments put forward previously to account for the discrepancies observed between DLVO prediction and experimental results of deposition of polystyrene latex particle on the RVC collector. It is believed that these arguments are applicable to the observed discrepancy between DLVO prediction and experimental results of deposition of *Hypercarb* on the RVC collector. Additionally, it is believed that the role of different characteristics of *Hypercarb* particles must be taken into account.

There are two main characteristics of the *Hypercarb* particles which differ greatly from that of latex particles. First the *Hypercarb* particles are made up of highly porous carbon material.

It was mentioned in section 4.3 (Chapter 4) that due to this high porosity there was problem associated with trapped air bubbles within the pores thus resulting in the need to use the non-ionic surfactant to disperse the particles. It is believed as discussed previously the presence of surfactant and of trapped gas bubbles within the pores may undermine the surface charge density values by interfering with the double layer interactions in a non-specific manner resulting in an incorrectly estimated value for the surface charge density of these particles (see Table 4.3). Second, the nature of functional groups present on the surface of *Hypercarb* particles may play a decisive role in the deposition process. The manufacturer reports that there are no functional groups present at the surface of particles but perhaps several carbon atoms at the edge of the graphitic sheet may be free to be attached to functional groups such as hydroxyl, carbonyl, carboxylic or perhaps amino functions.

Concluding the above argument to investigate the discrepancy observed between the deposition experiment and DLVO predictions, it is believed that emphasis must be placed on the role that the *Hypercarb* particles play in the process.

CHAPTER 7

TRAJECTORY ANALYSIS OF DEPOSITION

7.1 INTRODUCTION

In the previous two chapters the results of deposition experiments are discussed and these are then compared with the prediction of the DLVO theory. Attempts were made to justify any observed discrepancy between the prediction and experimental results.

It was discussed in Chapter 6 that a main contributing factor to the observed discrepancy between the theory and experiment at high volumetric flowrates was thought to be the effect of fluid drag on the particles. The transportation of non-Brownian particles to the vicinity of the collector occurs mainly by means of fluid flow. Consequently it was discussed in the previous chapter that the fluid flow in effect may play a dual role of transporting the particles to the vicinity of the collector and under some circumstances it may impose a drag force strong enough to prevent particles from depositing.

The DLVO prediction is based on the simulation of operating electrostatic forces between two surfaces. The total force of interaction is assumed to be the sum of the London-van der Waals and the repulsive electrical double layer forces.

A better representation of the deposition process should incorporate a number of other forces not included in the DLVO theory. It was discussed in the previous chapter that it was thought that the main forces contributing to the deposition process in the present system were the hydrodynamics and the surface forces. Therefore improvement to the DLVO prediction may

be obtained if these forces were incorporated.

The modelling of deposition of non-Brownian colloidal particles on spherical collector based on the trajectory analysis utilising the Happel's sphere-in-cell porous media model was discussed at length in section 2.3.1 (see Figure 2.3). The resulting semi-empirical relationship (equation (2.24)) is used in Chapter 5 to compare with theory the deposition experiments of polystyrene latex particles on the spherical glass bead collectors. It was decided to use the same modelling technique, i.e. trajectory analysis, to theoretically analyse the deposition experiments on the RVC collector.

The trajectory analysis in essence involves carrying out a force balance on the particle approaching a collector. The extent of deposition can be found from the location of the limiting trajectory, defined as the trajectory that divides the trajectory for deposition from that for non-deposition. A schematic representation of the limiting trajectory concept for the spherical collector can be seen in Figure 2.3 (Chapter 2).

7.2 DEVELOPMENT OF TRAJECTORY MODEL

To apply this analysis use was made of an approach developed by Spielman and Goren (1968) (see Table 2.5). This model utilises the trajectory analysis concept to simulate the particle capture by a *cylindrical* collector.

As discussed in Chapter 3, close observation of the SEM photograph of RVC as shown in Figure 3.3 reveals that RVC is in fact made up of *rectangular* elements 300 μm long and 37 μm wide, their thickness being negligible compared to the length. The major underlying

assumption for employing the trajectory analysis for the present study was that these rectangular elements may be assumed to behave as cylinders in so far as predicting the contribution of hydrodynamics. This may not necessarily cause problems, as will be discussed in the foregoing paragraphs, since hydrodynamic interaction between particle and collector becomes significant at short distances of separation. The polystyrene latex particles employed were 5.4 μm in diameter and at small separation distances the model, which will be utilised, considers the cylindrical collector to behave as a plane. It was also assumed that the bulk of the deposition occurs along the length of the cylinders and the end effects can be ignored.

The suspension will be assumed sufficiently dilute so that the interaction between particles may be neglected. Due to the low flowrates utilised the effects of inertial impaction was neglected and also since non-Brownian particles were employed the effect of Brownian diffusion was considered negligible. Therefore the force balance is assumed to be made up of the electrostatic, gravity and hydrodynamic forces.

Flow disturbances caused by the presence of a particle in the vicinity of a much larger collector has been tackled by several authors. Natanson (1957) assumed that the particle velocity deviates from the fluid velocity according to the Stoke's resistance law for the motion of a sphere in an infinite medium and therefore without the existence of an external force the particle moves along the undisturbed fluid motion.

Spielman and Goren (1968) improved upon Natanson's analysis by using the undisturbed flow field near the collector as the boundary condition on the particle motion. The 'exact' hydrodynamical interactions were considered by employing the available results of Stoke's equations.

The fluid motion is in general governed by the Navier-Stokes equations:

$$\frac{\partial U}{\partial t} + U.\,\nabla U + \frac{1}{\rho_f}\nabla p = \nu\,\nabla^2 U \tag{7.1}$$

and the continuity equation:

$$\nabla.\,U = 0 \tag{7.2}$$

for incompressible fluids. For slow motion it is possible to assume the inertial term U. ∇U and the time-dependent term, ∂U/ ∂t, negligible compared to the viscous term, $\nu\,\nabla^2$ U, and these simplifications result in the incompressible creeping flow equations:

$$\begin{aligned} \nabla p &= \mu\,\nabla^2 U \\ \nabla U &= 0 \end{aligned} \tag{7.3}$$

The particle freely translates and rotates according to its equations of motion under the influence of hydrodynamic and external forces. Therefore the particle creates a locally confined disturbance which is governed by the creeping flow equations (7.3). Where p is the disturbance pressure field, U the disturbance velocity and μ is the viscosity.

To determine the motion of the particle and its accompanied fluid the creeping flow equations (7.3) must be solved and consequently boundary equations are needed. The boundary conditions required for solving equations (7.3) are that the no slip condition applies at the collector and particle surfaces and far from the particle the fluid moves at velocity of the undisturbed flow past the cylinder (collector). Consequently, the undisturbed flow around a cylinder should be determined.

By assuming that the cylinder is infinitely long thus neglecting the end effects Speilman and Goren (1968) show that the undisturbed slow motion of fluid near a cylinder is given by the stream function:

$$\Psi = 2 A_F U a_f^{-1} (r - a_f)^2 \sin\alpha \qquad (7.4)$$

Where a_f is the cylinder radius, U the fluid velocity far from the collector, r the radial coordinate, α the angular coordinate as shown in Figure 7.2 and A_F is a parameter characterising the flow model. For isolated cylinders A_F is found from Lamb's (1932) solution :

$$A_F = 1/2 \left[1 - \ln \left(\frac{2 \rho_f a_f U}{\mu} \right) \right]^{-1} \qquad (7.5)$$

where μ is the fluid viscosity and ρ_f density. Spielman and Goren (1968) considered the fibres in a fibre mat as cylinders and obtained a relationship for A_F in terms of the voidage, β:

$$A_F = 1/2 \left[-1/2 \ln(1-\beta) - 1/2 + \frac{(1-\beta)^2}{2[1+(1-\beta)]^2} \right]^{-1} \qquad (7.6)$$

Happel (1959) also obtained a relationship for A_F:

$$A_F = 1/2 \left[-1/2 \ln(1-\beta) - 3/4 + (1-\beta) - \frac{(1-\beta)^2}{4} \right]^{-1} \qquad (7.7)$$

The undisturbed flow field far from a particle is resolved as shown in Figure 7.1 into two flows, one a planar stagnation flow, U_{st} (arising from that velocity component at infinity along the line of centres of the cylinder and particle) having a stagnation point at the collector surface, and a shear flow, U_{sh} (arising from the flow normal to the line of centres). The movement of particle and its disturbance field were similarly decomposed into the fields corresponding to its normal and tangential motions separately. Spielman and Goren (1968) argue that this is allowed since the equation of motion (7.3) is linear and consequently the boundary conditions are additive (see Figure 7.2).

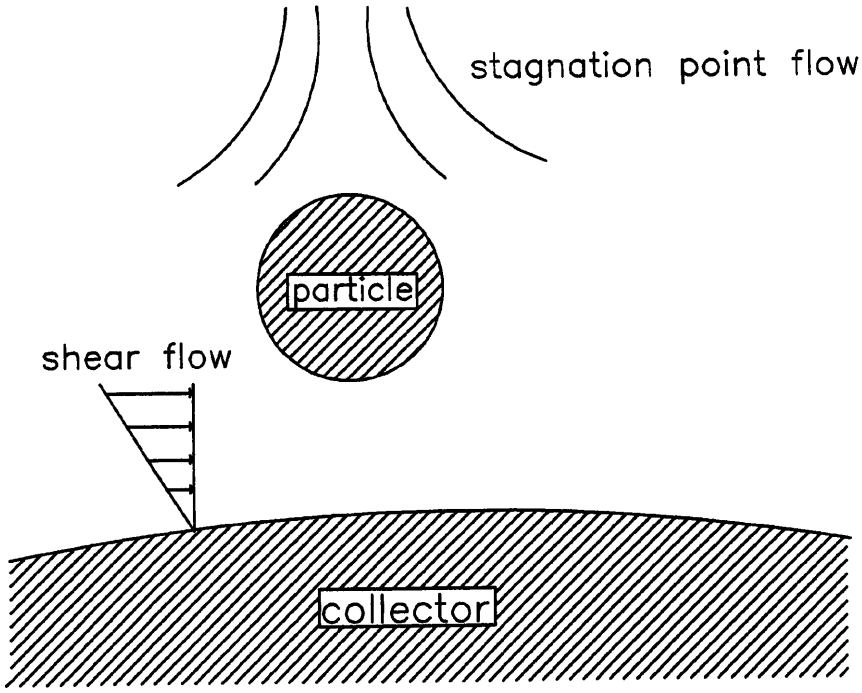

Figure 7.1 Schematic representation of the flows acting on a particle near a collector

For a two-dimensional planar motion the velocity components of the shear flow normal to the line of centre, U_{sh}, and the stagnation point flow along the line of centre, U_{st}, are found from the equation of the stream function as follows:

$$U_{st} = -\frac{1}{r}\frac{\delta \Psi}{\delta \alpha} \quad , \quad U_{sh} = \frac{\delta \Psi}{\delta r} \tag{7.8}$$

Where α is the angular coordinate as shown in Figure 7.2. The angular displacement of the particle from the forward stagnation point is α_p. As the particle moves in x direction over the collector surface to a new position shown by the dotted line OA in Figure 7.2, the angle α also changes. At this new position the radial velocity along the line of centre, U_{st}, remains the same while the component normal to the line of centre, U_{sh}, additionally contributes to the radial component by the amount given by the second term in equation (7.9).

$$U_{sh} = 4\,A_F\,a_f^{-1}\,U\,\sin\alpha_p\,y\,i_\alpha + 4\,A_F\,a_f^{-2}\,U\,\cos\alpha_p\,x\,y\,i_\alpha \tag{7.9}$$

$$U_{st} = -2\,A_F\,a_f^{-2}\,U\,\cos\alpha_p\,y^2\,i_R \tag{7.10}$$

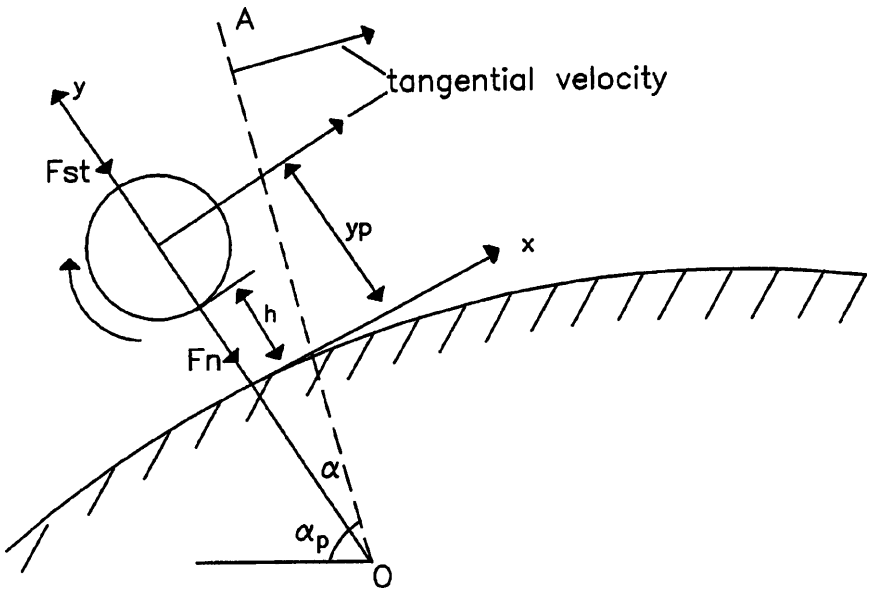

Figure 7.2 Schematic representation of the forces considered in the trajectory analysis

Therefore the velocity along the line of centre is given by:

$$u_{st} = 2\,A_F\,a_f^{-2}\,U\,\cos\alpha_p\left[\,2xy\,i_\alpha - y^2\,i_R\,\right] \tag{7.11}$$

Where $x=a_f\alpha$ and $y=r-a_f$ and i_α and i_R are unit vectors in the tangential and normal directions. These formulae for the undisturbed fluid velocity are valid for $a_f>(x^2+y^2)^{1/2}>a$.

Since the particle is much smaller than the collector it is assumed that the flow field past the cylinder is undisturbed by the presence of particles, except in the immediate vicinity of the

collector, and that at separations greater than several particle diameters, the particle centre moves along the undisturbed streamlines. Spielman and Goren (1968) argued that at close distances of separation it is important to take more realistic hydrodynamic interactions into account. The particles are so small compared to the cylinder that at small separation distances a particle trajectory differs significantly from an undisturbed fluid streamline and they assumed that the cylinder can be treated as a plane wall. If h is the minimum gap between the particle and the *flat* collector surface then the particle centre is located at x=0 and $y=y_p=(a+h)$.

The radially directed motion of the particle is imagined to be carried out under the influence of an external force F_n consisting of a molecular component and a hydrodynamic component. To arrive at an expression for the particle velocity under the influence of F_n, where Stoke's law applies, Spielman and Goren (1968) assume that the velocity should only depend on the parameters which enter into the equation of motion (7.3) and the boundary condition of the problem (i.e. no slip at the particle and collector surfaces and the Stoke's law):

$$v_R = \frac{dy_P}{dt} = \frac{dh}{dt} = F_1 \left[\mu , F_n , a , h \right] \tag{7.12}$$

Following dimensional analysis:

$$v_R = \frac{dy_p}{dt} = \frac{dh}{dt} = \frac{F_n F_1(H)}{6 \pi \mu a} \tag{7.13}$$

$F_1(H)$ is a universal function of the dimensionless gap width H=h/a. The value of $F_1(H)$ is known for all values of H from the exact solution of Stoke's equation obtained by Brenner (1961). Spielman and Fitzpatrick (1973) have discussed the asymptotic behaviour of this

function and following their analysis in the present study the following expressions were used:

$$F_1(H) \approx H \qquad \text{for} \quad h < a < a_f$$
$$F_1(H) \approx \left[1 - \frac{9}{8} (H + 1)^{-1} \right] \quad \text{for} \quad a < h < a_f \tag{7.14}$$

In the hydrodynamic component of the force F_n the particle was assumed to be held stationary in a field which became the stagnation point flow, U_{st}, far from the particle. They maintain that the no slip boundary conditions at the particle and collector applies therefore the particle is acted on in the radial direction by a force, F_{st}. Spielman and Goren (1968) argue that the expression for F_{st} should contain the same parameters that enter the boundary conditions (i.e. no slip at the particle and collector surfaces and equation (7.11) for U_{st}):

$$F_{st} = F_2 (\mu , a , h , a_f^{-2} A_F U \cos\alpha_p) \tag{7.15}$$

Following dimensional analysis the following expression for this radial force is obtained:

$$F_{st} = -6\pi \mu a^3 a_f^{-2} A_F U \cos\alpha_p F_2(H) \tag{7.16}$$

Where $F_2(H)$ is the universal function of the dimensionless gap width H=h/a and the expressions obtained by Spielman and Fitzpatrick (1973) for the asymptotic behaviour of this function was utilised in this study:

$$F_2(H) \approx 3.23 \qquad \text{for} \quad h<a<a_f$$
$$F_2(H) \approx \left[1 - \frac{9}{8} (H + 1)^{-1} \right]^{-1} \quad \text{for} \quad a<h<a_f \tag{7.17}$$

The particle and its accompanied fluid move in the radial direction under the influence of the forces discussed above. The motion of the particle can be determined by combining the flows discussed such that the net force on the particle is zero.

Therefore, this leads to the applied force F_n being equal to the hydrodynamic force F_{st} and an

external force F_{ext}:

$$F_n = F_{st} + F_{ext} \tag{7.18}$$

To visualise the above force balance better it may help to consider the settling of a spherical particle of radius a in an infinite unbounded fluid of viscosity μ. The particle settles under the influence of gravity against a frictional force F until the frictional force just balances the gravity force and consequently the particle will continue to settle at a uniform settling velocity of U i.e. Stoke's law which is derived from the incompressible creeping flow equations:

$$F = 6 \pi \mu a U \tag{7.19}$$

Close to an obstacle, e.g a cylinder, the same particle experiences additional forces such as hydrodynamic and for a charged particle electrostatic forces. Subsequently, the settling velocity, U, is now reinforced by two more fields in the same direction as U.

The external force, F_{ext}, in equation (7.18) is asumed by Spielman and Goren (1968) to consist of London-van der Waals and electrical double layer, however, in this study the gravity force will also be included to examine its effect on the simulations:

$$F_{ext} = F_{LO} + F_{EDL} + F_{Gr} \tag{7.20}$$

The London-van der Waals force was calculated from the expression obtained by Hamaker (1937):

$$F_{LO} = F_{ret} \times \frac{2}{3} \times \frac{A}{a} \times \frac{1}{(H+2)^2 H^2} \tag{7.21}$$

Where F_{ret} is incorporated to take into account the retardation effect. The value for F_{ret} was

discussed by Kruyt (1965) and Payatakes et al. (1974) provided the following limiting forms:

$$F_{ret} = \frac{1}{1 + 0.620725\ p + 0.075159\ p^2} \quad for\ \ 0 < p < 3 \qquad (7.22)$$

$$F_{ret} = \frac{1.024172}{p} - \frac{0.714228}{p^2} + \frac{0.555262}{p^3} \quad for\ \ 3 < p < \infty \qquad (7.23)$$

Where $p = 2\ \pi\ h\ /\omega$, h is surface-to-surface separation distance shown in Figure 7.2 and ω is the characteristic wavelength of the atoms (usually assumed 100 nm).

The electrical double layer force is estimated from the expression due to Hogg et al. (1966) for a sphere and a plane at constant potential:

$$F_{EDL} = \frac{\epsilon\ a\ \kappa\ (\ \psi_1^2 + \psi_2^2\ )}{2} \left[\frac{2\psi_1\ \psi_2}{(\ \psi_1^2 + \psi_2^2\ )} - e^{-\kappa h} \right] \frac{e^{-\kappa h}}{1 - e^{-2\kappa h}} \qquad (7.24)$$

Where ψ_1 and ψ_2 are surface potentials which will be assumed to be the measured zeta potential values for the particle and collector respectively and for the cases of the collector potentials being maintained externally the applied potential will be used. ϵ is the fluid permittivity and κ is called the Debye-Huckel reciprocal length, discussed in Chapter 2, and estimated from equation (2.7).

The gravity force contributes to both radial and tangential velocities and the radial component corrected for the fluid buoyancy is given by:

$$F_{Gr} = -\frac{4}{3}\ \pi\ a^3\ (\ \rho_p - \rho_f\ )\ g\ \cos\alpha \qquad (7.25)$$

Substituting equations (7.21), (7.24) and (7.25) into equation (7.20) and then substituting the resulting expression along with equations (7.13) and (7.16) into equation (7.18) yields the

following expression for the radial velocity component of

the particle:

$$\frac{dH}{dt} = -\frac{F_1(H)}{6\pi\mu a^2}\left\{ 6\pi\mu a^3 a_f^{-2} A_F U \cos\alpha_p F_2(H) + \frac{2}{3}\frac{A}{a}\frac{F_{ret}}{(H+2)^2 H^2} + \frac{4}{3}\pi a^3 (\rho_p - \rho_f) g \cos\alpha_p - \frac{\epsilon a \kappa (\psi_1^2 + \psi_2^2)}{2}\left[\frac{2\psi_1\psi_2}{(\psi_1^2 + \psi_2^2)} - e^{-\kappa h}\right]\frac{e^{-\kappa h}}{1 - e^{-2\kappa h}} \right\} \tag{7.26}$$

The particle velocity tangential to the collector surface, v_α, was obtained by considering the particle to freely rotate and translate. An expression for this velocity Spielman and Goren (1968) assumed, should only contain the parameters that enter the no slip boundary conditions at the particle and collector surfaces and also the expression for the shear flow, U_{sh}, normal to the line of centre of the cylinder far from the particle:

$$v_\alpha = F_3 (a , \mu , h , a_f^{-1} A_F U \sin\alpha_p) \tag{7.27}$$

Following dimensional analysis they obtain:

$$v_\alpha = a_f \frac{d\alpha_p}{dt} = a\, a_f^{-1} A_F U \sin\alpha_p f_3(H) \tag{7.28}$$

Where $F_3(H)$ is the universal function and in this study the approximate expressions obtained by Spielman and Fitzpatrick (1973) for the asymptotic behaviour of this function is utilised:

$$F_3(H) \approx \left[\frac{0.7431}{(0.6376 - 0.200 \ln H)}\right] \quad \text{for } h<a<a_f$$
$$F_3(H) \approx \left[1 - \frac{5}{16}(H+1)^{-3}\right] \quad \text{for } a<h<a_f \tag{7.29}$$

The second contributing flow field corresponds to the free rotation and translation of the particle under the force of gravity acting tangential to the collector surface. This problem is also solved by Goldman et al. (1967):

$$v_g\alpha = \frac{4}{3}\,\pi\, a^3\,(\,\rho_p - \rho_f\,)\,\frac{F_4(H)}{6\,\pi\,\mu\,a} \qquad (7.30)$$

The values for the universal function $F_4(H)$ was tabulated by Goldman et al. (1967) but in this study it is assumed to be unity for simplicity. Figure 7.3 shows the asymptotic behaviour of the hydrodynamic functions obtained by Spielman and Fitzpatrick (1973).

As with the radial velocity component it will be assumed that the rule of additivity of velocities applies and consequently total tangential velocity component can be found by adding equations (7.28) and (7.30) to give:

$$\frac{dv_\alpha}{dt} = \frac{a\,A_F\,\sin\alpha_p\,U}{a_f^2}\left[\,F_3(H) + N_G\,\frac{a}{a_f}\,\right] \qquad (7.31)$$

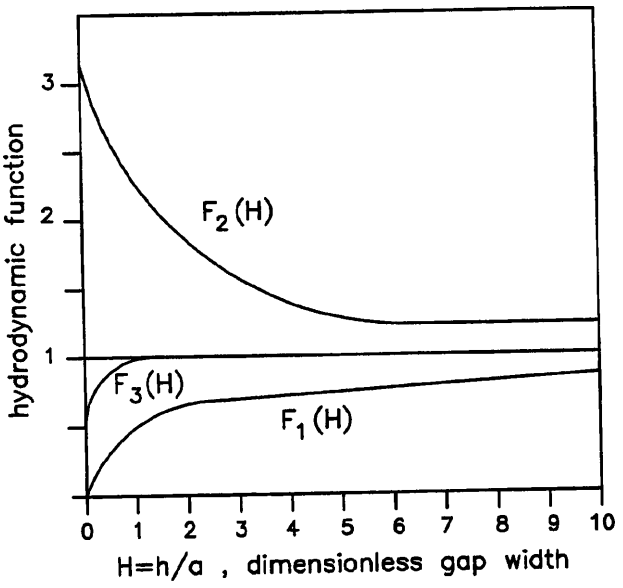

Figure 7.3 Variation of the hydrodynamic interaction functions for different gap widths

Eliminating the time derivative between equations (7.26) and (7.31) yields the trajectory

equation:

$$\frac{-\sin\alpha_p}{F_1(H)}\frac{dH}{d\alpha} = \frac{F_2(H)\cos\alpha_p + N_G\cos\alpha_p + ND_1\,(ND_2 - ND_3)\,ND_4 + N_{LO}\dfrac{F_{rel}}{(H+2)^2 H^2}}{F_3(H) + N_G\dfrac{a}{a_f}} \quad (7.32)$$

Where:

$$N_{LO} = \frac{A\,a_f^2}{(9\,\pi\,\mu\,A_F\,U\,a^4)} \quad , \quad N_G = \frac{2\,a_f^2\,g\,(\rho_P - \rho_f)}{9\,\mu\,U\,A_F}$$

$$ND_1 = \frac{\epsilon\,\kappa\,a_f^2\,(\psi_1^2 + \psi_2^2)}{12\,\pi\,\mu\,a^2\,A_F\,U} \quad , \quad ND_2 = \frac{2\,\psi_1\,\psi_2}{\psi_1^2 + \psi_2^2}$$

$$ND_3 = e^{-\kappa h} \quad , \quad ND_4 = \frac{e^{-\kappa h}}{1 - e^{-2\kappa h}} \quad , \quad H = \frac{h}{a} \qquad (7.33)$$

7.3 METHOD OF SOLUTION

For this thesis, the ordinary differential equation (7.32) was easily solved using the NAG library routine D02EAF available on Hewlett-Packard workstations which run the system V.2 Unix. This routine uses a variable-order variable-step method implementing the Backward Differentiation Formula (BDF). The Fortran programm TRAJ.F presented in Appendix D was written to carry out this task.

The limiting trajectory as explained in section 2.3.1 (Chapter 2) divides the trajectories for collection from those that pass the collector. The limiting trajectory must make contact with the collector at the rear stagnation point at an angle π from the forward stagnation point. This can be better visualised in Figure 7.4. The value of H^*, the separation distance, at the rear stagnation point corresponding to the limiting trajectory can be found by setting equation

(7.32) equal to zero at $\alpha=\pi$. Programm ROOT.F as shown in Appendix D was written to perform this task utilising the NAG library routine C05ADF. This routine finds a zero of a continuous function in a given interval by a combination of the methods of linear interpolation, extrapolation and bisection.

To locate the limiting trajectory the integration of equation (7.32) was initiated at points (H^*,π) and the integration was performed backward until the streamline coincided with the undisturbed fluid streamline far from the particle (usually a collector radius from the collector).

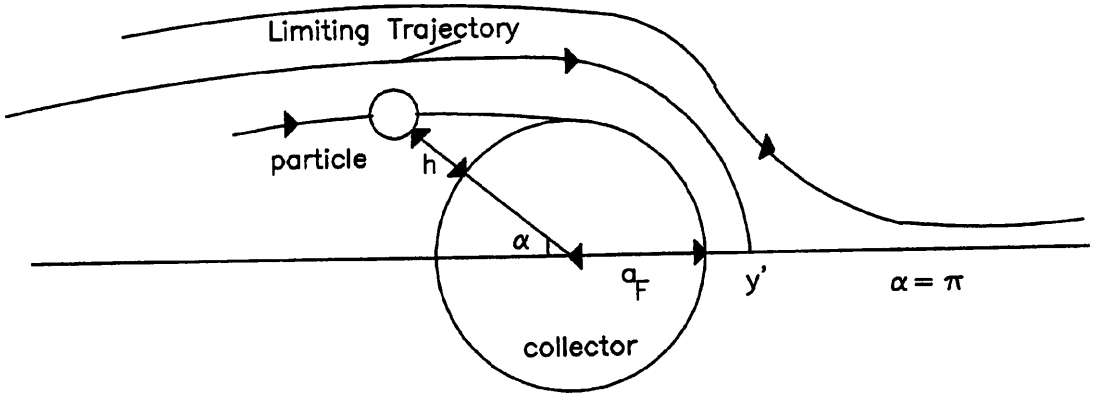

Figure 7.4 Schematic representation of the location of the limiting trajectory

7.4 SIMULATION RESULTS

Prior to comparing the trajectory predictions with the experimental results it is helpful to analyse the trajectory simulations and discuss any limitations imposed by the relationships used for estimation of forces.

7.4.1 Location of the limiting trajectory

The procedure for solution of the trajectory equation was discussed previously. The location of the limiting trajectory involves finding the value for H^* at the rear stagnation point. In the following paragraphs several simulation results will be discussed.

Figure 7.5 shows a typical variation of H^* with N_{LO} for fixed values of N_G. It can be seen from this figure that increasing the van der Waals attraction causes increases in the value of H^* i.e. the limiting trajectory extends further from the collector. Once the value of H^* was determined, for a set of experimental conditions, the trajectory equation (7.32) was integrated backwards until the streamline coincided with the fluid

streamline.

Figure 7.6 shows the variation of α with h^*, the separation distance, for the limiting trajectory estimated at KCl concentration of 0.0001 mol dm^{-3}, volumetric flowrate of 34 cm^3 min^{-1}, particle potential of -8.5 mV and collector potentials of -26.5 and 300 mV. The curve at RVC potential of +300 mV, where *favourable conditions* pertain, shows that the limiting trajectory starts at a distance of 64 nm from the rear stagnation point at an angle of 180° from the forward stagnation point and remains at this angle up to a distance of 180 nm and after this the trajectory moves vertically away from the collector. This pattern is the result of the force balance which below 180 nm predicts a strong attractive force and with a reducing attractive force as the particle moves away from the collector. Any particle following a trajectory which brings it to a separation distance more than 64 nm from the rear of collector will pass the collector and inversely any particle coming to a separation distance less than 64 nm will be considered collected.

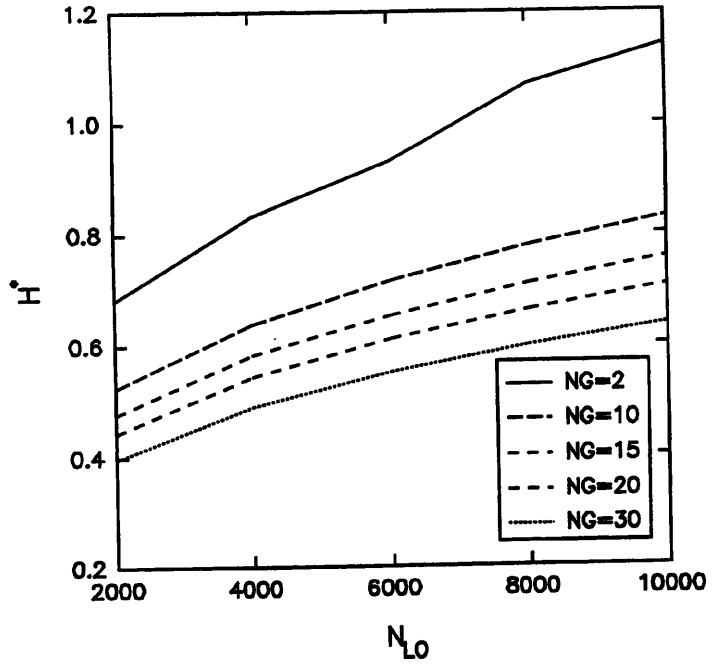

Figure 7.5 Variation of H^* with N_{LO} for fixed N_G, flowrate of 34 cm^3 min^{-1}, KCl concentration of 0.0001 mol dm^{-3}, particle potential of -8.5 and collector potential of -26.5 mV

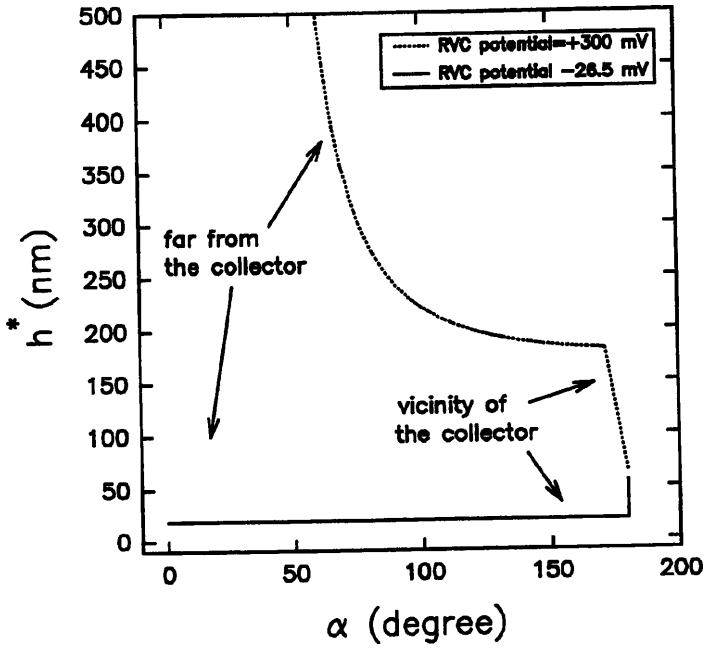

Figure 7.6 Variation of h^* with α for the limiting trajectory for KCl concentration of 0.0001 mol dm^{-3}, particle potential of -8.5 mV, volumetric flowrate of 34 cm^3 min^{-1} and collector potentials of -26.5 and +300 mV

The curve corresponding to the RVC potential of -26.5 mV remains close to the surface of the collector even at small angles. The program TRAJ.F was run with different initial conditions, keeping the particle-collector surfaces similarly charged, but still the same pattern was observed. This trend was also obtained in theoretical analysis by Tien et al. (1974). Tien et al. (1974) argue that the physical interpretation of this pattern is that for a particle to be captured the initial location has to be near the collector and there will be no need for the particle to penetrate into the region where the double layer dominates. This subsequently leads to low filter coefficient values which they argued to be in qualititative agreement with experiments.

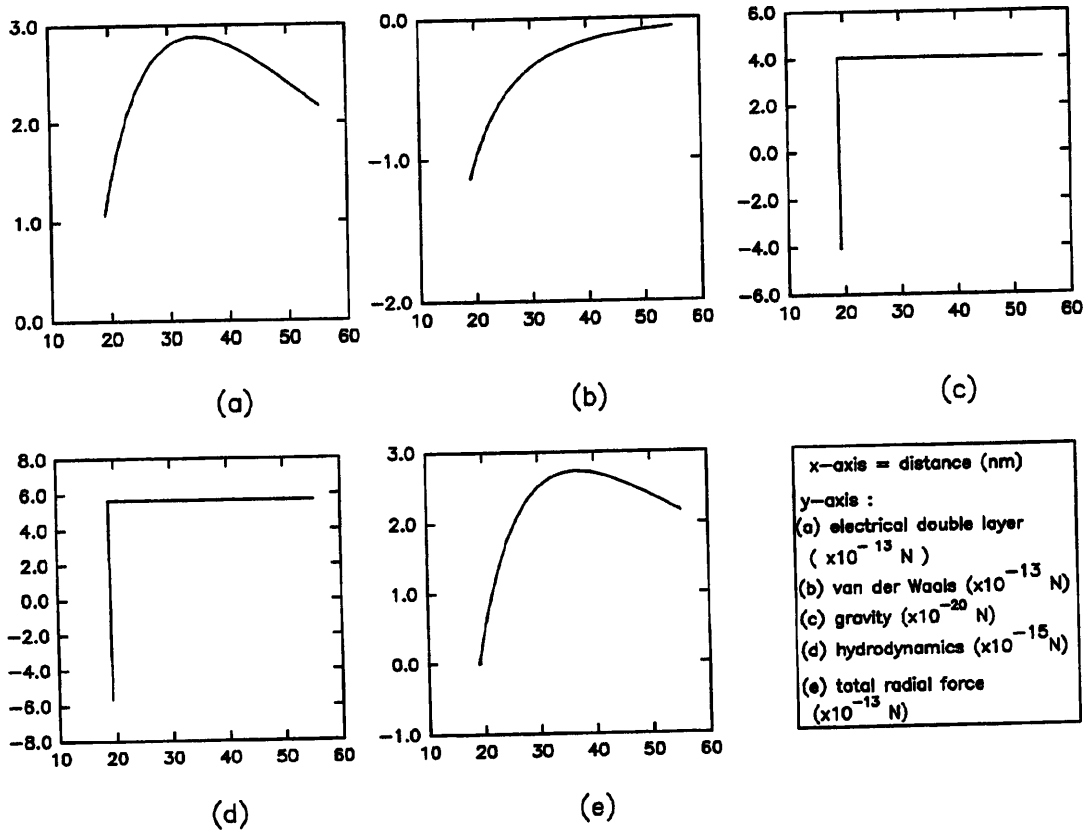

Figure 7.7 Variation with distance of various forces considered for obtaining the limiting trajectory presented in Figure 7.6 at KCl concentration of 0.0001 mol dm^{-3}, volumetric flowrate of 34 cm^3 min^{-1}, particle potential of -8.5 and collector potential of -26.5 mV

Figure 7.7 shows the variation with distance of various forces considered for estimation of the limiting trajectory at RVC potential of -26.5 mV. The electrical double layer (graph a) and van der Waals (graph b) forces can be compared in this figure and it can be seen that the total radial force (graph e) calculated was dominated by the electrical double layer which shows a maximum at separation distance of approximately 38 nm.

It was discussed previously that far from the collector the limiting trajectory was assumed to coincide with the fluid streamline. Assuming that this occurs sufficiently close to the collector that equation (7.4) holds then the collection efficiency can be estimated from :

$$\eta = \frac{\Psi_{lim}}{U\, a_f} \tag{7.34}$$

The filter coefficient, λ, was defined in Chapter 2 using equation (2.22). when all the collectors are the same size and shape the collection efficiency of a collector, η, and the filter coefficient, λ, were related to one another by Tien (1989):

$$\lambda_{the} = \frac{1}{l_c} \ln \frac{1}{1-\eta} = \frac{\eta}{l_c} \quad if \quad \eta < 1 \quad where \quad l_c = \frac{\pi^{\frac{1}{2}}\, a_f}{(1-\beta)^{\frac{1}{2}}} \tag{7.35}$$

Where l_c is defined as the length of periodicity or the axial distance of a unit collector. The experimental filter coefficient can be obtained from integration of equation (2.22):

$$\ln \frac{C_{in}}{C_{out}} = \lambda_{exp}\, L \tag{7.36}$$

Figures 7.8 to 7.11 show several simulation results obtained for the variation of the collection

efficiency and filter coefficient at volumetric flowrate of 34 cm^3 min^{-1}. It can be seen from Figure 7.8 that the collection efficiency and filter coefficient increase with increasing N_{LO} as shown previously in Figure 7.4.

At a volumetric flowrate of 34 cm^3 min^{-1} and a potassium chloride concentration of 0.0001 mol dm^{-3}, Figure 7.9 predicts that the deposition process is independent of the gravity force. Figure 7.10 shows the variation of collection efficiency and filter coefficient with RVC potential at KCl concentration of 0.0001 mol dm^{-3} and volumetric flowrate of 34 cm^3 min^{-1}. *The onset of favourable deposition condition above the RVC's potential of 0 mV is manifested in Figure 7.10 by the sharp increase in the slope of the curve.*

Figure 7.11 shows the variation of filter coefficient with KCl concentration at fixed volumetric flowrate. Above concentration of 0.01 mol dm^{-3} it can be seen that variation of KCl concentration does not affect the filter coefficient at *any* flowrate. It can also be seen that decreasing the flowrate increases the filter coefficient which is the result of increase in the residence time of particle leading to higher opportunity for particles to attempt deposition.

7.5 CONCLUSIONS AND IMPLICATIONS

Summarising the above results:

- the gravity force does not affect the deposition process significantly in comparison to other forces.
- variation of RVC potential in the unfavourable region does not produce any change in the collection efficiency as shown in Figure 7.10. However, variation of RVC potential in the favourable region may affect the overall deposition process at positive potentials up to a

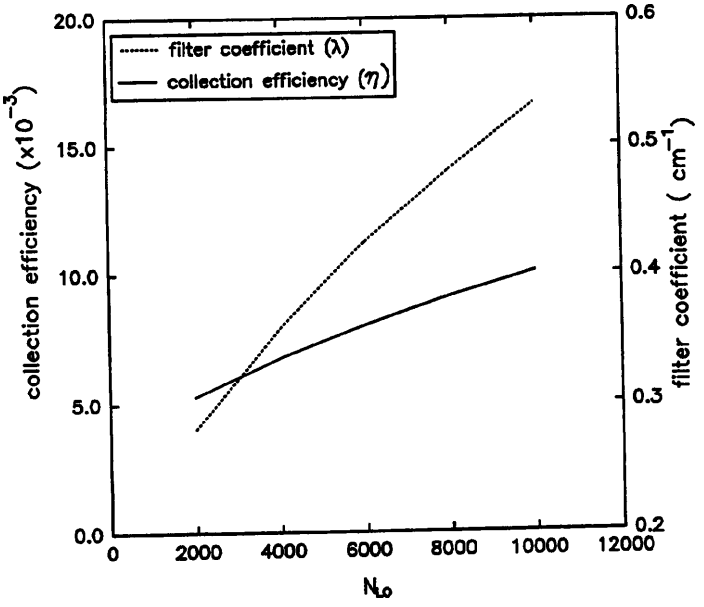

Figure 7.8 Variation of collection efficiency and filter coefficient with N_{LO} at volumetric flowrate of 34 cm^3 min^{-1}, KCl concentration of 0.0001 mol dm^{-3}, RVC potential of -26.5 mV and particle potential of -8.5 mV

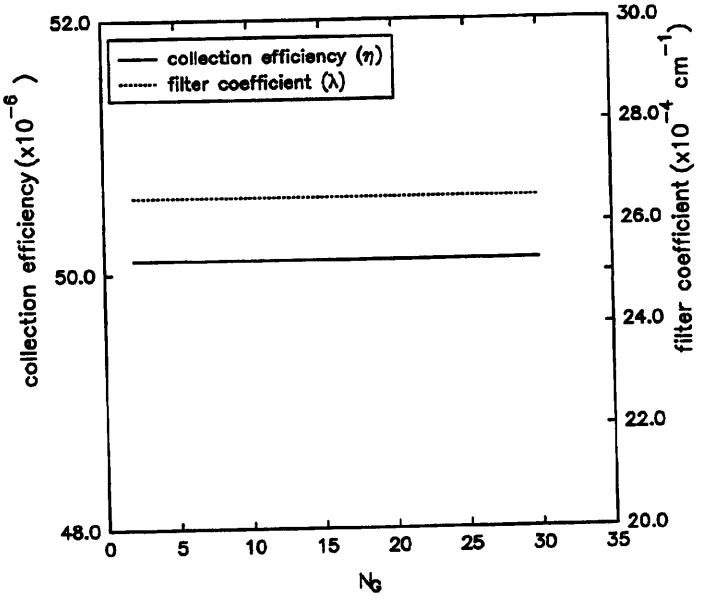

Figure 7.9 Variation of collection efficiency and filter coefficient with N_G at volumetric flowrate of 34 cm^3 min^{-1}, KCl concentration of 0.0001 mol dm^{-3}, RVC potential of -26.5 mV and particle potential of -8.5 mV

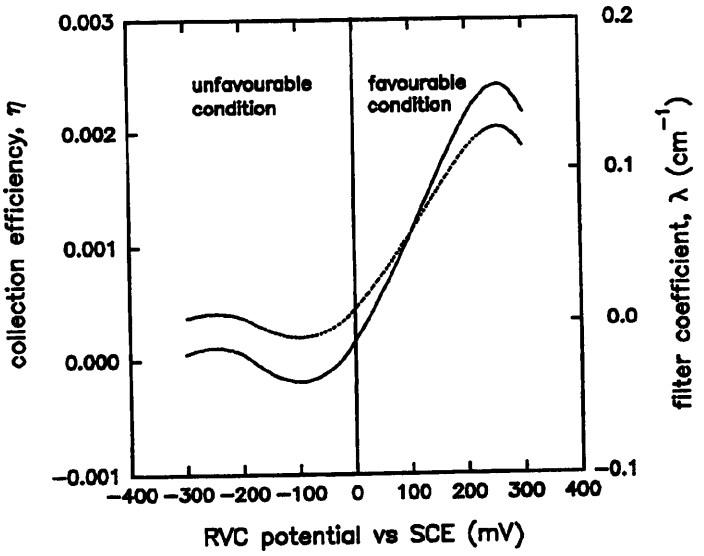

Figure 7.10 Variation of collection efficiency and filter coefficient with the RVC potential at KCl concentration of 0.0001 mol dm^{-3}, volumetric flowrate of 34 cm^3 min^{-1} and particle potential of -8.5 mV

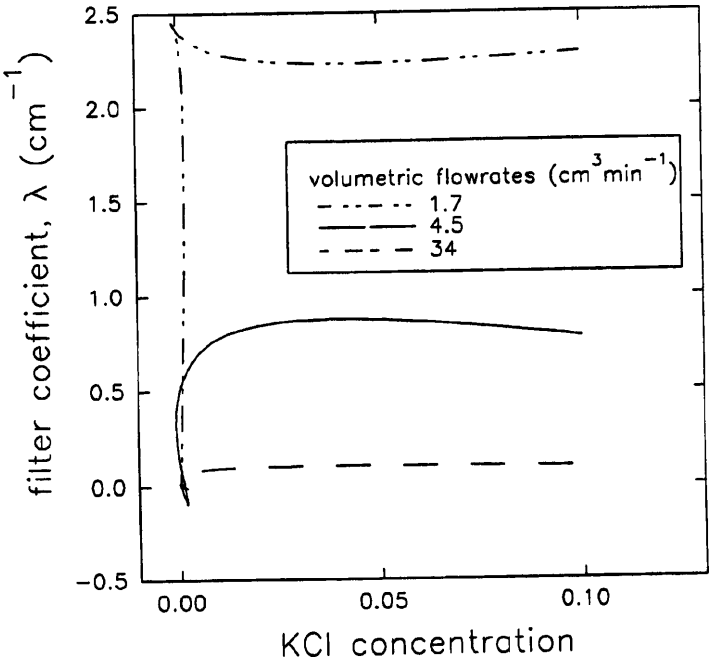

Figure 7.11 Variation of filter coefficient with KCl concentration at fixed volumetric flowrate

potential of +200 mV vs SCE as shown in Figure 7.10.

- variation of KCl concentration may affect the overall deposition process in a narrow range up to approximately 0.01 mol dm^{-3}, as shown in Figure 7.11, above which the electrical double layer will be compact leading to the shorter range of interaction.

It has to be taken into consideration that estimation of collector efficiency using equation (7.34) involves estimating the limiting trajectory, Ψ_{limit}, using the equation for the stream function for flow past a cylinder. This arises from the assumption stated in the beginning of this chapter that the individual RVC collector elements were taken to behave as cylinders. Ideally the stream function for flow past a rectangular plate would need to be employed.

To compare the theoretical predictions with the experimental results discussed in Chapter 6 care must be taken to recognise the fact that equation (7.36) applies to the initial clean bed removal time. This is usually defined in the literature as the time taken for the complete break-through of an inert tracer injected upstream into the column. It was discussed in Chapter 6 that the majority of experiments were carried out at KCl concentration of 0.001 mol dm^{-3} and volumetric flowrate of 1.7 cm^3 min^{-1}. It was also mentioned in section 6.1.1 that the inert tracer analysis carried out at volumetric flowrate of 1.7 cm^3 min^{-1} (see Figure 6.1b) showed a complete break-through time of approximately 3.6 hours. It must therefore be realised that the experiments carried out at the volumetric flowrate of 1.7 cm^3 min^{-1} did not achieve steady state and these must be excluded from any theoretical analysis.

Concluding from the above statement only a limited number of experimental results are used for the purpose of comparison with theory. However, the trends obtained in the experimental

results can be discussed. The results in Chapter 6 show that at volumetric flowrate of 34 cm^3 min^{-1} the surface forces were dominated by the hydrodynamic force but Figure 7.7 predicts that the surface forces to be dominant. The experimental results, discussed in Chapter 6 (section 6.1.4), were shown to be reproducible (see Figure 6.24) and this naturally leads to the argument that trajectory analysis should have predicted lower values for the surface forces or alternatively higher values for the hydrodynamic force to predict the experimental trend.

Figure 7.11 predicts that variation of KCl concentration above 0.1 mol dm^{-3} does not alter the filter coefficient values. Indeed this can be supported with experimental results which showed that at 0.1 mol dm^{-3} the electrical double layers became compact and thus deposition process could not be effected chemically.

It was concluded in Chapter 6 that the electrical double layer's role in the overall deposition process becomes evident at the low volumetric flowrate of 1.7 cm^3 min^{-1}. However, it was also concluded that at this low flowrate the variation of RVC potential in the unfavourable region did not produce significant variation in the deposition rate compared to that in the favourable condition region (see Figure 6.22). This follows the predictions offered by the trajectory analysis as shown in Figure 7.10.

The experimental and theoretical filter coefficients obtained and these have been plotted as shown in Figures 7.12 and 7.13. The experimental results show that the filter coefficient increases when RVC potential becomes positive, due to favourable deposition condition prevailing, and also it increases as the flowrate decreases, due to increase in the residence

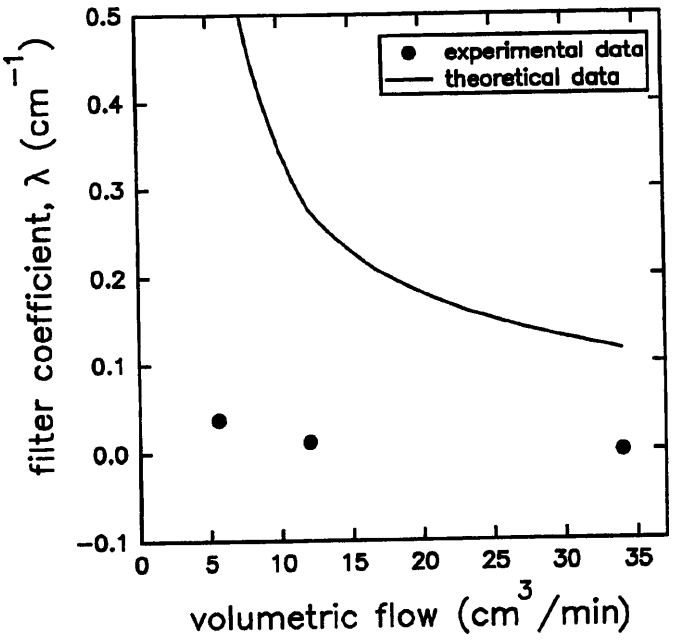

7.12 Comparison of theoretical prediction and experimental values of filter coefficient for various flowrates at KCl concentration of 0.0001 mol dm^{-3} and RVC potential of +300 mV vs SCE

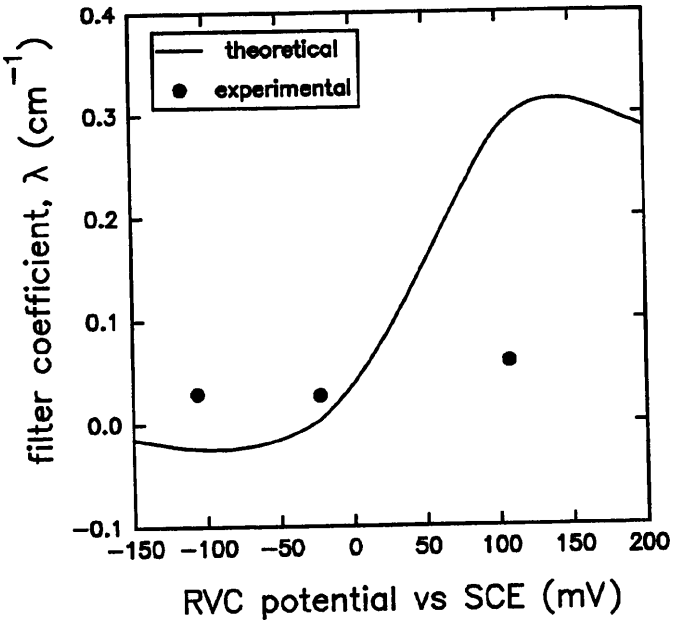

Figure 7.13 Comparison of theoretical prediction with experimental values of filter coefficient for various RVC potentials at KCl concentration of 0.0001 mol dm^{-3} and volumetric flowrate of 34 cm^3 min^{-1}

time. It can be concluded from these figures that the discrepancy observed presents itself under both favourable and unfavourable deposition conditions and thus there is a fundamental problem. In the literature the lack of agreement between theoretical and experimental results have been discussed. For example Elimelech (1990) provided a few possible explanation for the observed discrepancy.

- the two modes of the classical electrical double layer interaction considers interaction at constant charge and constant potential and these expressions yield different values for the double layer interaction. These expressions are classed as *static* since other dynamic processes such as distortion of double layers occurring during interaction are not included. It is possible a dynamic approach to the problem may improve the results.

- the trajectory equations consider the force balance under static condition and for a dynamic approach the convective-diffusive equation must be utilised.

- surface roughness of particles and collector and these are usually considered as half-spheres protruding from the smooth surface. It has been suggested that the total interaction should be calculated to be the sum of half-sphere interaction and smooth surface interaction.

- effect of blocking by the deposited particle which reduces the sites available for deposition. The deposited particle on the surface of the collector have the same sign of zeta potential and they consequently repel each other and also any incoming particle. However, it is believed that this may not cause problem for the present study as the surface coverage was low.

- the lack of evidence about the *true* RVC potential under potentiostatic control which was discussed at length in Chapter 6.

- the trajectory equation utilised in this study involved the deposition of particles on to cylindrical collectors. A more realistic approach for this study would be for deposition on to a plate. Indeed van de Ven and Adamczyk (1982) carried out a theoretical analysis of

deposition on to a plate using the convective-diffusion equation.

- the possibility of collection in the secondary minimum has not been accounted for in the limiting trajectory equation.

- the deposition process in known to be time dependent and this ageing effect has not been accounted for in the limiting trajectory equation.

- chemical type forces existing between surface has not been included in the trajectory equation.

Figure 7.14 shows in a different style the results previously discussed. The filter coefficient for experiments carried out under unfavourable condition have been boxed in as shown. It can be concluded from this graph that the major discrepancy between theory and experiment lie in the unfavourable deposition condition. As explained previously this finding has already been reported in the literature for example Adamczyk (1989) argues that the overall deposition process is determined by the transport step and the surface force may only provide an additional *transport* resistance.

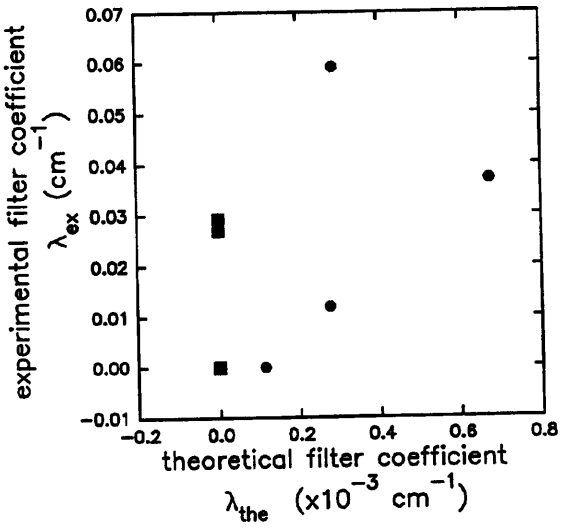

Figure 7.14 Comparison of theoretical and experimental filter coefficients

CHAPTER 8

CONCLUSION AND RECOMMENDATIONS FOR FUTURE WORK

In the introductory comments of Chapter 1 the industrial importance of deep bed filtration studies was discussed. The use of spherical glass bead collectors has been well established in the literature. The rate of deposition is commonly controlled by varying physical parameters such as the superficial fluid velocity, collector size, bed depth, particle size and concentration or chemically by changing the electrolyte concentration.

The availability of an additional control parameter to those mentioned above would increase the scope of deposition studies to cover such problems as the selective separation of a specific colloidal particle from a mixed species suspension. One such parameter is the external control of the collector potential, but not using such high voltages to result in electrophoretic separations. The main objective of the present study has been to investigate the effect of external variation of collector potential on the deposition process. Previous work on deposition has focused almost exclusively on packed beds of spheres. This work considers irregular packings in some detail.

Conclusions drawn from the experiments conducting using a novel adsorption column (section 8.1) and proposed modifications which may improve the current system (section 8.2) are discussed in this chapter.

8.1 CONCLUSIONS

The problems encountered in designing the column and the procedure for carrying out the experiments were discussed in Chapters 3 and 4. The principal conclusions are, viz:

8.1.1 Column design and experimental procedures

- Use of RVC as the filtration medium has been successfully studied. The RVC structure allows the control of its surface potential via a potentiostat. Furthermore, due to its rigidity and porosity it was possible to design a flow-through column resembling the conventional deep bed techniques.

- The column that was designed offered a robust structure under experimental conditions and can be dismantled with relative ease.

- The experimental procedures developed, as outlined in Chapter 4, were successfully employed. Before the particulate suspension could be fed into the column, an equilibration time was required to allow experimental variables such as outlet pH, conductivity, turbidity and cell current, potential and RVC potential stabilise. This preparation of column took approximately 1 hour.

- The duration of an experiment can be predetermined by carrying out inert tracer analysis.

- A technique for investigating the ohmic drop has been presented.

- Dialysis of latex particles for at least 1 month prior to experimentation removes contaminants, as shown by the conductometric titrations.

- It has been shown that it is possible to control the RVC potential potentiostatically and that distribution of potential throughout the bed is uniform.

8.1.2 Deposition experiments

Deposition of polystyrene latex particles

- Increasing the flowrate increases the deposition *rate* but the total amount deposited decreases. This is because at higher flowrates more particles are available for deposition.

- Deposition is proportional to the feed concentration. Hence with more particles per unit volume in the feed suspension the higher the total relative amount of deposit.

- For the present system of deposition the main forces contributing to the deposition process were the surface and hydrodynamic forces (and effect of inertia, gravity and Brownian forces are comparatively negligible).

- At the highest flowrate used in this study, 34 $cm^3\ min^{-1}$, the colloidal forces were shown to be negligible compared to the hydrodynamics effects. Indeed, the effect of surface forces at KCl concentration of 0.001 mol dm^{-3} apparently only become important at flowrates of 1.7 $cm^3\ min^{-1}$.

- At volumetric flowrate of 1.7 $cm^3\ min^{-1}$ and KCl concentration of 0.001 mol dm^{-3} the experimental results show clear evidence of the conditions governing the occurrence of favourable and unfavourable deposition conditions.

- The variation of RVC potential under unfavourable deposition conditions does not produce large changes in the deposition rate (with the average change of typically 2.0×10^{-11} g/s per mV) as shown in Figure 6.22. Variation of RVC potential under favourable deposition conditions produces significant changes in the deposition rate (with the average change of typically 2.67×10^{-10} g/s per mV) as shown in Figure 6.22.

- At RVC potential of -300 mV vs SCE hydrogen is evolved which is accompanied by the rise in the outlet pH. The rise in pH affects the particle and collector zeta potentials though slight but significant.

- Increasing the KCl concentration from 0.001 mol dm^{-3} to 0.0001 mol dm^{-3} increases the double layer thickness and subsequently the attractive colloidal forces extend further from the collector surface. This means that the collection distance around the surface of collector increases. It was concluded that at KCl concentration of 0.001 mol dm^{-3} the effect of surface forces became evident at volumetric flowrate of 1.7 cm^3 min^{-1} and this was argued to be partly due to increase in the residence time of particles and partly due to the decrease in the fluid drag force on the particles. Experiments show that the effect of surface forces on the deposition process at KCl concentration of 0.0001 mol dm^{-3} become evident at flowrate of 5.6 cm^3 min^{-1}. This means that decreasing KCl concentration from 0.001 to 0.0001 mol dm^{-3} the limiting flowrate, where the role of surface forces become evident, increases from 1.7 to 5.6 cm^3 min^{-1}.

Deposition of Hypercarb particles

- Establishing experimental conditions wherein surface forces become important proved more difficult in comparison to polystyrene latex particles. The difficulty was attributed to the characteristics of *Hypercarb* particles which have a highly porous structure. Hence surface charge variation and surface heterogeneity may become important. Variation of surface charge which may be accompanied by zeta potential sign variation can have the effect of a particle experiencing both favourable and unfavourable condition on different parts of its surface. The effect of surface roughness as discussed in Chapter 7 was that the colloidal forces were supposed to be made up of contributions from the smooth surface and the half-sphere protrusions from the surface.

Trajectory analysis

- The trajectory analysis proved to be a useful means of predicting the trends of experimental results. However, the values for experimental and theoretical filter coefficients differed by a factor of 10. The discrepancy was believed to arise from a variety of factors:

a) The assumption that RVC elements behave as cylinders is not wholly justifiable (see below) and stream function for flow past a rectangular plate would need to be employed together with other assumptions to take the complex RVC geometry into account.

b) The trajectory analysis only considers the steady state conditions of deposition whereas it would be more realistic to use a dynamic approach (e.g. through Monte Carlo simulation).

c) The possibility of collection in the secondary minimum has not been included in the trajectory analysis, however, the DLVO plots showed that in majority of cases there was no ground for assuming that a secondary minimum existed.

d) The role of surface roughness of RVC has not been included in the trajectory analysis. The protrusions from the surface of particles increase the surface area for contact and therefore more deposition occurs compared to a smooth particle.

- One of the fundamental characteristics of the RVC which has been simplified in the trajectory analysis is its three dimensional foam-like structure. The structure offers elements parallel, perpendicular and inclined to the flow path and this alters the flow characteristics within the matrix. To perform a microscopic particle simulation of deposition process incorporating a realistic model for the structure of the RVC (e.g. Jia (1993)) would make trajectory analysis redundant and obsolete. Either analytical technique for the estimation of deposition rate could be used. The full simulation is preferable but would require more extensive computation.

- The simulations involving the trajectory analysis for the experiments carried out under potentiostatic control assumes the RVC potential to be the value entered into the potentiostatic interface program but this value may not represent the true RVC potentia since the exact behaviour of the RVC double layer under potentiostatic control is not known. Additionally the use of SCE reference electrode against which the RVC potential has to be measured adds to uncertainty.

- At flowrate of 34 cm^3 min^{-1} and KCl concentration of 0.0001 mol dm^{-3} the experimental results show that the surface forces are negligible compared to the hydrodynamic force (see pages 143-146). Whereas, trajectory analysis simulations carried out at flowrate of 34 cm^3 min^{-1} and KCl concentration of 0.0001 mol dm^{-3} (see Figure 7.7) predicts that the surface forces to be the dominant forces. It was concluded that the discrepancy lies with assumptions inherent in the trajectory analysis e.g. the expressions used to quantify the hydrodynamic contributions.

Previous studies into the effect of external variation of collector potential notably by Albery et al. (1990) and Joscelyne (1993) have been based on the fundamental assumption that the secondary minimum can be directly monitored. However, it is believed that in this study it has been shown that there are several important practical hydrodynamic characteristics such as fluid drag, residence time and inertial effects which must be closely studied in order to arrive at a set of experimental conditions wherein the surface forces can be confidently said to be taking part in the deposition process.

Furthermore, the novel design offered in this study differs from the previous works by the fact the rigid three dimensional high porosity structure of RVC allows design of a larger volume column which may be more suited to certain 'process' applications (in contrast to the closely

packed fibre bed used by Joscelyne (1993) in which case the effect of each fibre on the neighbouring fibre may have adverse effect on the deposition process and in which the pressure drop across the column increases rapidly with only modest deposition in the bed).

8.2 RECOMMENDATIONS FOR FUTURE WORK

8.2.1 Improvement in experimental procedures

The experimental arrangement devised during this research has been shown to be robust and procedures that have been established lead to reproducible results. However, further improvements in experimental procedures could usefully be incorporated, viz:

- Some of the discrepancies observed between the DLVO predictions and experimental results were attributed to the evolution of gases. It was speculated that evolution of gases interferes with the deposition mechanism in various ways. It alters the local pH and hence zeta potential values of the particle and collector. This problem can be remedied by using buffered electrolyte solutions thus providing a stable operating pH. It may also be possible that due to hydrophobic nature of RVC it has a greater affinity for the evolving bubbles thus causing the attachment of gas bubbles and blockage of filter area. This problem can be counteracted by carrying out the experiments under an inert atmosphere.

- Measurement of particle number concentrations on-line provides a continuous analysis of the outlet and therefore an instantaneous response to an experimental variable may be monitored.

- Use of ion-exchange instead of the dialysis technique used in this study can remove contaminants from the suspension more effectively.

8.2.2 Elucidation of deposition mechanisms

- This research has shown that the effect of surface forces become evident at a limiting volumetric flowrate and that this limiting flowrate increases with decreasing KCl concentration. Further work should examine the effect of variation of RVC potential incrementally in both favourable and unfavourable deposition condition below and above the limiting flowrate to understand the detailed mechanism giving rise to this finding.

- Further, a judgment needs to be made on the applicability of DLVO theory to the experimental results i.e. by checking whether there is a close correspondence between DLVO predictions and experimental results and, if not, whether extension of DLVO to include structural forces such as hydrophobic attraction, hydration repulsion and steric repulsion can improve agreement. One method would be to utilise an atomic force microscope (AFM) (Wiesendanger (1994)) to measure the force-distance profile between a particle mounted on the AFM tip and a sample of the RVC membrane. Carrying out this measurement in different KCl electrolyte solutions would provide the necessary information to judge the applicability of the DLVO theory.

- Since the main conclusion of the work has been to show that at lower flowrate the surface forces become evident then naturally by removing the contribution of hydrodynamics to the deposition process the effect of surface forces can be better studied. The problem with carrying out such experiments under no flow condition primarily involves the method for detection of deposition. The particles may become mechanically trapped within the structure of the RVC and even sudden emptying of the column may not dislodge them. A possible scheme may involve using differing flow mode policies, for example, starting with a low throughput then stopping the flow and finishing the experiment at a high flowrate. In fact what happens in this scheme is that during the initial low flowrate the surface forces are small

but significant compared to the hydrodynamic then once the flow is stopped the effect of hydrodynamics is removed and the surface forces become dominant and eventually at high flowrate become negligible compared with the hydrodynamical transport mechanism.

- It may be postulated that there are two reasons for the inadequacy of the surface forces to affect the deposition rate:

(a) Particles do not possess high enough surface charge to interact effectively with the collector. To increase the surface charge of the particles a technique developed by Matijevic (1985) could be utilised wherein the process of depositing a layer of an inorganic compound on the surface of particles is described and by this it is reported that the sign and magnitude of the surface charge can be altered. For example if the surface charge can be increased on each particle and if the resulting experimental data obtained for the surface force controlled deposition region show significant increase in deposition rate, it may be argued that the surface charge of the particles are the determining.

(b) The RVC does not take part in the deposition process as expected perhaps due to hydrophobicity, low surface charge values, low electrical double layer capacity. This may also be studied further for example by carrying out deposition experiments after pretreating the RVC with a solution containing surfactant or a surface charge enhancement agent.

8.2.3 Means of achieving selective separation

Extension of the present system for selective *separation* of a specific colloidal particle from a mixed species suspension would be difficult unless better technique for enhancement of surface forces can be devised. This problem should be examined by investigating the individual roles that collector and particles play in the process.

Role of collector

The main conclusion of this study has been to show that the effect of surface forces only become evident at low flowrates and even then the deposition rates under favourable and unfavourable deposition conditions did not differ by appreciable amount. Hence as a separation process volumetric throughput would be small (1.7 $cm^3\ min^{-1}$). It therefore seems a good idea to carry out the experiments in a simpler collector to ascertain the conditions under which the surface forces become dominating. Use of collector geometries, with well defined flow characteristics, such as parallel plate, stagnation point flow and even a single spherical steel bead provides more control over the role of hydrodynamics in the deposition process.

The advantage of using RVC lies in its three dimensional structure thus allowing deposition occurring anywhere in the bed leading to higher removal capacity and this offers attractive potentials to the process scale application. Upon attaining better understanding of the role of collector in the deposition process as mentioned previously the attention should be directed towards improving the RVC cell designed in this study. For example the RVC used in this study has 100 pores per inch resulting in a porosity of 97% in contrast to the porosity of 40% typically found in glass bead deep beds. The decrease of RVC porosity let say to 50% would result in a higher pressure drop across the column for the same throughput. On the other hand the surface area available for deposition increases and additionally the residence time of particles also increases. The net effect would be an increase in deposition rate at the expense of higher pressure drop. This can also be seen from equation (7.35) in which it is shown that the filter coefficient is directly proportional to $(1-\beta)^{1/2}$. At 97% porosity this value is 0.17 and at 50% porosity it is 0.70 and although filter coefficient depends on other factors it can be seen that there is an appreciable increase in the filter coefficient value with decreasing

porosity.

Role of particles

Choice of particles would be important since different deposition rates determine their selective separation. It would be ideal to use two different particles that have zeta potential of opposite sign in the same electrolyte but this may cause the coagulation of the particles prior to deposition. Alternatively, two species of particles with the same sign of zeta potentials but of widely differing magnitudes may be used which would result in one type depositing at a higher rate than the other. Jia et al. (1993) in a theoretical study obtained particle-collector interaction energies of a mixed suspension of Al_2O_3/TiO_2. They concluded that when both particles were negatively charged a difference in particle zeta potential of at least 40 mV would be required in order to facilitate a possible selective separation.

The other problem encountered in the choice of particles would be the requirement to detect the concentration of particles of a specific type in the outlet. To do this some difference in optical, magnetic or compositional properties could be utilised.

8.2.4 Concluding perspective

It is believed that the main contribution of this study has been twofold:

First, it has been shown that it is possible to extend deep bed filtration techniques to the use of such structures as the RVC in an electrochemical cell. This has allowed the application of such theories as the DLVO and trajectory analysis to the deposition experiments.

Second, it has been shown that the surface forces do indeed play a part in the overall deposition process. However, the ability to utilise differences in surface forces to allow selective or non-selective separation using a controlled potential cell is constrained by the need to carefully control the prevailing hydrodynamic forces which tend to detach or prevent particle deposition. Consequently the volumetric throughputs in any RVC cell would need to be extremely low, in fact tending to quiescent conditions, if controlled deposition was to be achieved in practice.

REFERENCES

Adamczyk, Z., Colloid.Surfaces., 39, 1(1989)

Adamczyk, Z., van de Ven, T.G.M., J.Colloid.Interface.Sci., 84, 497(1981)

Albery, W.J., Fredlein, R.A., Kneebone, G.R., O'Shea, G.J., Smith, A.L., Colloid.Surfaces, 44, 337(1990)

Alince, B., Robertson, A.A., Inoue, M., J.Colloid.Interface.Sci., 65, 98(1978)

Almog, Y., British.Poly.J., 131(1982)

Amarasinghe, B.M.W.P.K., Hindered Sedimentation Behaviour of Concentrated Polydisperse Suspensions, Ph.D Thesis, University of Manchester Institute of Science and Technology, 1987

Attia, Y.A., Separation Science Technol., 17, 485(1982)

Bell, G.M., Levine, S., McCartney, L.N., J.Colloid.Interface.Sci., 33, 335(1970)

Brenner, H., Chem.Eng.Sci., 16, 242(1961)

Brinkman, H.C., App.Sci.Res., A1, 27(1947)

Bowen, B.D., Epstein, N., J.Colloid.Interface.Sci., 72, 81(1979)

Chapman, D.L., Phil.Mag., 25, 475(1913)

Choo, C., Tien, C., Separation Technology, 1, 122(1991)

Cowlard, F.C., Lewis, J.C., J.Mat.Sci., 2, 507(1967)

Czarnecki, J., J.Colloid.Interface.Sci., 72, 361(1979)

Dabros, T., van de Ven, T.G.M., Colloid. Polymer.Sci., 261, 694(1983)

Debye, P., Huckel, E., Physic. Z., 24, 185(1910)

Delahay, P., Double Layer and Electrode Kinetics, Wiley, Interscience, N.Y., 1965

Elimelech, M., J.Colloid.Interface.Sci., 146, 337(1991)

Elimelech, M., O'Melia, C., Colloid.Surfaces., 44, 166(1990a)

Elimelech, M., O'Melia, C., Langmuir, 6, 1153(1990)

Elimelech, M, Gregory, J., Williams, R.A., Jia, X., Particle Deposition and Aggregation, Meaurement, Modelling and Simulation, Butterworth, 1995

Feke, D.L., Prabhlu, N.D., Mann Jr, J.A., Mann III, J.A., J.Phys.Chem., 88, 5735(1984)

Fitzpatrick, J.A., Ph.D dissertation, Harvard University, Cambridge, Mass., 1972

Fowkes, F.M., Ind.Eng.Chem., 56, 40(1964)

Goldman, A.J., Cox, R.G., Brenner, H., Chem.Eng.Sci., 22, 637(1967)

Gouy, G., J.Phys.Radium, 9, 457(1910)

Graham, D.G., Chem.Rev., 41, 441(1948)

Gregory, J., J.Colloid.Interface.Sci., 83, 138(1981)

Hamaker, H.C., Physica, IV, 1058(1937)

Happel, J., A.I.Ch.E.J., 5, 174(1959)

Hansen, W.N., Wang, C.L.,Humpherys, T.W., J.Electroanal.Chem., 93, 87(1978)

Hogg, R., Healy, T.W., Fuerstenau, D.W., Trans.Faraday.Soc., 62, 1638(1966)

Hull, M., Kitchener, J.A., Trans.Faraday.Soc., 65, 3093(1969)

Hunter, R.J., Zeta Potentials in Colloid Science, Academic Press, 1981

Hunter, R.J., Foundations of Colloid Sciences, Oxford University Press, 1989

Israelachvili, J., Pashley, R., Nature, 300, 341(1982)

Ives, K.K., Proc.Inst.Civil.Eng., 16, 189-193(1960)

Jia, X., Williams, R.A., Chem.Eng.Comm., 91, 127(1990)

Jia, X., Computer Simulation of Colloidal Aggregation and Deposition, Ph.D thesis, University of Manchester Institute of Science and Technology, 1992

Joscelyne, S.M., Separations Using Controlled Potential Packed Beds, Ph.D Thesis, Oxford University, 1993

Judd, S.J., Solt, G.S., Colloid.Surfaces, 39, 189(1989)

Judd, S., Fletcher, P., Stephenson, T., Chem.Eng.Sci., 49, 2371(1994)

Kar, G., Chander, S., Mika, T.S., J.Colloid.Interface.Sci., 44, 347(1973)

Kruyt, H.R., Colloid Science, 1, Elsevier, N.Y., 1965

Kuwabara, S., J.Phys.Soc.Japan, 14, 527(1959)

Lamb, H., Hydrodynamics, 6th ed., Cambridge University Press, 1932

Levenspiel, O., Chemical Reaction Engineering, 2nd ed., N.Y., Wiley, 1972

Marshall, J.K., Kitchener, J.A., J.Colloid.Interface.Sci., 22, 342(1966)

Matijevic, E., Ann.Rev.Mat.Sci., 15, 483(1985)

Natanson, G.L., Dokl.Akad.Nauk.SSSR., 112, 100(1957)

Nir, S., Bentz, J., J.Colloid.Interface.Sci., 65, 399(1978)

Ohshima, H., healy, T.W., White, L.R., J.Colloid.Interface.Sci., 90, 17(1982)

Oren, Y., Soffer, A., Electrochemica Acta, 28, 1649(1983)

Oren, Y., Sep.Sci.Tech., 21, 679(1986)

Oren, Y., Tobias, H., Soffer, A., Bioelectrochemistry and Bioenergetics, 11, 347(1983)

Oren, Y., Glatt, I., Livnat, A., Kafri, O., Soffer, A., J.Electroanal.Chem., 187, 59(1985)

Oren, Y., Soffer, A., J.Electroanal.Chem., 206, 101(1986a)

Oren, Y., Golub, D., Soffer, A., J.Electroanal.Chem., 227, 41(1987a)

Oren, Y., Soffer, A., Hall, D., Priel, Z., Sep.Sci.Tech., 22, 1017(1987)

Overbeek, J.Th.G., J.Colloid.Interface.Sci., 58, 408(1977)

Pickett, D.J., Electrochemical Reactor Design, 2nd ed., Elsevier, 1979

Tien, C., Payatakes, A.C., Turian, R.M., A.I.Ch.E.J., 20, 889(1974)

Rajagopalan, R., Tien, C., A.I.Ch.E.J., 22, 523(1976)

Ruckenstein, E., Prieve, D.C., A.I.Ch.E.J, 22, 276(1976)

Shaw, D.J., Introduction to Colloid and Surface Chemistry, Butterworths, 4th ed., 1992

Soffer, A., Folman, M., Electroanalytical Chemistry and Interfacial Electrochemistry, 38,

25(1972)

Soffer, A., Cohen, H., Oren, Y., J.Colloid.Interface.Sci., 120, 272(1987)

Spielman, L.A., Goren, S.L., Environmental.Science.Technology., 2, 279(1968)

Spielman, L.A., Fitzpatrick, J.A., J.Colloid.Interface.Sci., 42, 607(1973)

Stechkina, I.B., Kirsch, A.A., Fuchs, N.A., Ann.Occup.Hyg., 12, 1(1968)

Stern, O., Z.Electrochem., 30, 508(1924)

Tamai, H., Hamada, A., Suzawa, T., J.Colloid.Interface.Sci., 88, 378(1982)

Tien, C., Granular Filtration of Aerosols and Hydrosols, Boston, Butterworths, 1989

Tobias, H., Oren, Y., Soffer, A., Bioelectrochemistry and Bioenergetics, 11, 347(1983)

Tobias, H., Taragan, E., Oren, Y., Soffer, A., Nuclear Technology, 77, 46(1987)

Tobiason, J.E., O'Melia, C.R., J.A.W.W.A., 54(1988)

Tobiason, J.E., Physicochemical Aspects of Particle Deposition in Porous Media, Ph.D dissertation, the John Hopkins University, Baltimore, MD, 1987

Tobiason, J.E., Colloids.Surfaces., 39, 53(1989)

van den Hull, H.J, Vanderhoff, J.W., J.Electroanal.chem., 37, 161(1972)

van de Ven, T.G.M., Adamczyk, Z., Chem.Eng.Sci., 37, 869(1982)

Verwey, E.J.W., Overbeek, J.Th.G., The Theory of Stability of Lyophobic Colloids, Elsevier, Amsterdam, 1948

Vogel, A.I., Textbook of Quantitative Inorganic Analysis Including Elementary Instrumentation, 4th ed., Longman, 1978

Von Fraunhofer, J.A., Potentiostat and Its Application, London, Butterworth, 1972

Wiese, G.R., Healy, T.W., Trans.Faraday.Soc., 66, 480(1970)

Wiesendanger, R., Scanninig Probe Microscopy, Cambridge University Press, 1994

Yao, K.M., Ph.D thesis, University of North Carolina, Chapel Hill, N.C., 1968

Yoshimura, Y., Ueda, K., Mori, F., Yoshioka, N., Int.Chem.Eng., 20, 600(1980)

Zebel, G., J.Colloid.Science., 20, 522(1965)

APPENDIX A

This appendix contains experimental data obtained for calibration of the turbiditimeter and also zeta potential meaurements of particles and collectors.

Table A1 Coulter Counter data obtained for calibration of the turbiditimeter

Background counts									Total counts								
1335	1249	1316	1308	1285	1425	1215	1211	1199	2972	2886	2960	2767	2846	2877	2810	2867	2756
Average Background=1283, Average Total Counts=2860									Number of particles in 1 cm^3 suspension=0.32 x 10^6								
Number of particles in 0.5 cm^3 Isoton=1577.0																	
Number of particles in 100 cm^3 Isoton=315510.0									Turbidity=13.3 NTU								
Background counts									Total Counts								
937	896	824	893	875	922	869	843	819	4003	3899	3878	3763	3724	3603	3729	3635	3705
Average Background=875, Average Total Counts=37712860									Number of particles in 1 cm^3 suspension=579140								
Number of particles in 0.5 cm^3 Isoton=2895																	
Number of particles in 100 cm^3 Isoton=579140									Turbidity=29.8 NTU								
Background counts									Total Counts								
768	751	777	745	770	708	735	739	773	6004	5940	5653	5741	5615	5651	5663	5622	5543
Average Background=751, Average Total Counts=5695									Number of particles in 1 cm^3 suspension=988740								
Number of particles in 0.5 cm^3 Isoton=4943																	
Number of particles in 100 cm^3 Isoton=988740									Turbidity=67.2 NTU								
Background counts									Total Counts								
1801	1758	1745	1840	1733	1746	1688	1738	1660	7616	7484	7582	7348	7471	7362	7232	7437	7245
Average Background=1745, Average Total Counts=7419									Number of particles in 1 cm^3 suspension=1134852								
Number of particles in 0.5 cm^3 Isoton=5674																	
Number of particles in 100 cm^3 Isoton=1134852									Turbidity=85.5 NTU								

Table A2 Zeta potenials of polystyrene latex particles for 0.01 mol dm^{-3} KCl and different pH

-12.2 -8.8	-12.0 -12.2	-16.9 -20.1	-20.4 -22.1	-14.9 -16.7	-16.5 -14.8	-20.0 -16.8	-23.3 -11.9	-13.4 -23.5	-15.0 -23.2			
Mean=-16.7, **pH=10.1**, Standard Deviation=4.39, Maximum=-8.8, Minimum=-23.5												
-9.8 -16.1	-8.8 -17.7	-7.0 -12.3	-17.4 -12.2	-13.8 -3.4	-15.6 -8.7	-15.9 -20.9	-15.5 -11.8	-17.6 -5.4	-12.3 -15.4	-17.4 -7.0	-13.7 -11.2	
Mean=-12.8, **pH=8.6**, Standard Deviation=4.4, Maximum=-3.4, Minimum=-20.95												
-13.3 -13.3	-11.0 -7.4	-11.1 -5.5	-12.8 -9.3	-5.6 -8.9	-9.3 -10.5	-9.2 -12.9	-9.1 -7.3	-3.7 -14.5	-12.8 -3.6	-7.3 -11.0	-10.9 -9.7	-11.1 -11.0
Mean=-9.7, **pH=7.3**, Standard Deviation=2.9, Maximum=-3.6, Minimum=-14.5												
-4.2 -10.2	-8.2 -12.3	-14.0 -3.8	-3.9 -7.0	-14.3 -7.1	-9.3 -6.4	-9.6 -19.2	-19.7 -24.2	-19.2 -6.4	-15.9 -5.7			
Mean=-11.7, **pH=6.0**, Standard Deviation=6.9, Maximum=-3.8, Minimum=-26.2												
-1.9 -1.9	-5.9 -3.7	-5.7 -4.3	-9.6 -10.7	-8.5 -9.5	-1.9 -4.5	-5.6 -7.7	-5.7 -17.6	-11.5 -13.6	-5.9 -9.3			
Mean=-7.6, **pH=4.8**, Standard Deviation=4.2, Maximum=-1.9, Minimum=-17.6												
-1.8 -5.4	-5.5 -7.4	-5.4 -6.5	-9.3 -3.7	-11.0 -3.6	-5.4 -12.7	-7.8 -14.5	-9.2 -9.3					
Mean=-7.5, **pH=4.3**, Standard Deviation=3.5, Maximum=-1.8, Minimum=-14.5												
-3.8 -7.0	-6.9 -6.4	-6.8 -13.7	-1.6 -1.6	-10.4 -8.8	-6.9 -8.8	-10.5 -8.6						
Mean=-7.3, **pH=4.1**, Standard Deviation=3.3, Maximum=-1.6, Minimum=-13.7												
-4.5 -3.4	-5.0 -8.4	-8.3 -11.5	-6.6 -7.3	-10.0 -10.1	-6.6 -6.6	-6.6 -14.7						
Mean=-9.8, **pH=4.0**, Standard Deviation=2.9, Maximum=-3.4, Minimum=-14.7												
-3.6 -8.8	-3.3 -6.5	-1.8 -3.8	-8.3 -7.0	-4.8 -11.4	-10.0 -6.4	-11.4 -6.5	-4.8 -6.5					
Mean=-6.6, **pH=3.90**, Standard Deviation=2.8, Maximum=-1.8, Minimum=-11.4												

Table A3 Zeta potenials of polystyrene latex particles for 0.001 mol dm^{-3} KCl and different pH

-8.8 -8.8	-12.4 -14.0	-12.8 -13.1	-11.5 -17.8	-11.8 -10.4	-10.2 -12.8	-7.5 -6.8	-15.6 -11.9	-10.9 -15.0	-9.5 -12.5	-16.0 -12.2	-9.89 -7.45	
Mean= -11.6, **pH=11.4**, Standard Deviation=2.82, Maximum=-6.8, Minimum=-17.8												
-13.8 -9.3	-11.9 -5.9	-6.5 -11.3	-8.4 -6.5									
Mean=-9.2, **pH=10.4**, Standard deviation=2.9, Maximum=-5.9, Minimum=-13.8												
-11.9 -16.0	-14.5 -13.5	-12.9 -11.6	-15.5 -10.7	-14.9 -10.5	-8.2 -7.8	-5.1 -11.3	-9.7 -5.6	-9.5 -4.5				
Mean=-10.8, **pH=9.9**, Standard Deviation=3.53, Maximum=-4.5, Minimum=-16.0												
-13.3 -15.1	-8.2 -5.8	-5.9 -10.9	-6.3 -5.9	-5.1 -9.6	-6.5 -3.7	-9.6 -12.7	-8.7 -10.2	-11.4 -7.0	-9.6 -9.1	-5.4 -3.2		
Mean=-8.3, **pH=6.0**, Standard Deviation=3.16,Maximum=-3.2, Minimum=-15.1												

Table A4 Zeta potenials of polystyrene latex particles for 0.0001 mol dm^{-3} KCl and different pH

-7.8 -13.3	-9.3 -10.4	-17.7 -20.4	-18.2 -18.1	-21.7 -17.9	-17.4 -18.5	-10.7 -15.1						
Mean= -15.1, **pH=5.1**, Standard Deviation=4.3, Maximum=-7.8, Minimum=-21.7												
-8.6 -6.8	-7.7 -10.7	-6.3 -2.4	-3.0 -2.3	-6.8 -10.9	-6.3 -3.2	-7.8 -10.2	-4.5 -1.5	-4.5 -6.8	-9.89 -1.41			
Mean=-6.1, **pH=6.0**, Standard deviation=3.1, Maximum=-1.4, Minimum=-10.9												
-15.9 -9.5	-22.4 -5.5	-10.4 -8.2	-6.9 -7.3	-25.5 -17.0	-14.2 -22.4	-20.3 -7.3	-22.4 -29.8	-19.2 -15.4	-17.4 -27.2			
Mean=-16.2, **pH=11.0**, Standard Deviation=7.4, Maximum=-5.5, Minimum=-29.8												

Table A5 Zeta potenials of polystyrene latex particles for 0.00001 mol dm^{-3} KCl and different pH

-3.9 -2.1	-1.6 -8.4	11.5 -3.2	3.3 3.3	0.0 0.0									
Mean=-0.1, **pH=4.0**, Standard deviation=5.4, Maximum=11.5, Minimum=-8.4													
-4.8 -6.4	+4.3 -8.8	-2.9 -11.9	0.0 -2.9	-7.4 -16.4	-1.5 -7.5	-6.0 -4.5	-10.5 -4.6	-6.0 0.0	-8.9 -7.5	-3.0 -7.5	-13.4 -8.9	-6.0 -8.9	-13.4 -8.9
Mean=-7.6, **pH=4.6**, Standard Deviation=3.6, Maximum=-1.5, Minimum=-16.4													
-32.5 -24.2	-26.0 -29.3	-23.5 -25.0	-29.4 -23.6	-25.0 -25.1	-33.0 -24.2	-24.2 -22.8	-17.9 -25.9	-21.0 -22.8	-18.5 -23.3				
Mean=-24.9, **pH=5.8**, Standard Deviation=3.8, Maximum=-17.9, Minimum=-33.0													
-40.9 -37.0	-36.1 -33.5	-29.1 -44.2	-41.1 -38.8	-32.6 -35.7	-39.8 -34.3	-37.2 -38.9	-37.1 -34.5	-32.7 -36.1	-28.5 -35.9	-34.5 -43.9	-37.5 -36.2	-33.0 -39.4	
Mean=-36.5, **pH=5.4**, Standard Deviation=3.8, Maximum=-28.5, Minimum=-44.2													
-45.6 -45.8	-38.5 -36.8	-49.3 -43.3	-52.5 -44.9	-46.1 -46.6	-49.4 -51.6	-54.2 -41.9	-49.3 -51.2	-47.8 -44.9	-43.1 -45.4	-47.9 -54.7			
Mean=-46.9, **pH=9.0**, Standard deviation=4.59, Maximum=-36.8, Minimum=-54.7													

Table A6 Effect of different concentrations of $CaCl_2$/KCl mixtures on the zeta potenials of polystyrene latex particles (no KCl solution, neutral pH)

$CaCl_2$=0.1 mol dm^{-3}												
-11.3	-11.1	-7.2	-29.5	-34.7	-17.2	-11.6	-3.8	-10.2	-3.9	-26.9	-13.5	
-3.4	-5.9	-22.7	-32.9	-20.9	-32.6	-22.2	-23.0	-23.5	-19.5	-30.7	-19.9	
Mean=-18.2, Standard deviation=9.9, Maximum=-3.4, Minimum=-34.7												
$CaCl_2$=0.01 mol dm^{-3}												
-4.1	-6.3	-9.8	-4.5	-10.7	-4.8	-6.0	-18.1					
-9.8	-13.3	-13.7	-7.8	-12.0	-14.3	-15.0	-10.4					
Mean=-10.0, Standard Deviation=4.21, Maximum=-4.1, Minimum=-18.1												
$CaCl_2$=0.001 mol dm^{-3}												
1.5	3.8	3.0	3.8	6.1	1.5	6.9	6.1	6.8	2.3	6.0	5.5	
2.9	3.7	7.5	6.8	6.3	3.2	7.2	4.5	3.8	4.5	3.9	3.0	
Mean=4.6, Standard Deviation=1.83, Maximum=7.5, Minimum=1.5												
$CaCl_2$=0.0001 mol dm^{-3}												
23.2	26.4	12.2	31.1	17.6	11.3	21.0	20.4	21.8	12.8	30.5	23.5	
21.2	29.1	19.9	29.3	29.8	22.7	24.5	20.5	18.6	16.7	27.7	30.5	
Mean=22.6, Standard Deviation=5.9, Maximum=31.1, Minimum=11.3												
$CaCl_2$=0.00001 mol dm^{-3}												
31.3	21.8	10.4	24.2	9.6	5.6	5.6	5.6	5.6	27.5	30.2	22.3	26.7	23.6
23.0	24.2	7.3	10.5	12.9	8.9	14.6	11.4	2.4	36.2	21.5	12.8	26.7	29.6
31.7	Mean=18.1, Standard Deviation=9.7, Maximum=36.2, Minimum=2.4												
19.1													

Table A7 Effect of different concentrations of $CaCl_2$/KCl mixtures on the zeta potenials of polystyrene latex particles (0.01 mol dm^{-3} KCl solution, neutral pH)

$CaCl_2$=0.1 mol dm^{-3}													
-6.6	-23.1	-7.3	-10.7	-18.2	-13.4	-3.6							
-31.4	-10.0	-22.1	-18.7	-9.7	-20.5	-3.7							
Mean=-14.2, Standard Deviation=8.3, Maximum= -3.6, Minimum=-31.4													
$CaCl_2$=0.01 mol dm^{-3}													
-2.5	-1.0	-2.9	-3.0	-3.6	-5.4	-6.1	-2.0	-17.9	-5.7	-5.6			
-4.2	-15.0	-17.6	-13.1	-15.5	-7.4	-14.1	-2.0	-23.2	-5.9	-3.5			
Mean=-8.0, Standard deviation=6.4, Maximum=-1.0, Minimum=-23.2													
$CaCl_2$=0.001 mol dm^{-3}													
6.5	6.0	1.8	11.9	6.9	1.6	3.4							
6.6	2.4	4.2	8.4	7.0	9.1	6.0							
Mean=5.8, Standard Deviation=2.9, Maximum=11.9, Minimum=1.6													
$CaCl_2$=0.0001 mol dm^{-3}													
-7.2	-9.7	-8.7	-1.8	-12.7	-12.5								
-11.0	-12.4	-13.4	-23.5	-10.6	-8.9								
Mean=-11.0, Standard deviation=5.0, Maximum=-1.8, Minimum=-23.5													
$CaCl_2$=0.00001 mol dm^{-3}													
-6.4	-1.6	-4.8	-18.1	-1.8	-6.5	-4.1	-6.1	-5.7	-4.2				
-20.1	-17.7	-2.4	-6.5	-5.6	-3.2	-3.0	-2.4	-12.8	-6.7				
Mean=-7.0, Standard Deviation=5.6, Maximum=-1.6, minimum=-20.1													
$CaCl_2$=0.000001 mol dm^{-3}													
-3.3	-1.6	-1.8	-2.4	-8.4	-5.2	-4.8	-1.6	-3.3	-21.9	-14.5			
-10.0	-22.8	-8.8	-1.6	-4.2	-1.8	-11.8	-9.3	-4.3	-11.8	-11.5			
Mean=-7.6, Standard Deviation=6.2, Maximum=-1.6, Minimum=-22.8													

Table A8 Effect of different concentrations of $CaCl_2$/KCl mixtures on the zeta potenials of polystyrene latex particles (0.001 mol dm^{-3} KCl solution, neutral pH)

$CaCl_2$=0.1 mol dm^{-3}													
-6.6	-14.2	-19.6	-15.9	-10.2	-3.6	-9.1	-18.5						
-6.4	-6.1	-9.1	-25.1	-6.0	-3.6	-5.9	-5.7						
Mean=-10.4, Standard Deviation=2.9, Maximum=-3.6, Minimum=-25.1													
$CaCl_2$=0.01 mol dm^{-3}													
-2.1	-13.2	-3.0	-3.4	-21.8	-2.0	-6.6	-9.5						
-1.9	-7.8	-1.9	-1.0	-9.8	-7.7	-9.6	-12.9						
Mean=-7.2, Standard deviation=5.6, Maximum=-1.0, Minimum=-21.8													
$CaCl_2$=0.001 mol dm^{-3}													
2.4	1.5	8.6	3.8	6.3	12.9	10.0	6.1	9.1	12.8				
10.7	8.4	6.9	8.6	7.0	25.9	3.0	4.6	13.1	10.1				
Mean=-8.6, Standard Deviation=5.3, Maximum=25.9, Minimum=1.5													
$CaCl_2$=0.0001 mol dm^{-3}													
15.1	16.1	13.7	1.6	4.5	11.1	9.6	11.3						
14.1	16.1	9.5	14.5	12.3	6.8	14.0	8.7						
Mean=11.2, Standard Deviation=4.2, Maximum=16.1, Minimum=1.6													
$CaCl_2$=0.00001 mol dm^{-3}													
17.0	14.0	1.6	14.5	20.3	12.0	16.4	22.1	11.5	22.8				
7.9	12.5	3.3	15.0	6.8	8.7	2.7	29.5	13.7	15.0				
Mean=13.4, Standard Deviation=7.1, Maximum=29.5, Minimum=1.6													
$CaCl_2$=0.000001 mol dm^{-3}													
16.0	6.0	2.7	7.4	11.4	5.1	7.5	5.9	9.6	16.7				
5.1	7.0	8.8	16.3	15.8	4.2	10.1	17.0	6.6	14.3				
Mean=9.7, Standard Deviation=4.7, Maximum=17.0, Minimum=2.7													

Table A9 Conductometric titration data for dialysed and non-dialysed polystyrene latex particles

Non dialysed particles		Dialysed particles	
Conductivity (μS)	cm^3 of 0.00001 mol dm^{-3} NaOH added	Conductivity (μS)	cm^3 of 0.00001 mol dm^{-3} NaOH added
7.33	0	7.22	0
7.07	0.5	7.16	0.3
6.99	0.7	7.07	0.5
6.87	1.0	6.84	1.0
6.78	1.2	6.41	2.0
6.67	1.5	6.07	3.0
6.6	1.7	5.71	4.0
6.51	2.0	5.45	5.0
6.44	2.2	5.29	6.0
6.38	2.5	5.2	7.0
6.33	2.7	5.21	8.0
6.32	3.0	5.26	9.0
6.28	3.2	5.30	10.0
6.24	3.4	5.44	11.0
6.22	3.6	5.64	12.0
6.2	3.8	5.85	13.0
6.16	4.0	6.02	14.0
6.45	4.2	6.18	15.0
6.45	4.5	6.29	16.0

Table A10 Zeta potentials of Hypercarb particles for neutral pH and different KCl solution

KCl=0.01 mol dm^{-3}												
-1.2 -7.4	-4.0 -5.5	-9.8 -4.1	-4.7 -5.6	-8.2 -11.7	-1.5 -8.7	-1.5 -7.8	-2.4 -7.1	-11.7				
Mean=-6.0, Standard Deviation=3.4, Maximum=-1.2, Minimum=-11.7												
KCl =0.001 mol dm^{-3}												
-9.0 -6.9	-8.2 -8.2	-5.6 -11.4	-6.6 -3.6	-6.3 -7.1	-9.4 -10.8	-4.3 -7.3	-9.3 -11.9	-10.8 -10.7	-5.7 -14.4	-13.0 -2.1	-18.0 -3.5	
Mean=-8.5, Standard deviation=3.7, Maximum=-2.1, Minimum=-18.0												
KCl =0.0001 mol dm^{-3}												
-8.9 -9.7	-14.0 -9.8	-15.5 -14.1	-9.7 -11.4	-16.7 -16.1	-18.6 -20.2	-12.9 -13.7	-26.6 -18.5	-17.7 -16.4	-17.8 -22.6	-26.7 -21.9	-21.1 -13.0	
Mean=-16.4, Standard Deviation=5.0, Maximum=-8.9, Minimum=-26.7												
KCl =0.00001 mol dm^{-3}												
-16.7 -27.8	-22.6 -25.4	-25.5 -29.5	-25.7 -29.0	-33.1 -26.2	-26.7 -28.2	-26.8 -18.5	-23.7 -30.0	-19.3 -21.3	-22.8 -21.5	-22.1		
Mean=-24.9, Standard Deviation=4.1, Maximum=-16.7, Minimum=-33.1												

Table A11 Zeta potenials of RVC for 0.1 mol dm^{-3} KCl and different pH

-19.3 -7.7	-7.8 -16.5	-8.1 -11.8	-28.4 -6.9	-7.9 -8.4	-4.1 -4.1	-3.7 -3.8	-3.9 -3.7	-11.8 -7.9	-4.3 -8.1	-4.2 -24.9			
Mean=-9.5, **pH=3.8**, Standard Deviation=6.95, Maximum=-3.7, Minimum=-28.4													
-3.7 -29.6	-3.7 -7.5	-3.8 -3.7	-22.7 -7.7	-7.9 -4.1	-11.9 -3.9	-3.9 -3.9	-3.9 -12.3	-7.8 -7.9	-15.5 -8.2	-8.1 -16.1	-11.5 -3.9	-8.2	
Mean=-8.9, **pH=3.9**, Standard Deviation=6.47, Maximum=-3.7, Minimum=-29.6													
-19.9 -14.5	-4.1 -19.6	-3.9 -12.5	-3.9 -3.9	-16.3 -8.2	-19.5								
Mean=-11.5, **pH=6.5**, Standard Deviation=6.85, Maximum=-3.9, Minimum=-19.9													
-8.2 -20.8	-8.1 -12.3	-3.9 -17.3	-3.9 -28.4	-8.1 -3.9	-15.8 -19.6	-3.8 -8.3	-8.3 -23.5						
Mean=-12.1, **pH=6.6**, Standard deviation=7.79, Maximum=-3.8, Minimum=-28.4													
-7.9 -4.1	-8.3 -8.2	-4.2 -8.3	-4.1 -4.1	-4.2 -8.2	-4.3 -4.2	-4.3 -8.2	-4.1 -4.1	-3.9 -17.2					
Mean=-6.2, **pH=6.8**, Standard Deviation=3.35, Maximum=-3.9, Minimum=-17.2													

Table A12 Zeta potenials of RVC for 0.01 mol dm^{-3} KCl and different pH

12.4 5.6	11.8 5.9	10.2 3.8	3.9 7.8	6.0 4.2	6.0 3.8	7.7 7.8	6.0 5.7	8.3 3.9	7.8 8.2	2.0 4.3	3.8 6.0	7.2 8.1	8.4
Mean=6.6, **pH=3.6**, Standard Deviation=2.5, Maximum=12.4, Minimum=2.0													
19.9 16.0	17.4 18.1	16.3 12.3	10.9 10.9	10.6 12.9	16.1 10.4	8.6 6.3	8.4 8.8	5.4 6.8	5.1 4.3	4.1 2.0	4.1		
Mean=10.2, **pH=3.9**, Standard Deviation=5.17, Maximum=19.9, Minimum=2.0													
-9.8 -2.0	-4.2 -4.3	-4.5 -2.1	-10.7 -8.9	-16.4 -14.2	-2.1 -2.1	-6.3 -6.5	-3.7 -7.2	-9.1 -7.3	-4.2 -6.1	-8.3 -6.6	-6.6 -8.7	-8.6	
Mean=-6.8, **pH=4.0**, Standard Deviation=3.6, Maximum=-2.0, Minimum=-16.4													
-2.1 -2.1	-2.1 -2.1	-4.1 -6.4	-4.1 -4.2	-2.0 -4.1	-4.2 -5.4	-5.4 -7.0	-8.7 -7.3	-7.2					
Mean=-4.6, **pH=4.13**, Standard deviation=2.13, Maximum=-2.0, Minimum=-8.7													
-13.3 -7.3	-7.0 -12.9	-12.4 -15.6	-14.2 -13.2	-16.4 -16.7	-4.2 -8.7	-25.3 -6.5	-4.2 -12.8	-7.4 -14.5	-7.3 -14.5	-12.9 -6.4			
Mean=-11.5, **pH=4.2**, Standard Deviation=5.0, Maximum=-4.2, Minimum=-25.3													
-15.9 -10.1	-13.3 -26.4	-16.5 -18.6	-16.9 -13.2	-18.3 -14.3	-21.7 -16.7	-12.7 -14.6	-12.9 -12.8	-17.9 -16.3	-14.3 -19.6	-19.5 -12.2	-16.3 -15.9		
Mean=-16.1, **pH=6.2**, Standard Deviation=3.52, Minimum=-26.4, Maximum=-10.1													
-11.1 -1.9	-5.9 -7.5	-9.3 -15.2	-16.6 -14.9	-24.1 -11.4	-14.5 -17.0	-14.9 -14.5	-12.8 -20.0	-11.0 -18.3	-20.4 -18.3	-16.5 -7.3	-5.2 -16.3	-10.9 -14.2	-23.3
Mean=-13.8, **pH=6.5**, Standard Deviation=5.4, Maximum=-1.9, Minimum=-24.1													
-11.1 -11.1	-13.6 -16.7	-17.4 -20.4	-17.4 -20.4	-18.1 -20.6	-21.9 -19.6	-20.9 -19.5	-20.1 -12.8						
Mean=-17.4, **pH=6.6**, Standard deviation=3.76, Maximum=-11.1, Minimum=-21.9													
-16.3 -19.1	-13.8 -19.2	-19.0 -16.7	-16.5 -12.8	-13.1 -16.0	-20.1 -13.4	-13.2 -13.3	-16.1 -19.7	-13.1 -16.4	-6.6 -13.1	-9.1 -18.1	-20.1 -23.0	-8.6 -20.3	-27.6 -25.3
-12.5 -18.8	-20.3 -23.2	-16.3 -6.5											
Mean=-16.4, **pH=11.7**, Standard deviation=4.9, Maximum=-6.5, Minimum=-27.6													

Table A13 Zeta potenials of RVC for 0.001 mol dm^{-3} KCl and different pH

3.8 10.4	15.2 15.2	17.4 9.8	10.1 8.6	6.6 3.4	6.6 3.3	3.4 8.4	6.8 1.8	1.6 3.3	15.9 12.0	10.2 8.4	4.8 8.2	3.3 7.9	
Mean=7.9, **pH=2.9**, Standard deviation=4.5, Maximum=17.4, Minimum=1.6													
-7.4 -3.2	-3.2 -4.8	-3.0 -3.0	-1.5 -1.5	-1.7 -4.6	-1.5 -7.9	-3.2 -1.5	-7.8 -1.5	-1.5 -1.7	-7.8 -6.1				
Mean=-3.7, **pH=4.0**, Standard Deviation=2.42, Maximum=-1.5, Minimum=-7.9													
-39.4 -29.8	-31.2 -36.3	-32.5 -39.0	-39.4 -37.2	-28.4 -25.1	-35.9 -31.4	-39.4 -36.4	-38.9 -37.2	-38.8 -32.7					
Mean=-34.9, **pH=5.8**, Standard Deviation=4.4, Maximum=-25.1, Minimum=-39.4													
-25.7 -28.7	-26.9 -23.5	-18.8 -19.2	-25.8 -20.7	-26.7 -23.6	-23.7 -25.3								
Mean=-24.0, **pH=6.6**, Standard deviation=3.1, Maximum=-18.8, Minimum=-28.7													
-33.4 -38.3	-36.7 -36.2	-35.8 -42.3	-37.8 -34.0	-35.0 -35.3	-38.4 -38.0	-33.4 -36.4	-33.5 -32.5	-36.7 -37.5					
Mean=-36.2, **pH=7.0**, Standard Deviation=2.4, Maximum=-32.5, Minimum=-42.3													

Table A14 Zeta potenials of RVC for 0.0001 mol dm^{-3} KCl and different pH

-14.3 -18.2	-12.9 -11.0	-10.7 -19.1	-15.4 -14.6	-12.7 -25.0	-16.1 -16.1	-16.3 -8.8	-5.2 -7.2	-12.7 -18.1	-14.5				8.48
Mean=-14.2, **pH=4.0**, Standard Deviation=4.55, Maximum=-5.2, Minimum=-25.0													
-30.4 -16.3	-3.4 -25.5	-31.4 -20.4	-24.1 -26.7	-26.7 -18.6	-26.0 -23.2	-23.1 -12.5	-27.1 -16.8	-22.4 -25.0	-19.6				
Mean=-22.1, **pH=4.5**, Standard Deviation=6.62, Maximum=-3.4, Minimum=-31.4													
-31.4 -30.7	-38.1 -40.8	-33.4 -37.6	-48.1 -30.7	-33.9 -37.7	-41.2 -37.7	-37.9 -32.5	-30.4 -39.8	-28.9 -36.3	-34.9 -27.2				
Mean=-35.5, **pH=5.7**, Standard Deviation=5.0, Maximum=-27.2, Minimum=-48.1													
-32.1 -39.4	-31.2 -38.0	-34.5 -42.0	-53.9 -48.4	-38.1 -42.1	-30.8 -41.2	-29.6 -38.6	-27.7 -31.4	-26.4 -40.0	-37.3 -23.5	-33.2 -31.3	-41.7 -28.1		
Mean=-35.9, **pH=6.7**, Standard deviation=7.1, Maximum=-23.5, Minimum=-53.9													
-46.2 -46.9	-45.3 -37.1	-40.8 -47.8	-43.9 -47.2	-54.2 -44.2	-39.8 -45.6	-35.3 -36.1	-35.7 -45.3	-52.4 -51.1	-38.2 -51.1	-35.3 -41.3			
Mean=-43.7, **pH=9.7**, Standard Deviation=5.8, Maximum=-35.3, Minimum=-54.2													
-31.6 -45.4	-46.3 -39.3	-35.8 -30.2	-34.0 -42.5	-51.5 -42.7	-41.6 -38.5	-43.8 -45.2	-35.2 -40.9	-44.2 -42.4	-47.8 -34.7				
Mean=-40.7, **pH=10.2**, Standard Deviation=5.6, Minimum=-51.5, Maximum=-30.2													

Table A15 Effect of different concentrations of $CaCl_2$/KCl mixtures on the zeta potenials of RVC (0.1 mol dm^{-3} KCl solution, neutral pH)

$CaCl_2$=0.1 mol dm^{-3}												
-26.4	-13.7	-4.6	-4.7	-4.7	-4.8	-9.8	-5.0	-8.9	-9.2	-4.6	-9.1	-4.6	-4.5
-8.8	-4.5	-9.6	-19.0	-4.8	-4.8	-10.2	-4.5	-13.7	-4.5	-18.6	-8.9	-8.9	-4.6
Mean=-8.6, Standard Deviation=5.4, Maximum=-4.5, Minimum=-26.4													
$CaCl_2$=0.01 mol dm^{-3}													
-16.4	-3.4	-14.1	-3.4	-14.6	-14.3	-3.6	-10.9	-3.6	-7.0	-6.9	-10.7		
-3.7	-14.0	-14.2	-7.3	-10.5	-10.7	-10.6	-7.2	-7.3	-3.6	-14.5			
Mean=-9.3, Standard deviation=4.4, Maximum=-3.4, Minimum=-16.4													
$CaCl_2$=0.001 mol dm^{-3}													
3.6	10.6	14.5	7.0	11.1	6.9	10.1	3.9	27.1	20.9				
13.8	3.3	3.6	20.6	3.6	6.8	3.7	16.9	14.1	6.8				
Mean=10.5, Standard Deviation=6.9, Maximum=27.1, Minimum=3.3													
$CaCl_2$=0.0001 mol dm^{-3}													
3.4	15.1	3.9	0.0	3.7	-8.6	8.2	0.0	0.0	4.1	-8.8	0.0	-8.7	-8.7
-7.7	12.2	6.4	4.2	-12.3	-12.0	4.3	4.2	-15.2	13.1	0.0	4.1	-4.3	4.2
-10.0	0.0	-7.0	0.0	-11.0	-6.9	0							
-7.2	-10.5	0.0	-3.3	-13.6	10.4	-3.4							
Mean=-1.3, Standard Deviation=7.7, Maximum=15.1, Minimum=-15.2													
$CaCl_2$=0.000001 mol dm^{-3}													
-3.3	-9.7	-6.5	-9.8	-13.8	-15.8	-12.9	-12.7	-9.6					
-19.6	-9.8	-6.6	-19.5	-19.9	-3.0	-9.7	-6.5						
Mean=-11.1, Standard Deviation=5.3, Maximum=-3.0, Minimum=-19.9													

Table A16 Effect of different concentrations of $CaCl_2$/KCl mixtures on the zeta potenials of RVC (0.01 mol dm^{-3} KCl solution, neutral pH)

$CaCl_2$=0.1 mol dm^{-3}													
-20.9 -4.6	18.5 9.6	8.8 15.9	9.1 4.6	-9.3 -5.1	10.2 0	4.6 -4.8	0 0	-5.2 0	10.1 4.8	9.7 0	4.8 5.1	-4.6 -24.8	4.7 0
0 -4.6	0 0	9.2 0	4.6 -8.9	4.7 -4.6	-9.2 0								
Mean=0.8, Standard Deviation=8.5, Maximum=18.5, Minimum=-24.8													
$CaCl_2$=0.01 mol dm^{-3}													
-15.0 -3.3	-13.3 -16.9	-3.2 -6.6	-3.2 -9.8	-9.8 -6.8	-10.0 -6.6	-6.9 -3.3	-7.2 -15.9	-4.6 -11.0	-8.7 -15.8	-13.7 -8.8	-4.2 -9.1	-13.4 -17.3	
Mean=-9.4, Standard deviation=4.5, Maximum=-3.2, Minimum=-17.3													
$CaCl_2$=0.001 mol dm^{-3}													
1.9 1.9	3.8 1.9	5.7 5.9	7.4 1.9	7.3 3.6	3.6 5.7	3.7 1.8	7.2 9.1	7.7 1.9	2.0 1.9	5.6 5.7			
Mean=4.4, Standard Deviation=2.4, Maximum=9.1, Minimum=1.8													
$CaCl_2$=0.0001 mol dm^{-3}													
13.2 9.5	7.4 18.8	20.9 9.5	12.9 12.7	7.4 18.8	12.7 21.9	13.1 12.7	1.8 5.5	5.6 3.7	15.0 11.4	16.5 5.5	9.5 16.3	16.8 14.9	5.5 14.7
Mean=11.9, Standard Deviation=5.3, Maximum=21.9, Minimum=1.8													
$CaCl_2$=0.00001 mol dm^{-3}													
-32.3 -34.3	-40.0 -37.1	-42.5 -38.4	-36.4 -38.8	-32.8 -37.9	-39.9 -31.7								
Mean=-36.8, Standard deviation=3.4, Maximum=-31.7, Minimum=-42.5													
$CaCl_2$=0.000001 mol dm^{-3}													
-34.5 -31.7	-31.7 -29.9	-29.5 -31.2	-27.7 -29.4	-32.9 -29.5	-27.6 -31.2	-34.3 -34.0	-32.9 -31.6						
Mean=-31.5, Standard Deviation=2.0, Maximum=-27.7, Minimum=-34.5													

Table A17 Effect of different concentrations of $CaCl_2$/KCl mixtures on the zeta potenials of RVC (0.001 mol dm^{-3} KCl solution, neutral pH)

$CaCl_2$=0.1 mol dm^{-3}												
16.1 8.1	8.1 20.5	8.3 4.2	27.5 16.1	11.9 24.2	21.0 12.2	3.8 23.9	27.9 31.6	40.7 3.8	24.5 19.9	7.8 12.2	32.2 35.9		
Mean=18.5, StandardDeviation=10.7, Maximum=40.7, Minimum=3.8													
$CaCl_2$=0.01 mol dm^{-3}													
-4.1 -5.0	-6.6 -2.5	-7.8 -7.5	-2.4 -5.0	-10.1 -7.7	-3.9 -5.1	-19.0 -10.1	-10.0 -7.8	-9.8 -5.2	-7.4 -10.2	-2.4 -2.0	-5.0 -7.5	-5.1 -2.4	
Mean=-6.9, Standard Deviation=3.7, Maximum=-2.0, Minimum=-19.0													
$CaCl_2$=0.001 mol dm^{-3}													
-5.7 -7.5	-1.8 -5.5	1.9 -7.5	1.9 3.7	1.8 1.8	-1.8 1.8	11.0 12.2	0 -1.8	1.8 5.2	6.9 3.4	7.2 -5.6	-7.4 -5.5	-1.8 7.4	0 5.4
7.3 9.2	1.8 9.1	1.8 5.4	1.8 7.2	-5.6 -3.7	-5.4 -5.4								
Mean=1.1, Standard deviation=5.5, Maximum=12.2, Minimum=-7.5													
$CaCl_2$=0.0001 mol dm^{-3}													
-16.4 -16.0	-21.8 -14.9	-18.5 -3.7	-14.9 -12.9	-9.1 -5.5	-7.8 -25.7	-7.9 -7.8	-3.8 -1.9	-11.4 -3.8	-3.9 -3.8				
Mean=-10.6, Standard Deviation=6.8, Maximum=-1.9, Minimum=-25.7													
$CaCl_2$=0.00001 mol dm^{-3}													
-32.9 -35.9	-30.2 -28.1	-28.1 -26.7	-36.2 -23.5	-22.7 -30.4	-26.4 -38.2	-20.0 -30.8	-29.0 -30.9	-29.0 -39.9	-25.5 -31.2	-30.5 -30.8	-40.8 -30.0	-31.1 -35.9	
Mean=-30.6, Standard Deviation=5.0, Maximum=-20.0, Minimum=-40.8													
$CaCl_2$=0.000001 mol dm^{-3}													
-34.0 -41.5	-28.6 -30.7	-15.4 -30.7	-36.7 -38.6	-35.5 -31.2	-31.3 -31.7	-18.5 -42.6	-18.5 -42.6	-37.0 -40.8	-35.2 -40.7	-28.0 -40.9	-35.8 -37.5	-37.7 -32.5	-36.3 -38.1
Mean=-34.2, Standard deviation=6.4, Maximum=-15.4, Minimum=-42.6													

APPENDIX B: Experimental results of deposition of polystyrene latex particles onto glass beads and onto RVC and also results for deposition of *Hypercarb* particles onto RVC

Table B1

C1	C2	C3	C4
90	0.28	0.19	0.45
250	1.35	0.19	0.45
405	2.06	0.21	0.50
660	2.83	0.21	0.50
887	3.20	0.22	0.51
984	3.80	0.23	0.54
1250	3.74	0.22	0.53
1462	5.10	0.25	0.58
1610	4.80	0.23	0.54
1770	5.35	0.24	0.56
1930	5.93	0.25	0.58
2110	6.20	0.25	0.60
2315	6.67	0.26	0.61
2471	7.11	0.26	0.62
2650	7.23	0.26	0.62
2909	8.41	0.28	0.66
3025	8.21	0.28	0.66
3440	8.89	0.28	0.66
3581	10.20	0.30	0.70
3820	11.45	0.31	0.73
4177	11.20	0.31	0.73
4515	11.40	0.31	0.73
4872	10.85	0.30	0.72
5165	11.75	0.31	0.74
5360	11.20	0.31	0.73
5540	12.25	0.35	0.82

Table B2

112	0.02	0.18	0.44
335	1.67	0.20	0.48
629	1.94	0.20	0.48
845	2.21	0.20	0.48
950	2.38	0.20	0.48
1210	2.90	0.21	0.51
1450	2.90	0.21	0.51
1654	3.35	0.22	0.54
1795	3.81	0.23	0.56
2000	3.82	0.23	0.56
2190	4.25	0.23	0.56
2318	4.09	0.23	0.56
2495	4.36	0.23	0.56
2655	4.53	0.24	0.58
2880	4.80	0.24	0.58
3030	4.90	0.24	0.58
3420	5.50	0.24	0.58
3560	5.41	0.24	0.58
3960	5.96	0.25	0.50
4228	7.84	0.26	0.63
4401	6.95	0.25	0.60
4625	6.50	0.25	0.60
4917	6.40	0.25	0.60
5063	6.30	0.25	0.60
5310	5.96	0.24	0.58
5655	6.60	0.25	0.60
5890	7.40	0.26	0.63

Table3 B3

60	4.23	0.23	0.52
165	12.46	0.33	0.75
310	13.52	0.34	0.77
452	15.15	0.37	0.84
640	16.95	0.37	0.84
750	18.10	0.38	0.86
945	18.45	0.39	0.88
1015	18.78	0.40	0.90
1155	19.15	0.40	0.90
1360	19.20	0.40	0.90
1530	19.70	0.41	0.93
1678	19.70	0.41	0.93
1798	19.80	0.41	0.93
1925	19.70	0.41	0.93
2064	19.70	0.41	0.93
2202	14.90	0.24	0.58
2387	15.50	0.24	0.58
2850	19.90	0.41	0.93
3029	19.96	0.41	0.93
3280	19.92	0.41	0.93
3445	19.95	0.41	0.93
3705	19.90	0.41	0.93
4323	19.90	0.41	0.93
4663	19.90	0.41	0.93
5155	19.90	0.41	0.93

Deposition of polystyrene latex particles onto glass beads. Table B1: run1 at KCl concentration of 0.01 mol dm^{-3}, Table B2: run2 at KCl concentration of 0.01 mol dm^{-3}, Table B3: run3 at KCl concentration of 0.001 mol dm^{-3}.

Columns C1: Time (second), C2: Turbidity (NTU), C3: Effluent particle number concentration ($x10^6$ particles/cm^3), C4: C/C_o

Table B4 Experimental conditions for the deposition of polystyrene latex and *Hypercarb* particles onto RVC

Experiments number	Volumetric flowrate (cm^3/min)	KCl Conc. (mol/dm^{-3})	Particle zeta potential (mV)	RVC potential (mV vs SCE)
Ex1	34	0.0001	-8.5	-26.5 [a]
Ex2	34	0.0001	-8.5	-200.0
Ex3	34	0.0001	-8.5	-300.0
Ex4	34	0.0001	-8.5	+300.0
Ex5	12	0.0001	-8.5	+300.0
Ex6	5.6	0.0001	-8.5	+300.0
Ex7	5.6	0.0001	-8.5	-300.0
Ex8	4.5	0.01	-4.0	+300.0
Ex9	4.5	0.01	-4.0	-300.0
Ex11	1.7	0.001	-8.5	-200.0
Ex12	1.7	0.001	-8.5	-300.0
Ex13	1.7	0.001	-8.5	-22.5 [a]
Ex14	1.7	0.001	-8.5	-130.0
Ex15	1.7	0.001	-8.5	184.0
Ex16	1.7	0.001	-8.5	172.0
Ex17	1.7	0.001	-8.5	444.0
Ex18	10.0	0.001	-8.5	-106.0
Ex19	10.0	0.001	-8.5	107.0
Ex20	10.0	0.001	-8.5	-22.5[a]
Ex21	1.7	0.001	-8.5	-417.0
Hyp1	2.5	0.0001	-16.0	-95.0
Hyp2	2.5	0.0001	-16.0	-30.0[a]
Hyp3	2.5	0.0001	-16.0	348.0
Hyp4	2.5	0.001	-8.5	-150.0
Hyp5	2.5	0.001	-8.5	-316.0
Hyp6	2.5	0.001	-8.5	-447.0

Note: a the zeta potential value used as the potential

Table B5 Ex1

C1	C2	C3	C4
0	0.00	0.00	0.00
35	0.86	0.18	0.30
85	5.15	0.25	0.40
165	22.20	0.43	0.70
250	35.00	0.58	0.95
330	36.20	0.60	0.98
405	37.00	0.61	1.00

Table B6 run Ex2

0	0.00	0.00	0.00
35	0.40	0.18	0.30
80	10.40	0.34	0.45
130	26.30	0.48	0.63
197	37.50	0.61	0.80
200	44.60	0.69	0.90
390	48.50	0.74	0.97
470	49.00	0.75	1.00

Table B7 run Ex3

0	0.00	0.00	0.00
30	0.75	0.18	0.30
70	6.70	0.26	0.38
105	19.50	0.40	0.58
195	34.00	0.57	0.83
265	41.20	0.65	0.94
350	42.80	0.68	1.00
435	43.70	0.69	1.00

Table B8 run Ex4

0	0.00	0.00	0.00
40	0.30	0.18	0.30
95	12.00	0.32	0.55
140	23.00	0.44	0.76
205	29.00	0.52	0.89
312	31.20	0.54	0.93
390	34.60	0.58	1.00

Table B9 run Ex5

0	0.00	0.00	0.00
75	1.20	0.20	0.36
160	2.10	0.23	0.41
262	10.30	0.30	0.53
380	19.90	0.41	0.73
500	25.90	0.48	0.86
620	26.00	0.48	0.86
740	26.20	0.48	0.86
860	27.10	0.49	0.87
990	27.20	0.49	0.87
1115	27.30	0.50	0.89
1240	28.10	0.50	0.89
1360	28.10	0.50	0.89
1580	28.20	0.51	0.91
1755	29.00	0.52	0.93
2005	29.00	0.52	0.93
2190	29.00	0.52	0.93
2395	29.00	0.52	0.93

Table B10 run Ex6

0	0.00	0.00	0.00
317	0.80	0.18	0.33
530	5.80	0.25	0.45
740	17.28	0.38	0.69
935	20.00	0.41	0.74
1145	20.10	0.41	0.74
1380	20.70	0.41	0.74
1605	21.50	0.43	0.78
1840	22.00	0.44	0.80
2075	22.10	0.44	0.80

Table B11 run Ex7

0	0.00	0.00	0.00
250	0.50	0.18	0.33
515	16.70	0.37	0.67
750	19.30	0.40	0.73
960	22.90	0.45	0.82
1165	25.90	0.48	0.87
1375	25.80	0.48	0.87
1568	26.40	0.49	0.89
1800	26.20	0.49	0.89
2000	26.20	0.49	0.89

Table B12 run Ex8

0	0.00	0.00	0.00
200	0.70	0.18	0.35
435	2.96	0.21	0.41
615	8.17	0.27	0.53
820	11.25	0.31	0.60
1040	14.30	0.35	0.68
1290	15.71	0.36	0.70
1520	16.40	0.37	0.72
1715	17.44	0.38	0.74
1970	17.40	0.38	0.74

Table B13 run Ex9

305	1.10	0.18	0.33
455	8.08	0.27	0.49
595	11.70	0.32	0.58
910	15.10	0.35	0.64
1140	19.20	0.40	0.73
1325	21.10	0.42	0.76
1545	22.90	0.44	0.80
1760	23.10	0.45	0.82
1915	23.90	0.46	0.84
2180	23.80	0.46	0.84
2395	23.60	0.45	0.82
2610	23.70	0.46	0.84
2760	23.90	0.46	0.84

Table B14 run Ex10

630	0.91	0.18	0.27
1230	8.60	0.28	0.43
1820	17.10	0.38	0.58
2400	22.70	0.44	0.67
3000	25.20	0.47	0.72

Table B15 run Ex11

645	1.56	0.20	0.23
1245	15.00	0.35	0.41
1920	30.60	0.54	0.64
2550	36.10	0.60	0.70
3240	41.30	0.66	0.78

Table B16 run Ex12

750	1.46	0.18	0.19
1395	3.14	0.23	0.24
1975	11.80	0.31	0.32
2550	20.00	0.41	0.43
3195	21.30	0.43	0.45
3790	22.00	0.44	0.46
4350	23.10	0.45	0.47
6950	22.80	0.44	0.46
7530	22.80	0.44	0.46

Table B17 run Ex13

0	0.00	0.00	0.00
615	1.12	0.18	0.20
1215	8.28	0.27	0.30
1830	19.90	0.41	0.46
2490	25.30	0.47	0.53
3075	26.50	0.48	0.54
3715	29.40	0.53	0.59
4335	28.80	0.52	0.58
4990	29.80	0.53	0.59

Table B18 run Ex14

0	0.00	0.00	0.00
750	3.91	0.23	0.31
1210	24.60	0.46	0.62
1845	31.30	0.54	0.73
2550	34.00	0.57	0.77
3165	35.80	0.59	0.79
3780	36.40	0.60	0.81
4440	35.60	0.59	0.80
4980	35.10	0.58	0.79
5740	35.00	0.58	0.78

6300	36.60	0.60	0.81
6720	36.20	0.60	0.81

Table B19 run Ex15

0	0.00	0.00	0.00
595	0.41	0.18	0.18
1155	11.45	0.31	0.32
1770	27.00	0.49	0.50
2360	35.70	0.59	0.60
3120	42.80	0.68	0.70
3600	45.10	0.70	0.72
4215	47.00	0.73	0.75

Table B20 run Ex16

645	1.70	0.20	0.23
1330	16.70	0.38	0.44
1920	25.90	0.48	0.56
2595	32.20	0.55	0.64
3225	35.70	0.59	0.68
3870	37.20	0.61	0.70
4440	36.40	0.60	0.69
5190	39.80	0.64	0.74
5830	48.90	0.74	0.86
6595	46.70	0.72	0.84

Table B21 run Ex17

720	0.79	0.18	0.20
1340	8.90	0.28	0.32
2040	20.40	0.41	0.46
2610	25.20	0.48	0.54
3210	30.60	0.54	0.61
3900	36.70	0.60	0.68
4590	37.70	0.62	0.70
5230	34.70	0.58	0.66
5910	33.40	0.57	0.64
6500	34.60	0.58	0.66

Table B22 run Ex18

0	0.00	0.00	0.00
140	1.00	0.18	0.28
255	7.30	0.26	0.38
325	14.40	0.35	0.51
405	21.40	0.43	0.63
525	26.80	0.49	0.72
645	29.80	0.53	0.78
755	31.30	0.54	0.79
890	32.30	0.55	0.80
1000	33.10	0.56	0.82
1110	33.20	0.56	0.82
1215	34.10	0.57	0.83
1320	34.00	0.57	0.84
1415	35.10	0.58	0.85
1525	34.40	0.57	0.84

Table B23 run Ex19

0	0.00	0.00	0.00
130	2.10	0.18	0.27
245	22.80	0.44	0.60
305	29.30	0.52	0.71
480	33.90	0.57	0.78
595	37.00	0.60	0.82
710	39.30	0.64	0.87
820	40.90	0.65	0.89
935	41.30	0.66	0.90
1040	42.50	0.67	0.91
1130	41.40	0.66	0.90
1235	41.90	0.66	0.90
1380	41.80	0.66	0.90
1645	41.60	0.66	0.90
1770	43.40	0.68	0.93
1890	44.00	0.69	0.94
2095	44.90	0.70	0.95
2275	44.90	0.70	0.95
2375	44.90	0.70	0.95

Table B24 run Ex20

0	0.00	0.00	0.00
155	2.46	0.20	0.27
270	10.51	0.30	0.42
380	21.80	0.44	0.61
490	29.80	0.53	0.73
600	31.80	0.55	0.76
710	34.00	0.57	0.79
820	35.10	0.58	0.80
915	35.80	0.59	0.81
1020	36.70	0.60	0.83
1150	36.70	0.60	0.83
1270	36.70	0.60	0.83
1380	36.80	0.60	0.83
1490	37.60	0.61	0.85
1605	38.70	0.62	0.85
1780	38.40	0.62	0.85
1995	38.40	0.62	0.85
2130	38.40	0.62	0.85
2360	38.40	0.62	0.85

Table B25 run pH1

720	4.60	0.23	0.25
1310	10.70	0.30	0.33
1970	19.30	0.40	0.43
2630	23.10	0.44	0.48
3170	24.00	0.45	0.49
3895	26.40	0.48	0.52
4515	26.90	0.49	0.53
5140	27.90	0.50	0.54
5580	26.70	0.49	0.53
6195	24.50	0.46	0.50
6810	22.40	0.44	0.48
7420	20.80	0.42	0.45
8205	21.00	0.42	0.45

Table B26 rub Hyp1

270	0.00	0.00	0.00
640	0.00	0.00	0.00
1065	2.40	0.20	0.44
1545	9.35	0.29	0.64
1935	9.20	0.28	0.62
2430	12.00	0.32	0.71
2790	11.20	0.31	0.69
3240	13.20	0.33	0.73
4035	13.71	0.34	0.75

Table B27 run Hyp2

930	0.33	0.18	0.69
1635	1.40	0.19	0.73
2025	3.40	0.22	0.84
2475	5.00	0.24	0.92
2870	5.10	0.24	0.92
3195	5.80	0.25	0.96
3610	6.14	0.25	0.96

Table B28 run Hyp3

753	2.10	0.20	0.71
1260	4.15	0.23	0.82
1626	4.80	0.24	0.86
2118	5.90	0.25	0.89
2487	8.32	0.25	0.89
2904	6.20	0.25	0.89
3381	6.20	0.25	0.89
3744	7.10	0.26	0.93
4089	6.82	0.25	0.89

Table B29 rub Hyp4

460	2.06	0.20	0.56
850	7.15	0.26	0.76
1265	9.25	0.28	0.82
1840	9.50	0.29	0.82
2400	9.40	0.30	0.88
3180	9.40	0.32	0.94
3505	14.30	0.34	1.00

Table B30 run Hyp5

435	4.10	0.23	0.69
855	4.90	0.24	0.73
1335	5.91	0.25	0.75
1755	5.60	0.24	0.73

Table B31 run Hyp6

420	4.40	0.23	0.69
1185	4.80	0.24	0.73

1630	6.70	0.25	0.76
2075	8.25	0.27	0.85
2395	8.00	0.27	0.85

Columns same as the tables for the glass bead experiments

APPENDIX C

Listing of computer programes written in the course of the study

Table C1 Description of the programes

Program name	Function
PPENERGY	particle-particle interaction energy
PCENERGY	particle-collector interaction energy
ROOT	root of trajectory equation
TRAJ.F	location of limiting trajectory

Program PPENERGY calculates and draws the van der Waals, electrical double layer, Born and the total interaction energies between *particles* in suspension.

```
PROGRAM PPENERGY
COMMON/A/COUNT
REAL H(250,250),VB(250,250)
REAL VA(250,250),VR(250,250)
REAL VT(250,250)
REAL VA1(250,250),VR1(250,250)
REAL M,A,KBT,AP,K,SIGMA,R
REAL U1,U2,B,Y,B1,B2,B3,B4
REAL MINX,MAXX,MINY,MAXY
INTEGER NP,NUMBER,COUNT,I,J
PARAMETER (RXLEFT=1.0E-3)

WRITE (*,*) "how many profiles needed?"
READ (*,*) NUMBER
DO 40 J=1,NUMBER
WRITE(*,*)"what is the electrolyte
 concentration (mol dm-3)?"
READ(*,*) M
WRITE(*,*) "what is the Hamaker
 constant (J)?"
READ(*,*) A
WRITE(*,*) "what is the particle
 potential (mv)?"
READ(*,*) Y
KBT=1.3805e-23*298
SIGMA=0.5
WRITE(*,*) "how many increments?"
READ(*,*) NP
WRITE(*,*) "what is the particle
 radius (nm)?"
READ(*,*) AP
aph=ap/1000.0

*retarded van der waals attraction by Gregory
*J.coloid.interf.sci.Vol.83, no.1, 1981
*electrical double layer by Bell et al.
*Born repulsion by Feke et al.

DO 10 I=1,NP
READ (J,*) H(I,J)
B=((5.32*H(I,J))/100.0)*
ALOG(1.0+(100.0/(5.32*H(I,J))))
VA(I,J)=((-A*AP)/(12.0*H(I,J)))*(1-B)
K=3.28*(M**0.5)
U1=4.0*3.14*78.5*8.854E-12*(Y**2.0)
U2=AP*((AP+H(I,J))/(H(I,J)+2.0*AP))
VR(I,J)=(U1*U2)*ALOG(1.0+(AP/
(AP+H(I,J)))*EXP(-AP*K))
R=(H(I,J)+2.0*AP)/AP
B1=(-2.0*R+6.0)/(R**7.0)
B2=(R**2.0+14*R+54.0)/((R+2.0)**7.0)
B3=(R**2.0-14.0*R+54.0)/((R-2.0)**7.0)
B4=(A*(SIGMA**6.0))/(37800.0*
R*(AP**6.0))
VB(I,J)=B4*(B1+B2+B3)
VT(I,J)=(VR(I,J)+VA(I,J)+VB(I,J))/KBT
VA1(I,J)=VA(I,J)/KBT
VR1(I,J)=VR(I,J)/KBT
10  CONTINUE
40  CONTINUE
 MINX=0.0
 MAXX=500.0
 MINY=-10.0
 MAXY=10.0
 COUNT=1
 CALL GROUTE(' ')
 CALL ROPEN
 CALL PSPACE(0.3,0.95,0.69,0.99)
```

```
CALL GLIMIT(RXLEFT,MAXX,MINY
 ,MAXY,0.,0.)
CALL SETGRAPH(MINX,MAXX,
 MINY,MAXY)
CALL GCLIP
CALL DRAWGRAPH(H,VT,NP,NUMBER)
CALL GNCLIP
CALL DRAWTEXT ( )
CALL PSPACE(0.2,0.5,0.35,0.65)
CALL GLIMIT(RXLEFT,MAXX,MINY
 ,MAXY,0.,0.)
CALL SETGRAPH(MINX,MAXX,
 MINY,MAXY)
CALL GCLIP
CALL DRAWGRAPH(H,VA1,
 NP,NUMBER)
CALL GNCLIP
CALL DRAWTEXT ( )
CALL PSPACE(0.65,0.95,0.35,0.65)
CALL GLIMIT(RXLEFT,MAXX,
 MINY,MAXY,0.,0.)
CALL SETGRAPH(MINX,MAXX,
 MINY,MAXY)
CALL GCLIP
CALL DRAWGRAPH(H,VR1,NP,
  NUMBER)
CALL GNCLIP
CALL DRAWTEXT ( )
CALL RCLOSE
STOP
END

SUBROUTINE SETGRAPH(MINX,MAXX,
 MINY,MAXY)
REAL MINX,MINY,MAXY,MAXX,HT
PARAMETER (RXLEFT=1.0E-3)
CALL GLIMIT(RXLEFT,MAXX,
 MINY,MAXY,0.,0.)
CALL GSCALE
HT=BOX2MM(0.50)*0.025
CALL RAXIS(2,MINX,HT,1)
CALL RAXIS(1,0,HT,1)
RETURN
END

SUBROUTINE DRAWGRAPH(H,VM,
 NP,NUMBER)
REAL H(250,250),VM(250,250),H1(250)
REAL VM1(250)
INTEGER NP,POS,POS1,NUMBER,CNT
DO 499 POS=1,NUMBER
CNT=1
DO 500 POS1=1,NP
H1(CNT)=H(POS1,POS)
VM1(CNT)=VM(POS1,POS)
  CNT = CNT + 1
500 CONTINUE
  CALL GVECT(H1,VM1,NP)
499 CONTINUE
  RETURN
  END

  SUBROUTINE DRAWTEXT()
  COMMON/A/COUNT
  REAL MINX,MAXX,MINY,
   MAXY,DISPX,DISPY
  INTEGER COUNT
  CALL GLIMIT(0.0,1.0,0.0,1.0,0.,0.)
  DISPX = 0.16
  DISPY = 0.3
  MINX = 0.0
  MAXX = 0.3
  MINY = 0.0
  MAXY = 1.0
  IF(COUNT.EQ.1) THEN
  CALL RTXHEI(4.0)
  CALL RTXANG(0.0)
  CALLRTX(-1,'(a)',MAXX-0.2,MINY-DISPY)
  CALL RTXANG(90.0)
  CALL RTX(-1, ' ENERGY (KT)
   ',MINX-DISPX,MINY+0.1)
  CALL RTXANG(0.0)
  CALL RTX(-1,' Distance (nm)',
   MAXX-0.3,MINY-0.1)
  CALL RTXANG(0.0)
  ELSE
  GOTO 11
  ENDIF
 11 CONTINUE
  IF(COUNT.EQ.2) THEN
  CALL RTXHEI(4.0)
  CALL RTXANG(0.0)
  CALL RTX(-1,'(b)', MAXX+0.2,MINY-0.3)
  CALL RTXANG(90.0)
  CALL RTX(-1, ' ENERGY (KT)
   ',MINX-DISPX,MINY+0.1)
  CALL RTXANG(0.0)
  CALL RTX(-1,' Distance (nm)',
   MAXX,MINY-0.1)
  ELSE
  GOTO 12
  ENDIF
 12 CONTINUE
  IF (COUNT.EQ.3) THEN
  CALL RTXHEI(4.0)
  CALL RTXANG(0.0)
  CALL RTX(-1,'(c)', MAXX+0.2,MINY-0.3)
   CALL RTXANG(90.0)
   CALL RTX(-1, ' ENERGY (KT)
    ',MINX-DISPX,MINY+0.1)
```

```
      CALL RTXANG(0.0)
      CALL RTX(-1,' Distance (nm)',
       MAXX,MINY-0.1)
      ELSE
      GOTO 13
      ENDIF
   13 CONTINUE
      COUNT=COUNT+1
      RETURN
      END

      SUBROUTINE PSPACE(X1,XR,Y1,YU)
      REAL X1,XR,Y1,YU
      REAL XORIG,YORIG,XSIZE,
       YSIZE,XLEN,YLEN
      LOGICAL FIRST
      DATA FIRST/.TRUE./
      SAVE XORIG,YORIG,XSIZE,FIRST
      XLEN=XR-X1
      YLEN=YU-Y1
      IF (FIRST) THEN
      CALL GACT(-1)
      CALL GVPORT(XORIG,YORIG,
       XSIZE,YSIZE) XSIZE=MIN(XSIZE,YSIZE)
      FIRST=.FALSE.
      ENDIF
      YSIZE=XSIZE
      CALL GVPORT(XORIG+X1*XSIZE,
       YORIG+Y1*YSIZE,XSIZE*
       XLEN,YSIZE*YLEN)
      CALL GWBOX(XLEN,YLEN,0.)
      RETURN
      END
```

Program PCENERGY calculates and draws the van der Waals, electrical double layer and the total interaction energies between *particle and collector*

```
      PROGRAM PCENERGY
      COMMON/A/COUNT
      REAL H(250,250),VA(250,250),
       VR(250,250),V(250,250)
      REAL A1(250,250),A2(250,250),
       A3(250,250),VT(250,250)
      REAL VA1(250,250),VR1(250,250)
      REAL M,A,Y1,Y2,KBT,
       AP,AA1,AA2,AA3,K
      REAL B1,A4,APR,EE,U1,U2,YY1,YY2
      REAL MINX,MAXX,MINY,MAXY,APH,B2
      INTEGER NP,NUMBER,I,J,COUNT
      PARAMETER (RXLEFT=1.0E-3)
      WRITE (*,*) "how many profiles needed?"
      READ (*,*) NUMBER
      DO 40 J=1,NUMBER
      WRITE(*,*)"what is the electrolyte
       concentration (mol dm-3)?"
      READ(*,*) M
      WRITE(*,*) "what is the Hamaker
       constant (J)?"
      READ(*,*) A
      WRITE(*,*) "what is the collector
       potential (mv)?"
      READ(*,*) Y1
      WRITE(*,*) "what is the particle
       potential (mv)?"
      READ(*,*) Y2
      KBT=1.3805e-23*298
      WRITE(*,*) "how many increments?"
      READ(*,*) NP
      WRITE(*,*) "what is the particle
       radius (nm)?"
      READ(*,*) AP
      APH=AP/10.0

*van der Waals attraction:
*Gregory at h<a and for h>(lambda/
4*pi) czarnecki
      DO 10 I=1,NP
      READ (J,*) H(I,J)
      IF(H(I,J).LT.APH) THEN
      GOTO 600
      ELSE
      B1=(H(I,J)+2*AP)
      A1(I,J)=((H(I,J)-AP)/(H(I,J)**2))
       -((H(I,J)+3*AP)/(B1**2))
      AA1=((2.45*100.0)/(60.0*3.14))*A1(I,J)
      A2(i,j)=((H(I,J)-2.0*AP)/
       (H(I,J)**3.0))-((H(I,J)+4.0*AP)/(B1**3.0))
      AA2=((2.17*10000.0)/(720.0*
       (3.14**2.0)))*A2(I,J)
      A3(I,J)=((H(I,J)-3*AP)/(H(I,J)**4))
       -((H(I,J)+5*AP)/(B1**4))
      AA3=((0.59*1000000.0)/(5040.0
       *(3.14**3)))*A3(I,J)
      VA(I,J)=A*(AA1-AA2+AA3)
      ENDIF
      GOTO 800
  600 B2=((5.32*H(I,J))/100.0)*
       ALOG(1.0+(100.0/(5.32*H(I,J))))
      VA(I,J)=((-A*AP)/(6.0*H(I,J)))*(1-B2)
  800 A4=((1.3805e-16*298.0)/(4.7976e-10))
      K=3.28*(M**0.5)
      APR=AP*0.0000001
       U1=(4.7976e-10*(Y1/(1000.0*
        299.8)))/(4.0*1.3805e-16*298.0)
       U2=(4.797e-10*(Y2/(1000.0*
```

```
     299.8)))/(4.0*1.3805e-16*298.0)
     EE=2.71828182
     YY1=(EE**U1-EE**(-U1))/
      (EE**U1+EE**(-U1))
     YY2=(EE**U2-EE**(-U2))
      /(EE**U2+EE**(-U2))
     V(I,J)=16.0*0.0796*78.5*(A4**2)*APR*
      YY1*YY2*exp(-H(I,J)*K)
     VR(I,J)=V(I,J)/(10000000.0)
     VT(I,J)=(VR(I,J)+VA(I,J))/KBT
     VA1(I,J)=VA(I,J)/KBT
     VR1(I,J)=VR(I,J)/KBT
     WRITE(J+2,*) H(I,J),VT(I,J)
10    CONTINUE
40    CONTINUE
     MINX=0.0
     MAXX=1000.0
     MINY=-20.0
     MAXY=20.0
     COUNT=1
     CALL GROUTE(' ')
     CALL ROPEN
     CALL PSPACE(0.3,0.95,0.69,0.99)
     CALL GLIMIT(RXLEFT,MAXX,MINY,
      MAXY,0.,0.)
     CALL SETGRAPH(MINX,MAXX,
      MINY,MAXY)
     CALL GCLIP
     CALL DRAWGRAPH(H,VT,NP,NUMBER)
     CALL GNCLIP
     CALL DRAWTEXT ( )
     CALL PSPACE(0.2,0.5,0.3,0.6)
     CALL GLIMIT(RXLEFT,MAXX,MINY,
      MAXY,0.,0.)
     CALL SETGRAPH(MINX,MAXX,
      MINY,MAXY)
     CALL GCLIP
     CALL DRAWGRAPH(H,VA1,
      NP,NUMBER)
     CALL GNCLIP
     CALL DRAWTEXT ( )
     CALL PSPACE(0.65,0.95,0.3,0.6)
     CALL GLIMIT(RXLEFT,MAXX,MINY,
      MAXY,0.,0.)
     CALL SETGRAPH(MINX,MAXX,
      MINY,MAXY)
     CALL GCLIP
     CALL DRAWGRAPH(H,VR1,
      NP,NUMBER)
     CALL GNCLIP
     CALL DRAWTEXT ( )
     CALL RCLOSE
     STOP
     END

     SUBROUTINE SETGRAPH(MINX,MAXX,
      MINY,MAXY)
     REAL MINX,MINY,MAXY,MAXX,HT
     PARAMETER (RXLEFT=1.0E-3)
     CALL GLIMIT(RXLEFT,MAXX,MINY,
      MAXY,0.,0.)
     CALL GSCALE
     HT=BOX2MM(0.50)*0.025
     CALL RAXIS(2,MINX,HT,1)
     CALL RAXIS(1,0,HT,1)
     RETURN
     END

     SUBROUTINE DRAWGRAPH(H,VM,NP,
      NUMBER)
     REAL H(250,250),VM(250,250),H1(250)
     REAL VM1(250)
     INTEGER NP,POS,POS1,NUMBER,
      CNT,DAT(5)
     DATA DAT/17,20,21,22,5/
     DO 499 POS=1,NUMBER
     CNT=1
     DO 500 POS1=1,NP
     H1(CNT)=H(POS1,POS)
     VM1(CNT)=VM(POS1,POS)
     CNT = CNT + 1
500   CONTINUE
     CALL BDIMX (1, H1, NP)
     CALL BPOINT(DAT(POS),1,VM1,NP,4.0,5)
     CALL GVECT(H1,VM1,NP)
499   CONTINUE
     RETURN
     END

     SUBROUTINE DRAWTEXT()
     COMMON/A/COUNT
     INTEGER COUNT
     REAL MINX,MAXX,MINY,
      MAXY,DISPX,DISPY
     CALL GLIMIT(0.0,1.0,0.0,1.0,0.,0.)
     DISPX = 0.16
     DISPY = 0.3
     MINX = 0.0
     MAXX = 0.3
     MINY = 0.0
     MAXY = 1.0
     IF(COUNT.EQ.1) THEN
     CALL RTXHEI(4.0)
     CALL RTXANG(0.0)
     CALL RTX(-1,'(A)',MAXX-0.1,MINY-0.3)
     CALL RTXANG(90.0)
     CALL RTX(-1, ' Energy (KT)
       ',MINX-DISPX,MINY+0.1)
      CALL RTXANG(0.0)
      CALL RTX(-1,' Distance (nm)',
```

```
     MAXX-0.2,MINY-0.1)
     ELSE
     GOTO 11
     ENDIF
  11 CONTINUE
     IF(COUNT.EQ.2) THEN
     CALL RTXANG(0.0)
     CALL RTXHEI(4.0)
     CALL RTX(-1,'(B)',MAXX+0.2,MINY-0.3)
     CALL RTX(-1,' Distance (nm)',
      MAXX,MINY-0.1)
     CALL RTXANG(90.0)
     CALL RTX(-1, ' Energy (KT)
      ',MINX-DISPX,MINY+0.1)
     CALL RTXANG(0.0)
     CALL RTXHEI(5.0)
     CALL RTX(-1,'Interaction energy profile',
      MAXX,MINY-0.6)
     CALL RTXHEI(3.0)
     CALL RTX(-1,'(A) Total energy of
      interaction', MAXX,MINY-0.7)
     CALL RTX(-1,'(B) van der Waals energy',
      MAXX,MINY-0.8)
     CALL RTX(-1,'(C) Electrical double layer',
      MAXX,MINY-0.9)
     CALL RTXANG(0.0)
     CALL RTXHEI(3.0)
     ELSE
     GOTO 12
     ENDIF
  12 CONTINUE
     IF (COUNT.EQ.3) THEN
     CALL RTXHEI(4.0)
     CALL RTXANG(0.0)
     CALL RTX(-1,'(C)',MAXX+0.2,MINY-0.3)
     CALL RTXANG(90.0)
     CALL RTX(-1, ' Energy (KT)
      ',MINX-DISPX,MINY+0.1)
     CALL RTXANG(0.0)
     CALL RTX(-1,' Distance (nm)',
      MAXX,MINY-0.1)
     CALL RTXANG(0.0)
     ELSE
     GOTO 13
     ENDIF
  13 CONTINUE
     COUNT=COUNT+1
     RETURN
     END

     SUBROUTINE PSPACE(X1,XR,Y1,YU)
     REAL X1,XR,Y1,YU
     REAL XORIG,YORIG,XSIZE,YSIZE,
      XLEN,YLEN
     LOGICAL FIRST
     DATA FIRST/.TRUE./
     SAVE XORIG,YORIG,XSIZE,FIRST
     XLEN=XR-X1
     YLEN=YU-Y1
     IF (FIRST) THEN
     CALL GACT(-1)
     CALL GVPORT(XORIG,YORIG,
      XSIZE,YSIZE)
     XSIZE=MIN(XSIZE,YSIZE)
     FIRST=.FALSE.
     ENDIF
     YSIZE=XSIZE
     CALL GVPORT(XORIG+X1*XSIZE,
      YORIG+Y1*YSIZE,XSIZE*XLEN,
      YSIZE*YLEN)
     CALL GWBOX(XLEN,YLEN,0.)
     RETURN
     END
```

Program ROOT calculates the position at the rear stagnation point of the collector corresponding to the limiting trajectory used in the program trajectory as the initial condition for the differential equation.

```
     PROGRAM ROOT
     COMMON/SET B/AF,AP,U,M,MU
     COMMON/SET C/PI,HAMAK,AAF
     COMMON/SET E/PPOTEN,CPOTEN
     COMMON/SETH/NLO,NG
     DOUBLE PRECISION KAPPA,NG
     DOUBLE PRECISION M,CPOTEN,FM,RM
     DOUBLE PRECISION NLO,PPOTEN,FLOW
     DOUBLE PRECISION AF,AP,U,MU,
      PI,HAMAK,AAF
     DOUBLE PRECISION A,B,EPS,ETA,X,DG,F
     INTEGER IFAIL,NUMBER
     EXTERNAL F,C05ADF

*DATA FOR SOME PARAMETERS GIVEN
*AF=COLLECTOR RADIUS (M)
*AP=PARTICLE RADIUS (M)
*MU=FLUID VISCOSITY (KG/M.S)
*M=KCL CONCENTRATION (MOL/L)
*PPOTEN=PARTICLE POTENTIAL (MV)
*CPOTEN=COLLECTOR POTENTIAL (MV)
*U=FLUID VELOCITY FAR FROM THE
COLLECTOR (M/S)
*HAMAK=HAMAKER CONSTANT (J)

      PI=3.14159D0
      AF=18.5D-6
      AP=2.7D-6
      MU=8.9D-4
```

```
      M=0.0001D0
      CPOTEN=-26.5D0
      PPOTEN=-8.5D0
      U=453.33D-6
      HAMAK=1.7D-20
      NUMBER=1
      CALL PARAMETER (AAF,NUMBER)
      CALL NLONDON(NLO)
      CALL NNG(NG)

*NAG ROUTINE PARAMETERS GIVEN

      A=0.0D0
      B=1000.0D0
      EPS=1.0D-6
      ETA=0.0D0
      IFAIL=1
      CALL C05ADF(A,B,EPS,ETA,F,X,IFAIL)
      IF (IFAIL.GT.0) GOTO 20
 20   WRITE(*,*) 'IFAIL= ',IFAIL
      STOP
      END

      DOUBLE PRECISION FUNCTION F(X)
      COMMON/SET C/PI,HAMAK,AAF
      COMMON/SETH/NLO,NG
      DOUBLE PRECISION B1,B2,B3,B4
      DOUBLE PRECISION NLO,NG,AAF
      DOUBLE PRECISION X
      DOUBLE PRECISION PI,HAMAK

      B1=(NLO*FRET(X))/((X**2.0D0)
       *((X+2.0D0)**2.0D0))
      B2=F2(X)*COS(PI)
      B3=COS(PI)*NG
      B4=EDL(X)
      F=B1+B2+B3-B4
      RETURN
      END

      SUBROUTINE NLONDON(NLO)
      COMMON/SET B/AF,AP,U,M,MU
      COMMON/SET C/PI,HAMAK,AAF
      DOUBLE PRECISION NLO,PI,MU,AF,U,M
      DOUBLE PRECISION AP,HAMAK,AAF
      NLO=HAMAK*(AF**2.0)/(9.0*PI*
       MU*AAF*U*(AP**4.0))
      RETURN
      END

      SUBROUTINE PARAMETER
       (AAF,NUMBER)
      DOUBLE PRECISION AAF,ALPHA,C1,C2
 INTEGER NUMBER
*     ALPHA=FRACTION OF SOLIDS

 ALPHA=0.03
 IF (NUMBER.GT.1) GOTO 11
*ESTIMATION OF THE FLOW
  PARAMETER AAF
*METHOD 1: LAMB'S SOLUTION
 C1=-0.5*DLOG((ALPHA))-0.5
 C2=(ALPHA**2.0)/(2.0*(1.0+(ALPHA**2.0)))
 AAF=1.0/(2.0*(C1+C2))
 GOTO 12
*METHOD 2: EXPRESSION BY HAPPEL (1959)
 11  AAF=0.5/(-0.5*DLOG((ALPHA))-
(3.0/4.0)+ALPHA-(ALPHA**2.0)/4.0)
 12  CONTINUE
 RETURN
 END

 FUNCTION F1(Y)
 COMMON/SET B/AF,AP,U,M,MU
 DOUBLE PRECISION Y,AFP,AP,AF,YY
 DOUBLE PRECISION H,APN,U,M,MU

 *APN=PARTICLE RADIUS (NM)
 *AFP=COLLECTOR RADIUS (NM)

 APN=AP*(10.0**9.0)
 AFP=AF*(10.0**9.0)
 H=Y
 YY=H*2700.0
 IF(YY.LT.APN.AND.YY.LT.AFP) THEN
 F1=H
 ENDIF
 IF(YY.GT.APN.AND.YY.LT.AFP) THEN
 F1=(1.00-(9.00/8.00)*((H+1.00)**(-1.00)))
 ENDIF
 RETURN
 END

 FUNCTION F2(Y)
 COMMON/SET B/AF,AP,U,M,MU
 DOUBLE PRECISION Y,AFP,AP,AF,YY
 DOUBLE PRECISION H,APN,U,M,MU

 *APN=PARTICLE RADIUS (NM)
 *AFP=COLLECTOR RADIUS (NM)

 APN=AP*(10.0**9.0)
 AFP=AF*(10.0**9.0)
 H=Y
 YY=H*2700.0
      IF(YY.LT.APN.AND.YY.LT.AFP) THEN
      F2=3.230
      ENDIF
      IF(YY.GT.APN.AND.YY.LT.AFP) THEN
```

```
      F2=(1.00-(9.00/8.00)*((H+1.00)**
       (-1.00)))**(-1.00)
      ENDIF
      RETURN
      END

      SUBROUTINE NNG(NG)
      COMMON/SET C/PI,HAMAK,AAF
      COMMON/SET B/AF,AP,U,M,MU
      DOUBLE PRECISION
       FF1,FF2,AF,G,ROP,ROF
      DOUBLE PRECISION MU,AAF,NG
      DOUBLE PRECISION PI,HAMAK,AP,M,U

* AP=COLLECTOR RADIUS (CM)
* G-GRAVITATIONAL ACCELERATION (M/S2)
* ROP=PARTICLE DENSITY (KG/M3)
* ROF=FLUID DENSITY (KG/M3)
* MUC=VISCOSITY (KG/M.S)
*  U=FLUID VELOCITY FAR FROM THE
COLLECTOR (M/S)

      G=9.81
      ROP=1050.0
      ROF=1000.0
      FF1=2.0*(AF**2.0)*G*(ROP-ROF)
      FF2=9.0*MU*U*AAF
      NG=FF1/FF2
      RETURN
      END

      FUNCTION FRET(H)
      DOUBLE PRECISION H,P,PI
      PI=3.141592654
      P=(2.0*PI*H*2700.0)/100.0
      IF(P.GT.3.) GOTO 30
      FRET=1.0/(1.0+0.620725*P+0.075159*(P*P))
      GOTO 50
   30 FRET=(1.024172/P)-((0.714228)/
      (P*P))+(0.555262)/(P**3.0)
   50 CONTINUE
      RETURN
      END

      FUNCTION EDL(Y)
      COMMON/SET C/PI,HAMAK,AAF
      COMMON/SET B/AF,AP,U,M,MU
      COMMON/SET E/PPOTEN,CPOTEN
      DOUBLE PRECISION NE1,NE2,NE3,NE4
      DOUBLE PRECISION
       PPOTEN,CPOTEN,Y,H
      DOUBLE PRECISION PHIP,PHIC,KAPPA
      DOUBLE PRECISION AF,AP,U,M,MU,EPS
      DOUBLE PRECISION PI,HAMAK,AAF
      DOUBLE PRECISION AFC,APC,MUC,UC
      PHIP=PPOTEN/(1000.0*299.80)
      PHIC=CPOTEN/(1000.0*299.80)
      KAPPA=3.28*(M**(0.5))
      AFC=AF*100.0
      MUC=MU*10.0
      APC=AP*100.0
      UC=U*100.0
      EPS=81.0
      H=Y*2700.0D0
      NE1=(EPS*(KAPPA*(10.0**7.0))*
       (AFC**2.0)*((PHIP**2.0)
       *(PHIC**2.0)))/(12.0*PI*
       MUC*APC*AAF*UC)
      NE2=((2.0*PHIP*PHIC)/((PHIP**2.0)
       +(PHIC**2.0)))
      NE3=EXP(-KAPPA*H)
      NE4=EXP(-KAPPA*H)/(1.0-EXP(-2.0*
       KAPPA*H))
      EDL=NE1*(NE2-NE3)*NE4
      RETURN
      END
```

Program TRAJ.F calculates the limiting trajectory for a particle approaching a cylindrical collector. The integration is initiated at the rear stagnation point and continues until the angle alpha was very small. This happened at approximately a collector radius from the collector.

```
      PROGRAM TRAJ.F
      COMMON/SET B/AF,AP,U,M,MU
      COMMON/SET C/PI,HAMAK,AAF
      COMMON/SETH/NLO,NG
      COMMON/SETP/PPOTEN,CPOTEN
      COMMON/SETL/FDL
      COMMON/SET ET/ETA2
      INTEGER          NOUT
      INTEGER          IFAIL,NUMBER
      INTEGER          N, IW
      PARAMETER        (NOUT=4)
      PARAMETER        (N=1,IW=(12+N)*N+50)
      DOUBLE PRECISION TOL, X, XEND,NG
      DOUBLE PRECISION W(IW),
       Y(N),ETA,STMLN,LAMBDA
      DOUBLE PRECISION NLO
      DOUBLE PRECISION
       AF,AP,U,M,MU,PI,HAMAK,AAF
      DOUBLE PRECISION
       CPOTEN,PPOTEN,FDL,ETA2
      EXTERNAL         D02EAF, FCN

*     AF=COLLECTOR RADIUS (M)
*     AP=PARTICLE RADIUS (M)
```

```
*     MU=FLUID VISCOSITY (KG/M.S)
*     M=ELECTYROLYTE CONCENTRATION
     (MOL/DM3)
*     HAMAK=HAMAKER CONSTANT(J)
*     CPOTEN=COLLECTOR POTENTIAL (MV)
*     PPOTEN=PARTICLE POTENTIAL (MV)
*     U=VELOCITY (M/S)

      PI=3.14159D0
      AF=18.5D-6
      AP=2.7D-6
      MU=8.9D-4
      U=6.0D-5
      M=0.01D0
      HAMAK=1.7D-20
      NUMBER=1
      CPOTEN=300.0D0
      PPOTEN=-4.5D0
      CALL PARAMETER (AAF,NUMBER)

      CALL NLONDON(NLO)
      CALL NNG(NG)
      XEND = PI/500.0D0
      TOL = 10.0**(-5.0D0)
      Y(1) =98.0431D0/2700.0D0
      X = PI
      IFAIL = 1
      CALL D02EAF(X,XEND,N,Y,TOL,
       FCN,W,IW,IFAIL)
      CALL STREAM(X,Y(1),ETA,
       STMLN,LAMBDA)
      WRITE(*,*)'ETA=',ETA,'
       LAMBDA=',LAMBDA
      STOP
      END

      SUBROUTINE FCN(T,Y,F)
      COMMON/SET B/AF,AP,U,M,MU
      COMMON/SETH/NLO,NG
      COMMON/SET C/PI,HAMAK,AAF
      COMMON/SETL/FDL
      INTEGER       N
      PARAMETER     (N=1)
      DOUBLE PRECISION T,B1,B2,B3,B4,B5
      DOUBLE PRECISION NLO,NG,FDL
      DOUBLE PRECISION AF,AP,U,M,MU
      DOUBLE PRECISION F(N), Y(N),R
      DOUBLE PRECISION PI,HAMAK,AAF
      R=AP/AF
      B1=(F1(Y(1))*NLO*FRET(Y(1)))
       /(((Y(1)+2.0D0)**2.0D0)*(Y(1)**2.0D0))
      B2=(F1(Y(1))*F2(Y(1))*COS(T))
      B3=F1(Y(1))*NG*COS(T)
      B4=F1(Y(1))*FEDL(Y(1))
      B5=NG*R*SIN(T)
      F(1)=-(B1+B2+B3-B4)/(SIN(T)*F3(Y(1))+B5)
      RETURN
      END

      FUNCTION FRET(H)
      COMMON/SET C/PI,HAMAK,AAF
      DOUBLE PRECISION H,P,PI,HAMAK,AAF
      P=(2.0D0*PI*H*2700.0D0)/100.0D0
      IF(P.GT.3.) GOTO 30
      FRET=1.0D0/(1.0D0+0.620725D0*P+
       0.075159D0*(P*P))
      GOTO 50
   30 FRET=(1.024172D0/P)-((0.714228D0)/(P*P))
       +(0.555262D0)/(P**3.0D0)
   50 CONTINUE
      RETURN
      END

      SUBROUTINE NLONDON(NLO)
      COMMON/SET B/AF,AP,U,M,MU
      COMMON/SET C/PI,HAMAK,AAF
      DOUBLE PRECISION NLO,PI,MU,AF,U,M
      DOUBLE PRECISION AP,HAMAK,AAF

*     MU=VISCOSITY (KG/M.S)
*     U=VELOCITY (M/S)
*     HAMAK=HAMAKER CONSTANT (J)
*
      NLO=HAMAK*(AF**2.0D0)/(9.0D0*PI*
      MU*AAF*U*(AP**4.0D0))
      RETURN
      END

      SUBROUTINE PARAMETER
      (AAF,NUMBER)
      DOUBLE PRECISION AAF,ALPHA,C1,C2
      INTEGER NUMBER

*     ALPHA=FRACTION OF SOLIDS

      ALPHA=0.03D0
      IF (NUMBER.GT.1) GOTO 11
*           METHOD 1: LAMB'S SOLUTION
      C1=-0.5D0*DLOG(ALPHA)-0.5D0
      C2=(ALPHA**2.0D0)/(2.0D0*(1.0D0+
       (ALPHA**2.0D0)))
      AAF=1.0D0/(2.0D0*(C1+C2))
      GOTO 12
*           METHOD 2 : HAPPEL
   11 AAF=0.5D0/(-0.5*DLOG(ALPHA)
       -(3.0D0/4.0D0)
       +ALPHA-(ALPHA**2.0D0)/4.0D0)
   12 CONTINUE
      RETURN
      END
```

```
      FUNCTION F1(Y)
      COMMON/SET B/AF,AP,U,M,MU
      DOUBLE PRECISION Y,AFP,AP,AF
      DOUBLE PRECISION H,APN,U,M,MU

*     APN=PARTICLE RADIUS (NM)
*     AFP=COLLECTOR RADIUS (NM)


      APN=AP*(10.0D0**9.0D0)
      AFP=AF*(10.0D0**9.0D0)
      H=Y
      YY=H*2700.0D0
      IF(YY.LT.APN.AND.YY.LT.AFP) THEN
      F1=H
      ENDIF
      IF(YY.GT.APN.AND.YY.LT.AFP) THEN
      F1=(1.0D0-(9.0D0/8.0D0)*((H+
       1.0D0)**(-1.0D0)))
      ENDIF
      RETURN
      END

      FUNCTION F2(Y)
      COMMON/SET B/AF,AP,U,M,MU
      DOUBLE PRECISION Y,AFP,AP,AF
      DOUBLE PRECISION H,APN,U,M,MU

*     APN=PARTICLE RADIUS (NM)
*     AFP=COLLECTOR RADIUS (NM)

      APN=AP*(10.0D0**9.0D0)
      AFP=AF*(10.0D0**9.0D0)
      H=Y
      YY=H*2700.0D0
      IF(YY.LT.APN.AND.YY.LT.AFP) THEN
      F2=3.230D0
      ENDIF
      IF(YY.GT.APN.AND.YY.LT.AFP) THEN
      F2=(1.0D0-(9.0D0/8.0D0)*
       ((H+1.0D0)**(-1.0D0)))**(-1.0D0)
      ENDIF
      RETURN
      END

      FUNCTION F3(Y)
      COMMON/SET B/AF,AP,U,M,MU
      DOUBLE PRECISION Y,AFP,AP,AF
      DOUBLE PRECISION H,APN,U,M,MU

*     APN=PARTICLE RADIUS (NM)
*     AFP=COLLECTOR RADIUS (NM)

      APN=AP*(10.0D0**9.0D0)
      AFP=AF*(10.0D0**9.0D0)
      H=Y
      YY=H*2700.0D0
      IF(YY.LT.APN.AND.YY.LT.AFP) THEN
      F3=0.74310D0/(0.63760D0-0.20D0*
       DLOG(H))
      ENDIF
      IF(YY.GT.APN.AND.YY.LT.AFP) THEN
      F3=(1.0D0-(5.0D0/16.0D0)*((H+
       1.0D0)**(-3.0D0)))
      ENDIF
      RETURN
      END

      SUBROUTINE
       STREAM(THETA,Y,ETA,STMLN
       ,LAMBDA)
      COMMON/SET C/PI,HAMAK,AAF
      COMMON/SET B/AF,AP,U,M,MU
      COMMON/SET ET/ETA2
      DOUBLE PRECISION
       YY,Y,MU,R,AP,AF,M,MUC,PI
      DOUBLE PRECISION
       ROF,U,AAF,STMLN,LAMBDA,YM
      DOUBLE PRECISION
       ETA,HAMAK,THETA,UC,AFC,ETA2

*     MUC=FLUID VISCOSITY (G/CM.S)
*     ROF=FLUID DENSITY (G/CM3)

      YY=Y*2700.0D0
      YM=Y+1.0D0
      MUC=MU*10.0D0
      AFC=AF*100.0D0
      UC=U*100.0D0
      R=AP/AF
      ROF=1.05D0
      ETA2=2.0D0*AAF*(R**2.0D0)*
       (YM**2.0D0)*SIN(THETA)
      STMLN=2.0D0*AAF*UC*(1.0D0/AFC)*
       (((YY/(10.0D7))-
       AFC)**2.0D0)*SIN(THETA)
      ETA=STMLN/(UC*AFC)
      LAMBDA=ETA/0.0189D0
      RETURN
      END

      FUNCTION FEDL(Y)
       COMMON/SET C/PI,HAMAK,AAF
       COMMON/SET B/AF,AP,U,M,MU
       COMMON/SETP/PPOTEN,CPOTEN
       COMMON/SETL/FDL
       DOUBLE PRECISION
        NE1,NE2,NE3,NE4,NE11
       DOUBLE PRECISION
        PPOTEN,CPOTEN,Y,H
```

```
      DOUBLE PRECISION PHIP,PHIC,KAPPA
      DOUBLE PRECISION AF,AP,U,M,MU,EPS
      DOUBLE PRECISION PI,HAMAK,AAF,FDL
      DOUBLE PRECISION AFC,APC,MUC,UC
      PHIP=PPOTEN/(1000.0D0*299.80D0)
      PHIC=CPOTEN/(1000.0D0*299.80D0)
      KAPPA=3.28D0*(M**(0.5D0))
      AFC=AF*100.0D0
      MUC=MU*10.0D0
      APC=AP*100.0D0
      UC=U*100.0D0
      EPS=81.0D0
      H=Y*2700.0D0
      NE1=(EPS*(KAPPA*(10.0D0**7.0D0))*
       (AFC**2.0D0)*((PHIP**2.0D0)+
       (PHIC**2.0D0)))/(12.0D0*PI*MUC*
       (APC**2.0D0)*AAF*UC)
      NE2=((2.0D0*PHIP*PHIC)/
       ((PHIP**2.0D0)+(PHIC**2.0D0)))
      NE3=EXP(-KAPPA*H)
       NE4=EXP(-KAPPA*H)/(1.0D0-
        EXP(-2.0D0*KAPPA*H))
       FEDL=NE1*(NE2-NE3)*NE4
       NE11=(EPS*(KAPPA*(10.0D0**7.0D0))*
        APC*((PHIP**2.0D0)
        +(PHIC**2.0D0)))/2.0D0
      FDL=NE11*(NE2-NE3)*NE4
      RETURN
      END

      SUBROUTINE NNG(NG)
      COMMON/SET C/PI,HAMAK,AAF
      COMMON/SET B/AF,AP,U,M,MU
      DOUBLE PRECISION
       FF1,FF2,AF,G,ROP,ROF
      DOUBLE PRECISION MU,AAF,NG
      DOUBLE PRECISION PI,HAMAK,AP,M,U

*G-GRAVITATIONAL   ACCELERATION
(M/S2)
*ROP=PARTICLE DENSITY (KG/M3)
*ROF=FLUID DENSITY (KG/M3)
*U=FLUID  VELOCITY  FAR  FROM  THE
COLLECTOR (M/S)

      G=9.81
      ROP=1050.0D0
      ROF=1000.0D0
      FF1=2.0D0*(AF**2.0D0)*G*(ROP-ROF)
      FF2=9.0D0*MU*U*AAF
      NG=FF1/FF2
      RETURN
      END

       SUBROUTINE VELOCITY
        (DIS,THETA,VRAD,VTAN,VTOT)
      COMMON/SET B/AF,AP,U,M,MU
      COMMON/SET C/PI,HAMAK,AAF
      COMMON/SETL/FDL
      DOUBLE PRECISION AF,AP,U,M,MU
      DOUBLE PRECISION PI,HAMAK,AAF
      DOUBLE PRECISION FDL,MS
      DOUBLE PRECISION APC,AFC,MUC,UC
      DOUBLE PRECISION
       DIS,THETA,VRAD,VTAN,VTOT
      DOUBLE PRECISION
       FL1,FL2,FL,FD,FGR,FHR,FTR
      DOUBLE PRECISION
       ROP,ROF,G,FHT,FGT,PI,FTT
      APC=AP*100.0D0
      AFC=AF*100.0D0
      MUC=MU*10.0D0
      UC=U*100.0D0
      ROP=1.05D0
      ROF=1.0D0
      G=0.0981D0
      FL1=-FRET(DIS)*2.0D0*HAMAK*
       (10.0D0**7.0D0)
      FL2=APC*3.0D0*((DIS+2.0D0)**2.0D0)*
       (DIS**2.0D0)
      FL=(FL1/FL2*(10.0D0**7.0D0))
      FD=FDL/(10.0D0**7)
      FGR=-((4.0D0/3.0D0)*PI*(APC**3.0D0)*
       G*(ROP-ROF)*COS(THETA))/(10.0D0**7)
      FHR=-6.0D0*PI*MUC*(APC**3.0D0)*
       (1.0D0/(AFC**2.0D0))*AAF*UC*
       COS(THETA)*F2(DIS)*(10.0D0**(-7.0D0))
      FTR=FD+FL+FGR+FHR
      FHT=(APC*(1.0D0/AFC)*AAF*UC*
       SIN(THETA)*F3(DIS))/(10.0D0**7.0D0)
      FGT=((4.0D0/3.0D0)*PI*(APC**3.0D0)*
       (ROP-ROF)*G*SIN(THETA))/(6.0D0*PI*
       MUC*APC*(10.0D0**7.0D0))
       FTT=FHT+FGT
       RETURN
       END
```

APPENDIX D

Experimental data of the deposition experiments

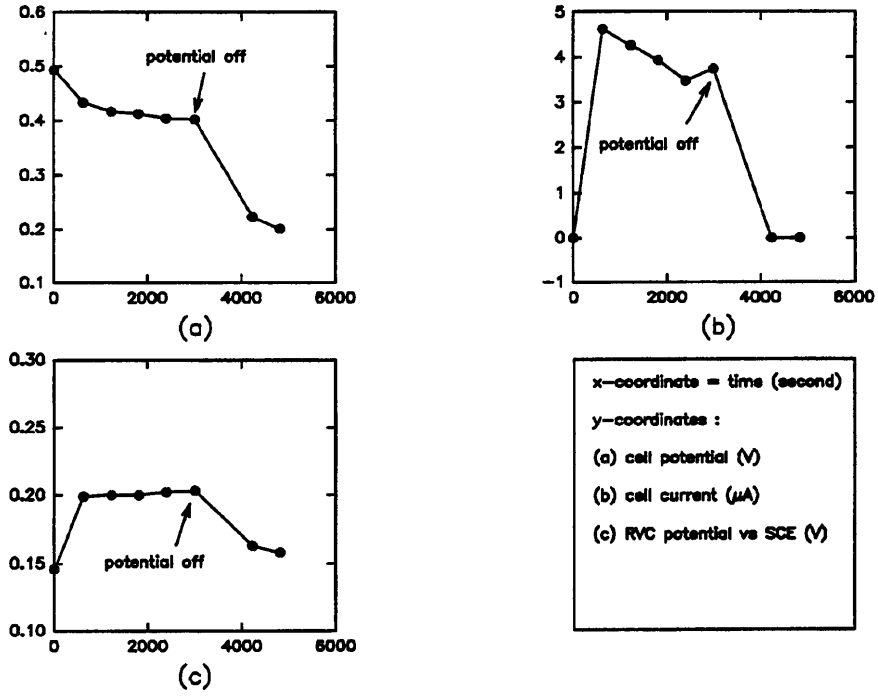

Figure D1 Experiment Ex10

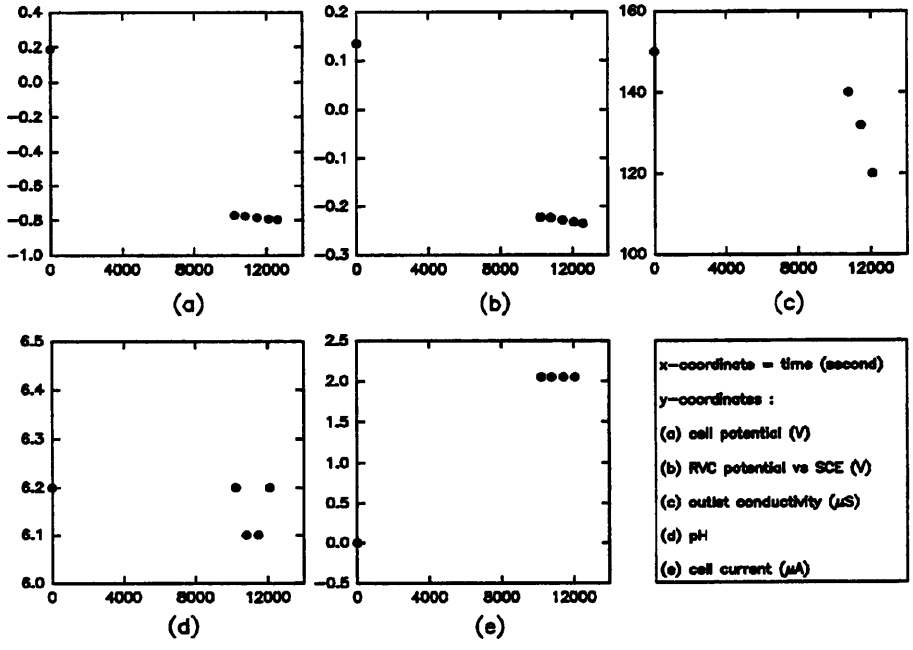

Figure D2 Experiments Ex11

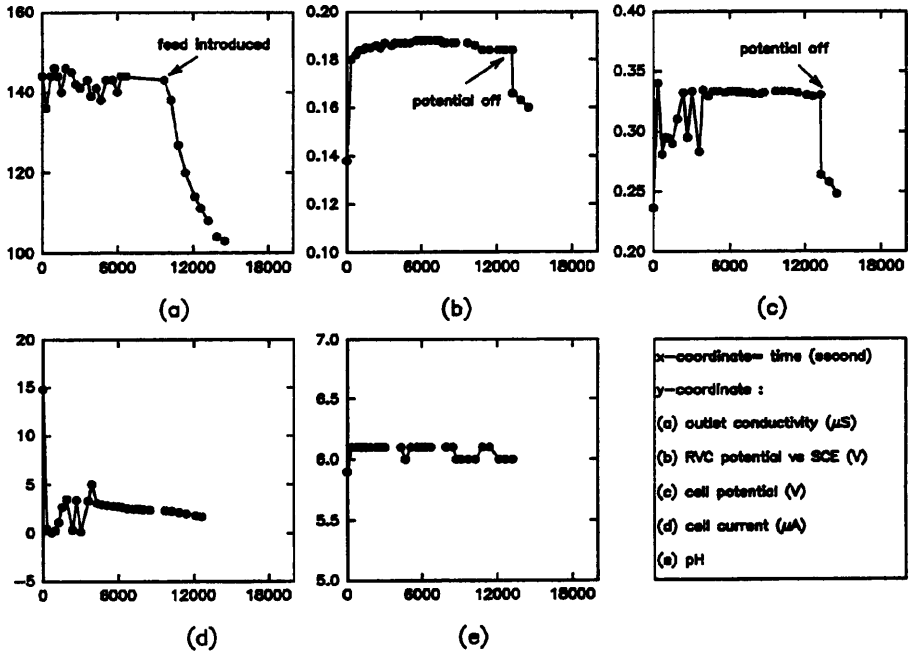

Figure D3 Experiments Ex15

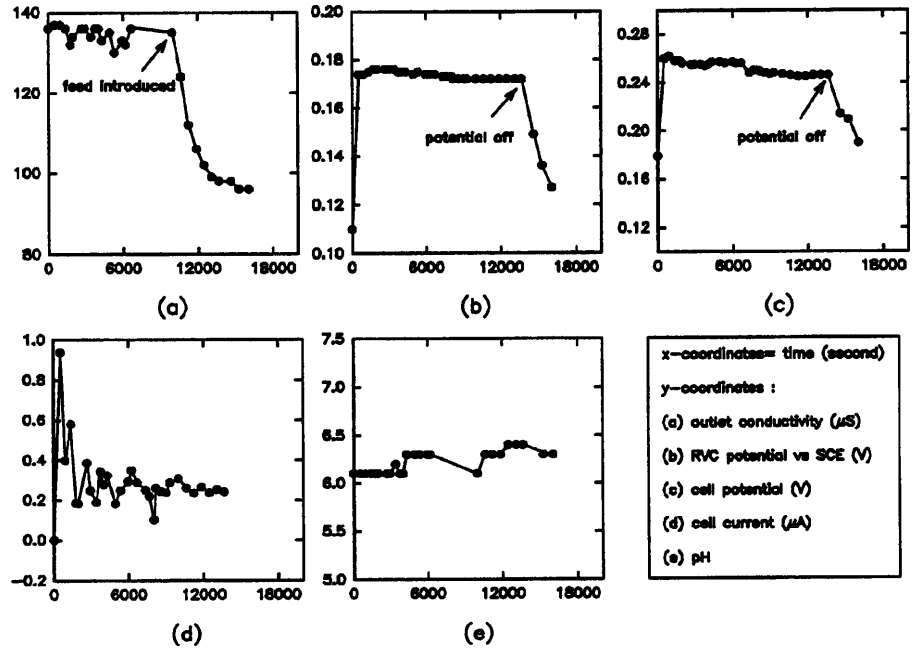

Figure D4 Experiment Ex16

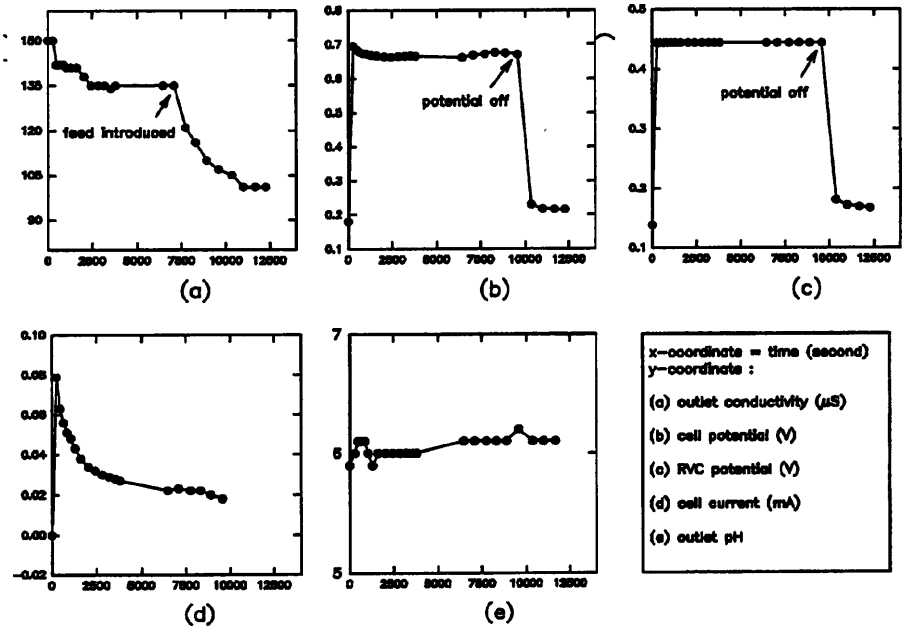

Figure D5 Experiment Ex17

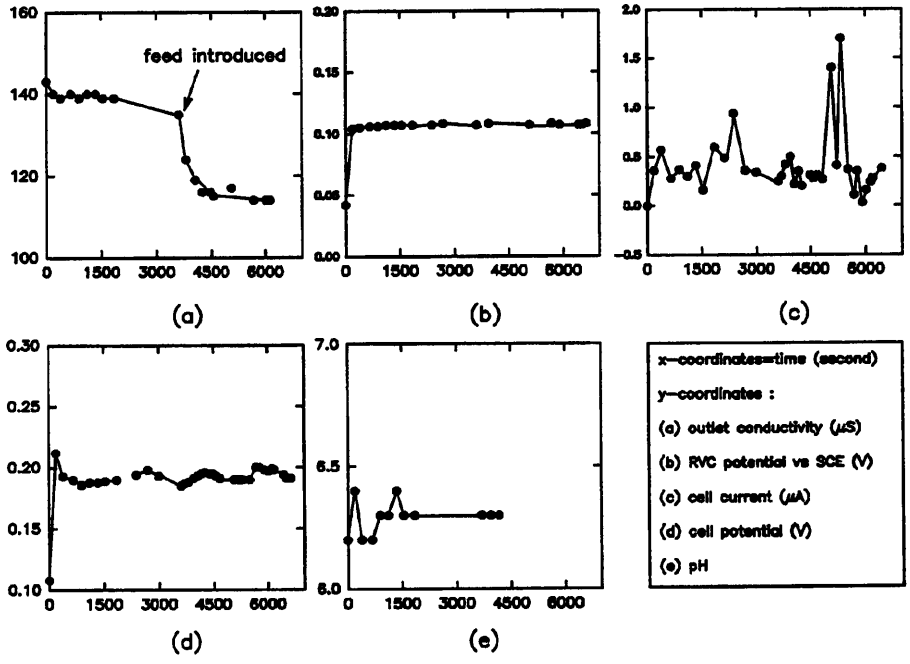

Figure D6 Experiment Ex19

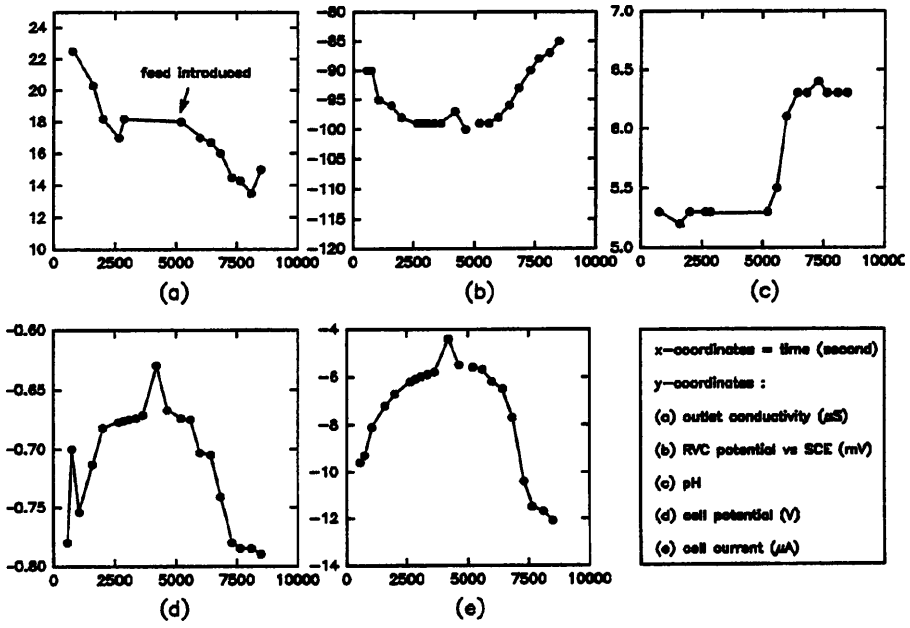

Figure D7 Experiment Hyp1

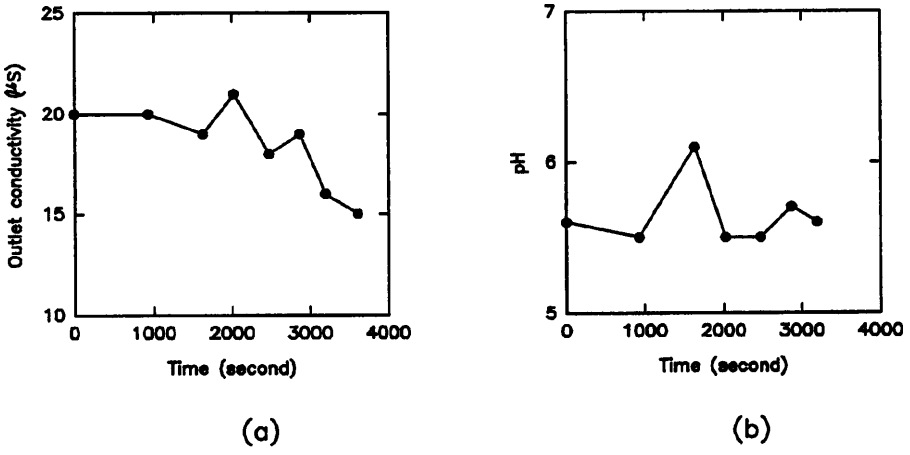

Figure D8 Experiment Hyp2

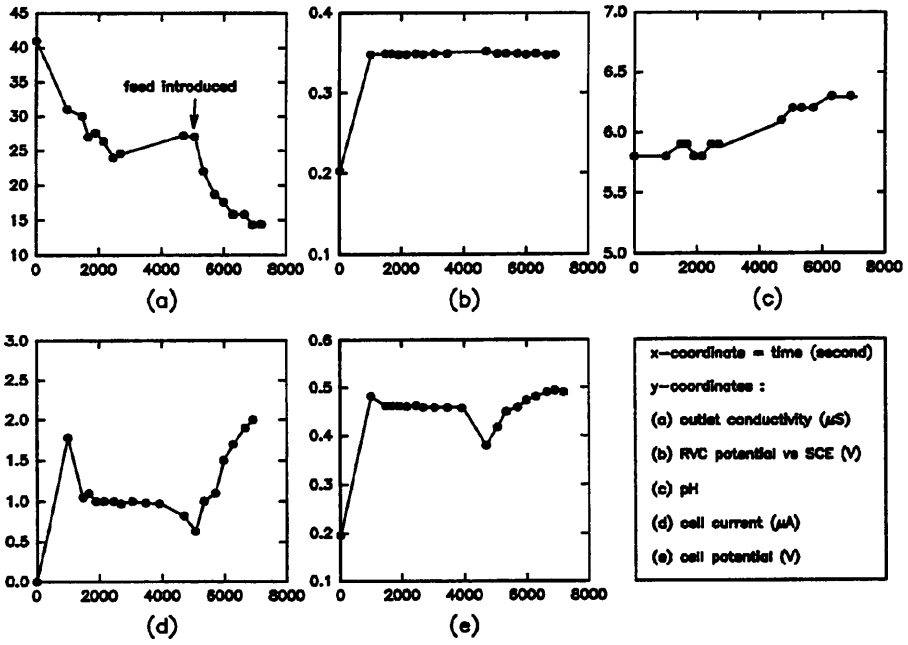

Figure D9 Experiment Hyp3

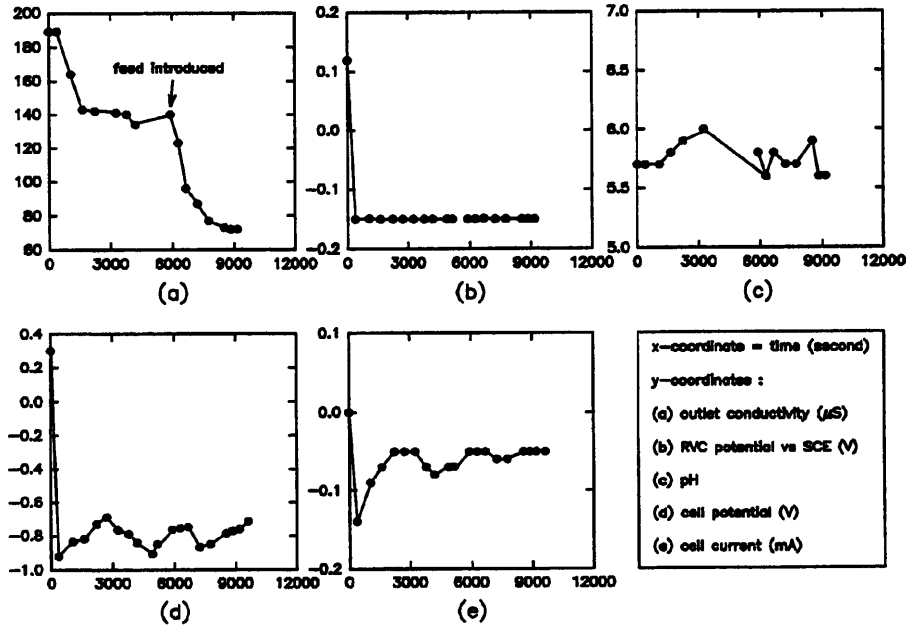

Figure D10 experiment Hyp4

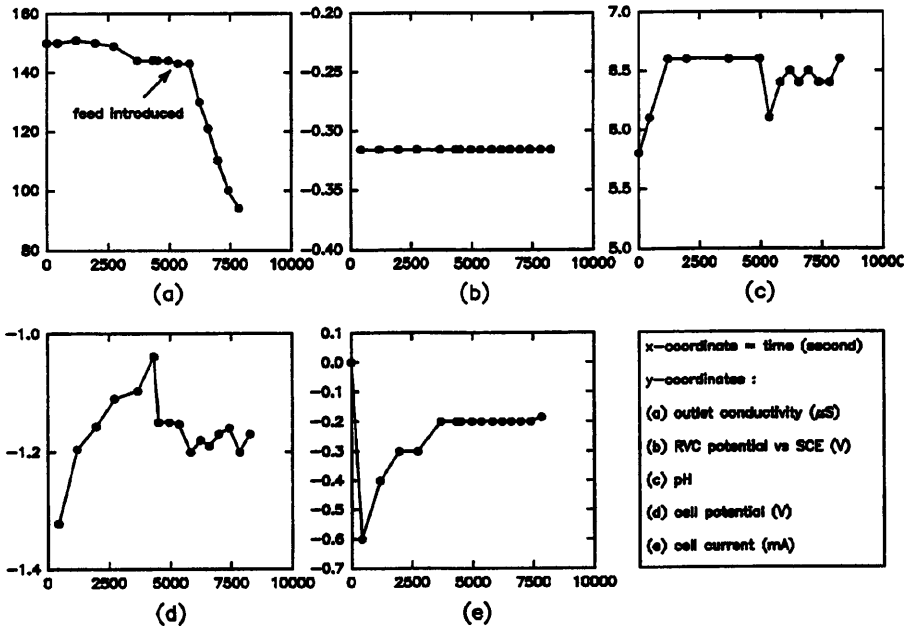

Figure D11 Experiment Hyp6

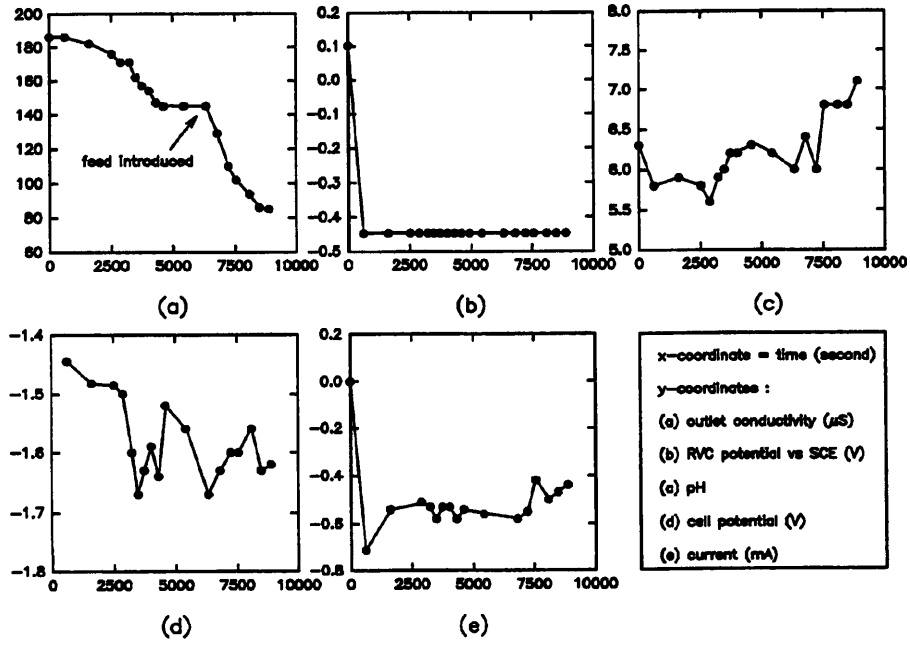

Figure D12 Experiment Hyp6

Appendix E

This appendix provides a comparison of the superficial and interstitial velocities used in this research project using the RVC column's porosity of 97%.

Volumetric Flowrate (cm^3/min)	Volumetric Flowrate ($x10^{-7}\ m^3/s$)	Superficial Velocity ($x10^{-4}$ m/s)	Interstitial Velocity ($x10^{-4}$ m/s)
34	5.67	4.5	4.4
12	2.00	1.6	1.5
5.6	0.93	0.74	0.72
1.7	0.28	0.22	0.22

The deposition experiments on to glass beads were carried out at the same volumetric flowrate of 22 $cm^3\ min^{-1}$. The corresponding superficial velocity for this flowrate is $2.41x10^{-4}$ m/s. Then from this value an interstitial velocity of $9.60x10^{-5}$ m/s can be estimated, using a typical bed porosity of 40% usually encountered in glass bead columns.